

**Advances in Synthetic, Structural and Reaction
Chemistry of Zinc and Zincate Complexes
Containing Alkyl and/or Amido Ligands**

Jennifer Anne Garden

A thesis submitted to the Department of Pure and Applied Chemistry, University
of Strathclyde, in part fulfilment of the requirements for the
degree of Doctor of Philosophy

March 2014

This thesis is the result of the author's original research. It has been composed by the author and has not been previously submitted for examination which has led to the award of a degree.

The copyright of this thesis belongs to the author under the terms of the United Kingdom Copyright Acts as qualified by University of Strathclyde Regulation 3.50. Due acknowledgement must always be made of the use of any material contained in, or derived from, this thesis.

Acknowledgements

Undertaking this PhD has been a rollercoaster journey. Having made it through final year, I began full of optimism and confidence about where the tracks that lay ahead would take me. It has been said that with a PhD, there is a negative correlation between how many things you know about, and how much you know about them, so that as you progress you become an expert in your specialism, although general knowledge and daily life skills may suffer as a result. I will admit that my experience has not felt like that of becoming an expert. For me, the journey has been challenging, stimulating, and at times overwhelming, as I tried to adjust to the constant questioning and evaluation of things I once thought I knew with certainty. This has meant that the “light bulb” moments, when things finally fell into place, have been worth celebrating all the more. Now that this journey has come to completion I can look back over the past three years and feel thankful for what I have achieved. I now understand that the reason I felt so far removed from my comfort zone was because I was constantly being pushed to develop and improve, often at a much faster pace than I was comfortable with. I have been incredibly lucky to have such wonderful family and friends who have supported me through the tough times, and celebrated with me during the good times. I will be forever grateful to every single one of you.

To mention a few people by name, I would like to thank George Fraser, whose exceptionally generous funding has enabled this research to take place.

I am extremely grateful to Prof Robert Mulvey for the opportunity to be a part of his research team. His project ideas, help and guidance along with inspirational discussions have been instrumental to the success of this work. On both a professional and a personal level, his counsel and support have been infinitely valuable. Additional help and input from Prof Eva Hevia and Dr Charlie O’Hara has added a wealth of ideas to this project and I am truly thankful for all their advice and encouragement.

I would like to thank Dr Alan Kennedy and Dr Stuart Robertson for their infinite patience in training me to perform X-Ray crystallography, in addition to Prof Bill Clegg and Dr Luca Russo, for all their help with the analysis of the compounds within this thesis. Dr Dave Armstrong has also been immeasurably helpful in performing the DFT calculations. I am extremely grateful to Dr John Parkinson and Craig Irving for insightful discussions into NMR techniques.

Special thanks go to all my lab colleagues, who have truly kept me going through the hard times. Knowing that “we’re all in this together” has been a huge source of comfort and a dance routine always makes things better! I am lucky to have been part of two generations of the Mulvey/Hevia/O’Hara contingent, and in no particular order, I would like to thank Ross, Matt, Liam, Gemma, Elaine, Zoe, Ben, Sharon, Emma, Sarah, Donna, Marina, Sylvia, Ana, Lewis, Marco, Sam, Andy, Laia, Stuart, Vicki, Jan, Thomas, Tobi, Markus, Antonio, Alberto, Javi, Chris and Janie-Anne for making the lab such an enjoyable place to work. I am incredibly thankful to have worked with so many wonderful people and these short acknowledgements cannot begin do justice to all their acts of kindness. Thank you for imparting your wisdom and experience, for making me laugh instead of tearing my hair out and for supplying the office with a steady stream of cakes. In particular, I would like to thank my glovebox counterparts, Ross and Sarah. A constant source of advice and amusement, Ross was full of novel ideas (3D noughts and crosses) and thought provoking questions (is an onion a vegetable?). Quite possibly the most considerate and patient person I know, Sarah has also been my partner in running and yoga, which has certainly helped me to keep my sanity during the writing of this thesis. I would like to thank every member of our lunchtime support group, which began with Zoe, Elaine, Ross and Vicki. Now in a new era, Donna, Emma, Marina, Andy and Sam regularly brighten up my lunch hour with their wit, anecdotes and support. I feel extremely grateful that I don’t just have colleagues at work, I have life-long friends.

I also owe thanks to Josh Trivett, a talented undergraduate student who made a significant contribution to the work presented in Chapter 5 and kept me entertained with stories of punching pigeons and how to survive a zombie apocalypse. An

enthusiastic final year student, Jemma Cowan had the misfortune to be mentored by me whilst I was ill with labyrinthitis and she bore this burden gracefully. Her wonderful baking helped me to keep going even when the world was spinning.

As a final note, just to quell the Mulvey myth that future students may hear...I'm really not that posh!

Abstract

One of the most important reactions in chemistry, metallation benefits society in general as it is utilised for the synthesis of many commodities used in daily life. While lithium-based monometallic compounds have long been the reagents of choice for metallation, bimetallic reagents are emerging as second generation metallating agents that can overcome many limitations of lithium reagents. This study extends “synergic” bimetallic chemistry focusing mainly on sodium, zinc and sodium zincate systems, investigating their syntheses, structures and reactions with organic substrates.

Probing the metallation of trifluoromethylbenzene, using ^tBuLi or ⁿBuNa activated by a donor (THF, TMEDA or PMDETA), established the metallation system dictated both regioselectivity and yield. The origin of the increased *ortho*-selectivity using sodium systems was uncovered through analysis of isolated metallated intermediates [(TMEDA)·Li(C₆H₄-CF₃)₂], **3**, [(TMEDA)·Na(C₆H₄-CF₃)₂], **4** and [(PMDETA)·Na(C₆H₄-CF₃)₂], **5**.

Since pyrrole is important within pharmaceuticals and zinc-pyrrole chemistry is remarkably underdeveloped, we have synthesised the first crystallographically-characterized zinc pyrrolyl complexes, with one, two, three or four pyrrole anions attached to zinc in [^tBuZn(NC₄H₄)(TMEDA)·HNC₄H₄], **7**; [Zn(NC₄H₄)₂(TMEDA)], **8**; [{"(THF)₂·NaZn(THF)(NC₄H₄)₃}_∞], **9**; [{"(TMEDA)·Na}₂Zn(NC₄H₄)₄], **10**; [{"(PMDETA)·Na}₂Zn(NC₄H₄)₄], **11**, as well as for comparison [{"(PMDETA)·Na(NC₄H₄)₂}, **12**.

Improving upon sub-ambient temperature protocols, ambient temperature zincation of *N*-Boc pyrrolidine was achieved *via* sodium zincate [(TMEDA)Na(μ-TMP)(μ-^tBu)Zn(^tBu)]. Metallated intermediate [(TMEDA)Na(TMP)(α-NC₄H₇NBoc)Zn(^tBu)] **13** was crystallographically characterised. Exploring the basicity of **13**, *in situ* side-reactions with toluene, ferrocene or anisole generated

[{(TMEDA)Na[OC(NC₄H₈)CHPh]}₂], **14**, [(TMEDA)(Boc-NC₄H₈)Na{(η²-C₅H₄)Fe(C₅H₅)Zn(^tBu)}₂], **16** and [(TMEDA)Na(μ-TMP)(μ-C₆H₄OMe)Zn(^tBu)], **17**, respectively.

Incorporating multifunctional 2,2'-dipyridylamide (dpa) into a bimetallic system produced neutral zinc, sodium and potassium zincates with unprecedented structures in [(dpa)Zn(^tBu)}₂]; **18**, [(TMEDA)₂Na₂(μ-dpa)₂Zn(^tBu)}₂]; **19**, [{Na(THF)₆}⁺{Zn(^tBu)₂(dpa)Zn(^tBu)₂}⁻]; **20**, [{K(THF)₆}⁺{Zn(^tBu)₂(dpa)Zn(^tBu)₂}⁻], **21**. Sodium zincates **19** and **20** *tert*-butylate benzophenone at the challenging *para*-position, whereas di-*tert*-butylzinc failed to react. Another difunctional amide, *N'*-benzyl-*N,N*-dimethylethylenediamide (BD) generated sodium zincate [(TMEDA)Na(μ-BD)(μ-^tBu)Zn(^tBu)], **25**, which successfully deprotonated both *N,N*-diisopropylbenzamide and anisole.

Publications

Publications in Peer Reviewed Journals

- [1] J. A. Garden, D. R. Armstrong, W. Clegg, J. García-Alvarez, E. Hevia, A. R. Kennedy, R. E. Mulvey, S. D. Robertson, L. Russo, Donor-Activated Lithiation and Sodiation of Trifluoromethylbenzene: Structural, Spectroscopic and Theoretical Insights, *Organometallics*, **2013**, 32, 5481.
- [2] D. R. Armstrong, J. A. Garden, A. R. Kennedy, S. M. Leenhouts, R. E. Mulvey, P. O’Keefe, C. T. O’Hara, A. Steven, Evaluating *cis*-2,6-Dimethylpiperidide (*cis*-DMP) as a Base Component in Lithium-Mediated Zincation Chemistry, *Chemistry – A European Journal*, **2013**, 19, 13492.
- [3] D. R. Armstrong, J. A. Garden, A. R. Kennedy, R. E. Mulvey, S. D. Robertson, Modifying Alkylzinc Chemistry with 2,2’-Dipyridylamide: Activation of *t*Bu-Zn Bonds Towards *Para*-Alkylation of Benzophenone, *Angewandte Chemie International Edition*, **2013**, 52, 7190.
- [4] L. Balloch, J. A. Garden, A. R. Kennedy, R. E. Mulvey, T. Rantanen, S. D. Robertson, V. Snieckus, Dizincation of a 2-Substituted Thiophene: Constructing a Novel Cage with a [16]crown-4 Zincocyclic Core, *Angewandte Chemie International Edition*, **2012**, 51, 6934. ***Hot Paper***
- [5] J. A. Garden, A. R. Kennedy, R. E. Mulvey, S. D. Robertson, Ambient Temperature Zincation of *N*-Boc Pyrrolidine and its Solvent Dependency, *Chemical Communications*, **2012**, 48, 5265.
- [6] J. A. Garden, A. R. Kennedy, R. E. Mulvey, S. D. Robertson, Neutral Zinc, Lower-Order Zincate and Higher-Order Zincate Derivatives of Pyrrole: Synthesis and Structural Characterisation of Zinc Complexes with One, Two, Three or Four Pyrrolyl Ligands, *Dalton Transactions*, **2011**, 40, 11945.

Conference Presentations (Oral)

- [7] J. A. Garden, A. R. Kennedy, R. E. Mulvey, S. D. Robertson, Co-op Bimetallics: New Zincate Chemistry, *Universities of Scotland Inorganic Conference (USIC-46)*, University of St Andrews, St Andrews, **2012**.
- [8] J. A. Garden, R. E. Mulvey, Synergic Stabilization of Sensitive Anions by a Sodium-Zinc Reagent: Applications to *N*-Boc Pyrrolidine Chemistry, *University of Strathclyde Inorganic Section Meeting*, West Brewery, Glasgow, **2012**.
- [9] J. A. Garden, R. E. Mulvey, Synergic Stabilization of Sensitive Anions by a Sodium-Zinc Reagent: Applications to *N*-Boc Pyrrolidine Chemistry, *243rd American Chemical Society National Meeting*, San Diego, USA, Abstract INOR 1198, **2012**.

Conference Presentations (Poster)

- [10] J. A. Garden, D. R. Armstrong, A. R. Kennedy, R. E. Mulvey, S. D. Robertson, Modifying Alkylzinc Reactivity with 2,2'-Dipyridylamide: Activation of *t*Bu-Zn Bonds for *para*-Alkylation of Benzophenone, *Universities of Scotland Inorganic Conference (USIC-47)*, University of Edinburgh, Edinburgh, **2013**.
- [11] R. E. Mulvey, J. A. Garden, A. R. Kennedy, S. D. Robertson, Fixing a Zinc Functional Handle on Pyrrole, *Universities of Scotland Inorganic Conference (USIC-45)*, University of Glasgow, Glasgow, **2011**.
- [12] R. E. Mulvey, J. A. Garden, A. R. Kennedy, S. D. Robertson, Fixing a Zinc Functional Handle on Pyrrole, *Annual Meeting of the Main Group Chemistry Specialist Interest Group*, Royal Society of Chemistry, Burlington House, London, **2011**.

Abbreviations

AMMM	Alkali-Metal-Mediated Metallation
AMMZn	Alkali-Metal-Mediated Zincation
BD	<i>N'</i> -benzyl- <i>N,N</i> -dimethylethylenediamide
BD(H)	<i>N'</i> -benzyl- <i>N,N</i> -dimethylethylenediamine
Boc	<i>tert</i> -butyloxycarbonyl
ⁿBu	<i>n</i> -butyl
ⁿBuLi	<i>n</i> -butyllithium
ⁿBuNa	<i>n</i> -butylsodium
^sBu	<i>s</i> -butyl
^tBu	<i>tert</i> -butyl
^tBuLi	<i>tert</i> -butyllithium
Bz	benzyl
CCDB	Cambridge Crystallographic Database
CIDNP	Chemically Induced Dynamic Nuclear Polarization
CIPE	Complex Induced Proximity Effect
COSY	Correlation Spectroscopy
Cy	cyclohexyl
DA	diisopropylamide
DA(H)	diisopropylamine
DIBA	diisobutylamide
DMAP	4-dimethylaminopyridine
DME	dimethoxyethane
DMP	<i>cis</i> -2,6-dimethylpiperidide
dpa	2,2'-dipyridylamide
dpa(H)	2,2'-dipyridylamine
DFT	Density Functional Theory
DMG	Directing Metallating Group
DoM	Directed <i>ortho</i> -Metallation
DOSY	Diffusion Ordered Spectroscopy

ESR	Electron Spin Resonance
Et	ethyl
EXSY	Exchange Spectroscopy
H₆-TREN	[<i>N</i> ^o , <i>N</i> ^o -bis(2-aminoethyl)ethane-1,2-diamine]
HMPA	hexamethylphosphoric triamide
HMDS	1,1,1,3,3,3-hexamethyldisilazide
HMDS(H)	1,1,1,3,3,3-hexamethyldisilazane
HSQC	Heteronuclear Single Quantum Correlation
LDA	lithium diisopropylamide
LIC-KOR	alkyllithium/potassium alkoxide Superbase
Me	methyl
Me₆-TREN	tris[2-(dimethylamino)ethyl]amine
NaTMP	sodium 2,2,6,6-tetramethylpiperidide
NOESY	Nuclear Overhauser Effect Spectroscopy
NMR	Nuclear Magnetic Resonance
PEPSSI	Pyridine-Enhanced Pre-catalyst Preparation Stabilisation and Initiation
Ph	phenyl
PMDETA	<i>N,N,N</i> ^o , <i>N</i> ^o , <i>N</i> ^o '-pentamethylethylenediamine
ppm	parts per million
ⁱPr	<i>iso</i> -propyl
ROESY	Rotating Frame Overhauser Effect Spectroscopy
TEMPO	2,2,6,6,-tetramethyl-1-piperidinyloxy
THF	tetrahydrofuran
TMCDA	<i>N,N,N</i> ^o , <i>N</i> ^o -tetramethylcyclohexane-1,2-diamine
TMDAE	tetramethyldiaminoether [bis{2-(<i>N,N</i> -dimethylamino)ethyl}ether]
TMEDA	<i>N,N,N</i> ^o , <i>N</i> ^o -tetramethylethylenediamine
TMP	2,2,6,6-tetramethylpiperidide
TMP(H)	2,2,6,6-tetramethylpiperidine
TriMEDA	<i>N,N,N</i> ^o -trimethylethylenediamine

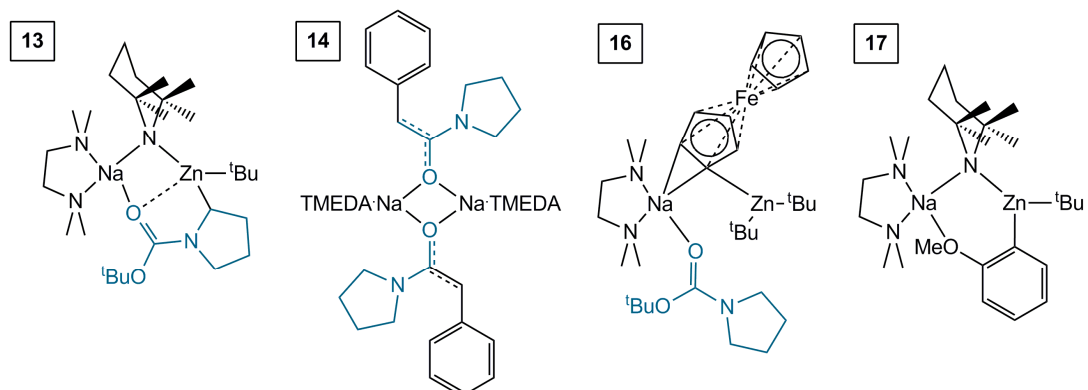
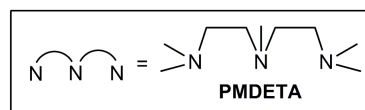
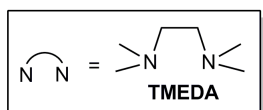
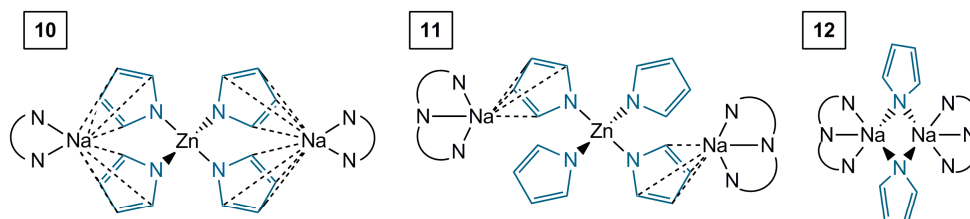
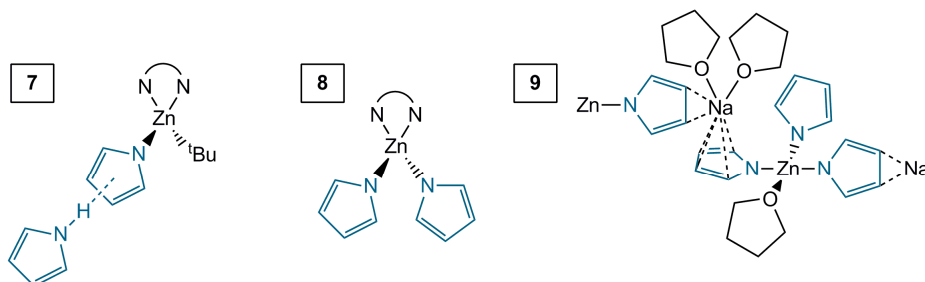
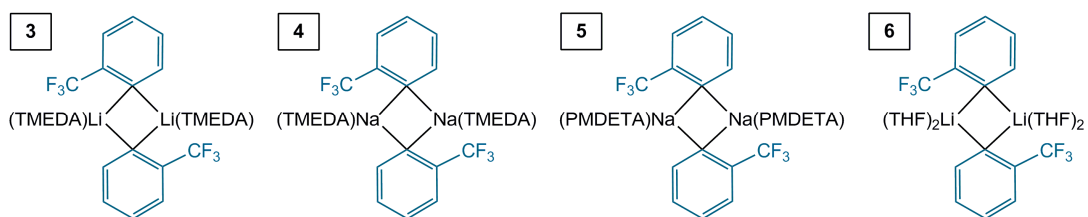
List of Numbered Compounds

- 1 [(TMEDA)Na(μ -TMP)(μ -^tBu)Zn(^tBu)]
- 2 C₆H₅CF₃
- 3 [(TMEDA)·Li(C₆H₄-CF₃)]₂
- 4 [(TMEDA)·Na(C₆H₄-CF₃)]₂
- 5 [(PMDETA)·Na(C₆H₄-CF₃)]₂
- 6 [(THF)₂·Li(C₆H₄-CF₃)]₂
- 7 [^tBuZn(NC₄H₄)(TMEDA)·HNC₄H₄]
- 8 [Zn(NC₄H₄)₂(TMEDA)]
- 9 [{(THF)₂·NaZn(THF)(NC₄H₄)₃}_∞]
- 10 [{(TMEDA)·Na}₂Zn(NC₄H₄)₄]
- 11 [{(PMDETA)·Na}₂Zn(NC₄H₄)₄]
- 12 [{(PMDETA)·Na(NC₄H₄)₂}]
- 13 [(TMEDA)Na(TMP)(α -NC₄H₇NBoc)Zn(^tBu)]
- 14 [{(TMEDA)Na[OC(NC₄H₈)CHPh]}₂]
- 15 [(TMEDA)Na(μ -TMP)(μ -Me)Zn(Me)]
- 16 [(TMEDA)(Boc-NC₄H₈)Na{(η ²-C₅H₄)Fe(C₅H₅)}Zn(^tBu)₂]
- 17 [(TMEDA)Na(μ -TMP)(μ -C₆H₄OMe)Zn(^tBu)]
- 18 [{(dpa)Zn(^tBu)}₂]
- 19 [(TMEDA)₂Na₂(μ -dpa)₂Zn(^tBu)₂]
- 20 [{Na(THF)₆}⁺{Zn(^tBu)₂(dpa)Zn(^tBu)₂}⁻]
- 21 [{K(THF)₆}⁺{Zn(^tBu)₂(dpa)Zn(^tBu)₂}⁻]
- 22 [(PMDETA)Na(dpa)]₂
- 23 [(TMDAE)Na(dpa)]₂
- 24 [(H₆-TREN)Na(dpa)]
- 25 [(TMEDA)Na(μ -BD)(μ -^tBu)Zn(^tBu)]
- 26 “NaZn(BD)(^tBu)₂”
- 27 [{(BD)Zn(^tBu)}₂]
- 28 C₆H₅C(O)NⁱPr₂
- 29 2-IC₆H₄C(O)NⁱPr₂

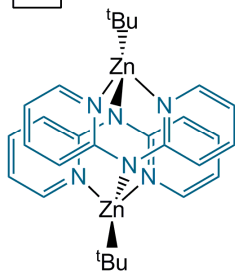
30 $2\text{-IC}_6\text{H}_4\text{C(O)H}$

31 $\text{C}_6\text{H}_5\text{C(O)H}$

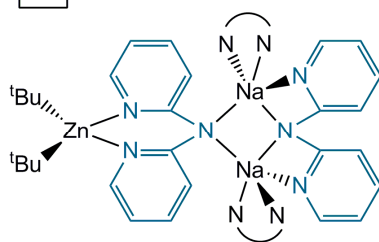
Compounds Prepared Within This Thesis



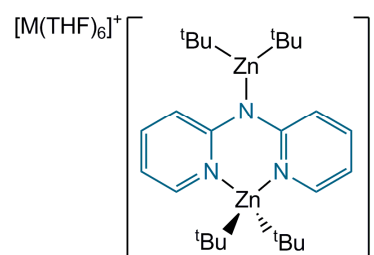
18



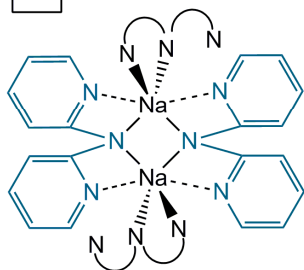
19



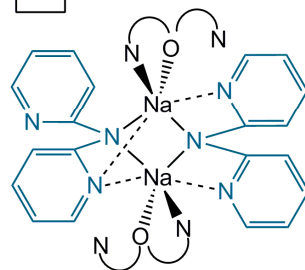
20 M = Na, 21 M = K



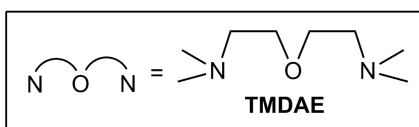
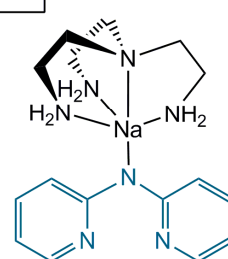
22



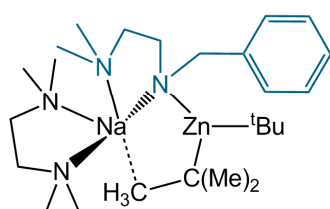
23



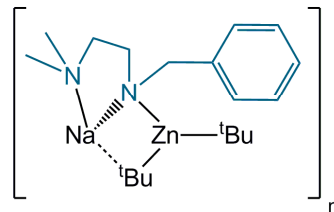
24



25



26



27

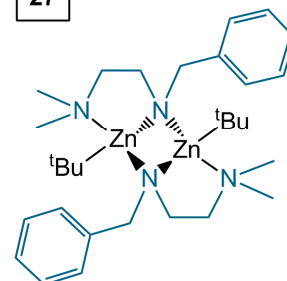


Table of Contents

Acknowledgements	iii
Abstract	vi
Publications	viii
Abbreviations	x
List of Numbered Compounds	xii
Compounds Prepared Within This Thesis	xiv
Table of Contents	xvi

1. An Introduction to C-H Bond Cleavage within Organometallic Chemistry **1**

1.1 A Brief Overview of C-H Bond Cleavage by Metallation	2
1.2 Conventional Metallation Reagents: A General Overview	3
1.3 Organoalkali Metal Reagents	5
1.4 Structure and Reactivity of Organolithium Reagents	7
1.5 Applications of Organolithium Reagents in Metallation Chemistry	13
1.5.1 Deprotonative Metallation	13
1.5.2 Metal Halogen Exchange	16
1.5.3 Reductive Lithiation	20
1.6 The LiCl Salt Effect	22
1.7 Grignard Reagents and their Turbo-Grignard Modifications	23
1.8 Organozinc Reagents: A Historical Perspective	26
1.9 Applications of Zinc Reagents	27
1.9.1 Reformatsky Reaction	28
1.9.2 Negishi Cross-Coupling Reaction	29
1.9.3 Simmons-Smith Cyclopropanation	30
1.9.4 Copolymerisation of Carbon Dioxide and Epoxides	30
1.9.5 Ring Opening Polymerisation	32
1.9.6 Zinc Alkoxides and Zinc Alkylperoxides: Epoxidation of Enones	32
1.9.7 Radical Addition Reactions Initiated by R ₂ Zn/O ₂ Systems	34
1.9.8 Hydroamination Reactions	35
1.10 Zinc-Zinc Bonding	36
1.11 Benefits and Shortcomings of Monometallic Reagents	38
1.12 A General Overview of Heterobimetallic Chemistry	39
1.13 Mixed Alkali Metal Mixed Ligand Compositions	41
1.14 Alkali-Metal-Mediated Metallations	42
1.15 Aims of the PhD Research Project	51

2. Lewis Base-Activated Lithiation and Sodiation of Trifluoromethylbenzene: Structural, Spectroscopic and Theoretical Insights **53**

2.1 Summary	54
2.2 Introduction	55
2.2.1 Directed <i>ortho</i> -Metallation: A Powerful Synthetic Tool	55
2.2.2 Background to the Metallation of Trifluoromethylbenzene	56
2.3 Results and Discussion	58
2.3.1 Alkali metallation of trifluoromethylbenzene	58
2.3.2 Solid State Molecular Structures	59
2.3.3 Solution NMR Spectroscopic Studies	65
2.3.4 DFT Computational Studies	70
2.3.5 Post-metallation NMR Spectroscopic Analysis: Electrophilic Quenching Studies with Iodine	73

2.4 Conclusions	76
2.5 Future Work	77
2.6 Experimental	79
3. Neutral Zinc, Lower-Order Zincate and Higher-Order Zincate Derivatives of Pyrrole: Synthesis and Structural Characterisation of Zinc Complexes with One, Two, Three or Four Pyrrolyl Ligands	84
3.1 Summary	85
3.2 Introduction	86
3.3 Results and Discussion	88
3.3.1 Synthesis and Solid State Characterisation of Neutral Zinc Pyrrolyl Formulations	89
3.3.2 Synthesis and Solid State Characterisation of Lower- and Higher-Order Sodium Zincates	94
3.3.3 Synthesis and Solid State Characterisation of a Sodiopyrrole Species	101
3.3.4 Solution NMR Spectroscopic Studies	103
3.4 Concluding Remarks on Metal Derivatives of Pyrrole	106
3.5 Future Work	106
3.6 Experimental	109
4. Ambient Temperature Zincation of <i>N</i>-Boc Pyrrolidine: Synthesis, Structure and Reactivity of a Sodium Pyrrolidide-Zincate Reagent	114
4.1 Summary	115
4.2 Introduction to Achieving the α -sp ³ Functionalisation of Pyrrolidine	115
4.3 Results and Discussion	117
4.3.1 The Quest for Ambient Temperature Metallation	117
4.3.2 Uncovering the Solvent Dependency of the Reaction	121
4.3.3 Examining the Alkyl Analogue: Reactivity Studies of the Related Sodium Methyl Zincate	126
4.3.4 Exploring the Scope of the Methodology: Reactivity towards Alternative Aromatic Substrates	127
4.4 Concluding Remarks on the Synergic Metallation of <i>N</i> -Boc Pyrrolidine	133
4.5 Future Work	134
4.6 Experimental	134
5. Modifying Alkylzinc Chemistry with 2, 2'-Dipyridylamide: Activation of ^tBu-Zn Bonds Towards Para-Alkylation of Benzophenone	142
5.1 Summary	143
5.2 Introduction to Polar Metal Amides	144
5.3 Results and Discussion	146
5.3.1 Synthesis and Characterisation of Alkylzinc and Alkali Metal Zincate Compounds with Unprecedented Structural Motifs	146
5.3.2 Reactivity Studies: Initial Investigation into the Alkylation of Benzophenone	155
5.3.3 Extending the Scope of Synergic Alkali-Metal Zinc Mediated Alkylation Chemistry	157
5.3.4 Modification of the Donor Ligand: Synthesis of a Series of Sodium Dipyridylamide Metalloligands	158
5.3.5 Structural Insights into Sodium Dipyridylamides 22-24	159
5.3.6 Solution State Characterisation of Sodium Amides 22-24	167
5.3.7 Evaluating the Formation of a Bimetallic Sodium-Zinc Product upon Co-Complexation of ^t Bu ₂ Zn with Sodium Amides 22, 23 or 24	169
5.3.8 Reactivity Studies: Investigating the Outcome of Varying the Lewis Donor upon the Alkylation of Benzophenone	172
5.3.9 Evaluating the Reaction Dependency of the Alkali Metal	175

5.3.10 Exploring the Reaction Dependency on the Solvent	176
5.3.11 Evaluating the Effect of Substituting ${}^t\text{Bu}_2\text{Zn}$ by ${}^t\text{BuLi}$ as the <i>tert</i> -Butyl Source	178
5.3.12 Evaluating the Addition of TEMPO to the Reaction System	179
5.3.13 Mechanistic Insights	179
5.4 Concluding Remarks on Dipyrildylamine Chemistry	182
5.5 Future Work	182
5.6 Experimental	184
6. Cooperative Bimetallics: Synthesis, Characterisation and Reactivity Studies of a New Sodium Zincate Derived from a Difunctional Amine	195
6.1 Summary	196
6.2 Introduction	196
6.2.1 It Takes Two: Advantages of Cooperative Bimetallic Bases	196
6.2.2 Introduction of a Donor Appended Amine to Sodium Zincate Chemistry	198
6.3 Results and Discussion	200
6.3.1 Incorporation of a Donor Appended Amine into a Sodium Zincate Framework: Synthesis and Characterisation	200
6.3.2 Mechanistic Insights: The Two-step Mechanism	205
6.3.3 Transamination Reactions within Sodium Zincate Chemistry	207
6.3.4 Sodium Amidozincates and their Disproportionation Tendency	208
6.3.5 In the Absence of TMEDA: Synthesis and Characterisation of a Neutral Alkylzinc Amide	212
6.3.6 Reactivity Studies: Metallation of <i>N,N</i> -diisopropylbenzamide	217
6.4 Conclusions	224
6.5 Future Work	225
6.6 Experimental	226
7. The Outlook for Organometallic Chemistry: Past, Present and Future	231
8. General Experimental Techniques	236
8.1 Schlenk Techniques	237
8.2 Glove Box	238
8.3 Solvent Purification	239
8.4 NMR Solvent Purification	240
8.5 Purification of Hydroscopic Liquids	240
8.6 Commercial Reagents Used	241
8.7 Standardisation of Organolithium Reagents	241
8.8 Preparation of Common Starting Materials	242
8.8.1 Preparation and Isolation of ${}^n\text{BuNa}$	242
8.8.2 Preparation and Isolation of ${}^t\text{Bu}_2\text{Zn}$	243
8.9 Instrumentation for Characterisational Procedures	244
8.9.1 Nuclear Magnetic Resonance (NMR) Spectroscopy	244
8.9.2 Elemental Microanalysis	245
8.10 X-Ray Diffraction Studies	245
9. Bibliography	246

Chapter 1

An Introduction to C-H Bond Cleavage within Organometallic Chemistry

“The most exciting phrase to hear in science,
the one that heralds new discoveries,
is not ‘Eureka!’ but ‘That’s funny...’”

Isaac Asimov

American biochemist and author

1.1 A Brief Overview of C-H Bond Cleavage by Metallation

Opening up a pathway to forming new compounds in fine chemical synthesis, C-H bond cleavage or deprotonation is defined within organometallic chemistry as the conversion of a C-H bond to a reactivity enhanced $C^{\delta-}$ -metal $^{\delta+}$ (often C-lithium) bond.^[1] This enhanced reactivity makes it possible to then convert the C-metal bond to other C-C or C-X bonds using compatible tandem bond forming strategies. Frequently exploited in the conversion of inert C-H bonds to other functional groups, C-H bond cleavage plays a pivotal role within the synthesis of many commodity chemicals, such as Zocor (used to lower cholesterol)^[2] and Trileptal (used in the treatment of epilepsy).^[3] Furthermore, in a climate where valuable petrochemical feedstocks are rapidly diminishing, their replacement by less expensive, more abundant alkanes would be highly desirable. Thus the ability to convert alkanes into more useful products through C-H bond activation is greatly sought-after, though at present it has not been realised. As highlighted in a recent roundtable discussion between a panel of organometallic experts, C-H bond cleavage is a therefore topical area of interest.^[4] Economical, environmental and social factors are driving the quest for improved metallation reactions which are atom economical, fast, cost efficient and can be performed safely under environmentally benign reaction conditions.

Long established conventional metallation procedures, which typically are the domain of organolithium reagents (alkyls or amides), tend to fall short of these desired properties. For example, the ferocious reactivity of organolithium reagents often necessitates expensive, energy wasteful cryogenic cooling systems, in order to prevent decomposition of sensitive functional groups or side reactions with solvents. Furthermore, restricted regioselectivity and the use of expensive, toxic solvents provide further limitations.

Recent advances have been made using bimetallic reagents, where two metals contained within the same molecular environment can work together to achieve reactivities and selectivities that more often or not are inaccessible to either monometallic component. This chemistry, which can be considered synergic in

origin, has associated benefits. For example, increased functional group tolerance enables reactions to be performed at ambient temperature, avoiding expensive cryogenic cooling systems. Furthermore, bimetallic reagents have often led to “synergic surprises”, achieving unprecedented regioselectivities.

As the extension of monometallic and bimetallic deprotonation strategies forms the central pillar of this PhD study, this introduction aims to give an overview of metallation agents currently employed within C-H bond cleavage. Firstly, conventional monometallic reagents shall be discussed, with emphasis on organolithium, organomagnesium and organozinc reagents. Secondly, the application of bimetallic bases towards the metallation of organic substrates shall be reviewed.

1.2 Conventional Metallation Reagents: A General Overview

The advent of s-block metallation chemistry has had a global impact upon chemistry, where metallation refers to the conversion of a relatively inert, non-polar carbon-hydrogen bond into a more polar, hence more reactive carbon-metal bond. Such metal-hydrogen exchange reactions are of great importance as they precede and enable carbon-carbon or carbon-heteroatom bond forming reactions. Therefore, metallation enables synthetic chemists to construct sophisticated molecular architectures. S-block organometallic reagents, especially those containing an alkali metal, have proven their worth in this field as strong Brønsted bases with the capability to perform selective deprotonation of organic substrates. Possibly the most famous of the pioneers of s-block chemistry is the Nobel laureate Victor Grignard, best known for his development of Grignard reagents with the general (although simplistic) formula “RMgX”.^[5] These reagents still carry his name more than a century after their initial discovery.

The German scientist Wilhelm Schlenk is perhaps most commonly associated with the innovative glassware, apparatus and experimental techniques he designed for the

synthesis and manipulation of pyrophoric chemicals.^[6] This development has facilitated rapid expansion of the field of reagent organometallic chemistry, enabling highly reactive materials to be handled safely without decomposition through reaction with oxygen or water. In addition, Schlenk is regarded by many as the father of organolithium chemistry. He reported the revolutionary synthesis of organolithium reagents in 1917, observing that:

“...the numerous yellow-glowing sparks thrown out by the red flame make the burning of methyllithium a magnificent sight”.^[7]

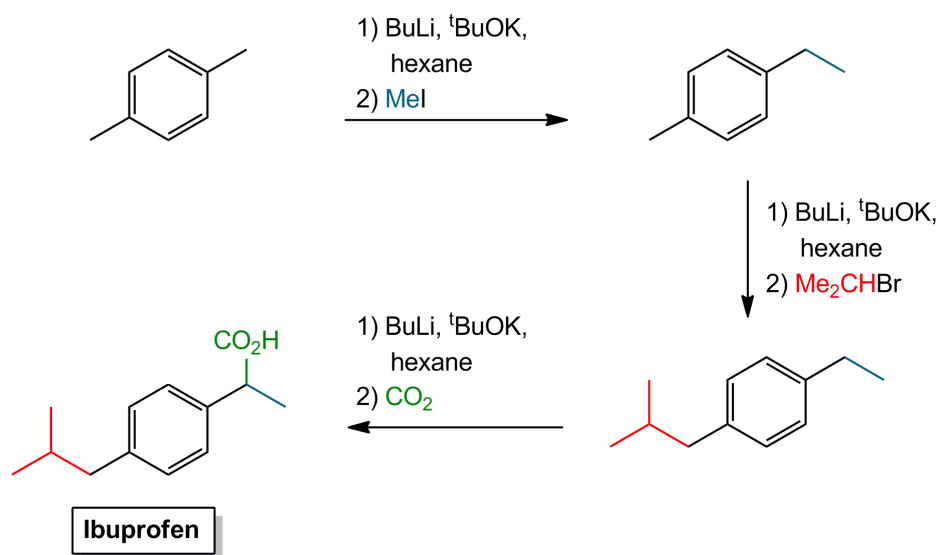
For this reason, Mulvey has recently suggested that organolithium reagents should be referred to as Schlenk reagents.^[8] Schlenk received a Nobel Prize nomination for this ground-breaking research, although the true significance of organolithium reagents was not realized at the time of their initial discovery. These reagents have since shot to stardom within the synthesis of commercial commodities including pharmaceuticals,^[9] agrochemicals,^[10] biochemicals,^[11] dyes,^[12] perfumes^[13] and electronic materials.^[14] Moreover, lithium batteries represent a major application of lithium chemistry.^[15] The usefulness of organolithium reagents within the chemical industry was recently highlighted in a survey compiled by Hans Reich, a world authority in organolithium chemistry. This survey revealed lithium diisopropylamide (LDA) to be the most frequently utilized organometallic reagent within the wide range of total syntheses investigated.^[16] Reflecting the high industrial demand for lithium reagents, FMC, the second largest world supplier of lithium chemicals behind Rockwood Lithium, initiated a 30% capacity expansion in Argentina in 2010.^[17]

1.3 Organoalkali Metal Reagents

Simple organometallic reagents based upon the group 1 metals bear the general formula $[RM\cdot(\text{donor})_x]_n$, where R is any organic fragment, M is an alkali metal (typically Li, Na or K), x represents the number of donor ligands per metal centre and n gives the aggregation state of the structure. As different metals, different organic fragments and different donor ligands can be mixed within the same compound, this general formula does not cover every such compound. These useful reagents owe their remarkably reactive nature to their electron deficient structures and highly polar, reactive, $R^{\delta-}-M^{\delta+}$ bonds. The electronegative R functionalities have the capacity to function as a source of carbanions, formally R^- . Upon descending group 1, the increased atomic radius,^[18] in conjunction with greater electronegativity differences between the alkali metal and the organic fragment, gives longer, weaker and more polarised bonds,^[19] thus stronger deprotonation reagents. Henceforth, organopotassium reagents generally exhibit a greater reactivity than their organosodium and organolithium analogues. Reflecting this, both alkylsodium and alkylpotassium reagents can achieve the deprotonation of benzene. In contrast, alkyllithium reagents can only do so when their reactivity is boosted by the presence of a donor ligand such as TMEDA (where TMEDA is *N,N,N',N'*-tetramethylethylenediamine).^[20] In spite of this, organolithium reagents are the most commonly encountered in industry, largely thanks to their solubility in both ethereal and hydrocarbon solvents.

Furthermore, alkali metal dialkylamides have a long track record as excellent deprotonation reagents.^[21] For instance, M-TMP reagents (M = Li, Na, K) can be employed as powerful Brønsted bases to selectively deprotonate organic substrates.^[22] Advantageously the absence of β -hydrogen atoms within TMP averts the potentially problematic side reaction of β -hydride elimination. Although M-TMP reagents are less reactive than their rival alkali metal-alkyl (M-C) counterparts, they provide other benefits such as reduced nucleophilicity (leading to fewer side-reactions) and greater solubility in hydrocarbon solvents.^[23]

Known for almost a century, organolithium reagents have for the past forty or so years been an indispensable component of the synthetic chemist's toolbox.^[24] As an exemplar, organolithium reagents are used in each of the three sequential stages in one synthesis of Ibuprofen (Scheme 1.1),^[25] whereas the original synthetic method patented by Boots requires six steps.^[26] Firstly, the mixed alkali metal base ⁿBuLi/^tBuOK executes the lateral deprotonation of *para*-xylene. Performing a methyl iodide quench subsequently converts the metallated methyl derivative to an ethyl group. Upon addition of a second equivalent of the mixed-metal base, followed by quenching with 2-bromopropane, the second methyl group is transformed to an *iso*-butyl group. Ibuprofen is ultimately generated through a final deprotonation followed by a carbon dioxide quench.



Scheme 1.1 One-pot synthesis of Ibuprofen, employing three sequential deprotonation-lithiation steps.

Further demonstrating their versatility and usefulness in synthesis, organolithium reagents also have applications as initiators in polymerisation reactions, thus are used in the synthesis of rubber and plastics.^[27] The demand for organolithium reagents shows no signs of diminishing, as the chemical company FMC recently opened butyllithium plants in Hyderabad, India and Zhangjiagang, China, to meet the growing industrial requirements for pharmaceuticals in the emerging Asian market.

1.4 Structure and Reactivity of Organolithium Reagents

Originally discovered in Stockholm, Sweden, lithium derives its name from the Greek word “lithos”, meaning “stone”, as it is found naturally as a mineral ore. Organolithium reagents are highly reactive species, owing largely to their electron deficient structures and their polar, reactive metal-carbon bonds.^[24d] In hydrocarbon solvents, organolithium species have a tendency to form aggregates, which attenuates their reactivity through steric shielding of the reactive carbanion. The aggregation state of an organolithium reagent depends on the nature of the organic functional group, R, the solvent, and the presence or absence of a co-ligand, such as TMEDA.

X-ray crystallographic characterisation of organolithium reagents remained a challenge well into the 20th century, with their extreme air- and moisture-sensitive nature (some are even pyrophoric) providing a major hurdle to overcome. However, in 1963, Dietrich reported the structural elucidation of ethyllithium by X-ray crystallography, a landmark event within organolithium chemistry.^[28] Distinguished as solvent free tetrameric aggregates, four Li(C₂H₅) units combine together to form a {C₄Li₄} heterocubane scaffold. Years later, in 1993, the solid state structures of *n*-butyllithium (Figure 1.1) and *t*-butyllithium (Figure 1.2) were revealed,^[29] as made possible through the advent of custom-built crystallographic apparatus designed by Stalke.^[30] Although structures in solution are often more complicated than those in the solid state, revelation of the molecular structures of *n*-butyllithium (ⁿBuLi), *t*-butyllithium (^tBuLi) and methyllithium (MeLi)^[31] in the solid state sheds light upon the corresponding differences in reactivity.

The molecular structures of ⁿBuLi and ^tBuLi were discovered to be discrete, electron deficient aggregates. In the hexameric structure of ⁿBuLi (Figure 1.1), six Li centres adopt a distorted octahedral conformation, with six long Li···Li separations (average length 2.939 Å) and six short Li···Li separations (average length 2.429 Å).^[29] This arrangement creates eight triangular faces, six of which are asymmetrically capped by ⁿBu groups, with two short (average length 2.159 Å) and one long (average length

2.270 Å) Li-C_α interaction. An additional Li-C_β electrostatic interaction provides the Li centre with further steric protection.

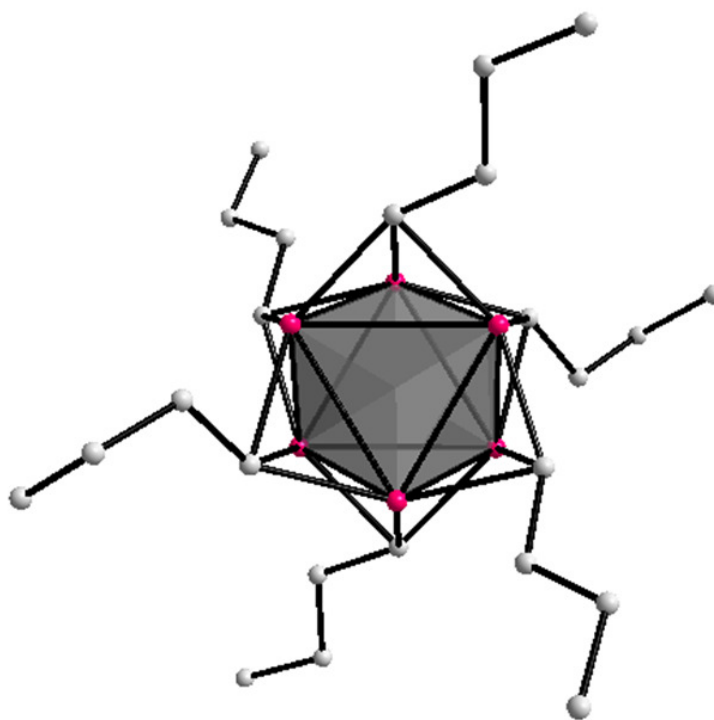


Figure 1.1 Molecular structure of [n-BuLi]₆, highlighting the hexameric “Li₆” core.^[29]

Two major factors influence the greater reactivity of ^tBuLi compared to ⁿBuLi. Firstly, the presence of two additional electron donating alkyl groups on the charge bearing carbon centre increases the anionic charge, enhancing the polarity of the M-C bond and so increasing the reactivity of the overall compound. Secondly, the greater steric bulk of the formal carbanion hinders aggregation, as the sterically encumbered *tert*-butyl ligands cannot pack so closely. Therefore, the solid state structure of donor free ^tBuLi is tetrameric, with interpenetrating Li₄ and C₄ tetrahedra (Figure 1.2).^[29] Four Li centres combine into one tetrahedron, where each triangular Li₃ face is capped with a *tert*-butyl unit, where the Li-C_α bond distance is 2.246 Å. Three methyl groups of the *tert*-butyl unit eclipse the three Li centres of the triangular face below, suggesting that additional Li-C_β interactions (average Li-C_β distance 2.374 Å) provide further stabilisation for the Li centres.

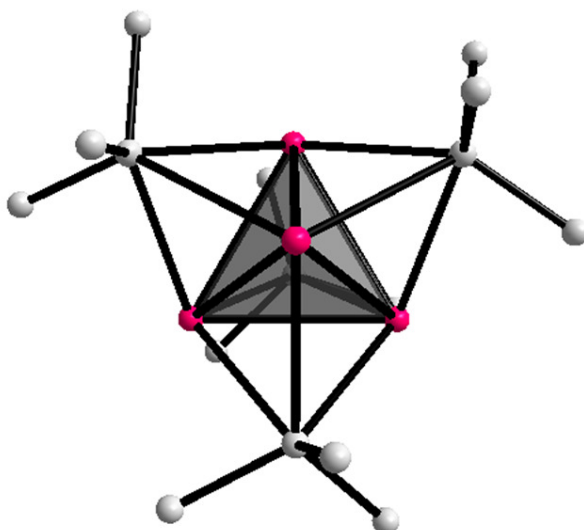


Figure 1.2 Molecular structure of electron deficient $[\text{t-BuLi}]_4$, highlighting the tetrameric “Li₄” core.^[29]

Analogous to t-BuLi , the simplest organolithium compound MeLi also adopts a distorted cubane arrangement.^[31] However, due to the reduced steric demands of the Me group, individual cubane units form a polymeric network through intermolecular agostic interactions, which diminishes the reactivity of MeLi in concentrated solutions. Unlike the majority of organolithium species, MeLi is insoluble in hydrocarbon media unless a donor solvent is present, an artefact of its three dimensional polymeric arrangement.

Structure and reactivity are intrinsically linked, and in the case of organolithium reagents the structure depends to a large extent on the aggregation state. The presence of an electron pair donor solvent can play a key role in the structure and hence reactivity of organoalkali metal reagents, through decreasing the aggregation state, as cation-anion aggregation bonds compete with cation-neutral donor dative bonds. This aids exposure of the reactive $\text{R}^{\delta-}$ component, and increases the kinetic mobility of the RLi unit which enhances reactivity and basicity. For example, the didentate donor TMEDA has long been exploited in enhancing the reactivity of alkali metal amides towards the deprotonation of aromatic substrates.^[32] However, this viewpoint may well be an oversimplification. Indeed, a thought-provoking review by

Collum suggests that strong solvation, increased reactivity and decreased aggregation often become a self-fulfilling prophecy, with the observation of two being taken as self-based evidence of the third.^[33] In reality organolithium chemistry is highly convoluted in the solution state. A mixture of aggregates and compounds are therefore anticipated, the relative proportions of which are influenced by temperature, solvent and concentration.

In contrast with the aggregated, hexameric structure adopted by ⁿBuLi in cyclohexane, smaller, more kinetically labile tetramers are formed in the presence of the monodentate donor solvent THF (where THF is tetrahydrofuran, Figure 1.3).^[34] Upon increasing the donor strength by moving to the difunctional amine TMEDA, two different solid state structures conforming to the general formula [ⁿBuLi]_x·(TMEDA)_y were discovered, where the nature of the prevalent structure formed depended on the relative stoichiometry of TMEDA and ⁿBuLi. When present in excess, TMEDA functions as a chelate donor, which decreases the aggregation state of ⁿBuLi through cleavage of the hexameric units into [ⁿBuLi]₂·(TMEDA)₂ dimers (Figure 1.4).^[34] Alternatively, sub-stoichiometric quantities of TMEDA insufficient to coordinate to every lithium centre gave a zig-zag shaped polymer of ⁿBuLi tetramers, [ⁿBuLi]₄·TMEDA]_∞, where only two of the four Li centres are solvated by TMEDA (Figure 1.5). Propagation of the polymeric chain occurs through monodentate, bridging Li-N(Me)₂CH₂CH₂(Me)₂N-Li, which each connect two ⁿBuLi tetrameric units.^[35] As perhaps would be expected, substitution of TMEDA with the isoelectronic oxygen donor DME (where DME is dimethoxyethane) gave a closely related polymeric structure, with a chain of tetrameric ⁿBuLi units linked by DME ligands.^[34]

Although other organolithium species are structurally recognised as monomers in the presence of tridentate donor PMDETA (where PMDETA is *N,N,N',N'',N''*-pentamethylethylenediamine), such as phenyllithium^[36] and trimethylsilylmethylithium,^[37] solid state crystallographic analysis of ⁿBuLi·PMDETA revealed it to possess the formula [ⁿBuLi]₂·PMDETA]₂ (Figure 1.6). This unusual looking aggregate was interpreted as consisting of a dimeric ⁿBuLi

core, stabilised by two terminal ${}^n\text{BuLi}\cdot\text{PMDETA}$ units.^[38] However, low temperatures proved necessary to prevent the lithiation of PMDETA by Brønsted basic ${}^n\text{BuLi}$, demonstrating one of the drawbacks of using such highly reactive organolithium reagents, especially in low aggregation states. Perhaps the best comparison for this alkyllithium species is provided by the lithium amide complex $[(\text{R}_2\text{NLi})_3\cdot\text{PMDETA}]_2$ (where R_2N represents the cyclic amide $\text{H}_8\text{C}_4\text{N}$, pyrrolidide).^[39] In contrast to the ${}^n\text{BuLi}$ complex, this lithium amide variant comprises a central ladder core with four $\text{R}_2\text{N-Li}$ rungs, potentially as a result of the reduced steric bulk associated with the “tied back” heterocyclic amide. However, similar to the ${}^n\text{BuLi}$ analogue, there are two terminal $\text{R}_2\text{N-Li}$ units which branch off from the central ladder framework. Each terminal lithium centre is stabilised through the dative coordination of a tridentate PMDETA ligand.

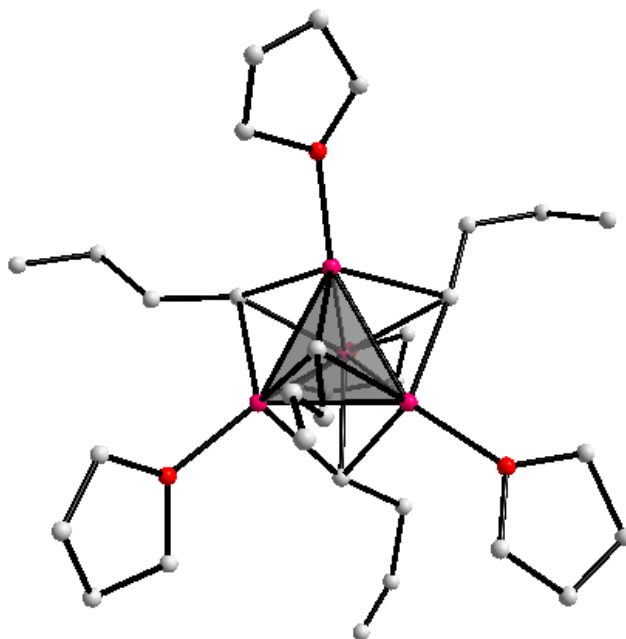


Figure 1.3 Molecular structure of THF solvated tetramers, $[\text{}^n\text{BuLi}\cdot\text{THF}]_4$, highlighting its tetrameric “ Li_4 ” core.^[34]

This trend of decreasing aggregation state upon moving to donor solvents of increased denticity is also found with trimethylsilylmethyl lithium. Similar to *n*-butyllithium, this silyl-substituted alkyllithium adopts a hexameric structure in the absence of a donor solvent.^[40] However, upon introduction of a didentate donor

molecule such as TMEDA or chiral (-)-sparteine, dimeric structures $[\text{LiCH}_2\text{SiMe}_3 \cdot \text{TMEDA}]_2$ and $[\text{LiCH}_2\text{SiMe}_3 \cdot (-)\text{-sparteine}]_2$ are formed in the solid state. Further increasing the steric bulk and donor atom capacity of the donor solvent, for example through the use of tridentate PMDETA, forces trimethylsilylmethyl lithium into a monomeric arrangement, $[\text{LiCH}_2\text{SiMe}_3 \cdot \text{PMDETA}]$, with a single Li-C bond.^[37]

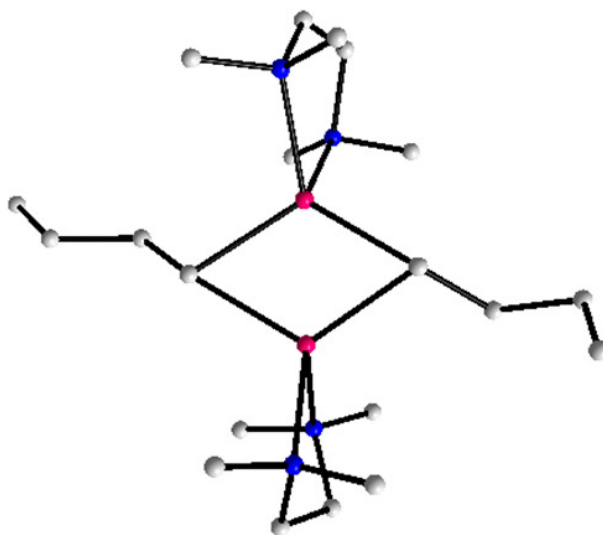


Figure 1.4 Molecular structure of the TMEDA solvated dimer, $[(^n\text{BuLi})_2 \cdot (\text{TMEDA})_2]$.^[34]

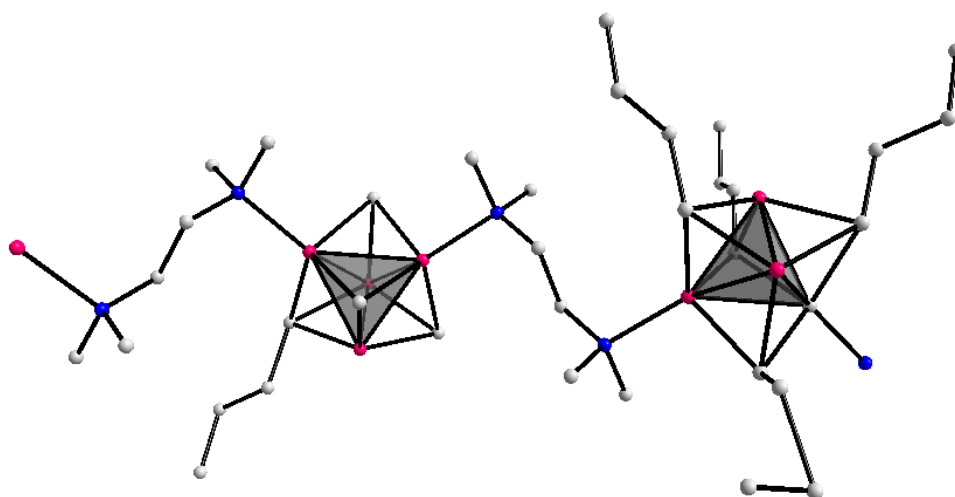


Figure 1.5 Polymeric structure of partially TMEDA solvated $\{^n\text{BuLi}\}_4$ tetramers, $[(^n\text{BuLi})_4 \cdot \text{TMEDA}]_{\infty}$.^[34-35]

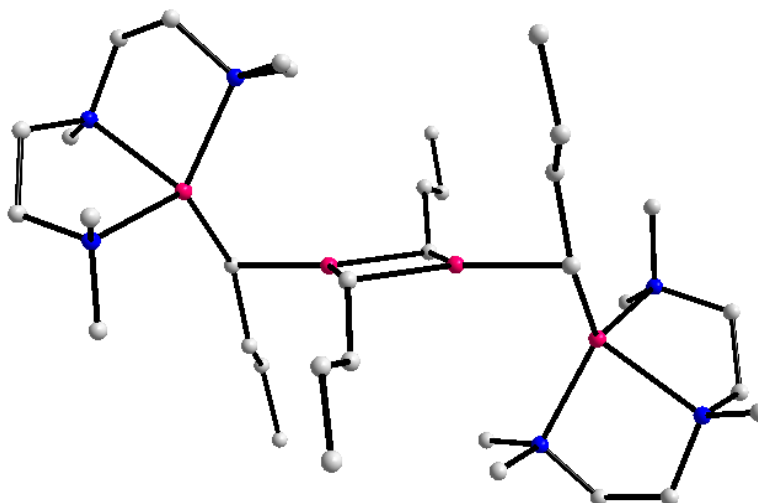


Figure 1.6 Molecular structure of the hemi PMDETA solvate $[\{^n\text{BuLi}\}_2 \cdot \text{PMDETA}]_2$.^[38]

1.5 Applications of Organolithium Reagents in Metallation Chemistry

In constant demand by the synthetic practitioner, organolithium reagents are one of the most widely used classes of organometallic reagents, rivalled only by Grignard reagents. These group 1 bases are typically synthesised by one of three principal methods: deprotonative metallation (including directed *ortho*-metallation, DoM), metal-halogen exchange, and reductive lithiation. This section aims to give a brief overview of each of these methods in turn.

1.5.1 Deprotonative Metallation

Deprotonative metallation was first recorded in 1908, when Schorigin obtained phenylsodium from the reaction of sodium metal with diethylzinc in benzene solvent.^[41] Over a century later, synthetic chemists frequently exploit directing metallating groups (DMGs) in the activation of a C-H site towards metal-hydrogen

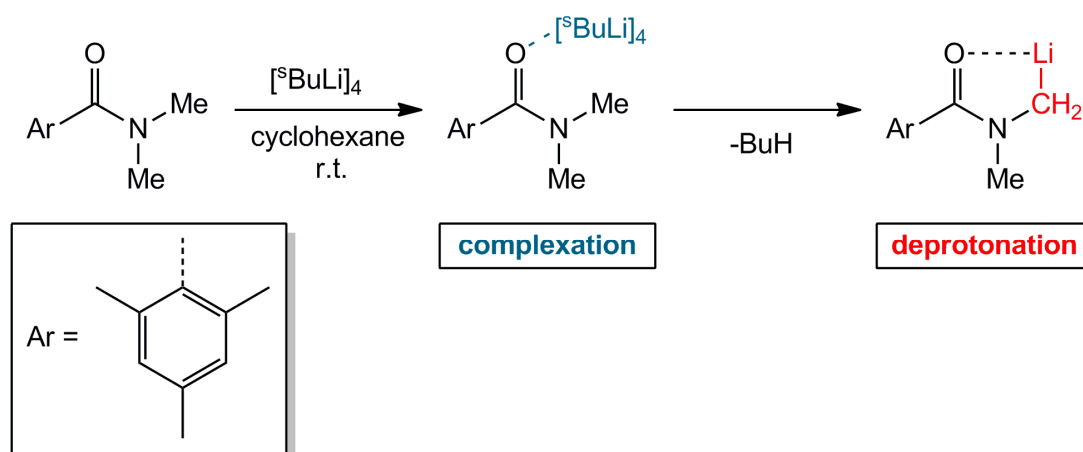
exchange. When selecting a DMG, it is of the utmost importance that the directing-substituent is not itself preferentially attacked by the strong nucleophilic organometallic base. If an attack does occur, it is stated that the base has a low functional group tolerance level.

At the simplest level, the rate of metallation is enhanced when a stabilised “carbanion” is formed. To this end, the presence of an electron withdrawing DMG aids metal-hydrogen exchange through the inductive acidification of a nearby hydrogen atom. Also, the greater the s orbital character of a hybridised carbon centre, the greater the stabilisation of the conjugate carbanion. Therefore, the metallation of alkane (or any sp^3 hybridised carbon) substrates generally presents a greater challenge than that of vinylic, aromatic (sp^2 hybridised) or alkyne (sp hybridised) substrates. Typically, the carbanions of vinylic and aromatic substrates can be further stabilised through resonance delocalisation. Those DMGs that involve an electron rich heteroatom (commonly N, O, or S) can also promote metallation by providing a Lewis basic coordination point for the incoming Lewis acidic organolithium base, a phenomenon which is commonly referred to as a complex induced proximity effect (CIPE).^[42]

An unsaturated heteroatomic ring such as thiophene therefore provides a prime candidate for α -metallation. The sulfur centre plays a dual role, as not only does it provide a Lewis basic coordination point for the CIPE, it also inductively acidifies the α -hydrogen atoms. In general, the higher the electronegativity of the heteroatom, the stronger the inductive effect, hence the more facile the deprotonation reaction. However, the first row elements (N, O and F) do not necessarily conform to this trend, as significant lone pair electronic repulsion between the heteroatom and the carbanion occurs. An artefact of their similar atomic radii, this electronic repulsion ultimately destabilises the metallated product.

Providing an example of a substituted arene bearing a strong DMG, the tertiary amide *N,N*-dimethyl-2,4,6-triisopropylbenzamide combines a Lewis donor coordination point ($C=O$), with inductive acidification of the NCH_3 hydrogens.

Investigation into the $^s\text{BuLi}$ executed deprotonation of this tertiary amide revealed that the rate of coordination far exceeds that of deprotonation (Scheme 1.2).^[43] Using stop-flow infrared spectroscopy, the reaction progress was followed through monitoring the carbonyl stretching frequency of the benzamide. Initially, a rapid decrease from 1650 cm^{-1} to 1625 cm^{-1} occurred, attributed to the Lewis basic amide forming a coordination complex with the Lewis acidic organolithium reagent. Over a longer time, a further decrease to 1588 cm^{-1} was observed, with deuterium quenching studies confirming that this species was the lithiated amide. Further developing this study, the reaction was repeated in the presence of the Lewis donor molecule TMEDA. As mentioned previously, it is often thought that TMEDA boosts the reactivity of an organolithium reagent through lowering its aggregation state. However, Beak and Smith suggest that within this benzamide system, TMEDA may promote $^s\text{BuLi}$ basicity by stabilising the metallated intermediate formed, through Lewis basic coordination to the Lewis acidic lithium centre.^[44]



Scheme 1.2 Complexation of $^s\text{BuLi}$ to N,N -dimethyl-2,4,6-triisopropylbenzamide, followed by α -lithiation.^[43]

Perhaps the most singularly important application of organolithium reagents is within DoM reactions. An invaluable process within the synthesis of commodity chemicals, chiefly in the pharmaceutical and agricultural industries, DoM is employed in the systematic synthesis of a multitude of substituted aromatic substrates.^[45] A functionalised aromatic substrate bearing a DMG is deprotonated in the *ortho*-

position by a strong organolithium base. This activates the resultant carbanion towards subsequent reaction with an electrophile, enabling regioselective functionalisation of the substrate.^[42] This process is discussed in more detail in Chapter 2.

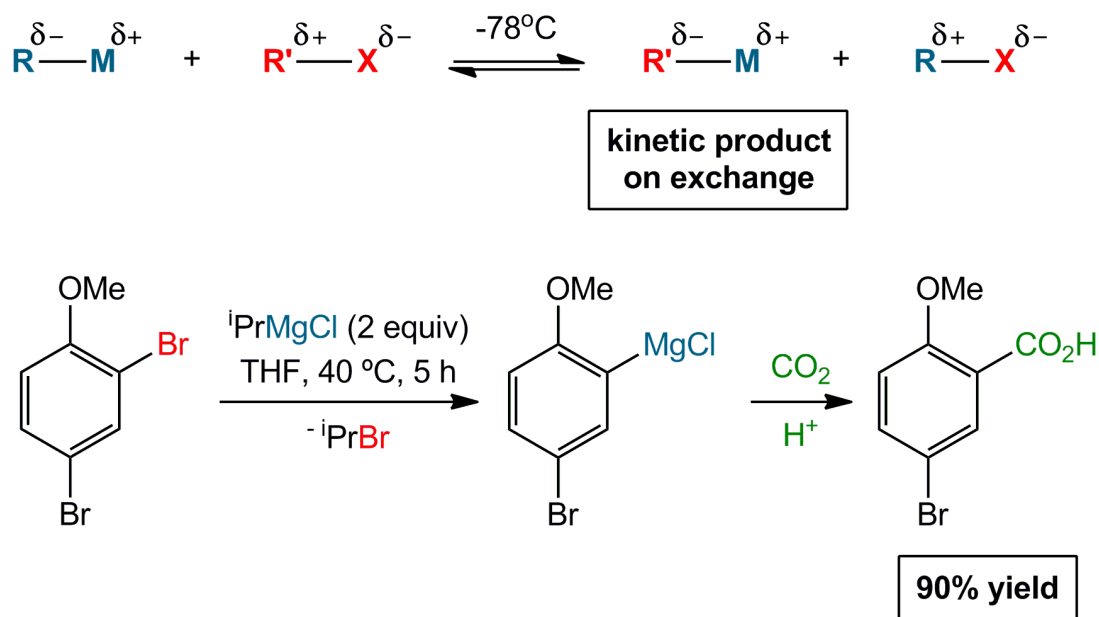
Within metallation (and in particular lithiation) chemistry, ethereal solvents including THF and ether are a popular choice, as they not only solubilise a whole host of organic substrates but also assist the deaggregation of organolithium reagents, which can enhance their reactivity. However, there are also several drawbacks associated with such solvents, namely their hygroscopic nature, the potential formation of explosive peroxides and their propensity to be attacked by organolithium reagents. Use of non-polar hydrocarbon solvents such as hexane overcomes these problems; however, such solvents present their own disadvantages. The major issue is the limited solubility of substrates and organolithium reagents. Indeed, the lack of a Lewis basic donor solvent means that the organolithium reagent will predominantly exist in its highest aggregation state.^[46]

Recent advances have shown that the solubility issues associated with non-polar solvents can be overcome through the addition of a Lewis donor, such as TMEDA or THF.^[32c; 46] Effectively, the presence of sub-stoichiometric quantities of a Lewis base catalyses the DoM reaction through aiding disaggregation of the organolithium reagent. This phenomenon has been termed “deficiency catalysis”. High yielding, atom economical DoM reactions can therefore be achieved in hydrocarbon solvents, providing the synthetic chemist with a safe, sustainable, green methodology as an alternative to using polar, ethereal solvents.

1.5.2 Metal Halogen Exchange

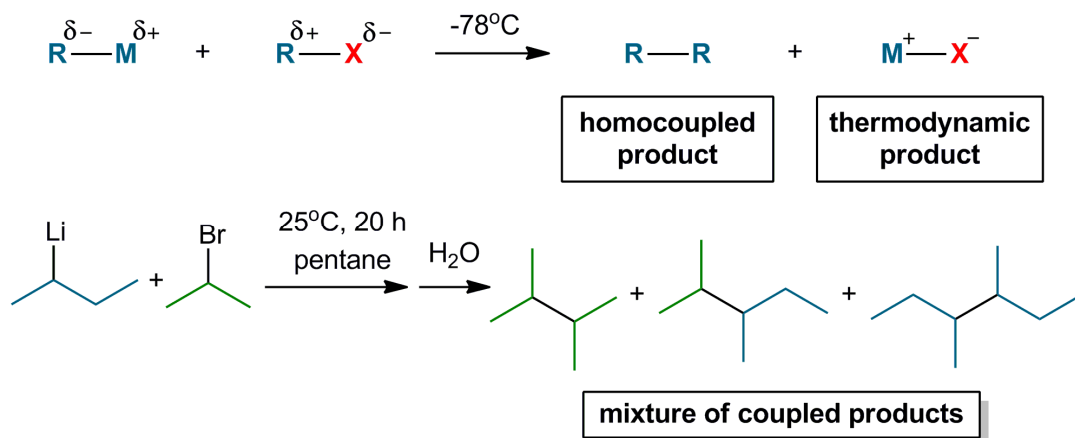
Metal halogen exchange is another fundamentally important vehicle for the preparation of reactive organolithium reagents, although these reactions must normally be performed at low temperatures. This versatile, selective reaction is a

phenomenon based upon kinetic control. In the reaction of an organometallic species (frequently an organolithium reagent) with an alkyl halide, the thermodynamically favoured product would clearly be the metal halide salt, with its high lattice energy providing the driving force for the reaction. However, cryogenic cooling facilitates a metathesis reaction where the two alkyl species swap their metal and halide partners to generate the kinetic product (Scheme 1.3). Propelling this reaction is the formation of the most stable alkyl “carbanion”.



Scheme 1.3 General schematic for metal-halogen exchange (top) and its application towards the conversion of 2,4-dibromoanisole to 5-bromo-2-methoxybenzoic acid (bottom).^[47]

A major advantage of metal-halogen exchange reactions is their high regioselectivity, as the metal occupies the site previously held by the halogen. Furthermore, the low temperatures often required for this reaction give rise to a wide functional group tolerance. Nonetheless, the formation of undesired side products presents a disadvantage, through Wurtz coupling (where R-X cannibalises R-M to form the homo-coupled R-R species alongside MX) (Scheme 1.4) and the formation of mixed aggregates.

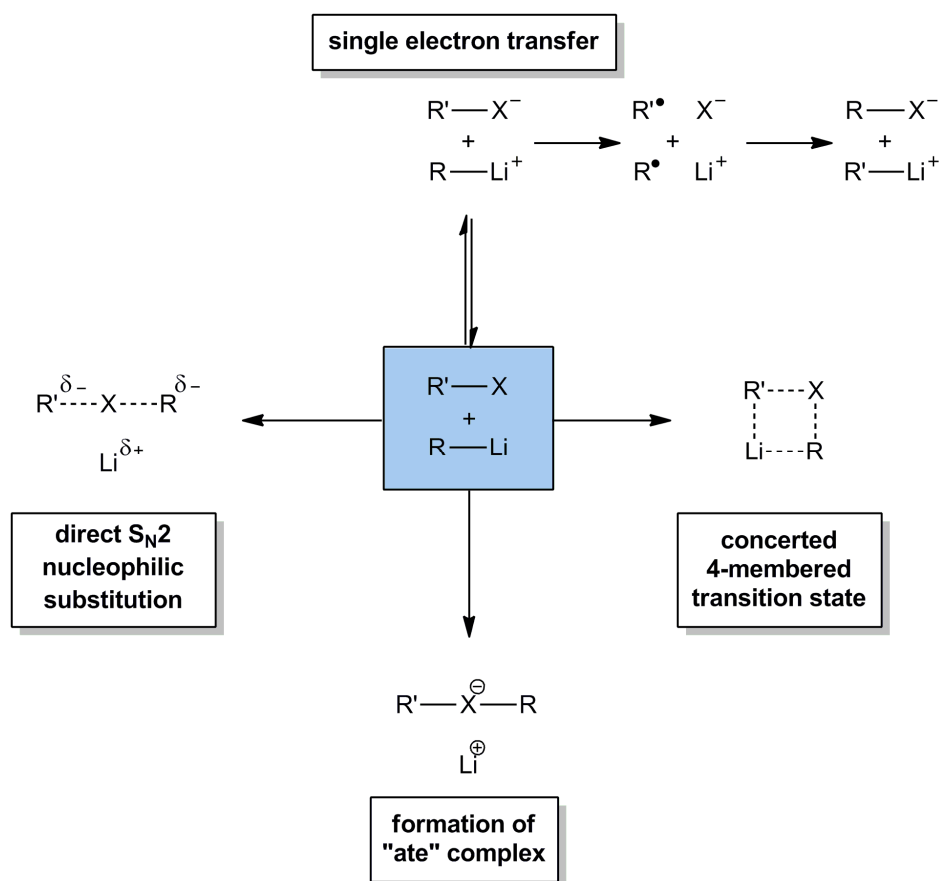


Scheme 1.4 General schematic for Wurtz coupling (top) and the mixture of homo- and heterocoupled products observed upon reaction of $^s\text{BuLi}$ with $^i\text{PrBr}$ (bottom).^[48]

In a recent, eye-catching study, the ability of aryllithium reagents to undergo coupling reactions was successfully exploited. This preparative method, which used a Pd-PEPPSI based catalyst (where PEPPSI is pyridine-enhanced pre-catalyst preparation stabilisation and initiation), was applied to the synthesis of a range of substituted biaryl compounds, including 1-(2,6-dimethoxyphenyl)naphthalene and 2'-methoxy-2,6-dimethyl-1,1'-biphenyl.^[49]

The concept of metal halogen exchange can be further extended to metal metalloids exchange, where metalloid typically refers to S, Se, Br, Sn, Te, I or Hg.^[50] Replacement of a halogen with a metalloid can present certain advantages, for example, lithium-tin exchange is more selective and can be used under milder reaction conditions than lithium halogen exchange.^[51] Conversely, it is also more expensive.

As metal-halogen exchange is a widely used synthetic methodology, it would be beneficial to understand the reaction mechanism clearly. However, the situation is not simple. Over time, many reaction mechanisms have been postulated, including nucleophilic substitution *via* a concerted transition state (through either a four centre transition state or an $\text{S}_{\text{N}}2$ mechanism), formation of an “ate” complex, or through a radical, single electron transfer (SET) reaction (Scheme 1.5).



Scheme 1.5 Postulated reaction pathways for metal-halogen exchange.

Experimental evidence to support each hypothesis has been accrued. For example, a kinetic study by Rogers, which probed the reaction of ⁿBuLi with a range of substituted bromobenzenes, revealed that the reaction rate was increased by the presence of an electron withdrawing substituent on the aromatic ring.^[52] This suggests that there is a build up of electron density on the aryl ring as the reaction proceeds, consistent with the formation of a concerted transition state (either four-centred or S_N2) or an “ate” complex as the rate limiting step.

Providing evidence to support the formation of an “ate” complex, kinetic^[53] and spectroscopic^[54] investigations of the combination of PhLi with PhI reveal that these reagents exist in a reversible equilibrium with the ate complex Li⁺Ph₂I⁻. Low temperature ⁷Li and ¹³C NMR spectroscopic monitoring of PhLi:HMPA (where HMPA is hexamethylphosphoric triamide) and PhI in a THF/HMPA solvent system

showed simultaneous disappearance of the PhLi·HMPA resonances, alongside the formation of a new set of resonances attributed to the ate complex $\text{Li}^+\text{Ph}_2\text{I}^-$. Based upon the observation of ^7Li - ^{31}P coupling, the lithium cation is thought to be stabilised by HMPA donor ligands. Complexes of lithium with HMPA as a supporting donor ligand are well known.^[55] Low temperature NMR spectroscopy has shown that the formation of such lithium iodinate complexes can also be achieved with other ligands, such as 5-methylthiophene.^[56] In addition, the molecular structure of the lithium iodinate $[\text{Li}(\text{TMEDA})_2]^+[\text{I}(\text{C}_6\text{F}_5)_2]^-$ has been elucidated through X-ray diffraction studies.^[57] Despite the observation of these ate species, definitive proof that they are involved in the rate limiting step of the metal halogen exchange reaction has not yet been forthcoming.^[58]

Experimental evidence has also been presented for a single electron transfer mechanism. Coupling products arising from radical origins were observed in the reaction of BuBr with BuLi in cumene solvent, namely butane, butene and octane. Also present was a significant quantity of (1,1,2-trimethyl-2-phenylpropyl)benzene $[\text{PhC}(\text{Me})_2\text{C}(\text{Me})_2\text{Ph}]$, formed through the abstraction of a hydrogen radical from cumene to produce a radical species, followed by dimerisation.^[59] Moreover, the cyclisation of alkyl radical probes has been observed within metal halogen exchange systems.^[60] In addition, spectroscopic techniques such as ESR (electron spin resonance) and CIDNP (chemically induced dynamic nuclear polarization) have also revealed the presence of radical species.^[61]

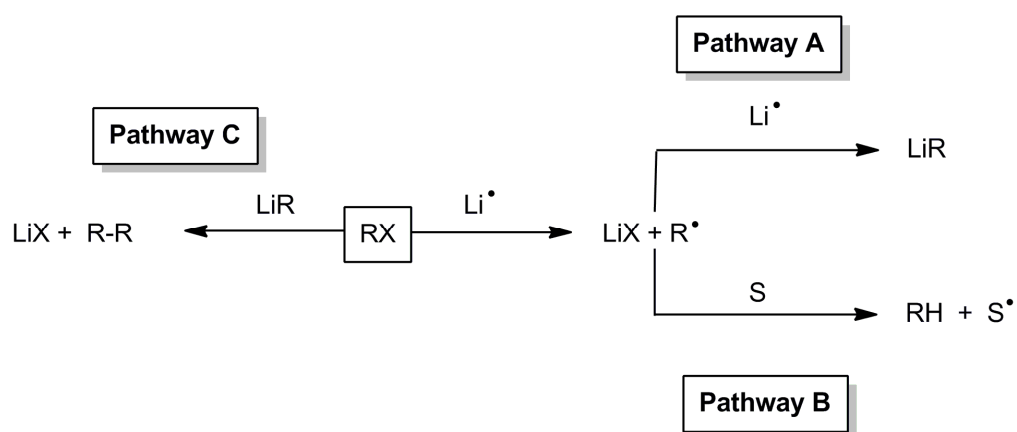
Despite the experimental evidence accrued to support each hypothesis, it seems that the “true” mechanism or mechanisms of metal-halogen exchange is still clouded in uncertainty and in likelihood varies from one reaction system to another.^[58; 62]

1.5.3 Reductive Lithiation

As the original preparative method for organolithium compounds, reductive lithiation has stood the test of time. Still used in the synthesis of commercially available

organolithium compounds, this method involves the reduction of an organohalide species by lithium metal.^[7] Alongside the production of a lithium halide salt, which provides a strong driving force for the reaction, an alkyl radical species is formed (R^\cdot). Upon reaction with a second equivalent of lithium metal, the organic fragment is converted to a formal carbanion to produce the organolithium reagent RLi (Scheme 1.6, Pathway A).

Although reductive lithiation proves one of the most popular methods of synthesising organolithium species, it comes with associated drawbacks. A primary limitation is the potential to form a mixture of products, which can occur through competitive reaction of the reactive radical species with the solvent (Pathway B). Moreover, by-products arising from cannibalisation of the organolithium product (LiR) by the unreacted starting material (RX) provide a further complication (Pathway C). Steps can be taken to disfavour this process, which is known as Wurtz coupling, such as alloying the lithium metal with 1-2% of sodium. Also, the selection of organochloride reagents instead of organobromides or organoiodides decreases the rate of this organolithium-organohalide coupling (note that organofluorides are never used on account of exceptionally strong C-F bonding). Finally, decomposition and side reactions can be dampened through the carefully considered choice of solvent and reaction temperature.



Scheme 1.6 General schematic representing the synthesis of organolithium reagents by reductive lithiation (Pathway A), along with potential side reactions with solvents (Pathway B) or Wurtz coupling (Pathway C).

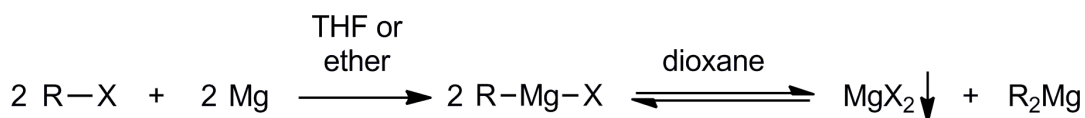
1.6 The LiCl Salt Effect

Though salt effects have been widely known in organolithium chemistry for many years,^[63] Collum has most recently exposed the effect LiCl impurities can impart upon the deprotonation of aromatic substrates by traditional organolithium reagents.^[64] As LiCl is present in commercially available lithium sources, many deprotonation reactions performed using LDA may have been reported without due acknowledgement of the substantial catalytic effect associated with the presence of LiCl. Addition of LiCl to an organometallic reaction system can improve the solubility, which is thought to occur through disaggregation of the organolithium reagent into smaller, more kinetically active aggregates, leading to an increased reactivity. Lithium chloride is also an excellent co-complexor as it can act as a Lewis acid (through “Li⁺”) or as a Lewis base (through “Cl⁻”).

Studies by Collum established that the trace presence of LiCl (0.5 mol% relative to the deprotonation reagent, LDA) can produce a remarkable rate enhancement of up to 100-fold upon the lithiation of arene substrates such as 1,4-difluorobenzene, 1,3-dichlorobenzene and 2,6-difluoropyridine.^[64] Furthermore, the presence of this inexpensive ionic salt can improve the reaction selectivity.^[65] Other lithium salts (LiBr, LiI, LiOCl₄, LiO^tBu) have also been shown to have a beneficial impact upon reaction rates and stereoselectivity.^[66] However, LiCl can alternatively play a detrimental role, giving birth to the description of its “Jekyll and Hyde” personality.^[67] Recent studies have highlighted the complex nature inherent within organolithium systems, where a multitude of transient solution state structures involving LiCl, pertinent to the deprotonation reaction investigated, were detected.^[68] Perhaps the most prominent use of LiCl has been in the development of turbo-Grignard reagents, where it is added stoichiometrically.

1.7 Grignard Reagents and their Turbo-Grignard Modifications

The ground-breaking work by Grignard, his discernment of the class of reagents with the empirical formula “RMgX”, has facilitated bond forming strategies for synthetic chemists worldwide.^[69] The importance of his work was internationally recognised when he received the Nobel Prize for Chemistry in 1912. Traditional Grignard reagents (of general formula RMgX), along with amino analogues (also known as Hauser Bases,^[70] R₂NMgX, so called due to the pioneering work of the American scientist Charles Hauser), still lie at the heart of magnesium chemistry today. Direct insertion of Mg metal into an alkyl halide bond provides a useful preparative method for Grignard reagents, as the reaction is atom economical, cheap, and environmentally benign thanks to the low toxicity of Mg (Scheme 1.7). However, the forcing conditions generally required limit the substrate tolerance. The oversimplistic empirical formula “RMgX” is perhaps misleading. In practice, a complex mixture of magnesium species exists in solutions of Grignard reagents, which involve different aggregation states and the coordination of commonly used donor solvents such as THF or ether. Furthermore, “Schlenk equilibria” occur, where a chemical equilibrium between RMgX on the one side and a mixture of R₂Mg and MgX₂ on the other side takes place.^[71] Enabling a greater degree of control, this equilibrium can be manipulated to the diorganomagnesium R₂Mg side through the addition of a donor ligand such as dioxane. Ultimately the equilibrium is driven towards the right through the precipitation of a MgX₂.dioxane complex.



Scheme 1.7 General route for the preparation of Grignard reagents.

Although organolithium reagents reign supreme as the leading organometallic reagents, organomagnesium reagents run them close, as they provide certain advantages including expansive functional group tolerance and greater thermodynamic stability, which enables higher reaction temperatures to be

employed. Perhaps it is thanks to their frequent use that research in this field is still blossoming today.

In 2004 Knochel reported the impact of salt effects upon the rate of metal-halogen (magnesium-bromine) exchange reactions.^[72] It transpired that whilst the addition of LiBr, LiI or LiClO₄ led to a minor increase in the reaction yield, LiCl gave a dramatic improvement. This important finding gave birth to the newest incarnation of Grignard reagents, popularly referred to as turbo-Grignard reagents on account of their increased reactivity, regioselectivity and functional group tolerance in comparison to their mainstream predecessors. Thought to bear the general formula RMgX·LiCl or R₂NMgX·LiCl, it seems likely that in qualitative terms the addition of LiCl promotes the reactivity of the Grignard reagent through decreasing the aggregation state while at the same time increasing solubility.^[73] These reagents are relatively facile to prepare, as performing the direct magnesiation of an alkyl halide in the presence of LiCl circumvents the forcing conditions required for conventional Grignard reagents. As a result, this method can be applied to substrates more sensitive than Grignard reagents or organolithium reagents can handle, as it demonstrates a much greater functional group tolerance.^[65] The impact of this research upon industry is perhaps best demonstrated by the commercial availability of TMPMgCl·LiCl, sold by Sigma Aldrich less than a decade after it was first reported.

Experimental evidence to support the formation of a lithium-magnesium co-complex has since been provided by the Mulvey group.^[74] Unveiling the molecular structures of the Hauser base TMPMgCl (Figure 1.7a) and turbo-Hauser base TMPMgCl·LiCl (Figure 1.7b), these compounds were crystallised, isolated and structurally elaborated through an X-ray diffraction study. Providing insight into the origins of the heightened reactivity of the turbo-Hauser base, this study established the full composition of [(THF)Mg(μ-Cl)(TMP)]₂ and [(THF)₂Li(μ-Cl)₂Mg(THF)(TMP)]. Intriguingly, lithium chloride is intimately involved in the molecular structure of the turbo-Hauser base; chloride anions adopt a bridging stance connecting the two metal centres. Formally, TMPMgCl·LiCl can be viewed as a lithium magnesiate. A TMP

unit occupies a terminal site on the tetra-coordinate Mg centre, adjacent to a THF molecule. The centre of reactivity is thought to be the vacant site created at the Mg centre upon the departure of THF, facilitating the approach of an organic substrate prior to its metallation.

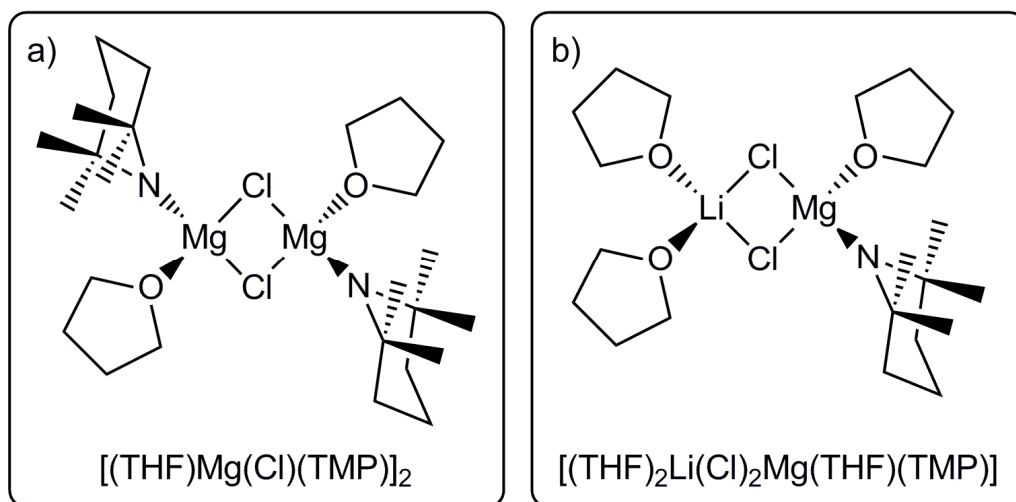


Figure 1.7 a) Molecular structure of Hauser base $[(\text{THF})\text{Mg}(\mu\text{-Cl})(\text{TMP})]_2$ b) Molecular structure of turbo-Hauser base $[(\text{THF})_2\text{Li}(\mu\text{-Cl})_2\text{Mg}(\text{THF})(\text{TMP})]$.^[74]

It is true that solid state structures can sometimes be simplistic in comparison to the dynamic chemistry often taking place in solution. Solution state ^1H and ^7Li DOSY (diffusion ordered spectroscopy) and EXSY (exchange spectroscopy) NMR experiments revealed that the solution state structures of turbo-Grignard reagents $[(\text{THF})_2\text{Li}(\mu\text{-Cl})_2\text{Mg}(\text{THF})(\text{TMP})]$ and $[\{(\text{THF})_2\text{Li}(\mu\text{-Cl})_2\text{Mg}(\mu\text{-DA})\}_2]$ differ from the solid state structures. Upon dissolution in d_8 -THF, solvent-separated ion pairs were formed.^[75] However, the solution state chemistry is complex, with temperature and concentration dependant dynamic exchange occurring between different structures. This study confirmed the specific involvement of lithium in the solution state structure(s) of the magnesium reagents, reinforcing that lithium performs a vital role in the reactivity enhancement, rather than simply observing as a spectator.

Further developing the rich chemistry associated with turbo-Grignard based metallating agents, the addition of the transition metal salt MnCl_2 to $\text{TMPMgCl}\cdot\text{LiCl}$

forms the trimetallic complex $\text{TMP}_2\text{Mn}\cdot\text{MgCl}_2\cdot 4\text{LiCl}$.^[76] This heterometallic reagent proves highly successful in the metallation of substrates that $\text{TMPMgCl}\cdot\text{LiCl}$ cannot deprotonate, such as the heterocycle 2-phenyl-1,3,4-oxadiazole.

1.8 Organozinc Reagents: A Historical Perspective

Igniting the field of organometallic chemistry both figuratively and literally, the British chemist Edward Frankland synthesised the first organozinc compounds, namely dimethylzinc (Me_2Zn) and diethylzinc (Et_2Zn), at the young age of 23.^[77] Not only were these species amongst the first organometallic compounds to be synthesized but further studies on these compounds also led to the development of valence theory. Referring to the reaction of dimethylzinc with water, Frankland made the following insightful observation:

“On pouring a few drops of water upon the residue, a green-blue flame, several feet long, shot out of the tube, causing great excitement among those present... which diffused an abominable odour throughout the laboratory”.^[77b]

Despite the dramatic nature of Frankland's initial discoveries, organozinc reagents are generally far less reactive than their s-block counterparts. Organozinc reagents such as ZnR_2 , $\text{Zn}(\text{NR}_2)_2$, $\text{RZn}(\text{NR}_2)$ and RZnX are soft nucleophiles, owing to the greater covalent character of the Zn-C bond. As a result, they exhibit a far greater functional group tolerance and are compatible with a wider range of solvents, although their reactivity falls well short of their lithium and magnesium counterparts.

Reflecting the challenge in performing X-ray diffraction studies upon such pyrophoric materials, with low melting points providing a further obstacle (Me_2Zn melts at $-42\text{ }^\circ\text{C}$), it took another 160 years following Frankland's epochal preparations until the molecular structures of Me_2Zn and Et_2Zn were finally revealed (Figure 1.8).^[78] Providing a marked contrast to the electron deficient, highly

aggregated molecular structures typically encountered for organolithium species, dialkylzinc formulations generally exhibit localised, two centre-two electron bonding. This reflects the greater covalency of Zn-C bonds in comparison to their Li-C analogues. For example, Me_2Zn , Et_2Zn and ${}^t\text{Bu}_2\text{Zn}$ ^[79] all possess discrete, linear molecular structures, where the C-Zn-C bond angle lies close to 180° [Me_2Zn , $180.0(2)^\circ$; Et_2Zn , $176.2(4)^\circ$; ${}^t\text{Bu}_2\text{Zn}$, $177.41(13)^\circ$]. Within both Et_2Zn and ${}^t\text{Bu}_2\text{Zn}$, the two organic fragments are orientated in an eclipsed geometry with respect to each other.

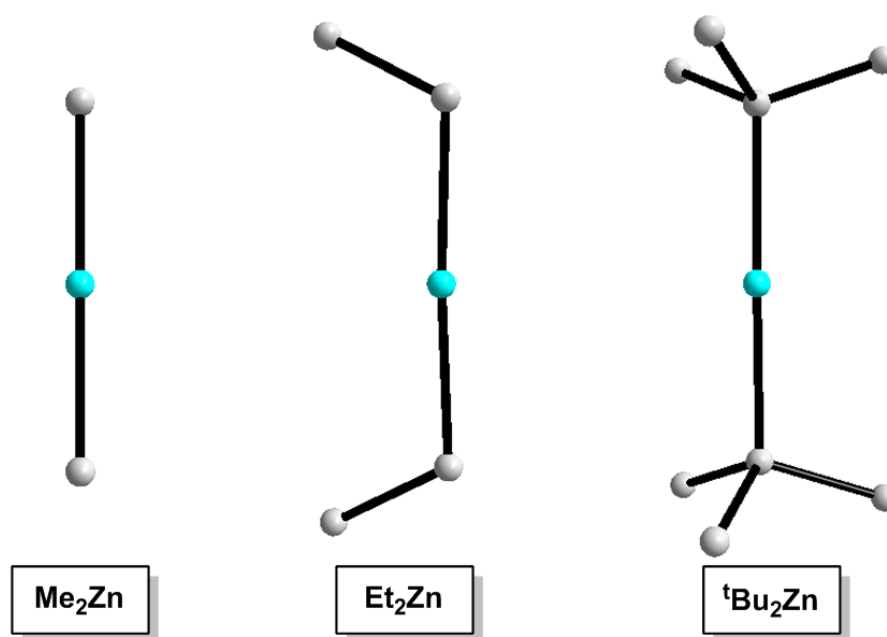


Figure 1.8 X-ray crystallographically determined molecular structures of organozinc species Me_2Zn , Et_2Zn and ${}^t\text{Bu}_2\text{Zn}$.

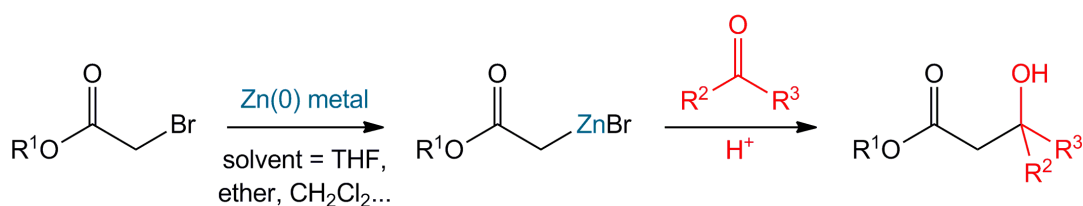
1.9 Applications of Zinc Reagents

Although organozinc reagents are less widely used in deprotonation chemistry than their more reactive s-block relatives, there has been a recent renaissance within organozinc chemistry, thanks to their applications within important synthetic processes such as C-C bond forming reactions.^[77b] In comparison to other metals,

zinc is relatively cheap and non-toxic, making it an attractive choice. Key reactions of this type are now outlined briefly.

1.9.1 Reformatsky Reaction

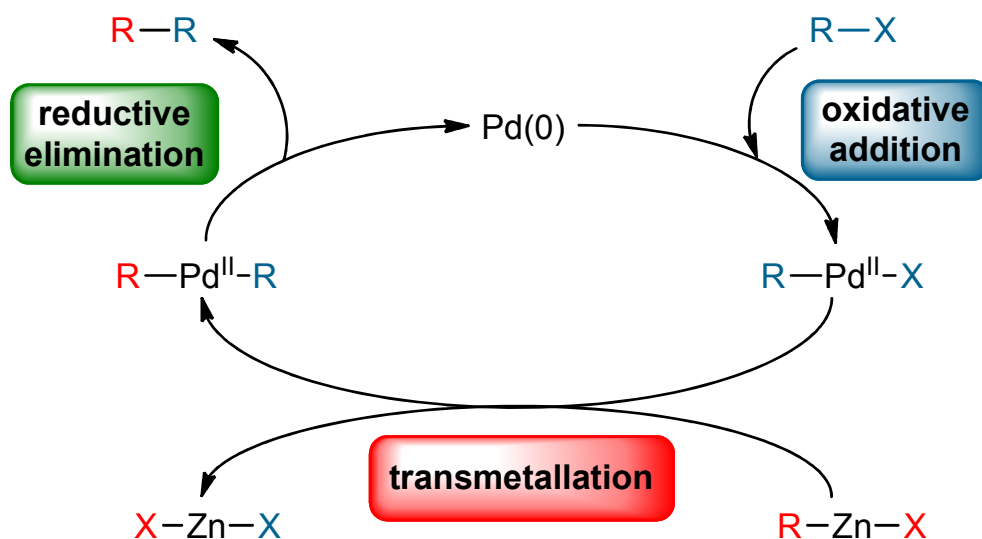
First described in 1887 and now a well established preparative method for β -hydroxyesters, the Reformatsky reaction provides an early example of the application of organozinc reagents to C-C bond forming reactions (Scheme 1.8).^[80] In the first step, a reactive organozinc intermediate is generated through the oxidative insertion of zinc metal into the carbon-halide bond of an α -halo ester, in effect forming an activated Grignard reagent mimic. Subsequent nucleophilic addition towards an aldehyde or ketone, followed by an oxidative work up, yields the β -hydroxyester product.^[80a] Demonstrating the beneficial functional group tolerance of organozinc reagents, the sensitive electron withdrawing ester functionality is preserved in this reaction. However, this functional group tolerance is compromised by several major limitations, including sluggish reactivity and low to moderate yields. As a result, organolithium and Grignard reagents are generally selected over their organozinc counterparts for deprotonative metallation applications.



Scheme 1.8 Application of organozinc reagents in the Reformatsky reaction.

1.9.2 Negishi Cross-Coupling Reaction

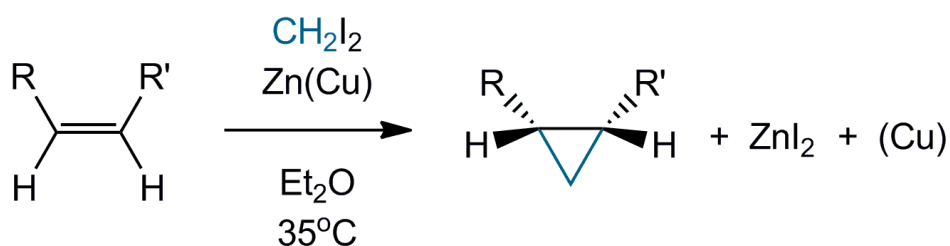
There exists a major benefit of organozinc reagents that has opened the gateway for facile C-C and C-N bond formation reactions. Negishi developed a Nobel Prize winning catalytic method for cross-coupling reactions which involves three principal steps as outlined in Scheme 1.9. Firstly, oxidative addition of RX to a Pd(0) [or Ni(0)] catalyst (where R = any organic fragment, X = halide, OTf, OAc₂ etc.) forms the Pd(II) species RPdX. Secondly, the low lying π -orbitals of Zn enable thermodynamically favourable transmetalation with R'ZnX to produce RPdR' (with the salt ZnX₂ formed as a by-product).^[81] Lastly, reductive elimination regenerates the Pd(0) catalyst. Although alternative metals can be used (for example Mg, Al, Cu, Zr, Cd, Sn and Hg), Zn displays far superior chemoselectivity and product yields. Furthermore, Zn reagents are generally facile to prepare and have a high functional group tolerance.^[82] This general cross-coupling method can therefore be successfully exploited to prepare a wide range of organic compounds including biaryls, enynes,^[83] and conjugated dienes^[84] that contain sensitive electrophilic functional groups.



Scheme 1.9 General catalytic cycle mechanism for a palladium catalysed cross-coupling reaction using organozinc substrates.

1.9.3 Simmons-Smith Cyclopropanation^[85]

Organozinc chemistry has also found applications in the synthesis of cyclopropanes, a process widely referred to as the Simmons-Smith cyclopropanation in honour of its discoverers. This versatile, stereospecific method can be used to synthesise substituted cyclopropanes through the reaction of an alkene with diiodomethane in the presence of a zinc/copper couple (Scheme 1.10).



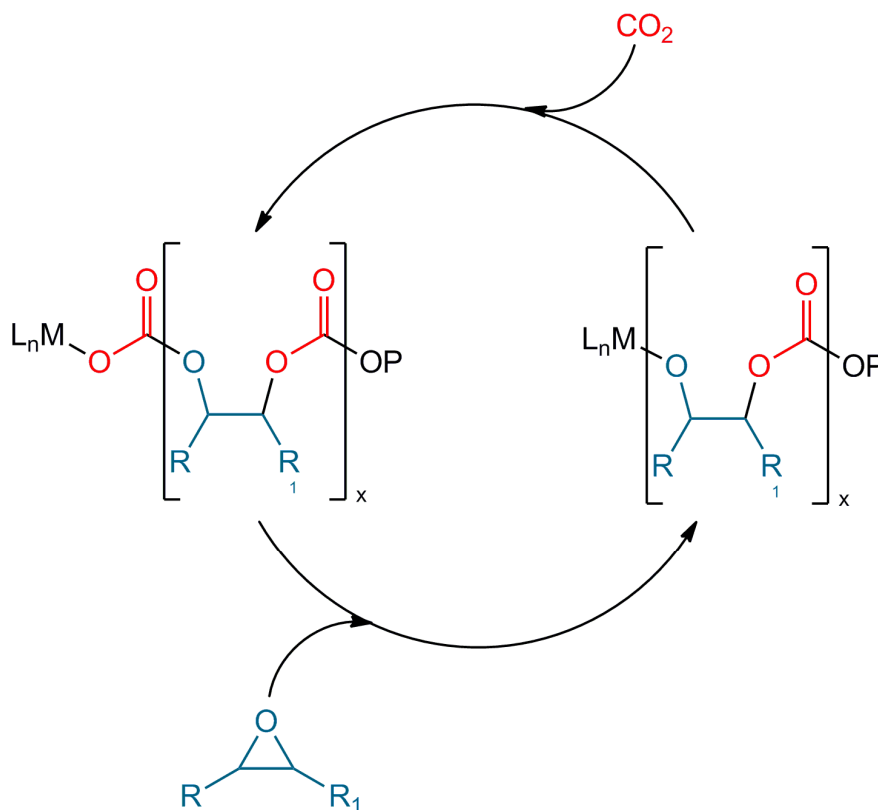
Scheme 1.10 General reaction scheme for the Simmons-Smith cyclopropanation.

1.9.4 Copolymerisation of Carbon Dioxide and Epoxides

With natural and synthetic polymers having come to play a vital role in our everyday existence, polymer synthesis is currently a vast area of research. Presently, the majority of polymers are synthesised from petroleum feed stocks. However, diminishing resources of oil are currently fuelling intense interest in the synthesis of polymers from renewable sources, including carbon dioxide and epoxides. In 1969, the seminal work of Inoue presented the first example of alternating carbon dioxide and epoxide (propylene oxide) copolymerisation. This was achieved by exploiting Et_2Zn as a catalyst, combined with H_2O in a 1:1 stoichiometry.^[86]

The employment of zinc catalysts has since dominated the copolymerisation of carbon dioxide and epoxides, despite other metals such as chromium and cobalt showing promising signs of catalytic activity.^[87] Although today most industrial scale productions of copolymers still employ heterogeneous catalysts, more recent

research has focussed upon homogeneous catalysts, which provide benefits such as narrow polydispersity indexes, faster reaction rates and improved selectivity. Furthermore, homogeneous catalysts allow greater control over the molecular weight, co-monomer incorporation and stereochemistry. Such catalysts conform to general formula L_nMR , where M is the active metal centre (often zinc), L is a ligand which remains bonded to the metal (thus influencing its activity), and R is the active group that can initiate polymerisation. For example, the phenol derivatives [(2,6-diphenylphenoxide) $_2$ Zn(THF) $_2$] and [(2,6-diphenylphenoxide) $_2$ Zn(OEt $_2$) $_2$] were the first single molecule zinc catalysts reported for this copolymerisation reaction,^[88] which inspired the development of many other zinc-based catalysts.^[87; 89] Moreover, structural analysis of such single molecule catalysts has advanced the understanding of the mechanisms involved in copolymerisation reactions (Scheme 1.11).^[87]



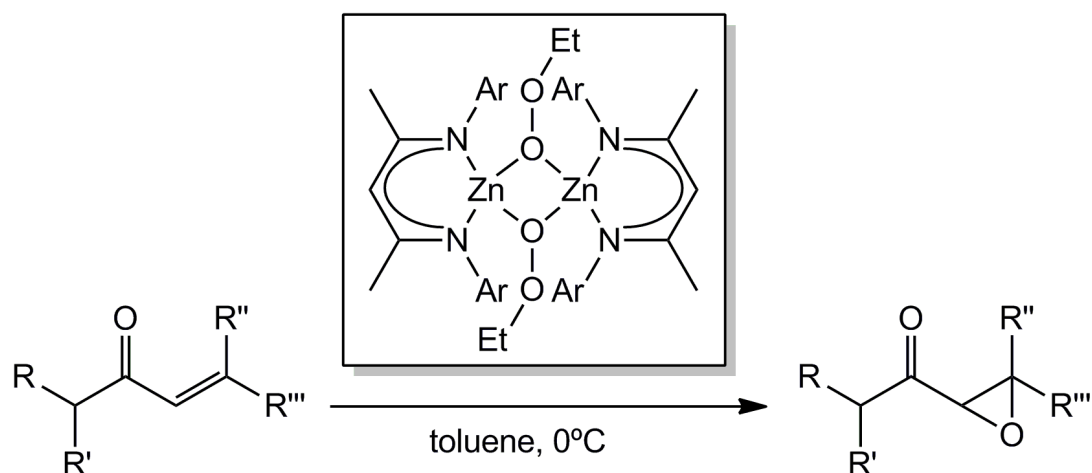
Scheme 1.11 General mechanism for alternating copolymerisation of carbon dioxide and an epoxide, where M = metal, L = ligand, P = polymer chain.^[87]

1.9.5 Ring Opening Polymerisation

In addition to their employment within copolymerisation reactions, homogeneous zinc catalysts have also been applied to ring opening polymerisations.^[90] Accordingly, the zinc alkoxide catalyst [(BDI)ZnOⁱPr] (where BDI refers to a 2,6-diisopropylphenyl substituted β -diiminate ligand), successfully enabled the stereoselective synthesis of polylactide.^[90a] Mass spectrometry investigations revealed that the polymerisation is initiated by the propoxide unit. Consequently, the Zn(BDI) fragment co-ordinates to the propagation site (that is, the alkanoate) at which the next monomer is incorporated. As the stereochemistry of poly(lactides) dictates their mechanical and physical properties, which dictates their applications, stereochemical control is therefore highly desirable. Interestingly, zinc alkoxides have outperformed analogous magnesium catalysts in this regard.^[91]

1.9.6 Zinc Alkoxides and Zinc Alkylperoxides: Epoxidation of Enones

The sensitivity of organozinc reagents towards air has been recognised since their initial discovery, although understanding and controlling this reactivity presents a significant challenge.^[77a; 92] Despite the restrictions imposed upon the handling of organozinc species, chemists have been able to turn this air-sensitivity to their advantage. Lewiński recently reported the first structurally characterised zinc alkylperoxide compound, [(BDI)ZnOOEt]₂, through the controlled reaction of [(BDI)ZnEt] with dry oxygen.^[93] As alkylzinc peroxide systems have applications within organic synthesis, the ability to prepare these compounds through the oxidation of alkylzinc species is highly useful.^[94] For example, the ethylperoxide [(BDI)ZnOOEt]₂ was successfully applied to the chemo- and regioselective oxidation of enones, producing high yields of substituted epoxides (Scheme 1.12).

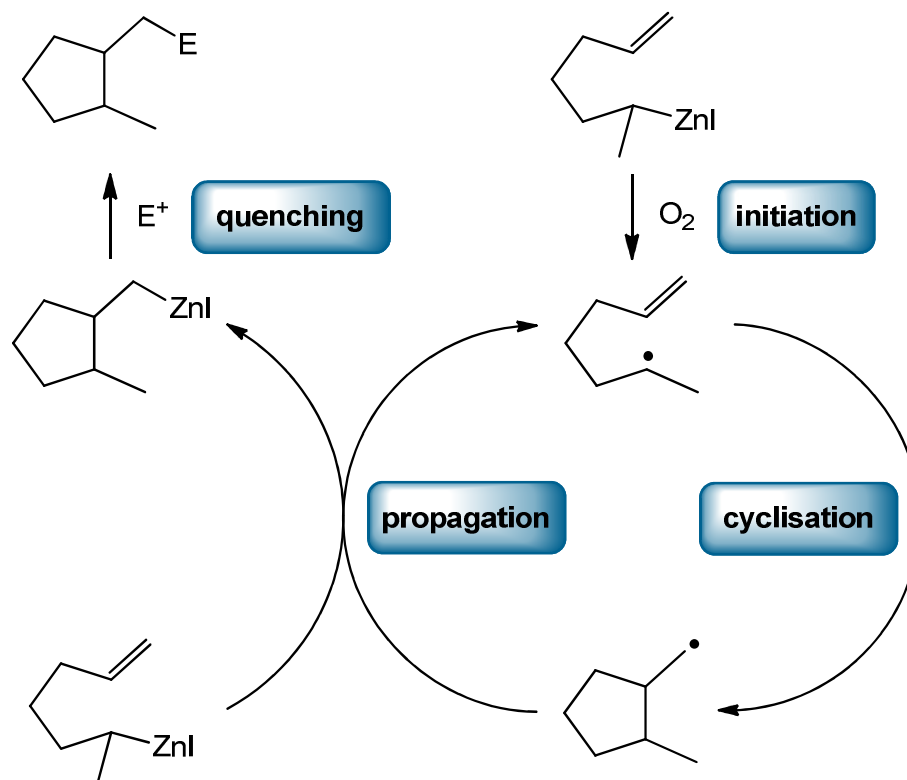


Scheme 1.12 Application of the zinc ethylperoxide $[(\text{BDI})\text{ZnOOEt}]_2$ to the epoxidation of enones.

Impressively, the controlled oxidation of alkylzinc species has been achieved,^[95] where the reaction outcome is strongly influenced by the chemical environment surrounding the zinc metal centre.^[96] For example, combining Et_2Zn and oxygen this time in the presence of azol-H (where azol-H is 1-aziridine ethanol) yielded the crystalline species $[\text{EtOOZn}(\text{azol})]_2[\text{EtZn}(\text{azol})]_2$.^[97] This dimeric complex contains two inequivalent ethyl groups, where the first type is involved in Zn-Et bonding and the second in O_2 -Et bonding. Despite the insertion of oxygen only occurring for half of the Zn-Et bonds, this peroxide was inert towards oxygen at -78°C . This concept of controlled oxidation has since been extended to the synthesis of zinc alkoxides, for example in the production of crystalline $\text{Me}_6\text{Zn}_7(\text{OMe})_8$ from dimethylzinc and oxygen.^[97] Furthermore, it has since been shown that the nature of the Lewis donor additive can enable control over whether an alkoxide or a peroxide species is formed.^[98] In the reaction of ${}^t\text{Bu}_2\text{Zn}$, oxygen and THF, the alkylzinc alkoxide dimer $[\{\text{Zn}{}^t\text{Bu}(\mu\text{-O}{}^t\text{Bu})(\text{THF})\}_2]$ was selectively produced. In contrast, replacing THF with the stronger Lewis base 4-methylpyridine (Me-pyr) yielded the alkylzinc peroxide species $[\{\text{Zn}{}^t\text{Bu}(\mu\text{-OO}{}^t\text{Bu})(\text{Me-pyr})\}_2]$.

1.9.7 Radical Addition Reactions Initiated by R_2Zn/O_2 Systems

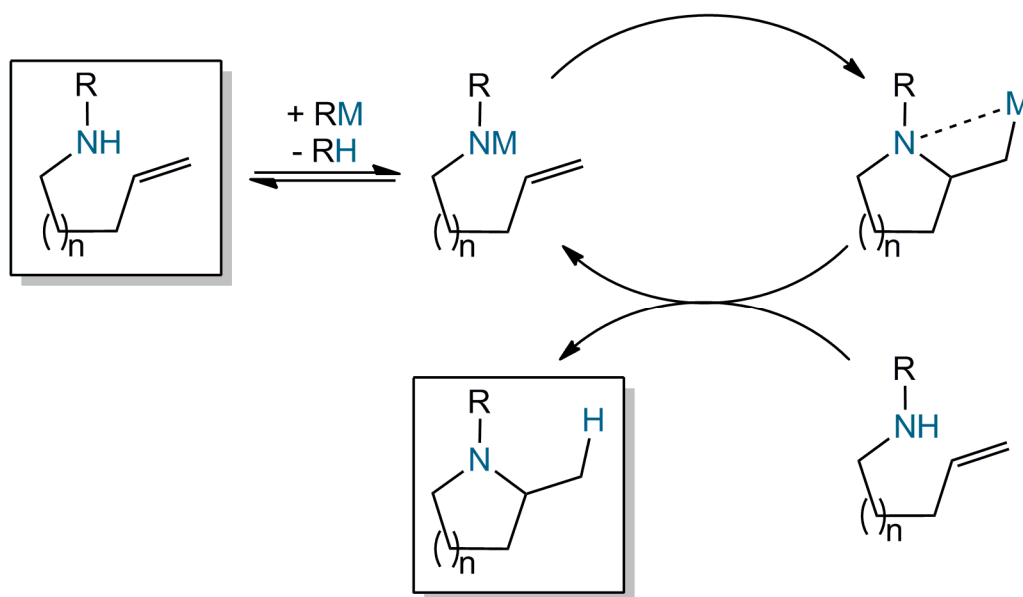
Zinc/oxygen systems have further applications as initiators within radical addition reactions, such as the cyclisation of terminally unsaturated alkenyl zinc iodides.^[99] Initiated by the presence of oxygen, this reaction is thought to proceed through a zinc radical transfer mechanism (Scheme 1.13). Supporting this hypothesis, the substitution of oxygen with the radical organotin initiator ($t\text{Bu}_3\text{Sn}$)₂ gave comparable results. Moreover, the stereochemistry of the cyclised products differed for alkylzinc halide systems in comparison to analogous organolithium or Grignard reagents, for which a polar carbometallation reaction mechanism is thought to be operative.



Scheme 1.13 Reaction mechanism for the oxygen initiated cyclisation of heteroleptic alkenyl zinc iodides.

1.9.8 Hydroamination Reactions

With C-N bond formation paramount in the synthesis of commodity chemicals, hydroamination (the addition of a N-H group from a primary or secondary amine across the unsaturated bond of an alkene or alkyne) provides a useful means to achieve this end (Scheme 1.14).^[100] This versatile, atom-economical, one-step reaction can be catalysed by various organometallic species involving an alkali metal,^[101] alkaline earth metal,^[102] early transition metal^[103] or lanthanide^[104] as the active metallic centre.^[105] Despite their efficiency, lanthanide based hydroamination catalysts are extremely air- and moisture- sensitive and intolerant of many functional groups, which limits their widespread application. In contrast, functional group tolerance is improved using late transition metal catalysts such as Ir,^[106] Rh,^[107] Pd,^[108] Pt^[109] and Ni^[110]. However, the expense of these noble metal catalysts is an undoubted drawback.



Scheme 1.14 General intramolecular hydroamination reaction mechanism.

One of the most impressive lines of development employs organozinc hydroamination catalysts. Stable to air, the zinc based catalyst $[\{(i\text{Pr})_2\text{ATI}\}\text{ZnMe}]$, [where ATI is *N*-isopropyl-2-(isopropylamino)troponiminato], was shown to catalyse the intramolecular hydroamination of functionalised alkenes and alkynes.^[100b] High

yields were secured, even for non-activated alkenes and for the synthesis of strained, seven-membered heterocycles. This catalyst displays advantages over its predecessors, demonstrating increased functional group tolerance and increased efficiency, along with robustness to air and moisture. Since this original report, other zinc based catalysts of general formula [RZnMe] have been developed, including those where R refers to a β -diketiminato ligand.^[100e]

Inexpensive, environmentally benign alkaline earth metal based catalysts have also shown excellent promise as catalysts for hydroamination reactions. In 2005, Hill reported an efficient calcium based catalyst for ambient temperature hydroamination, specifically a β -diketiminato calcium bis(trimethylsilyl)amido complex.^[102] This field of research has since been extended to incorporate alternative ligands^[111] and other alkaline earth metals such as Mg,^[112] Sr^[113] and Ba.^[114]

1.10 Zinc-Zinc Bonding

Revealing the first observation of a Zn-Zn bond, Carmona recently reported the compound [Zn₂(Cp*)₂] (Cp* = pentamethylcyclopentadienyl, C₅Me₅),^[115] where Zn is formally in a +1 oxidation state (Figure 1.9). The Zn-Zn bond length [2.305(3) Å] of this linear structure is significantly smaller than the sum of the covalent radii of two Zn centres (2.50 Å).^[116] Although this dizincocene presented the first structural elucidation of a Zn-Zn bond, this work was foreshadowed by the synthesis of Zn₂Cl₂ from a Zn/ZnCl₂ melt, where the observation of a [Zn₂]²⁺ dication suggested that Zn could be involved in low valent bonding.^[117] Since Carmona's pioneering discovery, there has been increasing interest in low valent metal-metal bonding,^[118] with the development of many Zn-Zn bonded compounds,^[119] in addition to the first observation of a crystallographically characterised Mg-Mg bond.^[120] The development of new dizincocenes includes [Zn₂(C₅Me₄Et)₂], which exhibits a strong structural similarity to [Zn₂(Cp*)₂].^[121] Contrastingly, attempts to synthesise analogous [Zn₂(Cp')₂] compounds (where Cp' is C₅H₅, C₅Me₄H, C₅Me₄SiMe₃ or

$\text{C}_5\text{Me}_4\text{tBu}$) were unsuccessful, revealing that the substituents of Cp^* play an important role in the stability of the dizincocene. Alternatively, Zn-Zn bonds can be stabilised by sterically demanding, often chelating Lewis bases such as β -diketiminato ligands. Presenting the first example of this type of compound, Robinson reported the zinc species $[\text{L}'\text{ZnZnL}']$ (where L' is $[(2,6\text{-}^i\text{Pr}_2\text{C}_6\text{H}_3)\text{N}(\text{Me})\text{C}]_2\text{CH}$).^[122]

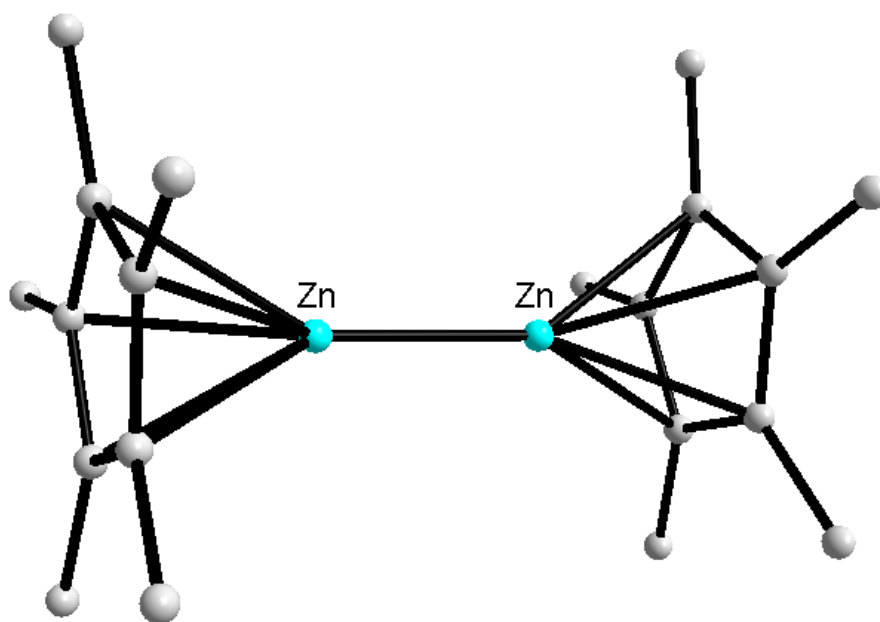
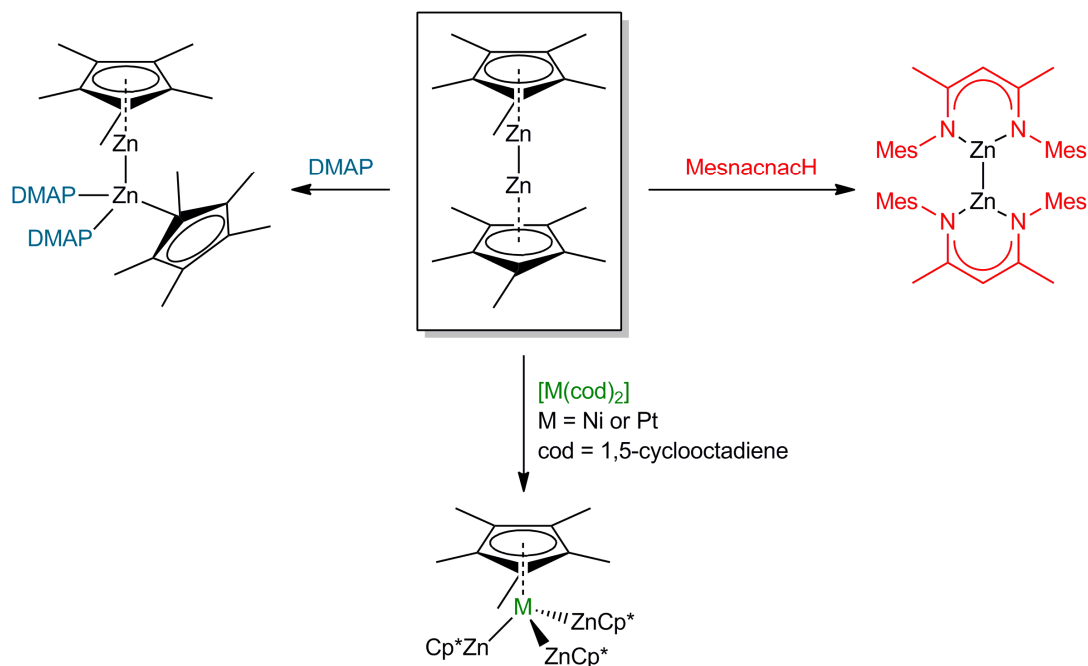


Figure 1.9 Molecular structure of $[\text{Zn}_2(\text{Cp}^*)_2]$.^[115]

The first reactivity studies of dizincocene $[\text{Zn}_2(\text{Cp}^*)_2]$ suggested that its reactivity was limited, as no reaction was observed with H_2 , CO or CO_2 . With H_2O or tBuOH disproportionation occurred to form Zn^0 metal, $\text{Zn}^{\text{II}}(\text{OH})_2$ or $\text{Zn}^{\text{II}}(\text{O}^t\text{Bu})_2$, and Cp^*H . Furthermore, no reaction occurred with a range of weak Lewis bases including NEt_3 , TMEDA and PPh_3 . However, in the presence of strong Lewis bases such as DMAP (4-dimethylaminopyridine), $[\text{Zn}_2(\text{Cp}^*)_2]$ can form a donor-acceptor complex, for example $[(\eta^5\text{-Cp}^*)\text{ZnZn}(\text{dmap})_2(\eta^1\text{-Cp}^*)]$ (Scheme 1.15).^[123] This dizincocene can also react with strong Brønsted acids. Ligand exchange occurs, and whilst the Zn-Zn bond persists, Cp^* is replaced, typically by a sterically demanding organic ligand, with concomitant formation of Cp^*H .^[124] Additional studies revealed that when reacted with the transition metal complex $[\text{M}(\text{cod})_2]$ ($\text{M} = \text{Ni}$ or Pt , $\text{cod} = 1,5$ -

cyclooctadiene), the dizincocene can act as a ZnCp^* and a Cp^* transfer agent. Cleavage of the Zn-Zn bond produces $[\text{Cp}^*\text{M}(\text{ZnCp}^*)_3]$ compounds which contain mixed metal (M-Zn) bonds.^[125] It has recently been shown that $[\text{Zn}_2(\text{Cp}^*)_2]$ has applications as a catalyst for intra- and intermolecular hydroamination reactions.^[126] Competitive with other hydroamination catalysts, $[\text{Zn}_2(\text{Cp}^*)_2]$ gives high product yields under ambient temperature conditions, and demonstrates a wide functional group tolerance.



Scheme 1.15 Reactions of $[\text{Zn}_2(\text{Cp}^*)_2]$ with Lewis base DMAP (left hand side), Brønsted acid Mesnacnach (right hand side) and transition metal complex $[\text{M}(\text{cod})_2]$ (bottom).

1.11 Benefits and Shortcomings of Monometallic Reagents

Although organolithium, organomagnesium and organozinc reagents can all be applied to the deprotonation of an organic substrate, each has associated advantages and disadvantages. Typically exhibiting the highest reactivity, organolithium

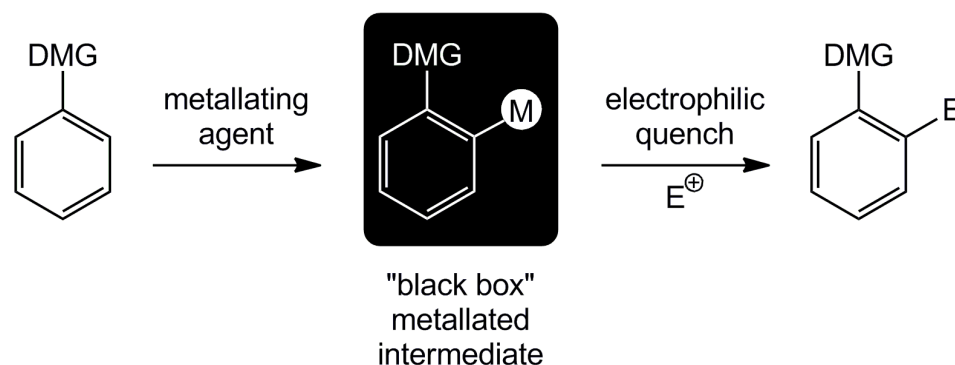
reagents currently reign supreme in C-H bond activation strategies. Although they are generally facile to prepare (or in many cases are commercially available), their highly reactive nature leads to a low functional group tolerance. In turn, this incurs expense, as low temperatures are often required to prevent decomposition. Similarly, Grignard reagents are readily available and exhibit moderate reactivity well below that of their organolithium counterparts, although the low selectivity and poor functional group tolerance often observed limits their use in metallation chemistry. In contrast, organozinc reagents are less easy to prepare and have a relatively low reactivity in comparison to their s-block relatives. Conversely, this is linked with high selectivity and good functional group tolerance. Although organozinc species have a wide range of applications within organic synthesis, they are less often used for the C-H deprotonation of aromatic and heteroaromatic substrates on account of their sluggish, kinetically slow reactivity. These observations prompt the question “how can we harness the beneficial properties of each metal reagent, whilst avoiding their shortcomings”? It seems that bimetallic reagents may provide one answer.

1.12 A General Overview of Heterobimetallic Chemistry

As organometallic reagents are essential for performing C-H bond deprotonation, it would be highly beneficial to develop reagents capable of overcoming the limitations associated with conventional monometallic strategies. Access to unusual regioselectivities and good functional group tolerance would feature highly on the wish list for an ideal deprotonation agent. Also, the ability to achieve dimetallation through a one step reaction would present a more efficient route to multi-substituted products. With green chemistry a topical issue,^[127] environmentally benign, ambient temperature reaction conditions, along with the use of non-toxic, cheap solvents are all highly desirable features. Along the same vein, atom economical bases, where each ligand within the metallator was capable of the deprotonation of an organic substrate would be ideal. At the heart of sought-after properties lies the ability to recycle the organometallic reagent. Within current lithiation methodologies, the

lithium reagent is often irrecoverably lost, for example, with BuLi, butane gas is released as a by-product.

Heterobimetallic (mixed-metal) systems have shown excellent promise towards achieving at least some of these goals. An area of international research, multimetal reagents are generating interest world wide, with prolific research groups across Europe (such as Knochel, Mongin, Mulvey and Wheatley) and Asia (such as Kondo and Uchiyama) developing cooperative bimetallic reagents. Examples include turbo-Grignard reagents of empirical formulas such as “(TMP)MgCl·LiCl”^[72] and the lithium zincate “LiZn(TMP)(^tBu)₂”.^[128] Often the focus of this research lies with the *in situ* employment of these bimetallic bases towards organic transformations. Therefore, the constitution of the reactive metallic species, and the metallated intermediates, are often unknown (Scheme 1.16). Mulvey has referred to this paucity of information as “black box” chemistry.^[129]



Scheme 1.16 General reaction scheme for the metallation of an aromatic substrate, highlighting the postulated metallated intermediate, followed by an electrophilic quench (DMG = directing metallating group).

Such synergic multi-metal complexes have often surprised their discoverers through exhibiting an exciting new reactivity, entirely individual to that of either of the component parts that make up the multicomponent reagent.^[8; 20; 73; 130] The two metals work together to create a novel, synergic effect, facilitating special regioselectivities and enabling reactions to be performed under milder reaction conditions, with a wider functional group tolerance than their homometallic

counterparts. The importance of this chemistry is reflected by the vast literature pertaining to heterobimetallic chemistry. Although this review aims to cover a range of examples, for brevity it is by no means exhaustive. Several excellent reviews have recently been published which provide a comprehensive summary of the literature pertaining to this synergic bimetallic chemistry.^[73; 130c; 130d; 131]

1.13 Mixed Alkali Metal Mixed Ligand Compositions

It has long been known that the deprotonative ability of *n*-butyllithium towards organic compounds, especially aromatic substrates, is enhanced when a bimetallic co-complex with potassium *tert*-butoxide is formed. Accordingly, the complex ${}^n\text{BuLi}\cdot\text{KO}^t\text{Bu}$, commonly written as LIC-KOR, is often referred to as the Schlosser-Lochmann “superbase”.^[132] In this context, the term “superbase” refers to a “base resulting from a mixing of two (or more) bases leading to new basic species possessing inherent properties”.^[133] In this special case LIC-KOR has a reactivity intermediate to that between BuLi (least reactive) and BuK (most reactive). Although LIC-KOR can be used to activate C-H bonds within a range of weakly acidic substrates, such as alkyl substituted benzenes, a mixture of regioselectivities are often observed.^[132d] Subsequent work by O’Shea has focused upon the related “LiNK” base, derived from the combination of ${}^n\text{BuLi}$, KO^tBu and TMP(H) in THF solvent.^[134] This mixed metal amide base offers improved regioselectivity over its LIC-KOR competitor, even when TMP(H) is only introduced in catalytic quantities.

In a recent, eye-catching study, the Schlosser-Lochmann superbase (${}^n\text{BuLi}\cdot\text{KO}^t\text{Bu}$) was successfully applied to the metallation of benzene.^[132e] Performed in THF solution at $-78\text{ }^\circ\text{C}$, the reaction yielded the mixed metal, hexanuclear Li_2K_4 aggregate $[(\text{PhK})_4(\text{PhLi})({}^t\text{BuOLi})(\text{THF})_6(\text{C}_6\text{H}_6)_2]$, which includes both phenyl and *tert*-butoxide anions (Figure 1.10). Interestingly, this compound represents the first crystallographically characterized example of a bimetallic aggregate to contain all the components of the Lochmann-Schlosser superbase (except perhaps for the most

important component, the active Bu^- base), including the metallated substrate (in this case, benzene). Formally a superbases itself, this bimetallic aggregate was subsequently shown to be capable of the deprotonation of toluene at the lateral Me site.

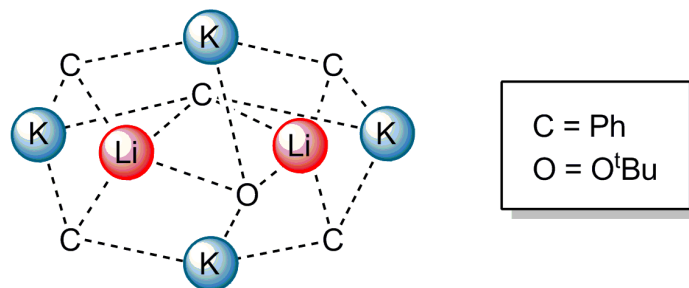


Figure 1.10 Central core of the molecular structure of bimetallic aggregate $[(\text{PhK})_4(\text{PhLi})(^t\text{BuOLi})(\text{THF})_6(\text{C}_6\text{H}_6)_2]$, where C represents Ph^- and O represents $^t\text{BuO}^-$. Solvating THF and benzene molecules have been omitted for clarity.^[132e]

Generally, multimetal superbases outperform their component unimetal superbases within deprotonation chemistry. However, Caubère's reagent is worthy of note.^[133] Having the formula $[\text{nBuLi}\cdot\text{Me}_2\text{N}(\text{CH}_2)_2\text{OLi}]$, this alkyllithium-lithium aminoalkoxide can be viewed as a unimetal analogue of LIC-KOR. An efficient metallating agent, Caubère's reagent can be applied to the metallation of sensitive pyridine derivatives.^[135] Despite the early recognition of the enhanced reactivity available using superbases, it is only within the past ten years or so that bimetallic bases combining two distinct metals from different groups within the periodic table have become an area of international focus.

1.14 Alkali-Metal-Mediated Metallations

Special, synergic chemistry can take place when two metals from different groups of the periodic table are combined within the same molecular environment. These heterometallic compounds typically comprise a hard alkali metal and a softer divalent metal (for example, Mg, Mn, Zn or Cd) or trivalent metal (for example, Al

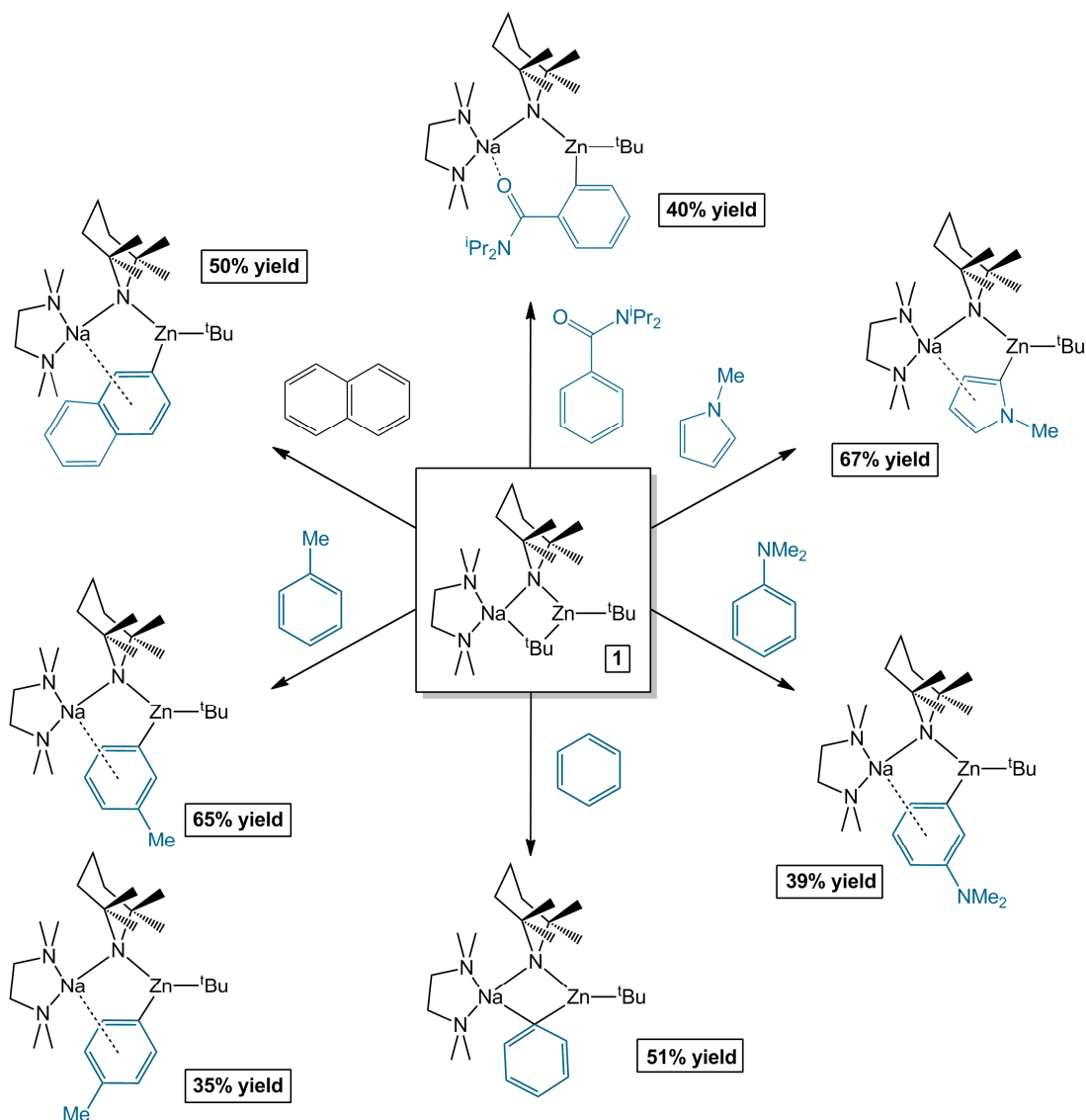
or Ga). Perhaps counter to expectation, it is typically the softer metal component which executes the deprotonation of organic substrates. However, the presence and participation of the alkali metal is essential for metallation to occur and so this phenomenon has been described as alkali-metal-mediated metallation (AMMM), where *M* represents the non-alkali metal.

Often used to describe heterobimetallic complexes, the term “ate” is prevalent throughout organometallic literature. Coined by Wittig, this suffix is used to indicate the anionic formulation of a metal centre. Observing that the trisphenyl complexes LiMgPh_3 and LiZnPh_3 exhibit a distinct chemistry to that of their individual homometallic components, Wittig insightfully attributed this effect to anionic activation of Mg/Zn by the surrounding phenyl ligands.^[136] Within a bimetallic environment, the softer, more carbophilic metal centre possesses an anionic formulation (such as MgR_3^- , ZnR_3^-), as the negative charge of the carbanions lies predominantly towards the metal that possesses the highest electronegativity (that is, Zn, $\chi = 1.6 > \text{Mg}$, $\chi = 1.2 > \text{Li}$, $\chi = 1.0$).^[137] Within Wittig’s zincate and magnesiate systems, the anionic metal centre is balanced by a lithium counteranion. Although a range of heterometallic bases have been developed using soft alkaline earth metals, transition metals or even p-block metals, sodium zincate systems provide the focal point for this PhD project. For brevity, the bulk of this introduction shall primarily cover developments within sodium zincate chemistry.

Preparation of the original zincate complex predated the term “ate” by almost a century.^[138] In 1858, Wanklyn synthesised the sodium trisalkylzincate “ $\text{Na}^+[\text{Zn}(\text{Et})_3]^-$ ” through the reaction of metallic elemental sodium with diethylzinc (which was prepared by his supervisor Frankland less than 10 years previously).^[139] Since this original unplanned synthesis, the construction of zincates has become increasingly sophisticated, with recent developments in the field including the rational design of a number of zincate bases that enable unprecedented reactions to be performed with ease.^[128; 140] In work carried out over a century after Wanklyn’s pioneering synthesis, the first structurally characterized zincate, the lithium tetraalkylzincate Li_2ZnMe_4 , was reported by Weiss.^[141]

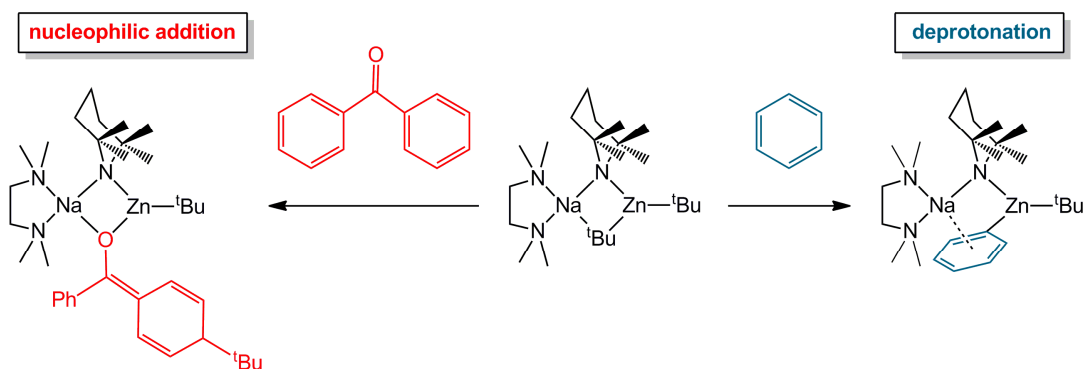
Highly useful because of its strong Brønsted basicity, significant steric bulk and low nucleophilicity, the monofunctional amide TMP is prevalent throughout alkali metal zincate chemistry. An important discovery within bimetallic chemistry was the development of the lithium amidozincate “LiZn(TMP)(^tBu)₂”, which has successfully been applied to the DoM of organic substrates. Subsequent elucidation of the molecular structure revealed the molecular formula to be [(THF)Li(μ-TMP)(μ-^tBu)Zn(^tBu)].^[142] In the solid state, Li and Zn are held within the same molecular environment, connected through a bridging TMP unit and a ^tBu fragment. Suggesting that the synergic effect associated with the pre-complexation of the two metal reagents plays an important role, the sequential reaction of the aromatic substrates with ^tBu₂Zn, LiTMP, and an electrophile did not form the *ortho*-substituted aromatic product. Advantageously, this lithium amidozincate was unreactive towards sensitive functional groups (for example, ester, amide, cyano) that are incompatible with conventional organolithium reagents, and was successfully used under ambient temperature reaction conditions.^[128]

The sodium analogue of bimetallic [(THF)Li(μ-TMP)(μ-^tBu)Zn(^tBu)], the heteroleptic complex [(TMEDA)Na(μ-TMP)(μ-^tBu)Zn(^tBu)], **1**, exhibits a fascinating reactivity towards a range of organic substrates (Scheme 1.17).^[140a; 143] One particularly impressive achievement was the metallation of unsubstituted (hence unactivated) benzene at ambient temperature within only 30 minutes, a feat which cannot be achieved by either NaTMP or Zn^tBu₂ on their own. Despite the greater reactivity of organosodium reagents in comparison to organozinc reagents, it is in fact the less electropositive zinc metal which is the source of reactivity within **1**. Formally, the C-H bond activations achieved by **1** manifest themselves as zincations, whereupon the reactivity of the zinc component is boosted by presence of the alkali metal. Due to its heteroleptic nature, **1** can function as an alkyl and/or an amido base (*vide infra*). Following the deprotonation of an organic substrate, the sodium zincate intermediate can be quenched with an electrophile or applied in a subsequent cross-coupling reaction.



Scheme 1.17 A selection of examples of alkali-metal-mediated-zincation reactions performed by sodium TMP-zincate **1**.^{128a, 131}

Intriguingly, **1** can also perform nucleophilic addition across unsaturated substrates. For example, **1**, 6-nucleophilic addition occurs upon reaction with benzophenone (Scheme 1.18).^[144] One significant advantage of bimetallic bases is their capacity to execute the dideprotonation of organic substrates. For example, the 1,4-dideprotonation of benzene was achieved through reaction with two molar equivalents of NaTMP and ^tBu₂Zn, followed by the addition of TMEDA.^[145]

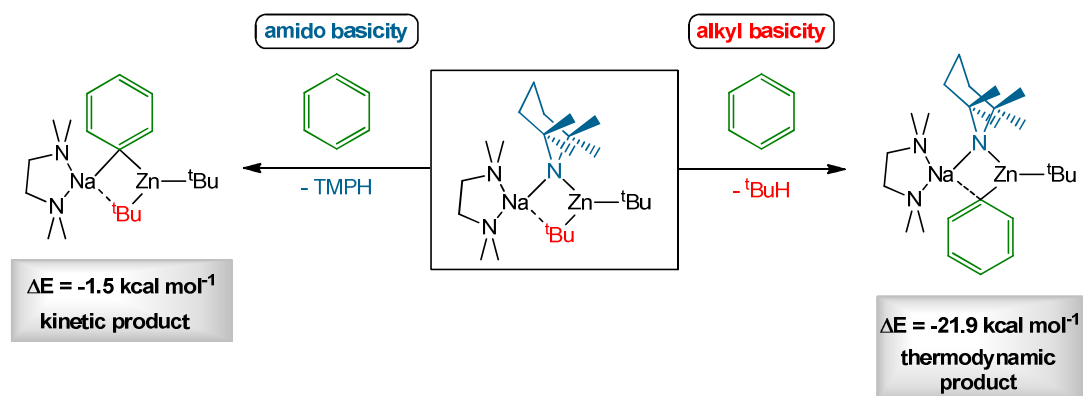


Scheme 1.18 Reaction of sodium TMP-zincate **1** as a nucleophilic addition agent towards benzophenone (LHS) and as a deprotonation agent towards the C-H bond activation of benzene (RHS).

This bimetallic cooperativity within **1** is further exemplified through the metallation of *N,N*-dimethylaniline.^[143c] As *N,N*-dimethylamine is a weak *ortho*-directing group, deprotonation in the *ortho*-position is observed with *n*-butyllithium under forcing conditions.^[146] Unexpectedly, reaction with **1** resulted in deprotonation in the *meta*-position, with concomitant formation of a Zn-C σ -bond. The greater stability of the *meta*-isomer was reinforced *via* DFT calculations. Despite the fact Zn bonds directly to the substrate, it is the relative strength of the Na- π C₆H₄ interaction which contributes significantly to the greater stability of the *meta*-isomer. Alternatively, *ortho*-metallation (sodiation) of *N,N*-dimethylamine can be performed through reaction with monometallic *n*-butylsodium under mild reaction conditions (stirred for 2 hours at 0 °C in hexane solution).^[147] Intriguingly, a sequential zincation of this arylsodium intermediate with di-*tert*-butylzinc selectively generates the *ortho*-isomer [(TMEDA)Na(μ -*o*-C₆H₄-NMe₂)₂Zn(^{*t*}Bu)], in contrast to the *meta*-regioselectivity observed using a direct, sodium mediated zincation approach. Thus the synergic combination of the two metals within one molecular environment, prior to reaction with *N,N*-dimethylaniline, plays an imperative role in the unprecedented regioselectivity obtained.

In 2008, Uchiyama published a theoretical study detailing the mechanistic pathway of the reaction of benzene with **1**.^[148] This insightful investigation emphasises the

complicated nature of this potentially alkyl or amido base. The amido ligand is calculated to be the more kinetically active base, performing the initial deprotonation of an organic substrate. This can be attributed in part to the greater polarity and hence lability of Zn-N bonds in comparison to Zn-C bonds. However, TMP then re-enters the complex as the thermodynamically driven protonation of the alkyl ligand (^tBu) occurs. *Iso*-butane is lost which means the reaction cannot go backwards. Overall, **1** therefore exhibits alkyl basicity. The donor ligand TMEDA also plays a part in the overall reactivity of the base as it enhances the deprotonation capacity of the TMP ligand. Although this study provides insight into the complex mechanism involved in this reaction, the theoretical calculations were performed using a simplified version of the base, [(TMEDA)Na(μ-NMe₂)(μ-Me)Zn(Me)]. This step-wise reactivity has also been reported for lithium zincate bases.^[149] The concept of the two-step mechanism, along with experimental evidence that has since been accrued to support these theoretical calculations, shall be discussed in further detail in Chapter 6.



Scheme 1.19 DFT modelled reaction of **1** with benzene, displaying amido basicity (LHS) or alkyl basicity (RHS).^[140a]

Due to the lesser stability of the resultant carbanion, the C-H bond activation of sp³ hybridised substrates presents a more challenging prospect than that of sp² hybridised substrates. However, sp³ C-H bond cleavage has been successfully achieved. For example, deprotonation of the CH₃ group of ketiminate ligands has been realised using heavier group 2 alkyl bases.^[150] Moreover, deprotonation of the cyclic ether

and common solvent THF can be achieved by conventional organolithium reagents. However the lithiated heterocyclic intermediate is highly unstable and spontaneously undergoes ring opening and cleavage even at subambient temperatures.^[151] Turning to the synergic sodium zincate base, [(TMEDA)Na(μ -TMP)(μ -CH₂SiMe₃)Zn(CH₂SiMe₃)], has enabled the deprotonation of THF (and its higher analogue tetrahydropyran) along with stabilization of this sensitive anion (Figure 1.11).^[152] As the deprotonated THF ring is encapsulated within the bimetallic framework, it is stabilized by both Lewis acidic metals and is not subjected to ring opening. Nucleophilic C₄H₇O can be applied to subsequent bond-forming reactions and be intercepted with an electrophile (benzoyl chloride).

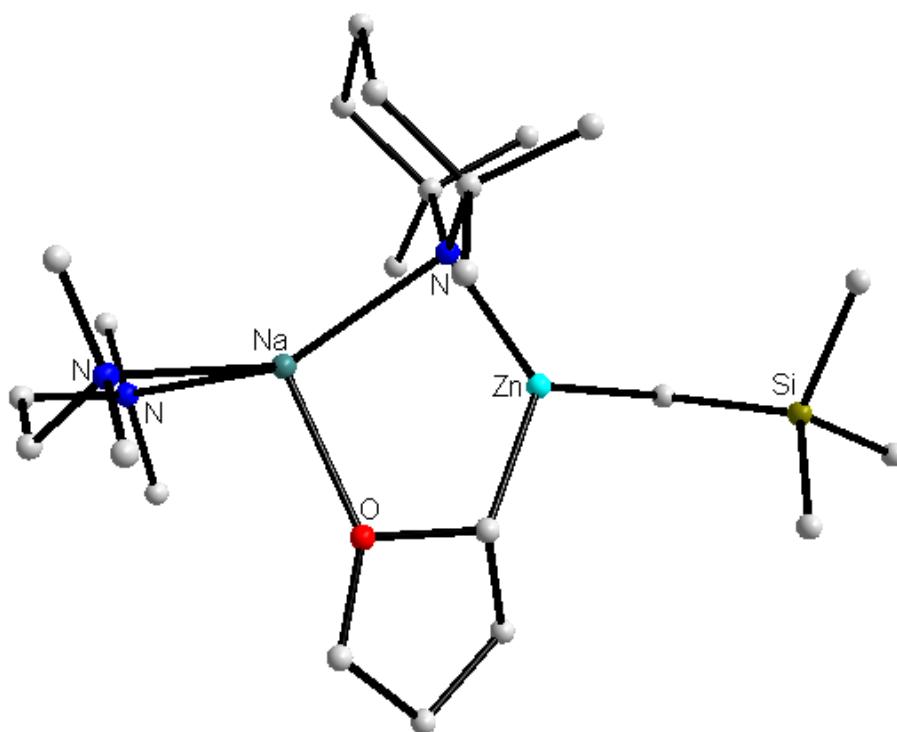


Figure 1.11 Molecular structure of [(TMEDA)Na(μ -TMP)(μ -C₄H₇O)Zn(CH₂SiMe₃)].^[152]

It is notable for comparison that the synergic aluminate base [(THF)Li(μ -TMP)(μ -TMP)Al(^{*i*}Bu)₂] has since been used to accomplish a similar deprotonation of THF.^[153] This aluminate base displays certain advantages over its sodium zincate counterpart, such as a faster reaction time, commercial availability of all starting materials and the stoichiometric addition of THF. In contrast, reaction of THF with

the sodium TMP-magnesiate [(TMEDA)Na(μ -TMP)(μ -CH₂SiMe₃)Mg(TMP)] resulted in cleavage of the cyclic ether. Heterocyclic THF only has thirteen bonds and in this extraordinary bimetallic executed reaction, six of them are cleaved. Each decomposition fragment was captured by a bimetallic framework; namely an oxygen dianion [encapsulated within a {Na₂Mg₂(TMP)₄} scaffold] (Figure 1.12a) and a remarkable 1,4-dimagnesiated butadiene product (Figure 1.12b).^[154]

Other unusual sp³ C-H bond activations have been achieved using bimetallic bases, such as the surprising generation of a TMP dianion.^[155] This was achieved through the combination of KTMP, (ⁱBu)₂Al(TMP) and TMEDA in a 1:1:1 stoichiometric ratio in a hydrocarbon medium, which produced crystalline potassium aluminate [(TMEDA)K(μ -TMP*)(μ -ⁱBu)Al(ⁱBu)]. Here, TMP* represents a dideprotonated TMP(H) unit, which has firstly been deprotonated at the most acidic secondary amine site, and secondly at the much more challenging, less acidic CH₃ position. Structural elucidation through X-ray diffraction studies, in conjunction with solution state analysis through multinuclear NMR experiments, confirmed that the product involves a TMP dianion, which functions as a didentate (C, N) donor towards aluminium in the solid state. Similarly, the bimetallic combination of LiTMP, (ⁱBu)₂Al(TMP) and one molar equivalent of TMEDA or PMDETA was used to achieve the deprotonation of TMEDA and PMDETA at the terminal N-CH₃ position.^[156]

These reactions demonstrate the unique reactivity that can be achieved through the harmonic cooperation of two metals, enabling unprecedented structures and reactivity to be achieved. Given the benefits associated with bimetallic reagents, especially considering their relative newness in comparison to their well developed monometallic relatives, suggests that in the future, bimetallic C-H bond activation strategies could overtake the current monometallic approaches. Therefore, the development of bimetallic chemistry, with an emphasis on sodium zincate reagents, was chosen as the primary focus of this PhD project.

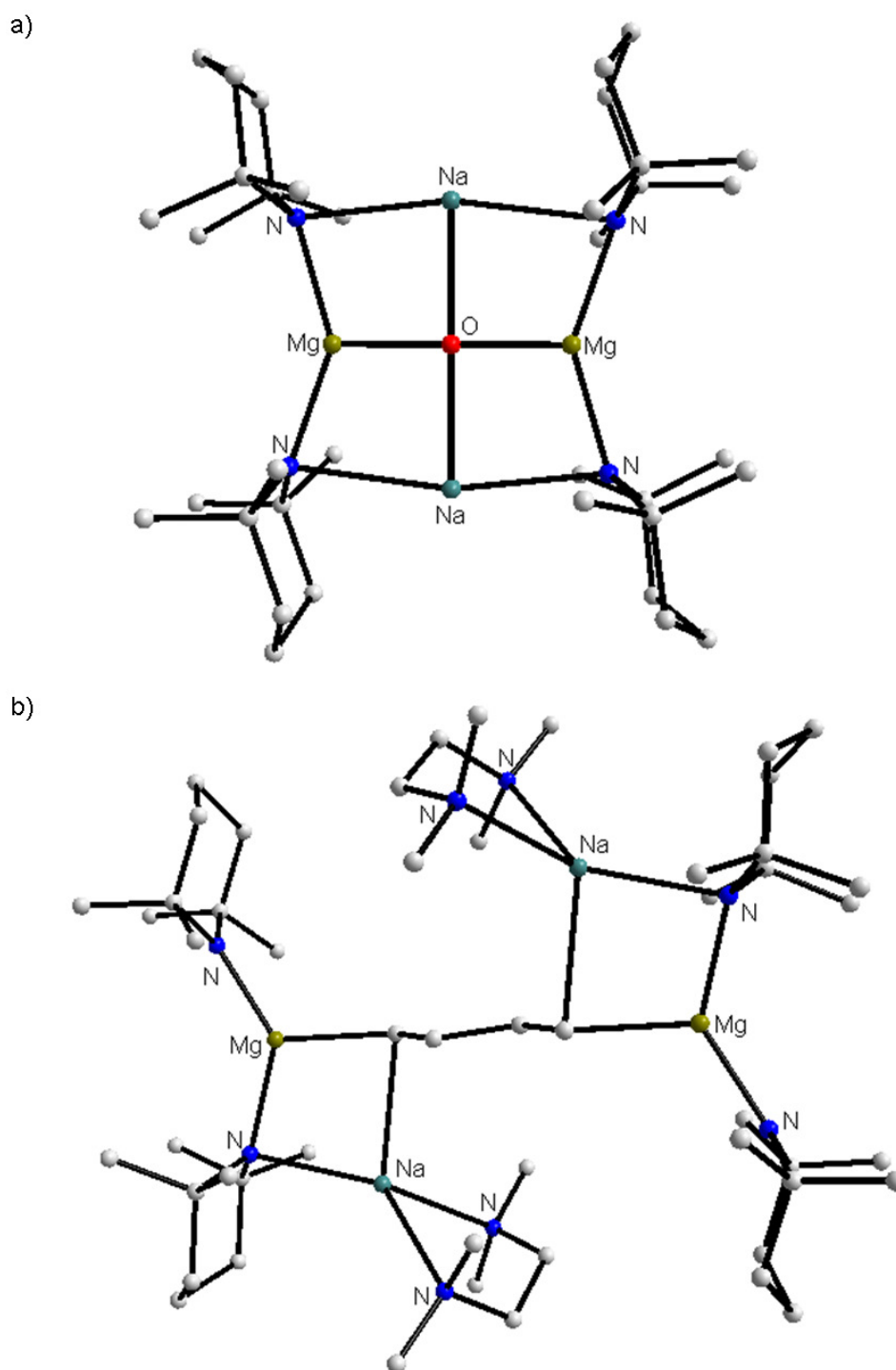


Figure 1.12 Molecular structure of products obtained from the cleavage of THF by $[(\text{TMEDA})\text{Na}(\mu\text{-TMP})(\mu\text{-CH}_2\text{SiMe}_3)\text{Mg}(\text{TMP})]$ into a) $[\text{Na}_2\text{Mg}_2(\text{TMP})_4\text{O}]^{[157]}$ and b) $[\{(\text{TMEDA})\text{Na}(\mu\text{-TMP})\}_2\{1,4\text{-}[\text{Mg}(\text{TMP})_2\text{-C}_4\text{H}_4]\}]^{[154]}$.

1.15 Aims of the PhD Research Project

The central thrust of this 42 month PhD project was to extend the deprotonation chemistry of organic substrates by organometallic bases, with an emphasis on synergic, sodium zincate systems. As structure and reactivity are closely connected, one of the key aims was therefore to develop new sodium zincates bearing unusual structural motifs. Subsequently, their reactivity towards C-H bond cleavage (or nucleophilic addition) was to be probed.

In order to gain structural insight into these reagents and subsequent reaction pathways, the isolation of crystalline sodium zincates and metallated reaction intermediates were targeted, to enable structural elucidation through X-ray diffraction studies. A further goal was to characterise these species in the solution state through a combination of NMR spectroscopic experiments including ^1H , ^{13}C , COSY, HSQC, NOESY and DOSY. Furthermore, electrophilic quenching and DFT calculations were to be applied where appropriate to gain further insights into the reaction pathways.

Specifically, the metallation of trifluoromethylbenzene with mono- and bimetallic bases has previously been reported, however a mixture of *ortho*-, *meta*- and *para*-metallated derivatives is typically observed. Our goal in this part of the work was therefore to improve the regioselectivity of the metallation of trifluoromethylbenzene (Chapter 2). This was approached systematically through the reaction of trifluoromethylbenzene with group 1 alkyl bases in the presence of different Lewis donor solvents, to study the yields and regioselectivity.

To the best of our knowledge, prior to the research described here no crystallographically-characterized zinc complex involving an unsubstituted pyrrole anion has ever been reported. Furthermore, the development of heteroleptic organometallic systems presents benefits within cross-coupling chemistry through reducing the number of potential coupled side-products. Thus another objective

within the overall aim was to synthesise a series of neutral zinc, lower-order and higher-order zincate pyrrole complexes (Chapter 3).

Owing to its predominance throughout active pharmaceutical ingredients, an additional goal of this project was to examine the metallation of *N*-Boc pyrrolidine using the sodium zincate base [(TMEDA)Na(μ -TMP)(μ -^tBu)Zn(^tBu)], with a view to developing a deprotonation strategy superior to the current ones published in literature (Chapter 4).

The majority of current sodium zincate systems are based on the bulky secondary amide TMP. With the aim to replace monofunctional TMP with a multifunctional amide within a sodium zincate framework, we hoped to develop sodium zincates with unprecedented structures. Multifunctional amines 2,2'-dipyridylamine [dpa(H)] (Chapter 5) and *N'*-benzyl-*N,N*-dimethylethylenediamine [BD(H)] (Chapter 6) were selected for this investigation. The supplementary goal was to test the reactivity of such sodium zincates towards C-H bond cleavage and nucleophilic addition.

Chapter 2

Lewis Base-Activated Lithiation and Sodiation of Trifluoromethylbenzene: Structural, Spectroscopic and Theoretical Insights

“Nothing has the power to broaden the mind
as the ability to investigate systematically
and truly all that comes under thy observation in life.”

Marcus Aurelius
Roman Emperor and philosopher

2.1 Summary

Aiming to accrue new information on the stability and constitution of the organometallic intermediates involved in directed *ortho*-metallation (DoM) processes, using trifluoromethylbenzene as a case study, this part of the PhD project investigates the deprotonation of trifluoromethylbenzene using the popular group 1 alkyl bases ^tBuLi and ⁿBuNa in the presence of the Lewis base additives TMEDA (*N,N,N',N'*-tetramethylethylenediamine), THF and PMDETA (*N,N,N',N',N''*-pentamethyldiethylenetriamine). Through a combination of structural, spectroscopic and theoretical studies, it is revealed that these donors have a strong influence upon the final outcome of the reaction. Not only does the donor ligand activate the alkali-metal base towards the deprotonation of the arene, it also tunes the regioselectivity of the reaction. Thus, while *ortho*-metallation of trifluoromethylbenzene is preferred using ^tBuLi and TMEDA, switching to THF gives a complex mixture of products with the *meta*-regioisomer being the major species in the solid state. This donor effect is significantly reduced when ⁿBuNa is employed, as *ortho* regioselectivity is observed almost exclusively using THF, TMEDA or PMDETA.

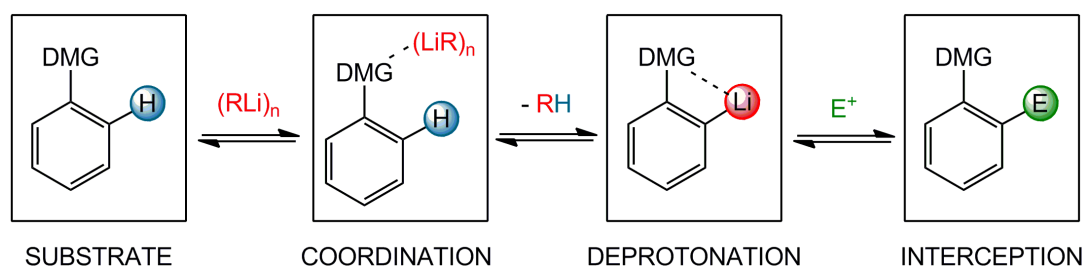
DFT calculations computing the relative energies of the *ortho*, *meta* and *para* regioisomers obtained from these metallating systems reinforce the experimental findings. These theoretical studies show that although in all cases the product of *ortho*-metallation is thermodynamically favoured, the energy difference between the three possible regioisomers is much larger for the Na systems than for the analogous Li systems. Furthermore, the structures of key metallated reaction intermediates have been elucidated by X-ray crystallographic studies. Interestingly, unusual Na \cdots F dative interactions are found for the Na derivatives, which appear to contribute to the overall stability of the *ortho*-metallated regioisomer, as they are absent from the *meta* and *para* structures.

2.2 Introduction

2.2.1 Directed *ortho*-Metallation: A Powerful Synthetic Tool

Recognised as familiar scaffolds within fine chemicals, poly-substituted aromatic rings are a commonly sought-after synthetic target. Their multistep synthesis often involves controlled, regioselective C-H bond cleavage and activation, succeeded by C-C bond formation. DoM (directed *ortho*-metallation), in particular directed *ortho*-lithiation, is well established as one of the most powerful synthetic preludes to achieving the direct functionalisation of aromatic molecules,^[24a; 24d; 45] where in this context, metallation refers to the conversion of a C-H bond to a C-metal (nearly always C-lithium) bond.

Pioneering studies by Wittig^[158] and Gilman^[159] on the lithiation of anisole constituted a milestone in the development of this synthetic methodology. Since then, the lithiation of this benchmark molecule in DoM chemistry has been much studied using NMR spectroscopy,^[160] semi-empirical calculations,^[160-161] kinetic isotope effects,^[162] and X-ray crystallography.^[163] Acting as a directing metallating group (DMG), the electron-rich MeO group provides a Lewis basic coordination point for an incoming organometallic reagent, bringing it into close proximity to an adjacent C-H unit enabling *ortho*-metallation (Scheme 2.1), although this mechanism still remains somewhat controversial with this particular substrate.^[33] This phenomenon is often referred to as a complex-induced proximity effect (CIPE).^[42]



Scheme 2.1 Sequential events of a general directed *ortho*-metallation (DoM) reaction.

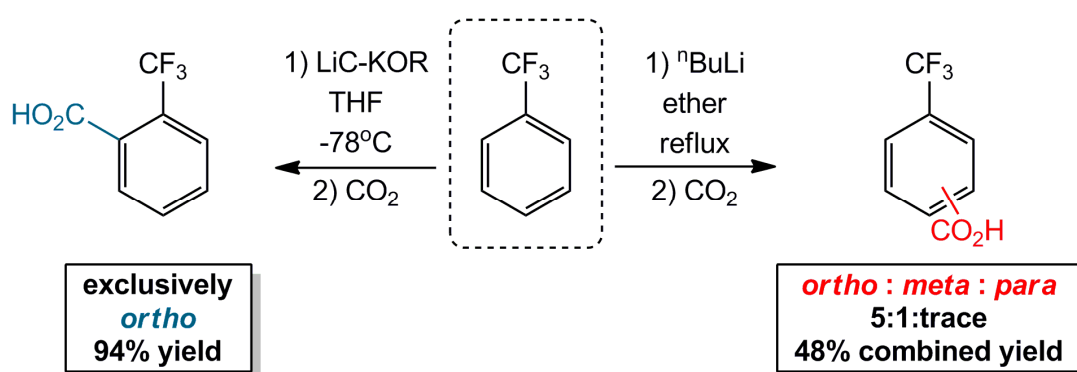
A second key factor in achieving this regioselectivity is the inductive effect of the MeO substituent, which enhances the acidity of the *ortho*-H atoms. For substrates bearing electron-withdrawing groups, (e.g., as in haloaromatic substrates),^[164] this can play a major role in directing the metallation. More than 70 years after the advent of DoM, a host of DMGs have been brought to light, the strongest of which promote *ortho*-metallation through a combination of the CIPE and inductive activation. Despite the extensive employment of organolithium reagents within DoM chemistry, there are surprisingly few known examples of structurally characterised *ortho*-lithiated intermediates.^[165]

2.2.2 Background to the Metallation of Trifluoromethylbenzene

Within this work, the substituted benzene we decided to focus our attention on was trifluoromethylbenzene, **2**. Often utilised as a solvent in organic synthesis,^[166] **2** is also a common intermediate in the synthesis of pharmaceuticals and agrochemicals.^[167] The CF₃ substituent of this aromatic fluorocarbon would be expected to promote DoM mainly on account of its strong electron-withdrawing capability. Indeed, *ortho*-metallation of **2** has been observed using ⁿBuLi in refluxing ether solution, although subsequent quenching by carbon dioxide gave an unexpected mixture of *ortho*- and *meta*-carboxylic acids in a combined 48% yield and in a ratio of 5:1 respectively, along with negligible quantities of the *para*-isomer (Scheme 2.2).^[168]

Intermediate in size between an ⁱPr and a ^tBu group, it is thought that the steric bulk of the CF₃ group disfavors *ortho*-metallation.^[169] Overcoming this, through applying the bimetallic “superbase” BuLi·KO^tBu (commonly written as LIC-KOR) in THF solvent at -78 °C,^[132a-d; 170] to the metallation of **2**, Schlosser observed regioselective *ortho*-deprotonation in a 94% yield.^[171] However, no metallated intermediates of these reactions prior to electrophilic interception were isolated or characterised within this work, and so the exact nature of the organometallic species involved is not yet known.

Bimetallic strategies have also been applied to the metallation of **2**. For example, it was recently shown that the direct zincation of **2** at room temperature using the zincate [(TMEDA)Na(μ -TMP)(μ -^tBu)Zn(^tBu)] gives a mixture of *ortho*-, *meta*- and *para*-zincated ring products in a respective ratio of 20:11:1 as determined by multinuclear NMR spectroscopy.^[172] Also, studies by Uchiyama of the alumination of **2** through reaction with the lithium TMP-aluminate [LiAl(TMP)(ⁱBu₃)] at 0 °C revealed the *meta*-product to be the predominant regioisomer (20% isolated yield), along with 10% of *ortho*- and 10% of *para*-metallation products.^[173] These moderate yields were achieved using an excess of the aluminate base (2.2 molar equivalents of base per 1 equivalent of substrate).



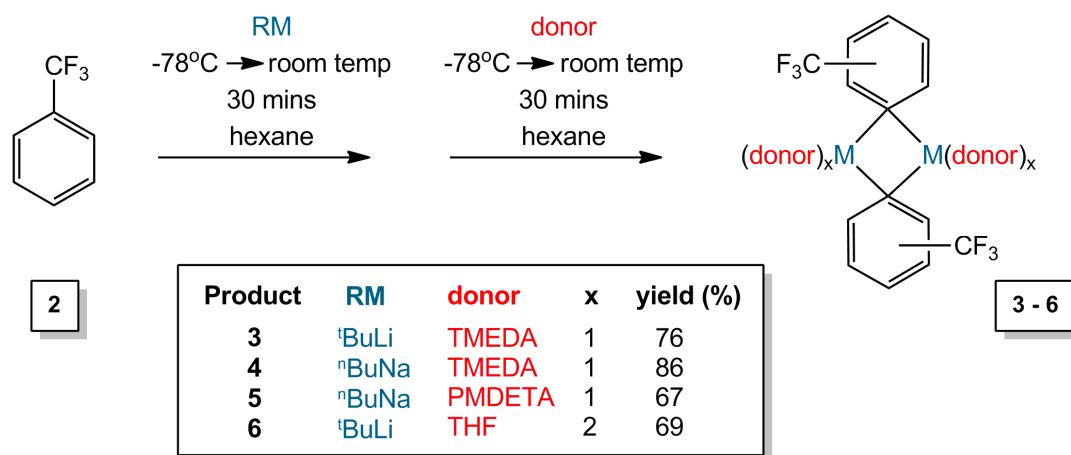
Scheme 2.2 Metallation of trifluoromethylbenzene using a group 1 monometallic (RHS)^[168] and bimetallic (LHS)^[171] base strategy.

To build on previous metallation studies of **2**, we have systematically investigated the deprotonation of **2** using the alkyl metallating reagents ^tBuLi and ⁿBuNa. Through combining spectroscopic and structural characterisation of the organometallic intermediates with theoretical calculations, this study offers new insights into the constitution and stability of the organometallic species involved and the influence that the application of the donors THF, TMEDA and PMDETA can have in improving the regioselectivity of the reaction.

2.3 Results and Discussion

2.3.1 Alkali metallation of trifluoromethylbenzene **2**

To start this part of the study the metallation of **2** by a group 1 alkyl base, specifically ${}^t\text{BuLi}$ or ${}^n\text{BuNa}$, in the presence of Lewis bases THF, TMEDA or PMDETA was investigated. Following the addition of either TMEDA or THF to the 1:1 stoichiometric reaction of ${}^t\text{BuLi}$ with **2**, a pale yellow solution was formed. The reaction of freshly prepared ${}^n\text{BuNa}$ with **2** produced a white suspension, which immediately changed colour to brown upon introduction of either TMEDA or PMDETA. Although the reactions were initially performed at $-78\text{ }^\circ\text{C}$ (Scheme 2.3), transferral of the resultant solutions to the refrigerator (at $-30\text{ }^\circ\text{C}$) allowed isolation of the crystalline solids $[(\text{TMEDA})\cdot\text{Li}(\text{C}_6\text{H}_4\text{-CF}_3)]_2$ (**3**), $[(\text{TMEDA})\cdot\text{Na}(\text{C}_6\text{H}_4\text{-CF}_3)]_2$ (**4**), $[(\text{PMDETA})\cdot\text{Na}(\text{C}_6\text{H}_4\text{-CF}_3)]_2$ (**5**) and $[(\text{THF})_2\cdot\text{Li}(\text{C}_6\text{H}_4\text{-CF}_3)]_2$ (**6**) after 1 day, in decent crystalline yields in the range 67%-86%. Homometallic compounds **3-6** were characterised in solution using multinuclear (${}^1\text{H}$, ${}^7\text{Li}\{{}^1\text{H}\}$, ${}^{13}\text{C}\{{}^1\text{H}\}$ and ${}^{19}\text{F}\{{}^1\text{H}\}$) NMR spectroscopy and the structures of **3-5** in the solid state were elucidated by X-ray crystallographic studies. Unfortunately, severe disorder in the crystallographic structure of **6** made it impossible to refine the molecular structure satisfactorily; hence no structural data can be presented.



Scheme 2.3 General synthesis of metallated aromatic products **3-6**.

2.3.2 Solid State Molecular Structures

Although solid state structures of polar organometallic compounds may not be replicated in solution, at the very least they provide a good guide to start unravelling the complexity of species normally encountered in solution.^[174] Accordingly, metallated intermediate complexes **3-5** were synthesised and isolated in a crystalline form suitable for the aforementioned X-ray crystallographic determinations. These metallated derivatives are intermediate in the sense they are still active and have not undergone the normal synthetic protocol of quenching these complexes with electrophiles.

Exhibiting a dimeric arrangement with the common formula [(donor)·M(C₆H₄-CF₃)]₂, (M = Li for **3**; M = Na for **4** and **5**), the molecular structure of each metallated intermediate complex contains a four-atom core in the form of a [MCMC] ring. Both metal corners are engaged in dative bonding with Lewis donors, namely one molecule of chelating TMEDA in **3** and **4**, and PMDETA in **5**. In each case, this [MCMC] ring is strictly (**3** and **4**) or essentially planar (**5**), where the sum of the endocyclic angles is 360° for **3**, 360° for **4** and 357° for **5**. This cyclic, dimeric motif is prevalent in alkali-metal chemistry, with known examples including alkali-metal alkyl,^[34; 175] alkali-metal aryl,^[176] alkali-metal amide^[177] and alkali-metal alkoxide^[22] complexes. In spite of these precedents, a surprisingly limited number of sodium based DoM intermediates (M = Na) have been isolated and structurally characterised. Thus, a search of the CCDB^[178] revealed that only three *ortho*-sodiated species have been published prior to the work reported herein.^[147; 179] One particularly relevant example comes from the *ortho*-sodiation of *N,N*-dimethylaniline by ⁿBuNa, which led to the isolation and structural characterisation of dimeric [{(TMEDA)·Na(*o*-C₆H₄-NMe₂)}₂].^[147]

There are two essentially identical distorted tetrahedral Li centres within lithiated intermediate **3**, each coordinated by two *ortho*-metallated trifluoromethylbenzene units and a chelating TMEDA (Figure 2.1). A crystallographic twofold axis in space group *C2/c* runs through both Li1 and Li2 and the centres of the C-C bonds of the

TMEDA ligands. The asymmetric unit therefore contains half of the dimeric molecule ($Z' = 0.5$). Equivalent within experimental error, the two distinct C-Li bond lengths in **3** [Li1-C1, 2.252(2) Å; Li2-C1, 2.251(2) Å] (Table 2.1) are comparable to those in the related lithium unsubstituted phenyl complexes [$\{\text{Li}(\text{C}_6\text{H}_5)\}_2\]_\infty (average Li-C bond length = 2.282 Å)^[180] and $[(\text{TMEDA})\cdot\text{Li}(\text{C}_6\text{H}_5)]_2$ (average Li-C bond length = 2.243 Å).^[181] It should be noted that no significant Li...F contacts are observed within **3**, with the shortest contact distance being Li2...F1 [3.2920(3) Å] which is essentially equal to the sum of the van der Waals radii for Li and F (3.29 Å, where the van der Waals radii of Li and F are 1.82 Å and 1.47 Å, respectively).^{[18:}
^{116]} This Li2...F1 distance is significantly longer than the Li-F bond length of 1.564 Å found within the LiF salt.^[182]$

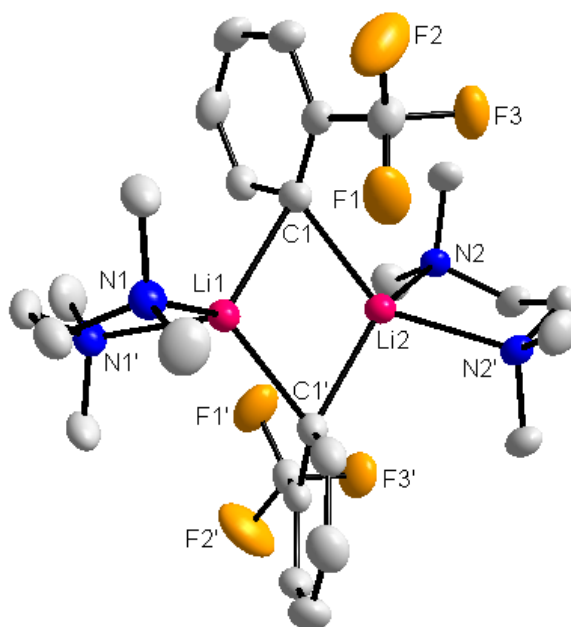


Figure 2.1 Molecular structure of **3** with displacement ellipsoids at the 50% probability level and hydrogen atoms omitted for clarity. Symmetry transformation used to generate equivalent atoms labelled ' : $1 - x, y, 0.5 - z$. Selected bond lengths (Å) and bond angles (°): Li1-N1, 2.238(3); Li1-C1, 2.252(2); Li2-N2, 2.244(3); Li2-C1, 2.251(2); N1-Li1-N1', 82.54(12); N1-Li1-C1, 112.52(5); N1-Li1-C1', 119.99(5); N1'-Li1-C1', 112.52(5); C1-Li1-C1', 108.05(15); N2-Li2-N2', 82.10(12); N2-Li2-C1, 98.26(5); N2-Li2-C1', 137.89(6); N2'-Li2-C1, 137.89(6); C1-Li2-C1', 108.09(14); Li1-C1-Li2, 71.93(10).

Table 2.1: Comparison of selected bond lengths and bond angles in metallated complexes [(TMEDA)·Li(C₆H₄-CF₃)₂], (**3**), [(TMEDA)·Na(C₆H₄-CF₃)₂], (**4**) and [(PMDETA)·Na(C₆H₄-CF₃)₂], (**5**).

Complex	Bond lengths and angles				
	M-F (Å)	M-C (Å)	C-M-C (°)	M-C-M (°)	M-F-C (°)
3	3.2920(3)	2.252(2)	108.05(15)	71.93(10)	101.583(3)
	3.4447(3)	2.251(2)	108.09(14)		90.593(3)
4	2.6415(7)	2.5580(12)	104.00(4)	76.00(4)	109.69(8)
5	2.6750(9)	2.7458(15)	102.20(4)	75.44(5)	113.55(5)
	3.2326(12)	2.6946(15)		77.13(5)	107.37(6)

Providing a comparison for **3**, the related aryl lithium, [(THF)₃·Li(C₆H₄F₄)], has a long, non-bonding Li···F interatomic distance of 3.448(4) Å.^[183] In contrast, significantly shorter Li···F bond lengths were observed for lithiated complexes [2,4,6-(CF₃)₃C₆H₂Li·OEt₂]₂ (2.252 Å)^[184] and [(THF)·{LiF(N^tBu)Si^tBu₂}₂]₂ (1.85 and 2.09 Å) (Figure 2.2).^[185] Within **3**, there is a dihedral angle of 77.31(6)° between the aryl ring plane and the Li1C1Li2C1' ring plane.

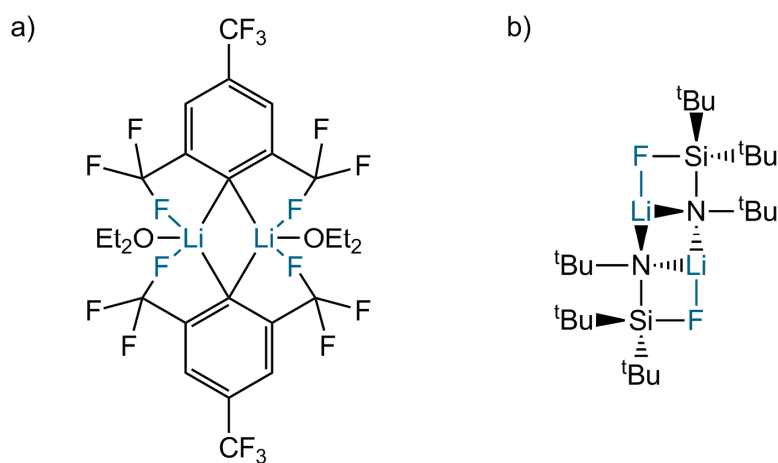


Figure 2.2 ChemDraw representation of the molecular structures of lithiated complexes a) [2,4,6-(CF₃)₃C₆H₂Li·OEt₂]₂^[184] and b) [(THF)·{LiF(N^tBu)Si^tBu₂}₂]₂ (THF solvent molecules omitted for clarity).^[185]

Presenting a rare example of an organometallic compound involving Na-F interactions, the crystal structure of **4** contains two independent molecules within its unit cell, which are essentially identical except for modest dimensional differences.

For brevity therefore the geometry of only one molecule shall be discussed (Figure 2.3). Each dimer lies about a $2/m$ centre with the twofold rotation axis running through the metal sites and the centres of the C-C bonds of the TMEDA and the mirror plane coincident with the plane of the aromatic group. The two symmetry-equivalent Na centres of each dimer of **4** are bridged *via* the *ortho*-C of deprotonated **2**, with an additional two dative Na-F interactions providing further stabilisation. Finally, a didentate TMEDA ligand completes the distorted octahedral geometry of Na [*cis* angles ranging from 68.38(4) to 104.00(4)° and *trans* angles ranging from 158.18(4) to 161.63(3)°].

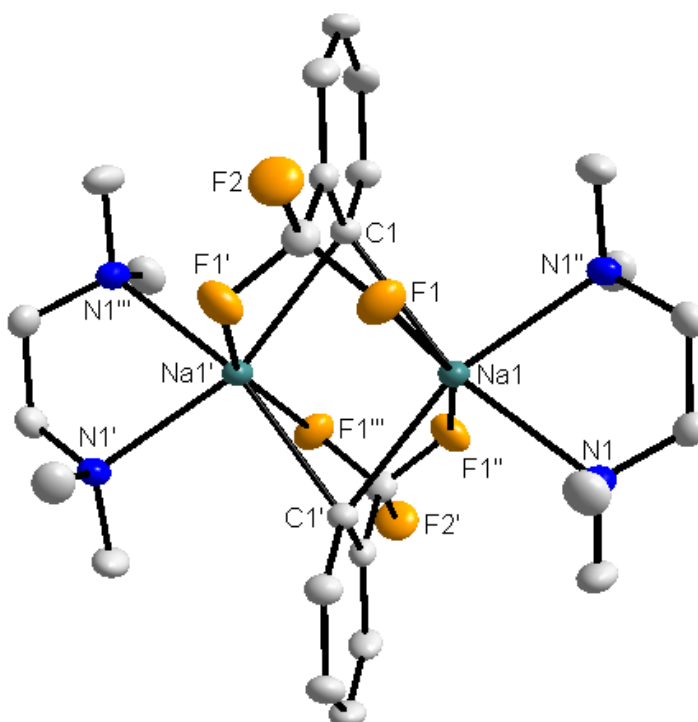


Figure 2.3 Molecular structure of **4** with displacement ellipsoids at the 50% probability level and hydrogen atoms omitted for clarity. Symmetry transformation used to generate equivalent atoms labelled ' : $x, -y, z$; '' : $1 - x, y, -z$; ''' : $1 - x, -y, -z$. Selected bond lengths (Å) and bond angles (°): Na1-F1, 2.6415(7); Na1-N1, 2.5234(10); Na1-C1, 2.5580(12); F1-C7, 1.3610(12); F2-C7, 1.3412(18); Na1-C1-Na1', 76.00(4); F1-Na1-F1'', 158.18(4); F1-Na1-N1, 102.39(3); F1-Na1-N1'', 95.29(3); F1-Na1-N1, 68.38(4); F1-Na1-C1', 97.78(4); N1-Na1-N1'' 71.77(4); N1-Na1-C1, 161.63(3); N1-Na1-C1', 92.78(3); C1-Na1-C1', 104.00(4).

Showing the ability of Na to raise its coordination number higher than that of its smaller congener Li, each Na centre is hexa-coordinate, whilst in contrast the Li centres within analogous **3** are only tetra-coordinate. This translates into a more acute bite angle of the chelating TMEDA ligand in **4** [N1-Na1-N1'', 71.77(4)°] in comparison to that of **3** [82.32° average]. Unlike the lithiated intermediate **3**, within **4** the CF₃ substituent of **2** is able to approach the sodium centre more closely, facilitating Na-F interactions that are further assisted by the higher coordination number achievable with Na. The Na1-F1 bond length of 2.6415(7) Å (Table 2.1) therefore lies significantly below the sum of the van der Waals radii for Na and F (3.74 Å; where Na is 2.27 Å and F is 1.47 Å),^[18; 116] although it is greater than the sum of the relevant ionic radii (2.31 ppm)^[137] and the bond length of the NaF salt (1.926 Å).^[182]

This interatomic metal-halide distance lies within the scope of Na-F bond lengths for other crystallographically characterised compounds, ranging from 2.175(3) Å for [Cr₃(dpa)₄F₂Na(H₂O)BF₄]BF₄·CH₃OH^[186] at the short end of the scale^[187] (where dpa = 2,2'-dipyridylamide) to 3.000(2) Å for [Na(*p*-HC₆F₄N(CH₂)₂NEt₂)₂Na(TMEDA)].^[188] Lying in the midst of this range, the related sodium zincate [(TMEDA)Na(μ-TMP)(μ-C₆H₄-CF₃)Zn(^tBu)] possesses a Na...F bond length of 2.435 Å, as modelled through DFT calculations for the *ortho*-zincated isomer.^[172] Within **4**, the near perfect tetrahedral Na1-F1-C7 bond angle of 109.69(8)° also suggests that one lone pair of electrons of a tetrahedral, sp³-hybridised F atom datively coordinates to Na.

Experimentally exchanging didentate TMEDA for tridentate PMDETA, in the reaction of **2** with ⁿBuNa, led to the formation and isolation of **5** (Figure 2.4). By switching to this higher denticity amine, this structure now possesses only one CF₃ interaction with the Na centre. Aside from taking part in this Na-F interaction, which measures 0.033 Å longer than those in **4**, Na bonds to all three N atoms of PMDETA, and to one *ortho*-C of two aryl anions. This generates a distorted octahedral Na geometry overall, where the *cis* angles range from 65.38(4) to 125.78(5)° and the *trans* angles vary from 144.85(5) to 154.84(5)°.

Within **5**, the aryl units act as asymmetrical bridges with non-equivalent Na-C bond lengths [Na1-C10, 2.7458(15) Å; Na1-C20, 2.6946(15) Å]. Forming a short interaction, the Na1-F2 bond length is 2.6750(9) Å whilst the Na1-F3 separation distance is elongated at 3.2326(12) Å (Table 2.1). Dimeric **5** crystallises in the monoclinic space group $P2_1/m$ with half a molecule in the asymmetric unit. The addition of the asymmetric PMDETA ligand results in loss of the two fold rotation symmetry seen in **3** and **4** with intramolecular symmetry now restricted to the mirror plane that is coincident with the aromatic ring planes, as shown in Figure 2.4.

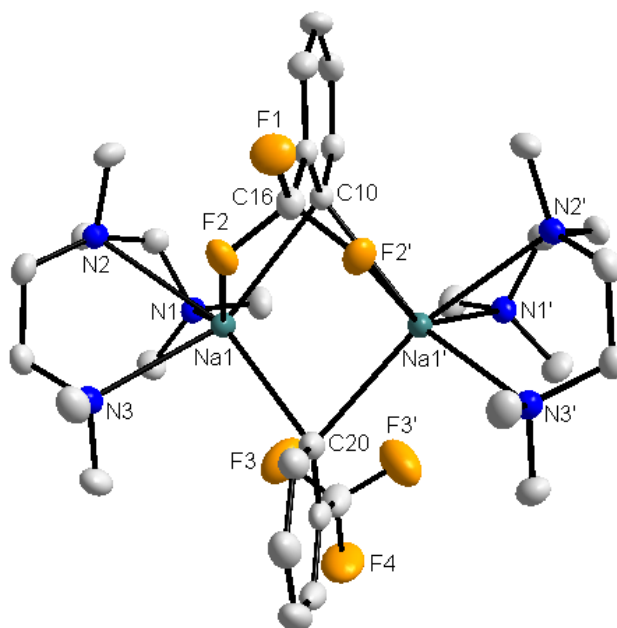


Figure 2.4 Molecular structure of **5** with displacement ellipsoids at the 50% probability level and hydrogen atoms omitted for clarity. Symmetry transformation used to generate equivalent atoms labelled ' : $x, 0.5 - y, z$. Selected bond lengths (Å) and bond angles ($^\circ$): Na1-F2, 2.6750(9); Na1...F3, 3.2326(12); Na1-N1, 2.6606(11); Na1-N2, 2.6824(12); Na1-N3, 2.6655(12); Na1-C10, 2.7458(15); Na1-C20, 2.6946(15); Na1-C20-Na1', 77.13(5); Na1-C10-Na1', 75.44(5); F2-Na1-N1, 148.42(3); F2-Na1-N2, 82.73(3); F2-Na1-N3, 82.17(3); F2-Na1-C20, 85.41(5); F2-Na1-C10, 65.38(4); N1-Na1-N2, 70.17(3); N1-Na1-N3, 102.01(4); N1-Na1-C20, 125.78(5); N1-Na1-C10, 99.25(4); N2-Na1-N3, 68.90(3); N2-Na1-C20, 154.84(5); N2-Na1-C10, 92.88(3); N3-Na1-C20, 87.58(4); N3-Na1-C10, 144.85(5); C20-Na1-C10, 102.20(4); Na1-F2-C16, 113.55(5).

Regrettably, severe disorder in the X-ray crystallographic analysis of the THF-solvated lithium aryl **6** prevented satisfactory elucidation of its molecular structure. However, from ^1H NMR spectroscopic analysis of the crystalline material it transpired that of the three potential regioisomers, the *meta*-metallated derivative of **2** was the prevailing product. In C_6D_6 solution, the relative ratio of *ortho:meta:para* isomers was established to be 1:10:3 (*vide infra*) from the relative integrals.

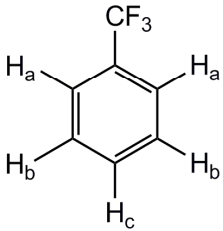
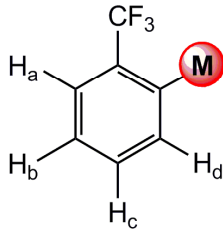
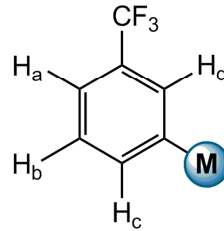
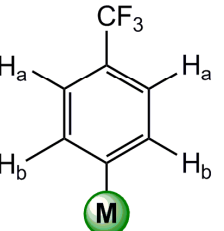
2.3.3 Solution NMR Spectroscopic Studies

Analysis of metallated intermediates **3-6** via multinuclear (^1H , $^7\text{Li}\{^1\text{H}\}$, $^{13}\text{C}\{^1\text{H}\}$ and $^{19}\text{F}\{^1\text{H}\}$) NMR spectroscopy in C_6D_6 solvent confirmed that in all cases a single C-H deprotonation of **2** has occurred (Table 2.2). Although only one equivalent of the group 1 alkyl base was employed within this study, other research has shown that the dimetallation of aromatic substrates is possible, through employing two equivalents of an organometallic base.^[189] For example, the remarkable 1,4-dimetallation of naphthalene was recently achieved using the synergic potassium magnesiate base “[NaMg(TMP)₂(ⁿBu)]”.^[189b] Reflecting the solid state structures (*vide supra*), only resonances corresponding to the *ortho*-isomer were observed for isolated crystals of **3-5**. The salient feature for each compound was the observation of four multiplets in the aromatic region of the spectrum, which are shifted downfield when compared with the resonances of precursor **2**. For example, the chemical shift for the *meta*-H (labelled as H_d and positioned adjacent to the site of metallation) moves significantly downfield, from 6.90 ppm in non-metallated **2**, to 8.32 ppm for **3**, 8.43 ppm for **4** and 8.48 ppm for **5** (Table 2.2).

Comparison of the ^1H NMR spectroscopic resonances attributed to TMEDA in **3** with that of non-coordinated TMEDA suggests that in C_6D_6 solution TMEDA remains coordinated to the electropositive metal centre, mirroring the solid state structure. This is manifested in a significant upfield shift for the corresponding NCH_3 and NCH_2 resonances, from 2.12 and 2.36 ppm respectively for free TMEDA to 1.71

and 1.64 ppm in **3**. Similarly, analogous upfield deviations are observed for TMEDA in **4**, PMDETA in **5** and THF in **6**, indicating that these Lewis donors also remain coordinated as would be expected in weakly-coordinating C_6D_6 solvent. Interpretation of the $^{13}C\{H\}$ NMR spectra reveals that varying the metal from Li in **3** to Na in congeneric **4** translates as a downfield movement of the C-M resonance, from 185.9 ppm to 192.5 ppm (Table 2.3), a difference of 6.6 ppm.

Table 2.2: Comparison of aromatic 1H NMR shifts (400.13 MHz, 300 K) in C_6D_6 solution for aromatic fluorocarbon **2** and metallated derivatives **3-6** (where M = Na or Li).

	2	3, 4, 5 and 6-ortho	6-meta	6-para
				
Compound	$\delta(H_a)$ ppm	$\delta(H_b)$ ppm	$\delta(H_c)$ ppm	$\delta(H_d)$ ppm
$CF_3C_6H_5$ (2)	7.32 (d)	6.90 (t)	6.97 (t)	-
$[(TMEDA) \cdot Li(C_6H_4-CF_3)]_2$ (3)	7.73 (d)	7.21 (t)	7.35 (m)	8.32 (d)
$[(TMEDA) \cdot Na(C_6H_4-CF_3)]_2$ (4)	7.76 (d)	7.16 (t)	7.32 (t)	8.43 (d)
$[(PMDETA) \cdot Na(C_6H_4-CF_3)]_2$ (5)	7.78 (d)	7.19 (t)	7.35 (t)	8.48 (d)
$[(THF)_2 \cdot Li(o-C_6H_4-CF_3)]_2$ (6-ortho)	7.74 (d)	7.21 (t)	7.38 (t)	8.31 (d)
$[(THF)_2 \cdot Li(m-C_6H_4-CF_3)]_2$ (6-meta)	7.56 (d)	7.31 (t)	8.40 (d)	8.63 (s)
$[(THF)_2 \cdot Li(p-C_6H_4-CF_3)]_2$ (6-para)	7.66 (d)	8.32 (d)	-	-

Whilst the NMR spectra of crystalline **3-5** displayed the resonances of a single metallated product resulting from *ortho*-deprotonation of **2**, the same analysis of the *in situ* reaction mixtures prior to crystallisation showed that, in the case of the reaction of $tBuLi/TMEDA$, small but significant amounts of *meta* and *para* lithiation products are present in solution (11% and 7% respectively, Table 2.4). As non-derivatised **2** is volatile, it is easily removed under vacuum and so residual **2** was not

detected *via* NMR spectroscopic analysis. Contrastingly, switching to ⁿBuNa as a metallating reagent in the reaction solutions producing **4** and **5** led to the almost exclusive formation of the *ortho*-metallated product.

Table 2.3: Comparison of metal-carbon ¹³C{¹H} NMR shifts (100.63 MHz, 300 K) in C₆D₆ solution for metallated products **3-6** (where M = Na or Li).

Compound	δ(C-M) ppm
[(TMEDA)·Li(C ₆ H ₄ -CF ₃) ₂], (3)	185.9
[(TMEDA)·Na(C ₆ H ₄ -CF ₃) ₂], (4)	192.5
[(PMDETA)·Na(C ₆ H ₄ -CF ₃) ₂], (5)	194.4
[(THF) ₂ ·Li(<i>o</i> -C ₆ H ₄ -CF ₃) ₂] (6-ortho)	185.9
[(THF) ₂ ·Li(<i>m</i> -C ₆ H ₄ -CF ₃) ₂] (6-meta)	179.5
[(THF) ₂ ·Li(<i>p</i> -C ₆ H ₄ -CF ₃) ₂] (6-para)	178.7

Table 2.4: *In situ* solution yields of the metallated aryl product.

Reaction	Metal Alkyl	Donor	Metallated Product Yield (%) ^a			
			<i>ortho</i> -	<i>meta</i> -	<i>para</i> -	Total
3	^t BuLi	TMEDA	67	11	7	85
4	ⁿ BuNa	TMEDA	76	0	0	76
5	ⁿ BuNa	PMDETA	81	0	0	81
6	^t BuLi	THF	35	26	12	73

a) Yields determined by ¹H NMR spectroscopy through addition of an internal standard (10 mol% hexamethylbenzene) to the metallated product solution.

Surprisingly given the pattern of results for **3-5**, NMR spectroscopic analysis of isolated crystals of **6** showed that in C₆D₆ solution the major product is the *meta*-isomer (Figure 2.5d), followed by *para* and *ortho* with a relative ratio of 10:3:1. However, NMR spectroscopic analysis of the crude reaction mixture, without removal of the crystalline solid (after stirring for 24 hours), revealed that overall, the *ortho* metallated product was the marginally preferred regioisomer (with a significantly closer *ortho:meta:para* ratio of 3:2:1, Table 2.4). Given that the solid isolated is predominantly **6-meta**, this suggests that the *meta*- product is the least

soluble and preferentially crystallises from solution. Within the $^{13}\text{C}\{^1\text{H}\}$ NMR spectra, the attenuating influence of the electron-withdrawing CF_3 substituent upon moving from **6-ortho**, to **6-meta**, to **6-para** significantly impacts upon the chemical shift of the metallated carbon atom, with an upfield sequential progression from 185.9, to 179.5, to 178.7 ppm, respectively (Table 2.3).

When analysed in C_6D_6 solution, ^1H NMR monitoring of crystalline **6** over a period of 5 hours revealed that the 1:10:3 ratio of *ortho:meta:para* regioisomers persisted. However, dissolution of **6** in deuterated THF solution induced a remarkably different outcome. Thus, as illustrated in Figure 2.5a, the aromatic resonances in the ^1H NMR spectrum of **6** in this polar solvent medium are considerably broad, and after 20 minutes in solution the almost complete conversion of both **6-meta** and **6-para** to **6-ortho** (Figure 2.5c) is witnessed. As heavier solvation generally favours reduced aggregation, it seems plausible that the dissolution of dimeric **6** in deuterated THF solvent promotes the formation of an externally solvated, monomeric intermediate. Solvent induced lithium migration could subsequently facilitate the conversion of the kinetic *meta*- and *para*-isomers to the thermodynamically favourable *ortho*-isomer. Within the context of DoM chemistry, Wheatley *et al.* have found that when isolated crystals of the *ortho*-lithiated product of 2-ethyl-*N,N*-diisopropyl-1-benzamide are dissolved in deuterated THF, a rearrangement takes place in solution, to give the product of lateral lithiation which in this case is most thermodynamically favoured.^[165d] It is worth noting that DFT calculations support the proposal that this lateral rearrangement occurs through a monomeric intermediate. In contrast, no changes were observed in the NMR spectra of crystalline **3-5** in either C_6D_6 or d_8 -THF solution, as would be expected on the basis that crystalline **3-5** include purely the *ortho*-metallated derivatives of **2**.

For completeness, we next monitored the regioselectivity of the lithiation of **2** (employing THF as the donor ligand) over a period of 24 hours. Accordingly, the *in situ* iodine quench products were analysed through ^1H NMR spectroscopy to probe the possibility of a thermodynamically driven rearrangement. The results of this study (Table 2.5) demonstrate that the relative ratio of *ortho*-, *meta*- and *para*-iodo-

trifluoromethylbenzene isomers remains largely consistent over time, although the collective yield after only ten minutes is considerably smaller than that after 100 minutes. Decomposition was observed when the reaction was performed over a longer time period of 24 hours and accordingly, the overall yield was lowered by 11%, from 80% after 100 minutes, to 69% after 24 hours. Therefore, these findings show that the presence of excess Lewis basic THF solvent is required for the thermodynamically driven rearrangement to the *ortho*-product. It is worth noting that the yields of the *ortho*-, *meta*- and *para*-iodo-trifluoromethylbenzene (Table 2.5) give good agreement with those of the *in situ* metallated aryl product (Table 2.4) obtained prior to iodine quenching.

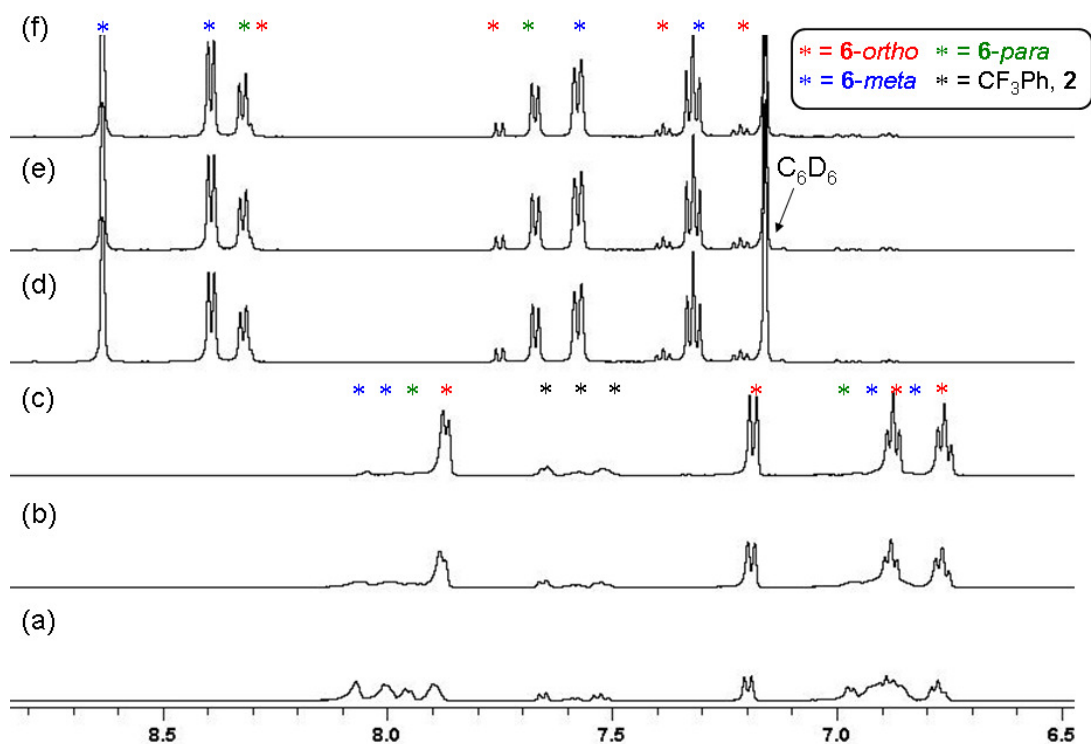
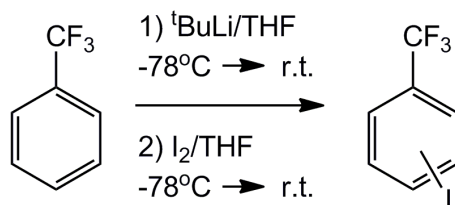


Figure 2.5 Aromatic region of ^1H NMR spectra for d_8 -THF solutions [(a-c)] and C_6D_6 solutions [(d-f)] of isolated crystals of **6** after a) 0 mins, b) 80 mins, c) 5 hours, d) 0 mins, e) 80 mins and f) 5 hours.

Table 2.5: Effect of reaction time on the yield and ratio of iodo-trifluoromethylbenzene regioisomeric products.

Entry	Metal Reagent	Donor	Reaction Time (h)	Iodinated Product Yield (%) ^[a]			
				<i>ortho</i> -	<i>meta</i> -	<i>para</i> -	Total
1	^t BuLi	THF	10 mins	8	8	4	20
2	^t BuLi	THF	100 mins	32	31	17	80
3	^t BuLi	THF	24 hrs	30	26	13	69

a) Conditions: CF₃Ph (2 mmol), ^tBuLi (2 mmol), THF (4 mmol), hexane (10 mL). Yields determined by ¹H NMR spectroscopy through addition of an internal standard (10 mol% hexamethylbenzene) to the iodinated product.

2.3.4 DFT Computational Studies

To attempt to quantify the energetics involved in the formation of these metallated species, the aforementioned solid state and solution studies were augmented by a complementary gas phase theoretical study investigating the reaction of **2** (model **2_{calc}**) with each of the following metal alkyl reagents ^tBuLi/TMEDA, ⁿBuNa/TMEDA, ^tBuLi/THF and ⁿBuNa/THF in turn. Calculations were carried out to probe the relative energies of the regioisomers of compounds **3** (model **3_{calc}**), **4** (model **4_{calc}**), **6** (model **6_{calc}**) and [(THF)₂·Na(C₆H₄-CF₃)]₂ (model **7_{calc}**), first utilising the B3LYP^[190] functionals and the 6-311G (d, p)^[191] basis set. The resultant optimised geometries were subjected to a frequency analysis, and the total energy computed by the DFT calculation was adjusted by inclusion of the zero-point energy contribution. These compounds were modelled as dimeric structures, to match the arrangements observed in the experimental structural studies.

A comparison of the geometrical parameters calculated for **3_{calc}** and **4_{calc}** with those observed experimentally from X-ray determination of the solid state structures show good agreement. For both **3_{calc}** and **4_{calc}**, the theoretical model resulting from *ortho*-deprotonation of **2** was determined to be the energetically preferred product. In each case, the energy difference between the *ortho* and *meta* regioisomers is much larger (+7.48 and 15.47 kcal mol⁻¹ respectively) than that between the *meta* and *para* ones (+3.10 and 3.68 kcal mol⁻¹ respectively), as shown in Figure 2.6.

It is discernible from the DFT calculations for **3_{calc}** and **4_{calc}** that there is a smaller energy difference between the regioisomers **3_{calc-ortho}**, **3_{calc-meta}** and **3_{calc-para}** (spanning 10.58 kcal mol⁻¹) than between those of the sodium congeners **4_{calc-ortho}**, **4_{calc-meta}** and **4_{calc-para}** (spanning 19.15 kcal mol⁻¹). Consequently, this supports the superior selectivity towards the *ortho*-isomer observed experimentally for the reaction of ⁿBuNa/TMEDA with **2**. This trend is mirrored to a less significant extent by models **6_{calc}** and **7_{calc}**, where the energy difference of **6_{calc-ortho}**, **6_{calc-meta}** and **6_{calc-para}** spans 11.25 kcal mol⁻¹ compared with 15.44 kcal mol⁻¹ for **7_{calc-ortho}**, **7_{calc-meta}** and **7_{calc-para}**. Comparing the geometrical parameters of model **3_{calc}** with those of compound **3** reveals a significant overestimation in the theoretical model for Li···F interactions [with lengths of 2.897 and 3.123 Å in contrast to experimental values of 3.2920(3) and 3.4447(3) Å]. A similar but more modest effect is observed for the Na···F contacts in **4_{calc}** and **4** [2.519 vs 2.6415(7) Å]. Therefore, this general trend predicts a similar overestimation for model **6_{calc}**, where the Li···F interatomic distances [2.995 and 3.001 Å] are too long to be significant.

Collectively, these DFT calculations reinforce the experimental observations within this investigation. However, the predominance of the *meta*-lithiated species (**6_{meta}**) in the solid state is surprising, as calculations show **6_{calc-ortho}** to be the most energetically stable product. Indeed **6_{ortho}** is the major product observed experimentally in the *in situ* reaction mixture. However, the predilection towards **6_{meta}** and **6_{para}** in the solid state may originate from the relatively large dimerisation energy gain associated with the formation of these species (-11.23 kcal mol⁻¹ for **6_{calc-meta}** compared to -9.32 kcal mol⁻¹ for **6_{calc-para}** and -5.18 kcal mol⁻¹

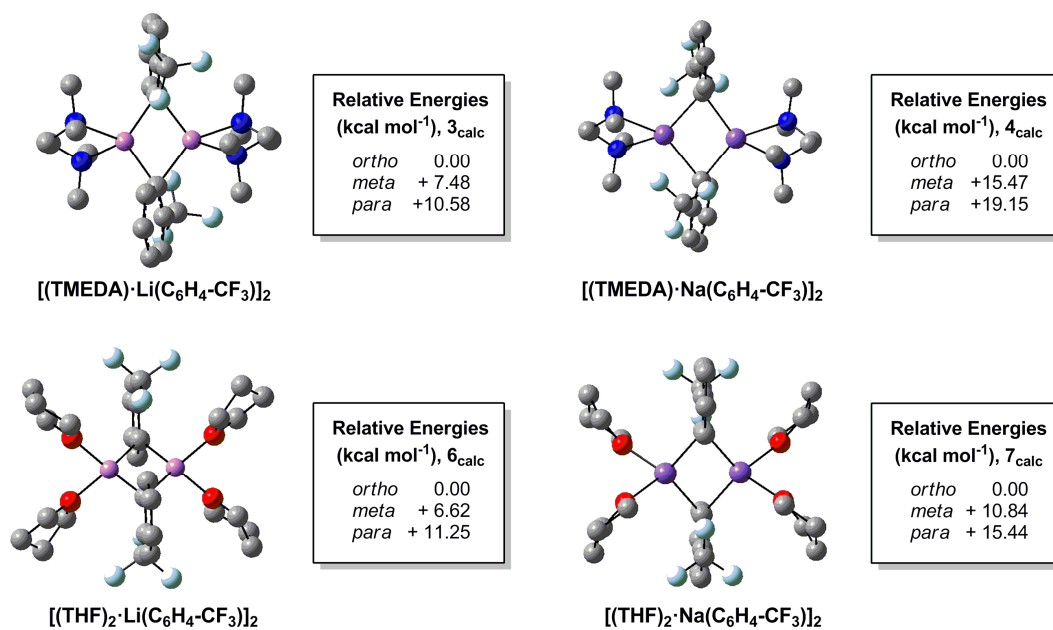
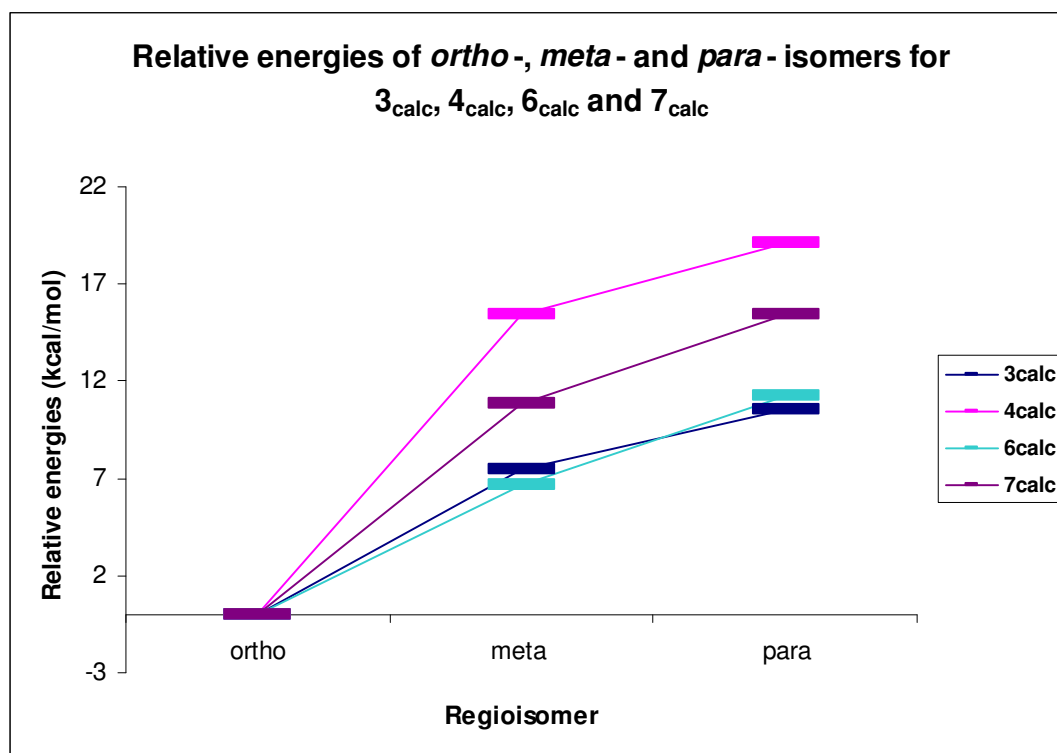


Figure 2.6 Relative energies of DFT-modelled compounds 3_{calc}, 4_{calc}, 6_{calc} and 7_{calc} (picturing the energetically favoured *ortho*-isomers).

for 6_{calc}-*ortho*). DFT modelling of 6_{calc} in the theoretical monomeric state shows the *ortho*-product to be more thermodynamically favourable than the *meta*- and *para*-

products (by +9.37 and +9.76 kcal mol⁻¹ respectively), which can be partly attributed to the presence of Li···F interactions. Although **6**_{calc-ortho} remains the energetically preferred product upon moving to the more realistic dimeric model, the balance swings in favour of **6**_{calc-meta} (+6.62 kcal mol⁻¹). It seems likely that the relatively low dimerisation energy gain associated with **6**_{calc-ortho} is influenced by the disruption of the Li···F interaction present in the monomeric model, as it is replaced by a secondary Li-C bond.

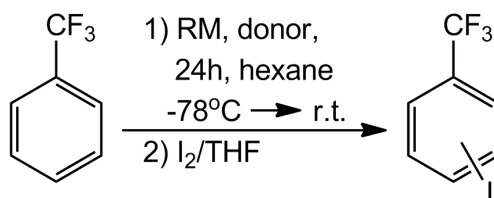
2.3.5 Post-metallation NMR Spectroscopic Analysis: Electrophilic Quenching Studies with Iodine

After running the metallation reactions for 24 hours at ambient temperature, *in situ* iodine quenching of reaction mixtures of compounds **3-6** was performed. Subsequent analysis of the quenched products *via* multinuclear (¹H, ¹³C{¹H} and ¹⁹F{¹H}) NMR spectroscopy in deuterated chloroform solvent revealed the successful mono-metallation of **2** that led to the formation of iodo-trifluoromethylbenzene,^[172] with further 2-dimensional (¹H-¹H COSY) NMR experiments confirming the presence of three regioisomers (*ortho*-, *meta*- and *para*-). Throughout the electrophilic quenching process, the reaction mixture was surrounded with a black bag to protect it from light due to the light-sensitive nature of iodo-trifluoromethylbenzene.^[16] This collection of results (Table 2.6) discloses that the careful choice of metal reagent and Lewis basic solvent enables us to improve the regioselectivity of metallation. Within this investigation, the best yield (82%) with high selectivity (80% *ortho*-directed) was secured employing the ⁿBuNa/PMDETA combination as the metallation system. In general, the yields of the iodinated products for entries 2-3 and 6-7 (Table 2.6) exhibit little deviation from the *in situ* metallated yields (Table 2.4) indicating that the quenching reactions were clean.

Relevant to the present study, one of the most interesting quotes about donor-activated organolithiums came from Schlosser, who stated that “Even if suspected to

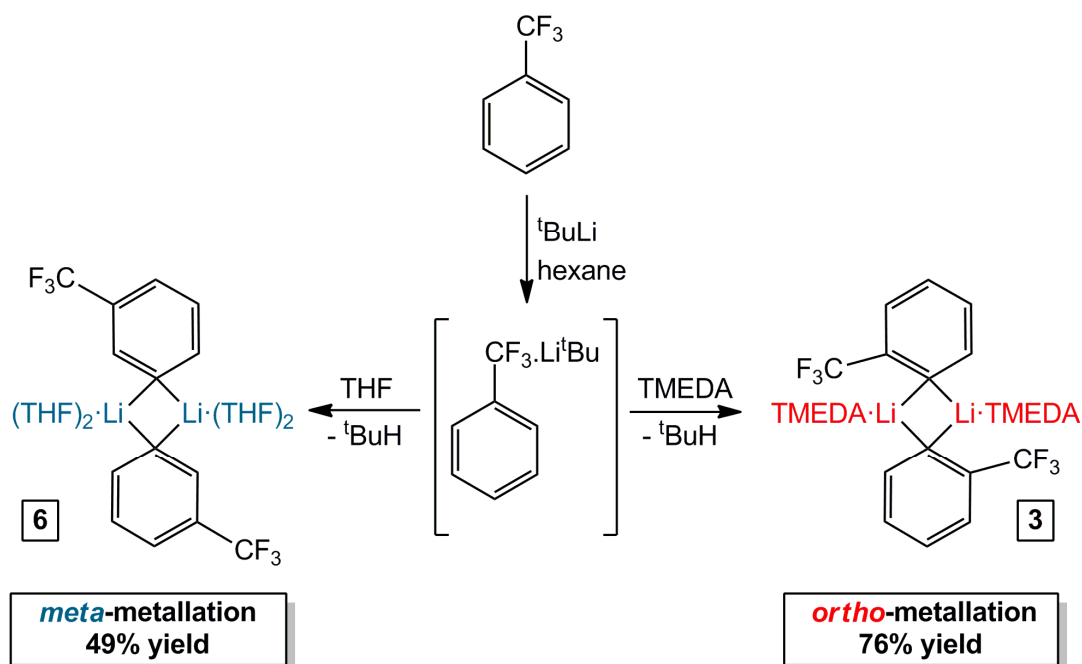
produce sometimes a “placebo effect”,^[33] *N,N,N',N'*-tetramethylethylenediamine (TMEDA) is often added to *n*-butyllithium as a reactivity enhancing complexand.”^[24d] It is a fact well exploited by synthetic chemists that the introduction of Lewis donors to polar organometallic reagents can greatly boost their reactivity.^[28] Accordingly, in this study we found that no metallation of **2** occurs when neat ^tBuLi was administered in hexane solution (Table 2.6, entry 1). Exemplifying the essential requirement for the donor solvent, use of ^tBuLi in tandem with THF gave *ortho*-, *meta*- and *para*-metallated **2** in a relative ratio of 30:26:13 (entry 2). Simply switching to the more basic TMEDA as the donor solvent improved the regioselectivity to a ratio of 65:10:6 (entry 3), diminishing the quantities of *meta*- and *para*-isomers and promoting the yield of the thermodynamically favoured *ortho*-product (Scheme 2.4). It is worth noting that the metallation of **2** using ^tBuLi and PMDETA was also investigated. However, spectroscopic analysis of the quenched reaction mixture revealed that a complex mixture of products was obtained with eight different product signals being observed in the ¹⁹F{¹H} NMR spectrum. Due to time constraints the complexity of this reaction system was not unravelled further.

Reflecting the absence of a reactivity-enhancing Lewis basic solvent, a poor yield of 8% of *ortho*-iodo-trifluoromethylbenzene was obtained upon treatment of **2** with ⁿBuNa alone (entry 4). It is highly plausible that the limited solubility of donor-free ⁿBuNa in hexane solvent is a factor which hinders the reaction yield. Upon turning from Li to Na, the formation of the *ortho*-products became much more favourable in line with increasing donor strength (entries 5-7). Notably, only 1% of *meta*- and *para*-iodotrifluoromethylbenzene were observed for PMDETA (entry 7) and these regioisomers were absent completely when Lewis donors THF or TMEDA were used, although this was counterbalanced by diminished yields. It seems likely that the increasing favourability of the *ortho*-metallation product upon moving from Li to Na is influenced by the increased atomic radius and increased coordination requirements of Na facilitating Na-F interactions, thus driving the regioselectivity towards *ortho*-metallation.

Table 2.6: Effect of varying the metal reagent and donor solvent on the ratio of iodo-trifluoromethylbenzene regioisomers.

Entry	Metal Alkyl	Donor	Iodinated Product Yield (%) ^a			
			<i>ortho</i> -	<i>meta</i> -	<i>para</i> -	Total
1	^t BuLi	None	0	0	0	0
2	^t BuLi	THF	30	26	13	69
3	^t BuLi	TMEDA	65	10	6	81
4	ⁿ BuNa	None	8	0	0	8
5	ⁿ BuNa	THF	43	0	0	43
6	ⁿ BuNa	TMEDA	72	0	0	72
7	ⁿ BuNa	PMDETA	80	1	1	82

a) Yields determined by ¹H NMR spectroscopy using hexamethylbenzene (10 mol%) as an internal standard.



Scheme 2.4 Regioselective metallation of **2** using ^tBuLi activated by THF or TMEDA (crystalline yields reported).

2.4 Conclusions

Using a systematic approach combining practical X-ray crystallographic and NMR spectroscopic studies with theoretical calculations, the metallation of trifluoromethylbenzene (**2**) by the group 1 bases ^tBuLi and ⁿBuNa in the presence of Lewis bases that are popular in organic synthesis (including TMEDA and THF) has been investigated. These studies have revealed not only that the use of these Lewis bases as additives is crucial for deprotonation to occur but also that they can play a major role in tuning the regioselectivity of the overall process. This is particularly noticeable for the lithiation reactions. Using the chelating diamine TMEDA yielded compound [(TMEDA)·Li(*o*-C₆H₄-CF₃)]₂ (**3-ortho**) where the metallation has occurred exclusively at the *ortho* position of **2**. Contrastingly when monodentate THF is employed compound [(THF)₂·Li(*m*-C₆H₄-CF₃)]₂ (**6-meta**) was the predominant isolated crystalline product. NMR spectroscopic analysis of crystalline **6** revealed a mixture of the three possible regioisomers for the deprotonation of **2**, showing a preference for the *meta*- and *para*- products with the *ortho*-isomer being the minor species present. Highlighting the complex behaviour of these organometallic intermediates in solution, these NMR spectroscopic studies also revealed that the observed ratio of the three regioisomers can be influenced profoundly by the bulk solvent employed. Thus, while in C₆D₆ solutions this ratio remains constant over time, when the Lewis donor solvent *d*₈-THF is used, complete equilibration of **6-meta** and **6-para** to **6-ortho** is observed after only 20 minutes at room temperature. Theoretical calculations predict **6-ortho** to be the energy minimum thermodynamically favourable regioisomer. These findings suggest that the CIPE, that is, the complexation of an organometallic reagent to the functional group of the substrate prior to proton-transfer, plays little or no role in determining the regioselectivity when CF₃ is present as the DMG. This differs significantly from the case with other, stronger DMGs.^[42]

Moving to ⁿBuNa as the metallating reagent also has important consequences for the regioselectivity of the reaction. Independently of the donor employed (THF, TMEDA or PMDETA), metal-hydrogen exchange occurs almost exclusively at the

ortho position of **2**. Supporting this superior regioselectivity, DFT studies comparing the relative stability of the three possible regioisomers for deprotonation of **2** by ^tBuLi/TMEDA or ⁿBuNa/TMEDA showed that although in both cases the *ortho* products are the most energetically preferred, the calculated energy differences between the *ortho*, *meta* and *para* regioisomers for the ⁿBuNa/TMEDA reactions are significantly larger than those observed for the corresponding ^tBuLi/TMEDA system. Finally, new structural insights on the constitution of the organometallic intermediates involved in these reactions have shed some light on the regioselectivities observed. Thus, sodium derivatives [(TMEDA)·Na(C₆H₄-CF₃)]₂ (**4**) and [(PMDETA)·Na(C₆H₄-CF₃)]₂ (**5**) contain stabilising dative Na···F interactions. Rarely observed in the solid state, these Na···F interactions appear to be a key factor in the stabilisation of the *ortho*-metallated products.

2.5 Future Work

Ultimately, the long term goal is to perfect the reaction regioselectivity, to realize the selective synthesis of *meta*- or *para*-metallated **2** in good yields. This presents a challenging prospect, as DFT studies have predicted the *ortho*-metallated derivative of **2** to be the thermodynamically preferred product in all cases. However, the nature of the organometallic reagent and the donor ligand has been shown to have a profound impact upon the reaction yield and the product distribution. Furthermore, the 49% yield of the crystalline *meta*-product obtained using Li/THF offers hope that regioselective *meta*-metallation is an achievable target.

Initial attempts to improve the *meta*-product yields could focus on the THF stoichiometry within the Li/THF metallation system. When crystalline **6** was dissolved in bulk THF solvent, a rearrangement from the kinetic *meta*- and *para*-products to the thermodynamically favourable *ortho*-product was observed. Potentially, using a sub-stoichiometric quantity of THF (with respect to the organolithium reagent) could therefore enhance the *meta*-product yield. Slocum *et al.* recently reported on the *ortho*-lithiation of a range of aromatic substrates, based on a

catalytic deficiency of the common Lewis donors TMEDA or ether.^[46] Using a sub-stoichiometric quantity of the bases THF, TMEDA and PMDETA should therefore be probed, to determine whether catalytic quantities of the Lewis donor component are sufficient to promote the metallation of **2**. Also, sterically encumbered Lewis donors such as Me₆-TREN should be investigated, as steric congestion between the metal/Lewis donor and the CF₃ substituent may disfavour *ortho*-metallation, thus promoting the yields of the isomeric *meta*- and *para*-products.

To seek improvement in the metallation methodology described in this chapter, these reactions should be repeated under a range of temperature conditions. This would help us to establish whether the metal-hydrogen exchange proceeds efficiently at ambient temperature, without decomposition, and so avoiding the need for expensive, cryogenic cooling. The reactions should also be performed at -78 °C, as this may increase the yields of the kinetic *meta*- and *para*- products. Kinetic trapping of the less stable *meta*- and *para*-isomers could subsequently be achieved through the fast reaction of the metallated derivatives of **2** with an electrophile.

Crystalline **6**, obtained from the metallation of **2** using the Li/THF system, favours the incorporation of the *meta*-product, although NMR spectroscopic analysis revealed that the *para*- and *ortho*-products are also present, albeit to a lesser extent. Therefore, the crystallisation conditions should be optimised, for example through variation of the concentration, solvent system and temperature, with the intention of crystallising purely the *meta*-isomer.

Furthermore, the dimetallation of **2** should be probed through the employment of two equivalents of the group 1 alkyl base and the donor ligand. Expanding upon the monometallic systems investigated within this work, the reaction of a range of cooperative bimetallic bases with **2** should be examined, as such reagents have a precedent for achieving unexpected *meta*-regioselectivities.^[27c; 42] For example, the 2,5-dimetallation of toluene^[189a] has previously been achieved using a synergic sodium magnesiate base, prepared *in situ* from the 1:1:3 stoichiometric combination of ⁿBuNa, ⁿBu₂Mg and TMP(H) in a hexane medium, with the resultant formation of an

inverse crown macrocycle. More recently, the remarkable 1, 4-dimetallation of naphthalene was realised using the special sodium magnesiate base “[NaMg(TMP)₂(ⁿBu)]”.^[189b] Thus, there is potential that **2** could also be dimetallated and transformed into a novel F-containing inverse crown using these or related reaction conditions.

2.6 Experimental

2.6.1 Synthesis of [(TMEDA)·Li(C₆H₄-CF₃)]₂, **3**

CF₃Ph (2 mmol, 0.25 mL) was added to a solution of ^tBuLi (2 mmol, 1.18 mL of a 1.7M solution in hexane) in hexane (10 mL) at -78 °C, and the reaction mixture was stirred for 30 minutes at ambient temperature. Subsequently, TMEDA (2 mmol, 0.30 mL) was added to the mixture at -78 °C and the reaction mixture was stirred for 30 minutes at room temperature to give a white precipitate. Briefly heating the suspension with a heat gun afforded a colourless solution, from which colourless crystals of **3** were deposited upon cooling this solution to -30 °C (yield 0.41g, 76%).

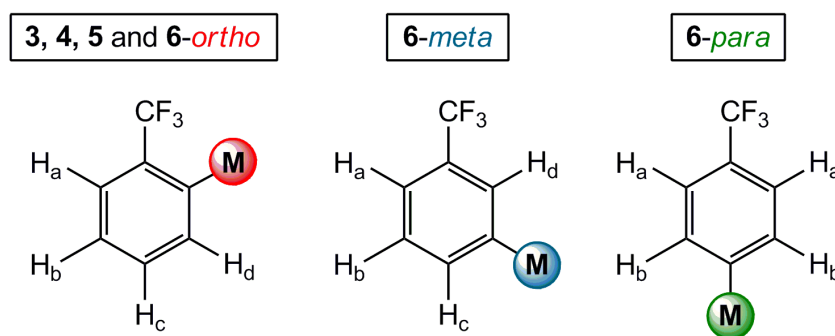


Figure 2.7 Labelling scheme for isomers of metallated **2**.

¹H NMR (400.13 MHz, C₆D₆, 300 K): δ = 8.32 [d, ³J(H,H) = 6.4 Hz, 2H, H_d-C₆H₄], 7.73 [d, ³J(H,H) = 7.62 Hz, 2H, H_a-C₆H₄], 7.35 [m, 2H, H_c-C₆H₄], 7.21 [t, ³J(H,H) = 7.7 Hz, 2H, H_b-C₆H₄], 1.71 and 1.64 ppm [s, 32H, CH₃ and CH₂-TMEDA respectively].

$^{13}\text{C}\{\text{H}\}$ NMR (100.63 MHz, C_6D_6 , 300 K): $\delta = 185.9$ [br. s, $\text{C}(\text{Li})\text{-C}_6\text{H}_4$], 142.5 [s, $\text{C}(\text{H}_d)\text{-C}_6\text{H}_4$], 141.8 [q, $^2\text{J}(\text{C},\text{F}) = 23.6$ Hz, $i\text{-C}_6\text{H}_4$], 130.6 [br. m, CF_3], 127.7 [s, $\text{C}(\text{H}_c)\text{-C}_6\text{H}_4$], 124.0 [s, $\text{C}(\text{H}_b)\text{-C}_6\text{H}_4$], 122.7 [q, $^3\text{J}(\text{C},\text{F}) = 3.0$ Hz, $\text{C}(\text{H}_a)\text{-C}_6\text{H}_4$], 56.7 [CH₂-TMEDA] and 45.3 ppm [CH₃-TMEDA]. $^7\text{Li}\{\text{H}\}$ NMR (155.50 MHz, C_6D_6 , 300 K, reference LiCl in D_2O at 0.00 ppm): $\delta = 2.0$ ppm. $^{19}\text{F}\{\text{H}\}$ NMR (376.40 MHz, C_6D_6 , 300 K): $\delta = -60.4$ ppm.

Due to the acute air sensitivity of **3**, satisfactory C, H, N analyses could not be obtained.

Crystal data for **3**: $\text{C}_{26}\text{H}_{40}\text{F}_6\text{Li}_2\text{N}_4$, $M_r = 536.50$, monoclinic, space group $C2/c$, $a = 14.9318(7)$, $b = 12.8892(7)$, $c = 16.7268(9)$ Å, $\beta = 116.089(7)^\circ$, $V = 2891.2(3)$ Å³, $Z = 4$, $\mu = 0.099$ mm⁻¹, 9846 reflections, 3119 unique, R_{int} 0.0248, final refinement to full-matrix least squares on F^2 gave $R = 0.0408$ (F , 2229 obs. data only) and $R_w = 0.1220$ (F^2 , all data), GOF = 1.063.

2.6.2 Synthesis of [(TMEDA)·Na(C₆H₄-CF₃)]₂, **4**

A suspension of ⁿBuNa (2 mmol, 0.16 g) in hexane (10 mL) was cooled to -78 °C and CF_3Ph (2 mmol, 0.25 mL) was added. The reaction mixture was subsequently stirred for 30 minutes at room temperature. TMEDA (2 mmol, 0.30 mL) was then added to the mixture at -78 °C and the mixture was stirred for 30 minutes at room temperature, which produced a white solid. Briefly heating the suspension with a heat gun produced a brown solution, from which crystalline **4** was afforded at -30 °C (yield 0.49g, 86%).

^1H NMR (400.13 MHz, C_6D_6 , 300 K): $\delta = 8.43$ [d, $^3\text{J}(\text{H},\text{H}) = 6.5$ Hz, 2H, $\text{H}_d\text{-C}_6\text{H}_4$], 7.76 [d, $^3\text{J}(\text{H},\text{H}) = 7.8$ Hz, 2H, $\text{H}_a\text{-C}_6\text{H}_4$], 7.32 [t, $^3\text{J}(\text{H},\text{H}) = 6.7$ Hz, 2H, $\text{H}_c\text{-C}_6\text{H}_4$], 7.16 [t, $^3\text{J}(\text{H},\text{H}) = 7.5$ Hz, 2H, $\text{H}_b\text{-C}_6\text{H}_4$] and 1.61 ppm [s, 32H, CH₂ and CH₃-TMEDA]. $^{13}\text{C}\{\text{H}\}$ NMR (100.63 MHz, C_6D_6 , 300 K): $\delta = 192.5$ [q, $^3\text{J}(\text{C},\text{F}) = 13.7$ Hz, $\text{C}(\text{Na})\text{-C}_6\text{H}_4$], 144.0 [s, $\text{C}(\text{H}_d)\text{-C}_6\text{H}_4$], 142.4 [q, $^2\text{J}(\text{C},\text{F}) = 23.8$ Hz, $i\text{-C}_6\text{H}_4$], 130.2 [br. m, CF_3], 123.4 [s, $\text{C}(\text{H}_c)\text{-C}_6\text{H}_4$], 121.9 [s, $\text{C}(\text{H}_b)\text{-C}_6\text{H}_4$], 121.8 [q, $^3\text{J}(\text{C},\text{F}) = 3.7$ Hz, $\text{C}(\text{H}_a)\text{-C}_6\text{H}_4$], 56.7 [CH₂-TMEDA] and 44.8 ppm [CH₃-TMEDA]. $^{19}\text{F}\{\text{H}\}$ NMR (376.40 MHz, C_6D_6 , 300 K): $\delta = -61.5$ ppm.

Due to the acute air sensitivity of **4**, satisfactory C, H, N analyses could not be obtained.

Crystal data for **4**: C₂₆H₄₀F₆N₄Na₂, M_r = 568.60, monoclinic, space group *C2/m*, *a* = 12.4249(6), *b* = 14.6166(5), *c* = 17.6830(8) Å, β = 110.919(5)°, *V* = 2999.7(2) Å³, *Z* = 4, μ = 0.126 mm⁻¹, 12224 reflections, 3945 unique, *R*_{int} 0.0179, final refinement to full-matrix least squares on *F*² gave *R* = 0.0335 (*F*, 3339 obs. data only) and *R*_w = 0.0890 (*F*², all data), GOF = 1.030.

2.6.3 Synthesis of [(PMDETA)·Na(C₆H₄-CF₃)]₂, **5**

CF₃Ph (2 mmol, 0.25 mL) was added to a suspension of ⁿBuNa (2 mmol, 0.16 g) in hexane (10mL) at -78 °C and the reaction mixture was stirred for 30 minutes. PMDETA (2 mmol, 0.42 mL) was subsequently added to the reaction mixture at -78 °C, which was then stirred at ambient temperature for a further 30 minutes. The resultant brown solution was transferred to the refrigerator, whereupon a crop of colourless crystals was deposited overnight (0.46g, 67% yield).

¹H NMR (400.13 MHz, C₆D₆, 300 K): δ = 8.48 [br. s, 2H, H_d-C₆H₄], 7.78 [br. s, 2H, H_a-C₆H₄], 7.35 [br. s, 2H, H_c-C₆H₄], 7.19 [br. s, 2H, H_b-C₆H₄], 1.91 [s, 24H, N(CH₃)₂ PMDETA], 1.86 [s, 16H, NCH₂-PMD ETA] and 1.59 ppm [s, 6H, NCH₃-PMD ETA].
¹³C{¹H} NMR (100.63 MHz, C₆D₆, 300 K): δ = 194.4 [q, ³J(C,F) = 15.0 Hz, C(Na)-C₆H₄], 144.0 [s, C(H_d)-C₆H₄], 142.1 [q, ²J(C,F) = 23.9 Hz, *i*-C₆H₄], 127.1 [s, C(H_c)-C₆H₄], 122.8 [s, C(H_b)-C₆H₄], 122.0 [s, C(H_a)-C₆H₄], 57.0 [s, NCH₂-PMD ETA], 54.7 [s, NCH₂-PMD ETA], 45.3 [s, N(CH₃)₂-PMD ETA] and 42.6 ppm [s, NCH₃-PMD ETA].
¹⁹F{¹H} NMR (376.40 MHz, C₆D₆, 300 K): δ = -60.7 ppm.

Due to the acute air sensitivity of **5**, satisfactory C, H, N analyses could not be obtained.

Crystal data for **5**: C₃₂H₅₄F₆N₆Na₂, M_r = 682.79, monoclinic, space group *P2₁/m*, *a* = 9.3966(2), *b* = 13.8611(3), *c* = 14.2631(3) Å, β = 94.259(2)°, *V* = 1852.60(7) Å³, *Z* = 2, μ = 0.114 mm⁻¹, 18861 reflections, 4871 unique, *R*_{int} 0.0258, final refinement to full-matrix least squares on *F*² gave *R* = 0.0416 (*F*, 3827 obs. data only) and *R*_w = 0.1125 (*F*², all data), GOF = 1.045.

2.6.4 Synthesis of [(THF)₂Li(C₆H₄-CF₃)]₂, **6**

A solution of ^tBuLi (2 mmol, 1.18 mL of a 1.7M hexane solution) in hexane (10 mL) was cooled to -78 °C and CF₃Ph (2 mmol, 0.25 mL) was added. The reaction mixture was subsequently stirred for 30 minutes at ambient temperature. Following this, THF (4 mmol, 0.32 mL) was added to the reaction mixture at -78 °C, producing a yellow solid. After stirring for 5 minutes at ambient temperature, a primrose solution was produced. Refrigeration of this solution at -30 °C afforded a crop of colourless crystals after 18h (yield 0.41g, 69% yield). NMR spectroscopic analysis of the crystals reveals a mixture of *ortho*, *meta* and *para* products in a respective ratio of 1:10:3. As labile THF is removed under vacuum upon isolation of crystalline **6**, ideal NMR integration values could not be obtained. Within the ¹H NMR spectra, overlapping resonances prevented the determination of coupling constants.

¹H NMR (400.13 MHz, C₆D₆, 300 K): δ = 3.22 [m, 9H, α-CH₂ THF] and 1.20 ppm [m, 9H, β-CH₂ THF];

6-ortho: δ = 8.31 [d, 1H, H_d-C₆H₄], 7.74 [d, ³J(H,H) = 8.0 Hz, 1H, H_a-C₆H₄], 7.38 [t, ³J(H,H) = 6.8 Hz, 1H, H_c-C₆H₄] and 7.21 ppm [t, ³J(H,H) = 7.5 Hz, 1H, H_b-C₆H₄].

6-meta: δ = 8.63 [s, 1H, H_d-C₆H₄], 8.40 [d, ³J(H,H) = 6.1 Hz, 1H, H_c-C₆H₄], 7.56 [d, ³J(H,H) = 7.7 Hz, 1H, H_a-C₆H₄] and 7.31 ppm [t, ³J(H,H) = 7.2 Hz, 1H, H_b-C₆H₄].

6-para: δ = 8.32 [d, 2H, H_b-C₆H₄] and 7.66 ppm [d, ³J(H,H) = 7.05 Hz, 2H, H_a-C₆H₄].

¹³C{H} NMR (100.63 MHz, C₆D₆, 300 K): δ = 68.1 [α-CH₂ THF] and 25.2 ppm [β-CH₂ THF];

6-ortho: δ = 185.9 [br, C(Li)-C₆H₄], 142.7 [s, C(H_d)-C₆H₄], 128.7 [s, C(H_c)-C₆H₄], 125.4 [s, C(H_b)-C₆H₄] and 122.8 ppm [q, ³J(H,H) = 3.6 Hz, C(H_a)-C₆H₄]. Signals for CF₃ and *i*-C₆H₄ were not detected.

6-meta: δ = 179.5 [s, C(Li)-C₆H₄], 146.1 [s, C(H_c)-C₆H₄], 142.4 [q, ³J(H,H) = 26.0 Hz, *i*-C₆H₄], 138.1 [br, C(H_d)-C₆H₄], 125.7 [s, C(H_b)-C₆H₄] and 122.1 ppm [br, C(H_a)-C₆H₄]. Signal for CF₃ not detected.

6-para: δ = 178.7 [br, C(Li)-C₆H₄], 142.5 [s, C(H_b)-C₆H₄] and 121.6 ppm [s, C(H_a)-C₆H₄]. Signals for CF₃ and *i*-C₆H₄ were not detected.

$^7\text{Li}\{^1\text{H}\}$ NMR (155.50 MHz, C_6D_6 , 300 K, reference LiCl in D_2O at 0.00 ppm): $\delta = 2.0$ ppm.

$^{19}\text{F}\{^1\text{H}\}$ NMR (376.40 MHz, C_6D_6 , 300 K) **6-ortho**: $\delta = -61.1$ ppm; **6-meta**: $\delta = -61.4$ ppm; **6-para**: $\delta = -61.6$ ppm.

Due to the acute air sensitivity of **6**, satisfactory C, H, N analyses could not be obtained.

2.6.5 Iodine Quench Studies – General Procedure

To a solution of $^t\text{BuLi}$ (2 mmol, 1.18 mL of a 1.7M hexane solution for compounds **3** and **6**) or a suspension of $^n\text{BuNa}$ (2 mmol, 0.16 g for compounds **4-5**) in hexane (10 mL), aromatic substrate **2** was injected *via* syringe at -78 °C. The cold bath was then removed and the reaction mixture was allowed to stir for 90 minutes at ambient temperature, prior to the addition of a donor solvent (TMEDA, 2 mmol, 0.30 mL for compounds **3** and **4**; PMDETA, 2 mmol, 0.42 mL for **5**; THF, 4 mmol, 0.32 mL for **6**) at -78 °C. Subsequently, the reaction mixtures were stirred for 24 hours at ambient temperature prior to treatment with a freshly prepared solution of iodine (4 mmol, 2 mL of a 2M THF solution) at -78 °C. Following the addition of iodine, the reaction was stirred at ambient temperature for 1 hour. As iodo-trifluoromethylbenzene is light-sensitive,^[16] the reaction was protected from light throughout the quenching process. A saturated solution of NH_4Cl (10 mL) was added, along with saturated $\text{Na}_2\text{S}_2\text{O}_3$ until bleaching occurred (20 mL). The organic layer was separated from the aqueous layer and the aqueous layer was washed with diethyl ether (4 x 15 mL). Magnesium sulfate was used to dry the combined organic layers. Following filtration, the solvent was removed *in vacuo* and the crude residue was spiked with 10 mol% hexamethylbenzene (0.0324 g, 0.2 mmol for 2 mmol scale reactions). ^1H NMR spectroscopic analysis was performed and the relative yields of *ortho*-, *meta*- and *para*-iodo-trifluoromethylbenzene were determined by relative integration.^[172]

Chapter 3

Neutral Zinc, Lower-Order Zincate and Higher-Order Zincate Derivatives of Pyrrole: Synthesis and Structural Characterisation of Zinc Complexes with One, Two, Three or Four Pyrrolyl Ligands

“Science is a way of thinking
much more than it is a body of knowledge”

Carl Sagan

American astrophysicist

3.1 Summary

With the aim of developing the zinc chemistry of the important five-membered nitrogen heterocycle pyrrole, this part of the PhD project reports the synthesis and characterisation of five crystalline zinc-pyrrolyl complexes. Pyrrolyl here means the *N-H* bond has been converted to an *N-Zn* bond. Two neutral complexes, [^tBuZn(NC₄H₄)(TMEDA)·HNC₄H₄] **7** and [Zn(NC₄H₄)₂(TMEDA)] **8**, containing one or two pyrrolyl ligands, were synthesised from ^tBu₂Zn and different amounts of pyrrole in the presence of TMEDA (*N, N, N', N'*-tetramethylethylenediamine). X-ray crystallographic studies established that both adopt mononuclear structures with the salient feature of the former the presence of an additional parent protonated pyrrole molecule which engages its anionic counterpart in *N-H*···*πC-C* interactions.

Applying a similar synthetic approach but also incorporating ⁿBuNa within the mixture delivered three distinct sodium zincate (anionic zinc) compounds: [(THF)₂·NaZn(THF)(NC₄H₄)₃]_∞ **9**, [(TMEDA)·Na]₂Zn(NC₄H₄)₄ **10**, and [(PMDETA)·Na]₂Zn(NC₄H₄)₄ **11** (PMDETA is *N,N,N',N'',N''*-pentamethyldiethylenetriamine). From their crystal structures, the 1:1, Na:Zn complex **9** can be classified as a lower-order zincate having three pyrrolyl ligands bound to zinc in a polymeric chain arrangement, while the 2:1, Na:Zn complexes **10** and **11** are molecular higher-order zincates having Zn centres fully saturated by four pyrrolyl ligands. Revealingly, the zinc-free sodiopyrrole complex [(PMDETA)·Na(NC₄H₄)₂] **12**, made and characterised for comparison, shows that on its own sodium prefers σ -bonding, but is forced to revert to π -bonding when combined with the stronger Lewis acid zinc in the zincate compositions.

3.2 Introduction

One of the most important molecular scaffolds in chemistry, the five-membered heterocyclic pyrrole ring (Figure 3.1) is utilised in a multitude of diverse topics ranging from agrochemicals^[192] and pharmaceuticals^[2] through to functional polymers^[193] and nanoparticles.^[194] This provides a large incentive to elaborate the structural characteristics of zincated pyrrole chemistry. These *N*-heterocycles are also of major significance in biochemistry often found linked together into macrocycles that act as receptors for metal ions (e.g., most significantly Fe in haem; Co in vitamin B12).^[195] Developed by Pfizer as a cholesterol lowering drug, atorvastatin is one of the highest revenue generating medicines in pharmaceutical history.^[196] Sold under the trade name Lipitor, this drug is estimated to have brought in over \$131 billion over the course of its patent and bears a central, fully substituted pyrrole motif at its core (Figure 3.2).

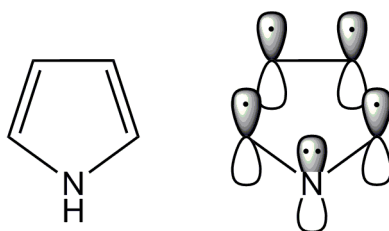


Figure 3.1 Molecular structure of and π -bonding within pyrrole.

Boasting so many uses and potential uses, this class of compound inevitably receives a great deal of attention from synthetic chemists, with the number of reported pyrrole derivatives growing substantially year by year. The pre-functionalisation of simple pyrroles through metallation is often a convenient starting point in synthetic pathways to more complex molecules. While high-polarity lithiation has usually been the method of choice for pyrrole^[197] and aromatic compound metallation in general,^[45; 159] new low-polarity metallation methods have been developed by Knochel,^[72; 198] Kondo^[128; 149] and Uchiyama,^[199] Mongin,^[140b; 200] Wheatley,^[201] and Mulvey,^[14] amongst others, that display significant advantages over the former method. Converting C-H (or N-H) bonds to C-M (or N-M) bonds where M is a

softer, less electropositive metal acid (e.g., Mg, Al, Mn, Zn, Cd) than lithium, promotes greater thermodynamic stability and higher functional group tolerance of the pre-functionalised metallo-organic intermediate. Nicely illustrated by Uchiyama and Mongin's reaction of *N*-Boc-pyrrole with a mixed lithium-zinc base^[202] (Scheme 3.1), low polarity metallations can be performed at ambient temperature in the presence of sensitive carbonyl functions, in cases where low temperature regimes (here, -80 °C) are necessary for conventional lithiation.^[197a] Moreover, when M is zinc, this new improved form of metallation (zincation) opens a door to utilising the metallo-organic intermediates in subsequent cross-coupling methodologies (Negishi type especially) that is normally closed to lithio-organics. Organ recently demonstrated the efficiency with which higher-order zincates can be applied to Negishi cross-coupling reactions.^[203] This research development provided an additional incentive to study a series of lower-order and higher-order zincates.

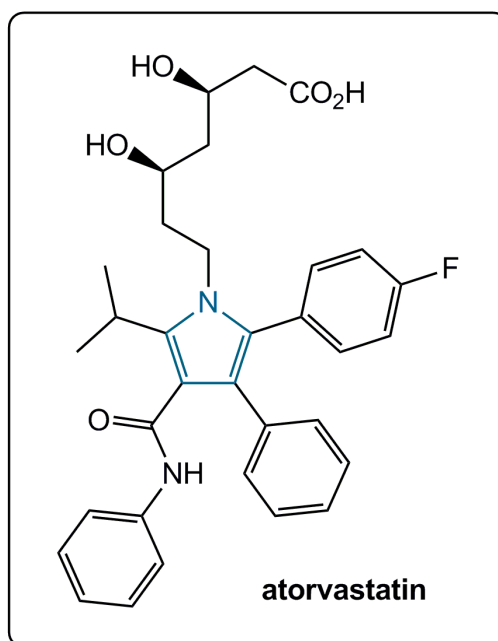
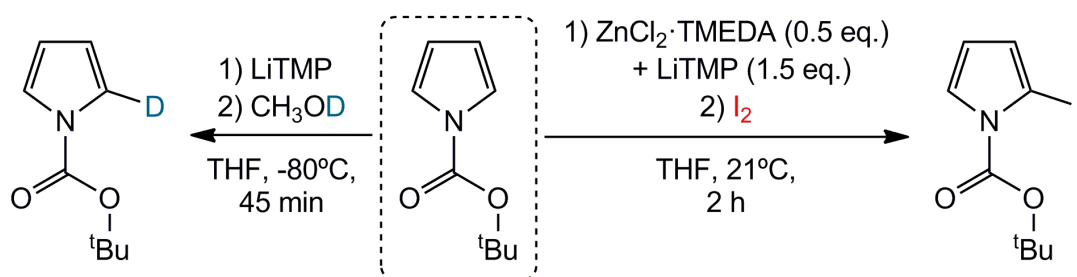


Figure 3.2 Structural formula of atorvastatin (sold under the trade name Lipitor), highlighting the five-fold substituted pyrrolyl core.

Stimulated by these synthetic advances and the lack of knowledge of zincated pyrrolyl intermediates (highlighted by the non-isolation/non-characterisation of the example in Scheme 3.1), this part of the PhD project aims to develop the zinc

chemistry of the pyrrole family of compounds. For this case study, the parent pyrrole molecule seemed the logical starting point, especially since, to the best of our knowledge, no zincated derivative of it has previously been isolated and characterised. It should be noted that the synthesis of bis(pyrrolyl)zinc, *via* the reaction of dimethylzinc with HNC_4H_4 , was reported in 1970.^[204] However, this compound was not structurally characterised *via* crystallographic or NMR spectroscopic studies and only elemental microanalysis was reported for it. Furthermore, no follow-up studies to this work have been published. As the deprotonated form of pyrrole $\text{C}_4\text{H}_4\text{N}^-$ is isoelectronic to the widely studied Cp^- (C_5H_5^-) ligand and can be considered an azacyclopentadienyl ligand with σ^- and π^- bonding capabilities, this provides an additional incentive to uncover the structural characteristics underpinning zincated pyrrole chemistry.



Scheme 3.1 Functionalisation of *N*-Boc-pyrrole *via* lithiation (LHS) or alkali-metal-mediated zincation (RHS).^[197a; 202]

3.3 Results and Discussion

This work introduces five new zinc derivatives of pyrrole, each of which has been synthesised, isolated from solution, characterised in the solid-state by X-ray crystallography and in solution by multinuclear [^1H , $^{13}\text{C}\{\text{H}\}$] NMR spectroscopy. This collection includes two neutral zinc compounds [$^t\text{BuZn}(\text{NC}_4\text{H}_4)(\text{TMEDA})\cdot\text{HNC}_4\text{H}_4$] **7** and [$\text{Zn}(\text{NC}_4\text{H}_4)_2(\text{TMEDA})$] **8**; three distinct sodium zincate (anionic zinc) compounds [$\{(\text{THF})_2\cdot\text{NaZn}(\text{THF})(\text{NC}_4\text{H}_4)_3\}_\infty$] **9**,

[{(TMEDA)·Na}₂Zn(NC₄H₄)₄] **10**, and [{(PMDETA)·Na}₂Zn(NC₄H₄)₄] **11**; and to allow comparisons the zinc-free solvated sodiopyrrole complex [{(PMDETA)·Na(NC₄H₄)₂] **12**. Structurally, each compound is unique within this set, while the pyrrole ligands attached to zinc or sodium have been deprotonated at the most acidic N-*H* site as would be anticipated, each compound within the collection is structurally unique in other ways.

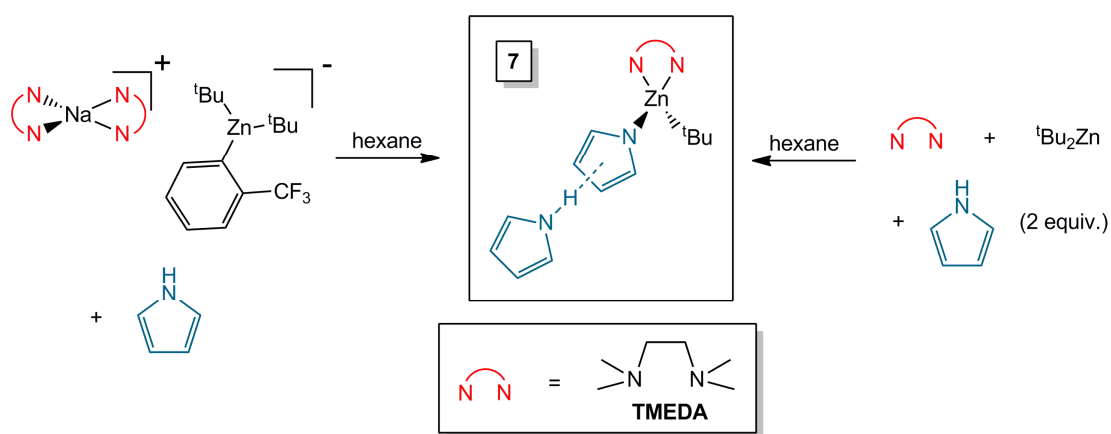
This study centred on the reactions of pyrrole with sodium zincate base mixtures. Low polarity zincations, especially of relatively inert C-H bonds (but less so in the case of more easily breakable N-H bonds), generally require the alkali metal to be present even though the deprotonation reactions taking place are C-H to C-Zn exchange processes or so it is thought. However, in the cases of **7** and **12** the solid products isolated from solution turned out to be homometallic compounds even though both sodium and zinc were present within the reaction mixtures. X-ray crystallographic studies were successfully carried out on the six new compounds **7** – **12**. Their structures are displayed in Figures 3.3 – 3.10 and selected bond parameters are listed in Table 3.1.

3.3.1 Synthesis and Solid State Characterisation of Neutral Zinc Pyrrolyl Formulations

Homometallic **7**, a heteroleptic alkyl-pyrrolyl zinc compound, was initially obtained unexpectedly by subjecting pyrrole to sodium bis(alkyl)-arylzincate [{(TMEDA)₂·Na}⁺{^tBu₂Zn(*o*-C₆H₄-CF₃)⁻}] (Scheme 3.2). The reaction was undertaken with a view to monitoring the effects of amines on the complicated *ortho*-, *meta*- and *para*-isomerisation processes taking place in zincated trifluoromethylbenzene. This circuitous route to **7** was not investigated further as it was established that direct rational synthesis from di-*tert*-butylzinc, pyrrole and TMEDA (Scheme 3.2) in bulk hexane solution produced good yields of **7** (approaching 80%). It is worth noting that the 1:1:1:2 combination of *n*-butyllithium,

di-*tert*-butylzinc, pyrrole and TMEDA in hexane solution also led to the formation of crystalline **7**.

Two molar equivalents of pyrrole had to be used in this room temperature direct reaction because a pyrrole molecule with its N–H intact, which plays a significant part in the structure and bonding of **7** (*vide infra*), is a component part of crystalline **7**. Repetition of this reaction under reflux conditions still produced **7**. Off-diagonal peaks in the ROESY^[205] (Rotating-Frame Overhauser Effect Spectroscopy) NMR spectrum of **7** are observed, which could be a result of chemical exchange between the pyrrolyl anion and free pyrrole. However, NOE interactions cannot be ruled out.



Scheme 3.2 Synthetic approaches: original fortuitous (LHS) and rational (RHS) preparations of **7**.

The crystal structure of **7** contains two essentially identical though crystallographically independent molecules within its unit cell, although for brevity only the geometry of one need be discussed. This molecule (Figure 3.3a), which has no crystallographically imposed symmetry, contains a central zinc atom having a distorted tetrahedral (NNNC) coordination comprising two anions (*t*-Bu and pyrrole) and a neutral bidentate TMEDA ligand. The unexpected extra feature is a second pyrrole molecule which has not been deprotonated, allowing its polarised N^{δ-}–H^{δ+} unit to interact with the π-system of the deprotonated pyrrole. To the best of our knowledge **7** represents the first crystallographically-characterised zinc compound

displaying an anionic unsubstituted form of pyrrole. Substituted variants are known including the diphenyl example $[(\text{THF})\cdot\text{Zn}(\text{2,5-Ph}_2\text{-NC}_4\text{H}_2)_2]^{[206]}$ which like **7** is a monomer but the steric needs of its dual phenyl substitution restricts zinc to a lower three-coordinate (NNO), distorted trigonal planar geometry.

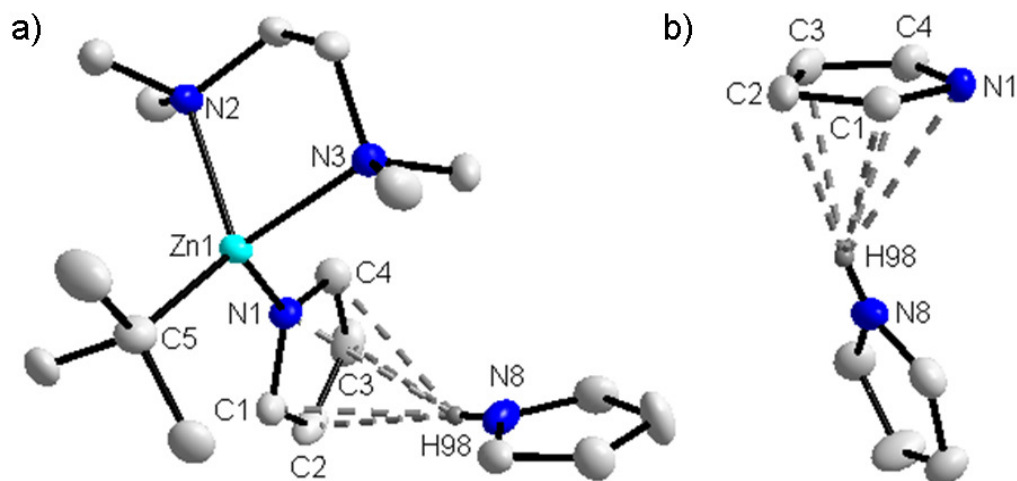
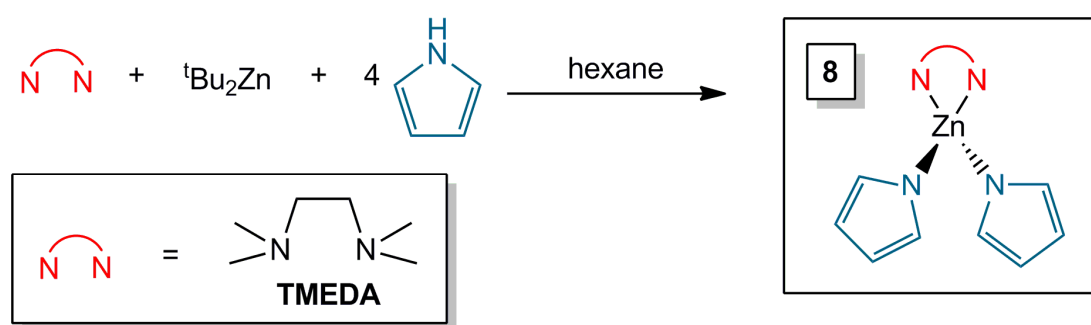


Figure 3.3 a) Molecular structure of **7** with thermal ellipsoids at 50% probability level and hydrogen atoms (other than pyrrole N-H) omitted for clarity. Only one of two independent molecules in the unit cell is displayed. The second molecule is identical within experimental error. Selected bond lengths (Å) and bond angles (°): Zn1-N1, 2.0040(15); Zn1-N2, 2.1841(15); Zn1-N3, 2.1850(15); Zn1-C5, 2.0040(15); N1-H98, 2.74(3); C1-H98, 2.55(3); C2-H98, 2.42(3); C3-H98, 2.53(3); C4-H98, 2.70(3); N1-Zn1-N2, 103.35(7); N1-Zn1-N3, 107.26(7); N1-Zn1-C5, 118.34(8); N2-Zn1-N3, 84.13(6); N2-Zn1-C5, 118.22(8); N3-Zn1-C5, 119.71(9); b) Fragment of **7** highlighting the NH \cdots π C-C interaction between the pyrrole/pyrrolyl molecules.

Although in general the bond dimensions within **7** are unexceptional, it is worth noting that those of the deprotonated and N-H intact pyrrole molecules lie within experimental error of each other and are nearly equivalent to those of free pyrrole. The pyrrolyl ligand engages Zn in a σ -manner with a Zn-N bond length of 2.0040(15) Å. In the pyrrole molecule the N-H hydrogen atom was located and freely refined and this unit forms a π -interaction with the pyrrolyl ring. This

interaction is not symmetrical over the NC₄ ring. Instead, it is displaced closer towards the C2-C3 back-edge (the N⋯C2 and N⋯C3 distances are 3.2469 Å and 3.3233 Å respectively, with the shortest distance from N to the C2–C3 bond being 3.2045 Å), with a dihedral angle of 76.4° between the pyrrole and pyrrolyl ring planes. This mirrors the intramolecular N–H⋯π interactions found in the crystal structure of free pyrrole causing its close-packed structure to be arranged in pairs where the distance of the N atom to the midpoint of its C2-C3 neighbour is 3.300(3) Å with a corresponding dihedral angle between its ring planes of 70.6°.^[207]

The next reaction looked at was that of di-*tert*-butylzinc and TMEDA with the addition of a four-fold stoichiometric excess of pyrrole. This combination resulted in the synthesis of homometallic **8** in a high crystalline yield of 89% based upon the di-*tert*-butylzinc stoichiometry (Scheme 3.3). It is noteworthy that only two of the four pyrrole ligands are present within **8**. In contrast, the use of a two- or three-fold stoichiometric excess of pyrrole resulted in the formation of **7**. TMEDA-free Zn(NC₄H₄)₂ has been previously synthesised, however elemental microanalysis alone was used to identify the product.^[204] To the best of our knowledge, **8** therefore represents the first non-substituted bis-pyrrolylzinc compound to be structurally characterised *via* X-ray crystallography and NMR spectroscopic analysis. Traces of **8** are observed in the ¹H NMR spectrum of **7**, implying that **8** is also formed as a minor product in the synthesis of aforementioned **7**.



Scheme 3.3 Synthesis of neutral zinc species **8** from an excess of pyrrole.

Unlike the molecular structure of heteroleptic **7**, complex **8** is homoleptic but is mononuclear and its Zn centre displays a distorted tetrahedral (NNNN) coordination (Figure 3.4). The coordination of two planar pyrrolyl ligands to the Zn centre is modestly less sterically demanding than the coordination of one pyrrolyl and one *tert*-butyl ligand present in heteroleptic **7**. This is reflected by a slight increase in the bite angle of the didentate TMEDA ligand, from 84.13(6)° in **7** to 86.041(1)° in **8**. Furthermore, the Zn-N_{pyrrolyl} bond lengths are shorter within **8** [Zn1-N1, 1.9461(15) Å; Zn1-N2, 1.9425(14) Å], than in **7** [Zn1-N1 2.0040(15) Å]. In spite of the addition of a four-fold excess of pyrrole (with regards to the Zn stoichiometry) in the reaction mixture, there is an absence of NH... π C-C interactions within **8**.

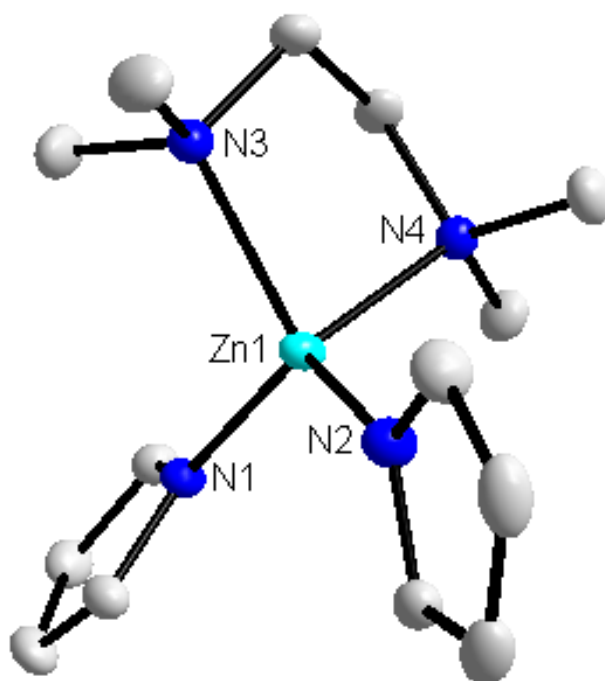
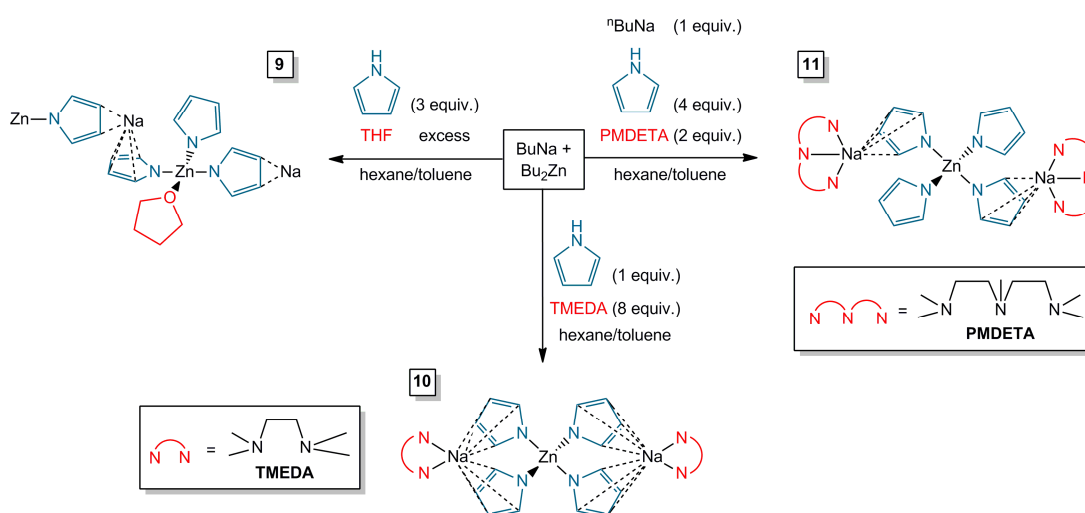


Figure 3.4 Molecular structure of **8** with thermal ellipsoids at 50% probability level and hydrogen atoms omitted for clarity. Selected bond lengths (Å) and bond angles (°): Zn1-N1, 1.9461(15); Zn1-N2, 1.9425(14); Zn1-N3, 2.1284(15); Zn1-N4, 2.0978(14); N1-Zn1-N2, 115.55(6); N1-Zn1-N3, 109.04(6); N1-Zn1-N4, 115.10(6); N2-Zn1-N3, 115.80(6); N2-Zn1-N4, 111.90(6); N3-Zn1-N4, 86.041(1).

3.3.2 Synthesis and Solid State Characterisation of Lower- and Higher-Order Sodium Zincates

New sodium zincates **9–11** all have homoleptic compositions with respect to their anionic, pyrrolyl ligands though they carry additional neutral donor ligands which differ for each compound. Scheme 3.4 illustrates the general synthetic method employed for the series. The reactions were performed in a bulk hexane medium, with the introduction of toluene for solubility purposes, where mixtures of *n*-butylsodium, di-*n*-butylzinc and pyrrole in various stoichiometric ratios were treated with the Lewis donor solvents THF (for **9**), TMEDA (for **10**) and PMDETA (for **11**). Crystalline products $[\{(THF)_2 \cdot NaZn(THF)(NC_4H_4)_3\}_\infty]$ **9**, $[\{(TMEDA) \cdot Na\}_2Zn(NC_4H_4)_4]$ **10**, and $[\{(PMDETA) \cdot Na\}_2Zn(NC_4H_4)_4]$ **11** were obtained in variable yields [28% for **9**; 12% for **10** based on the pyrrole stoichiometry, that is, out of a maximum of 25%; 61% for **11**].



Scheme 3.4 Synthesis of sodium pyrrolylzincates **9 – 11** starting from *n*-butylsodium and di-*n*-butylzinc.

Tris-pyrrolyl zincate **9** can be considered a lower-order zincate, as it possesses a 1:1 alkali metal:zinc stoichiometry with a monoanionic (R₃Zn)[−] moiety. Produced in line with its stoichiometry from a 1:1:3, ⁿBuNa: ⁿBu₂Zn: HNC₄H₄ mixture, the best yield of isolated crystalline material of **9** was a modest 28%. However, the actual yield

was higher as evidenced by NMR analysis of the filtrate, which also revealed that no other products were formed in the solution although resonances corresponding to free (unreacted) pyrrole were observed. Due to its polymeric constitution (*vide infra*), crystalline **9** exhibits poor solubility in benzene, though it dissolves well in the polar, stronger Lewis basic solvent THF. Notwithstanding, THF is easily lost from the isolated solid as reflected by low integration values in NMR spectroscopic analyses and variable microanalytical results.

Of the three sodium zincates reported in this study, lower-order zincate **9** is the most unique for adopting a polymeric structure of C_1 symmetry (Figure 3.5) with an assortment of contacts repeated along its chain which clearly differentiate the distinct bonding preferences of zinc and sodium. In essence, **9** comprises a chain of alternating Zn and Na atoms connected *via* σ -bonding (to Zn) and π -bonding (to Na) ambi-bridging pyrrolyl ligands with weaker donating THF ligands that plug the coordination gaps, one bound to Zn and two bound to Na.

Structurally characterised sodium zincate polymers of any ligand constitution are rare. A search of the CCDB^[178] revealed the majority of sodium zincate polymers are carboxylic acid,^[208] phosphinate/phosphate^[209] or porphyrin derivatives^[210] wholly unrelated to **9**. To the best of our knowledge, **9** is the first example of a polymer comprising sodium, zinc and pyrrole constituents. However, a particularly relevant structure within the CCDB is that of the triscyclopentadienyl [$\{(THF)_2 \cdot NaZn(C_5H_5)_3\}_\infty$], reported by Carmona in 2007 (Figure 3.6),^[211] which bears a striking likeness to its analogous pyrrole complex **9**. Both form infinite chains comprising alternate Na and Zn atoms bridged by two cyclic anions, with a third, terminal anion bound to Zn and involving two donor THF ligands coordinating to the Na centre. The similarity between these two structures reflects the isoelectronic and close structural relationship between the $C_5H_5^-$ and $NC_4H_4^-$ planar rings. A Na/Zn polymer involving 5-(2'-pyrimidyl)tetrazolate has also been prepared.^[212]

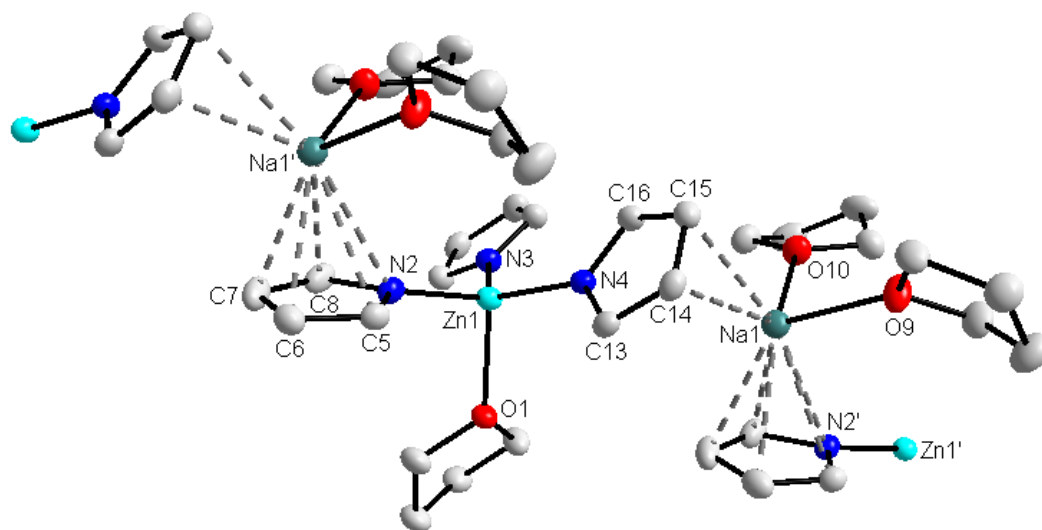


Figure 3.5 Section of the polymeric structure of **9** with thermal ellipsoids at 50% probability level and hydrogen atoms omitted for clarity. Selected bond lengths (Å) and bond angles (°): Zn1-N2, 1.9664(14); Zn1-N3, 1.9506(14); Zn1-N4, 1.9604(14); Zn1-O1, 2.1376(12); Na1-O9, 2.3285(14); Na1-O10, 2.2967(15); Na1-N2', 2.9191(15); Na1-C5', 2.8554(19); Na1-C6', 2.737(2); Na1-C7', 2.709(2); Na1-C8', 2.8172(19); Na1-C14, 2.7806(18); Na1-C15, 2.6908(18); N2-Zn1-O1, 96.48(5); N2-Zn1-N3, 117.39(6); N2-Zn1-N4, 112.27(6); N3-Zn1-O1, 102.56(6); N3-Zn1-N4, 118.76(6); N4-Zn1-O1, 96.48(5).

Occupying a distorted tetrahedral NNNO environment,^[213] the Zn atom in **9** bonds in a σ -manner to three pyrrolyl ligands and one THF ligand. No interaction takes place between Zn and the pyrrolyl π -system. This contrasts with the $\text{Zn}\cdots\eta^5\text{-NC}_4\text{-ring}$ π -bonding implicated in the free radical zinc monopyrrolyl half-sandwich structure $\text{ZnC}_4\text{H}_4\text{N}$ on the basis of laser-induced fluorescence evidence.^[214] Despite there being three distinct pyrrolyl ligands in **9**, within the σ -bonded coordination sphere of zinc the bond lengths to their N anions are essentially equivalent, with a mean bond length of 1.9591 Å with the dative Zn-O bond understandably longer [2.1376(12) Å] and weaker. π -Bonding distinguishes the pyrrolyl ligands. One pyrrolyl does not engage Na at all. Another (the N4C13-C16 ring) interacts with Na through a $\eta^2\text{-C}_2$ edge [Na1-C14, 2.7806(18) Å; Na1-C15, 2.6908(18) Å], with a significantly longer

contact to C16 [3.0681(19) Å] with the N atom remote [separation distance, Na1...N4, 3.3753 Å]. This Na... η^2 -C₂ interaction is best interpreted as the weaker intermolecular propagating point as the third pyrrolyl engages Na in a stronger η^5 -NC₄ interaction. Situated asymmetrically above the ring, the Na lies closer to the C6'-C7' back-edge [Na1-C6', 2.737(2) Å; Na1-C7', 2.709(2) Å] than to the more electronegative N centre [Na1-N2', 2.9191(15) Å; Na1-C5', 2.8554(19) Å; Na1-C8', 2.8172(19) Å]. There is no significant difference in the lengths of the Na-O bonds [Na1-O9, 2.3285(14) Å; Na1-O10, 2.2967(15) Å] which complete a coordination number of 9 for the alkali metal. Alternatively, viewing the pyrrolyl π -systems as single coordination points (the midpoint of C14-C15; and the centroid of N2'C5'-C8'), sodium occupies a more familiar distorted tetrahedral four-coordinate geometry.

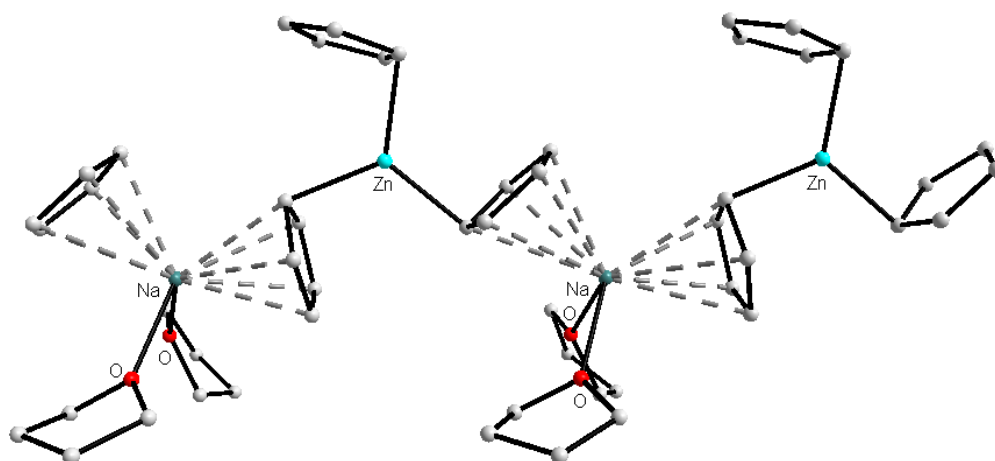


Figure 3.6 Polymeric structure of $[\{(THF)_2 \cdot NaZn(C_5H_5)_3\}]_\infty$.^[211]

Whereas monodentate THF could not deaggregate the polymeric arrangement within **9**, the stronger chelating donors TMEDA^[29] and PMDETA,^[165d; 215] two of the most utilised Lewis bases in alkali metal chemistry enforce molecular structures. Not directly comparable to **9** as it is lower-order trianionic, these higher-order tetraanionic zincates **10** and **11** could be considered text-book examples of how the different denticities and steric profiles of donor ligands can alter the structures of organic alkali metal compounds.^[130b; 175; 177a; 216]

Tetra-pyrrole zincate **10**, a higher-order zincate possessing a 2:1 alkali metal: zinc stoichiometry with a dianionic $[(R_4Zn)^{2-}]$ moiety, was produced from a 1:1:1, ${}^n\text{BuNa}$: ${}^n\text{Bu}_2\text{Zn}$: HNC_4H_4 mixture. This reaction mixture afforded a suspension which would not fully dissolve even upon addition of an eightfold excess of TMEDA. This suspension was consequently filtered and cooled giving a crop of colourless crystals in 12% yield, based upon the pyrrole stoichiometry (i.e. with a maximum yield of 25%). However the stoichiometry of **10** does not match that of its metal reactants as it is sodium rich (Na:Zn, 2:1) and contains four equivalents of deprotonated pyrrole. There must be at least one other product (rich in zinc) from this reaction and significantly a white solid precipitated from the mixture prior to the crystallisation of **10** in the filtrate. On the basis of NMR evidence (*vide infra*) this second product is thought to be $[\text{NaZn}(\text{NC}_4\text{H}_4)_3]_\infty$. While this still does not account for the mismatch of the stoichiometry, ${}^n\text{Bu}_2\text{Zn}$ is highly volatile and is easily removed under vacuum. It is therefore believed that ${}^n\text{Bu}_2\text{Zn}$ is present in the reaction mixture but is not detected *via* NMR spectroscopic analysis.

To the best of our knowledge, neither $\text{Zn}(\text{C}_4\text{H}_4\text{N})_2$ or $\text{Na}(\text{C}_4\text{H}_4\text{N})$ have previously been structurally characterised, although the (15-crown-5)sodium-pyrrolide crown ether complex has been reported.^[217] Repeating the reaction with the stoichiometry matching the components within **10** (i.e., 2 ${}^n\text{BuNa}$: 1 ${}^n\text{Bu}_2\text{Zn}$: 4 HNC_4H_4) and with an eight-fold excess of TMEDA increased its crude yield to 88%. However, NMR spectroscopic analysis revealed the crystalline solid obtained was significantly contaminated with the second apparently polymeric product so this yield is invalid. Alkali metal chemists whose research involves a lot of structural studies commonly substitute bidentate TMEDA for tridentate PMDETA to probe the structural consequences, so following suit here we repeated the reaction affording **10** but with this substitution. Mimicking the TMEDA reaction, a 2:1:4 mixture of the two metal alkyl reagents and pyrrole in hexane to which PMDETA (two molar equivalents were sufficient for dissolution of the precipitate, reflecting the stronger donating ability of PMDETA versus TMEDA) and toluene were added produced a solution which gave another tetra-pyrrolyl, higher-order zincate, solid product in **11** in a crystalline yield of 61%.

Both **10** and **11** have in common a distorted tetrahedral $[\text{Zn}(\text{NC}_4\text{H}_4)]^{2-}$ spine made up of strong Zn–N σ bonds: in **10**, all Zn–N bond lengths are equivalent at 1.984(2) Å; in **11**, the mean Zn–NC₄H₄ bond length is 1.9957 Å but how the pyrrolyl rings interact with the amine-chelated Na⁺ cations differs significantly. In **10**, possessing D₂ symmetry which dictates a strictly linear Na \cdots Zn \cdots Na unit, bidentate TMEDA fills two Na coordination sites leaving the other two available to be filled by η^5 -bonded NC₄H₄ ligands (Figure 3.7). The pattern of distances involved in this metal \cdots π -surface bonding [Na1–N1, 2.735(3) Å; Na1–C1, 2.786(3) Å; Na1–C2, 3.036(3) Å; Na1–C3, 3.129(3) Å; Na1–C4, 2.950(3) Å] shows the Na intrudes into the V-shaped, π -pocket to move closer to the electron-rich N atom than to the ring C atoms.

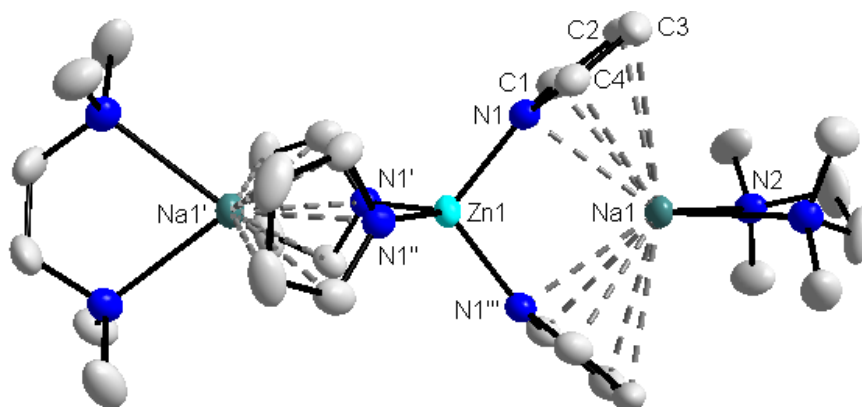


Figure 3.7 Molecular structure of **10** with thermal ellipsoids at 50% probability level and hydrogen atoms and minor disordered component omitted for clarity. Selected bond lengths (Å) and bond angles (°): Zn1–N1, 1.984(2); Na1–N1, 2.735(3); Na1–N2, 2.480(3); Na1–C1, 2.786(3); Na1–C2, 3.036(3); Na1–C3, 3.129(3); Na1–C4, 2.950(3); Na1 \cdots Zn1 \cdots Na1', 180.000(23); N1–Zn1–N1', 112.71(14); N1–Zn1–N1'', 111.26(14); N1–Zn1–N1''', 104.55(14); N1–Na1–N1''', 70.05(11); N1–Na1–N2, 132.12(8); N1–Na1–N2''', 128.43(8); N2–Na1–N2''', 75.81(13).

Contrastingly, in **11** the symmetry (C_1) is reduced which is reflected in a non-linear Na \cdots Zn \cdots Na unit [Na1–Zn1–Na1' is 155.445(2)°] (Figure 3.8). Although **11** displays two nearly identical molecules in its unit cell, for brevity the dimensions of only one molecule shall be discussed. Tridentate PMDETA fills three coordination sites on

Na, concomitantly increasing steric demands. Consequently, the V-shaped π -pocket is no longer sustainable as the approach of the extra bulky (compared to TMEDA.Na⁺) PMDETA.Na⁺ counter-ion forces one pyrrolyl ring (carrying N5 or N6) to rotate away from it to a remote position. The remaining pyrrolyl ring fills the fourth Na coordination site in a η^5 -manner. With respect to **10**, the bond lengths of **11** which involve Na1 are generally shorter [such as Na1–N4, 2.5884(18) Å; Na1–C10, 2.737(2) Å; Na1–C11, 2.993(2) Å; Na1–C12, 3.002(2) Å; Na1–C13, 2.746(2) Å due to reduced steric constraints caused by the remoteness of the non-coordinated (to Na) pyrrolyl ligand (Table 3.1)].

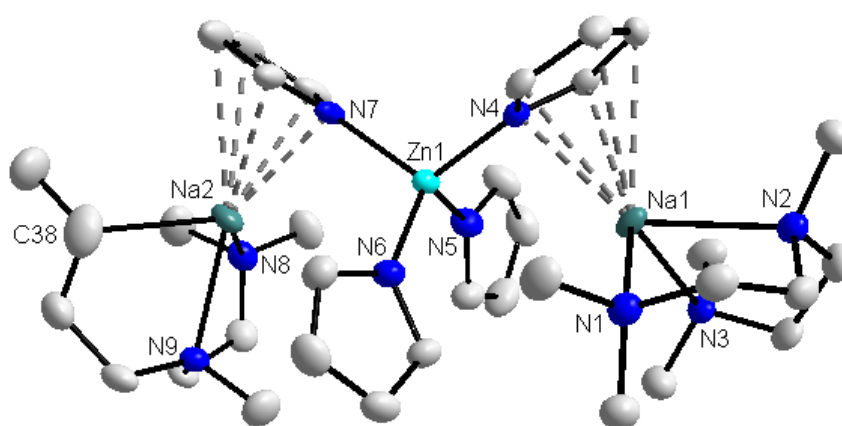


Figure 3.8 Molecular structure of **11** with thermal ellipsoids at 50% probability level and hydrogen atoms and minor disordered component omitted for clarity. Note N10 is eclipsed by C38. Only one of the independent molecules in the unit cell is displayed, the second molecule is identical within experimental error. Selected bond lengths (Å) and bond angles (°): Zn1–N4, 1.9978(19); Zn1–N5, 1.9792(19); Zn1–N6, 1.9995(19); Zn1–N7, 2.0062(18); Na1–N1, 2.448(2); Na1–N2, 2.473(2); Na1–N3, 2.4722(19); Na1–N4, 2.5884(18); Na2–N7, 2.551(2); Na2–N8, 2.530(2); Na2–N9, 2.461(2); Na2–N10, 2.506(2); N4–Zn1–N5, 108.44(8); N4–Zn1–N6, 108.38(8); N4–Zn1–N7, 110.87(7); N5–Zn1–N6, 113.06(8); N5–Zn1–N7, 108.60(8); N6–Zn1–N7, 107.50(8); N1–Na1–N2, 76.41(7); N1–Na1–N3, 108.60(7); N1–Na1–N4, 122.73(7); N2–Na1–N3, 75.27(6); N2–Na1–N4, 140.37(7); N3–Na1–N4, 120.75(7); N7–Na2–N8, 113.76(8); N7–Na2–N9, 146.11(7); N7–Na2–N10, 122.11(7); N8–Na2–N9, 73.43(7); N8–Na2–N10, 118.46(8); N9–Na2–N10, 74.44(7).

The basic metal–pyrrolyl skeletons of **10** and **11** could be considered *Weiss motifs* as this general electrostatically–favoured arrangement (Figure 3.9a) was reported for several alkali metal ate complexes in the seminal structural studies of Erwin Weiss, a pioneer of organolithium structural chemistry.^[216b] Surprisingly **10** and **11** represent the first *Weiss motifs* for a sodium zincate pyrrolyl compound, or indeed for a pyrrolyl compound of any metal combination, despite the prevalence of the *Weiss motif* within higher-order alkali metal zincate species. The closest *Weiss* analogy to **10** and **11** is the mixed alkyl–amido lithium zincate [(TMEDA)₂·Li₂Zn(Me)(NMe₂)₃],^[218] but there are also related structures in magnesiate chemistry (Figure 3.9b, *vide infra*). *Weiss motifs* also extend to transition metal ate systems as witnessed in the structure of the higher-order cobaltate [Li₂Co(O-*o*-Tol)₄(THF)₄].

Table 3.1: Comparison of Na⋯pyrrolyl bond lengths in complexes **9** – **11**.

Bond	Bond Length (Å)				
	9 ^[a]	9 ^[b]	10	11 ^[c]	11 ^[d]
Na-N	2.9191(15)	3.3753(1)	2.735(3)	2.5884(18)	2.551(2)
Na-αCH	2.8554(19)	3.1933(1)	2.786(3)	2.737(2)	2.821(2)
Na-α'CH	2.8172(19)	3.0681(19)	2.950(3)	2.746(2)	2.680(3)
Na-βCH	2.737(2)	2.7806(18)	3.036(3)	2.993(2)	3.100(3)
Na-β'CH	2.709(2)	2.6908(18)	3.129(3)	3.002(2)	3.008(3)

a) data for Na1⋯N2; b) data for Na1⋯N4; c) data for Na1⋯N4; d) data for Na2⋯N7.

3.3.3 Synthesis and Solid State Characterisation of a Sodiopyrrole Species

The final synthesis in this chapter was that of the homometallic sodiopyrrole complex **12**. It was the sole solid product obtained from a reaction containing a 2: 1: 2, ⁿBuNa: Et₂Zn: HNC₄H₄ stoichiometry to which PMDETA (two molar equivalents) was added (Scheme 3.5). Having a deficiency of zinc with respect to the number of moles of pyrrole present, this mixture held the prospect of generating a zinc-free sodiopyrrole product and such a product duly crystallised preferentially in a best

yield of 53%. The reaction was shown to be reproducible, and so the rational preparation was not attempted. A second product (the aforementioned compound **11**) was observed through ^1H NMR spectroscopic analysis of the filtrate.

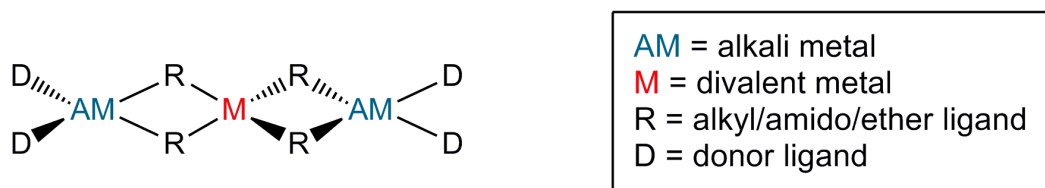


Figure 3.9a ChemDraw representation of a general *Weiss motif* structure for a higher order ate.

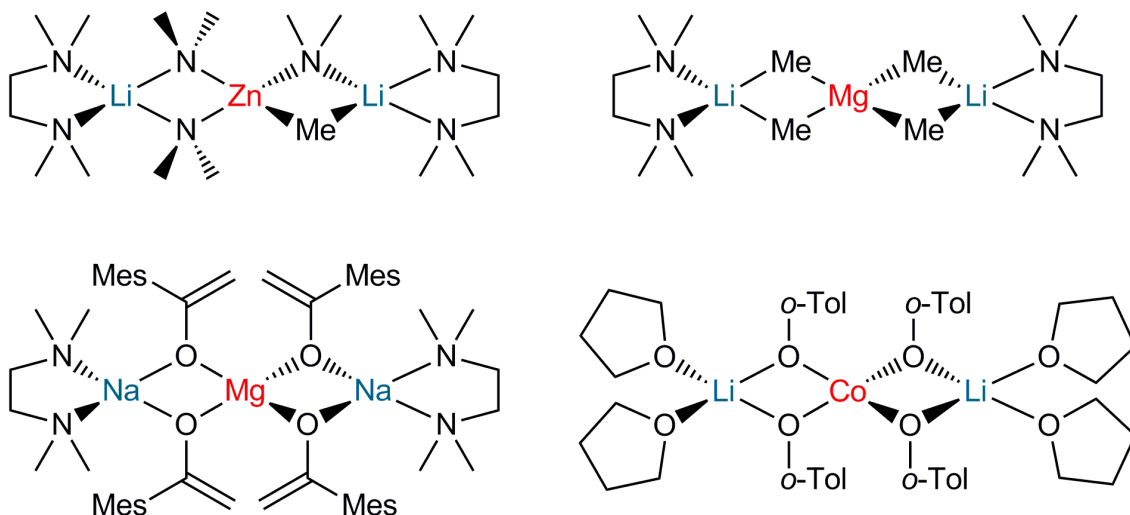
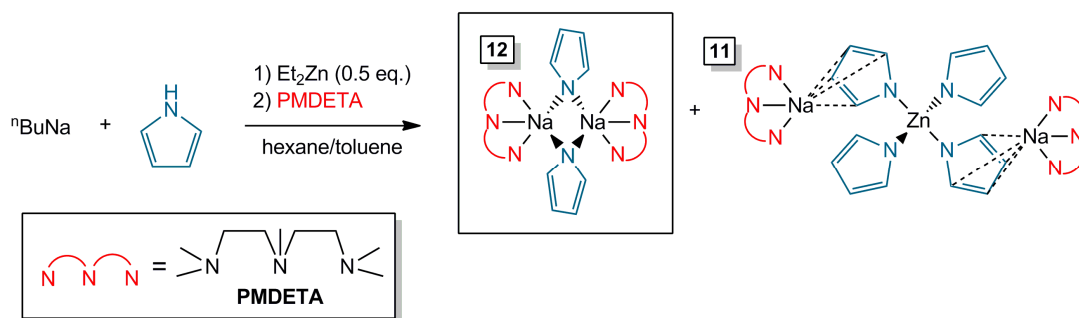


Figure 3.9b Literature examples of ate compounds displaying a *Weiss motif*; $[\text{Li}_2\text{Zn}(\text{NMe}_2)_3(\text{Me})(\text{TMEDA})_2]$,^[218] $[\text{Li}_2\text{Mg}(\text{Me})_4(\text{TMEDA})_2]$,^[219] $[\text{Na}_2\text{Mg}(\mu\text{-OC}(\text{=CH}_2)\text{Mes})_4(\text{TMEDA})_2]$ ^[220] and $[\text{Li}_2\text{Co}(\text{O-}o\text{-Tol})_4(\text{THF})_4]$.^[221]

In all three of the sodium pyrrolylzincate structures uncovered through this research, without exception, the sodium cation engages with the π -system of the *N*-heterocycle. To investigate the structural and bonding effects of removing the zinc bis-pyrrolyl component, the crystal structure of **12** was determined. The chelating PMDETA ligands were modelled as disordered over two sites. This complex is formally the (zinc bis-pyrrolyl component)-free variant of sodium zincate **11**. Possessing C_i symmetry, the molecular structure of **12** (Figure 3.10) is dimeric with a

central, planar ($\text{NaN}_{\text{pyrrolyl}}\text{)}_2$ ring, the metal corners of which carry tridentate-attached PMDETA ligands. Dimeric ring motifs of this type are well preceded in sodium (and especially lithium) amide chemistry as for example in $[\{(\text{TMEDA})\cdot\text{Na}(\text{NPh}_2)\}_2]$,^[177c] $[\{(\text{PMDETA})\cdot\text{Na}(\text{NHPH})\}_2]$ ^[177b] and $[\{(\text{TMEDA})\cdot\text{Li}(\text{C}_4\text{H}_3\text{NPh})\}_2]$.^[176]



Scheme 3.5 Synthesis of homometallic sodiopyrrole **12**.

Interestingly the Na cation in **12** interacts exclusively with the anionic N of the pyrrolyl ligand avoiding π -contact with the NC_4H_4 ring C atoms. This signifies a major departure from the π -bonding modes exhibited by the $\text{Na}-\text{NC}_4\text{H}_4$ contacts in the zincates **9–11**. There are grounds therefore for arguing that a metal–metal cooperative effect is in operation within the zincate systems, with zinc forcing sodium to amend its bonding stance towards the coordinatively–flexible heterocyclic ligand as zinc demands the σ bonding component of the N atom.

3.3.4 Solution NMR Spectroscopic Studies

As a consequence of pyrrole metallation, significant downfield shifts are observed for the signals attributed to the heterocycles α - and β -positions, evident in both the ^1H and $^{13}\text{C}\{\text{H}\}$ NMR spectra (refer to Table 3.2 and Table 3.3 for comparative data). Owing to the increased polarity of the M–N bond (M = Zn/Na), the N centre experiences a greater negative charge in comparison to the more covalent N–H unit in free pyrrole. This in turn decreases the deshielding experienced by the α -hydrogen

atoms. For example, the ^1H chemical shift increases from 6.37 to 7.42 ppm for compound **11** (whilst the $^{13}\text{C}\{\text{H}\}$ chemical shift increases from 117.5 to 127.3 ppm). Comparison of the chemical shifts for **11** and **12** reveals that the largest deviation for the α -CH pyrrole resonance is observed for sodium zincate **11** (with a deviation of 1.05 ppm from free pyrrole), rather than for the sodium analogue **12** (with a deviation of 0.84 ppm). It therefore seems that the ate effect outweighs the greater electropositive nature of sodium in comparison to zinc. The β -H atoms, which are further removed from the N centre, experience an attenuated deshielding effect (from 6.31 to 6.58 ppm for **11**). For ^1H and $^{13}\text{C}\{\text{H}\}$ NMR spectra analysed using C_6D_6 solvent, pyrrole metallation leads to increased chemical shift separation between α - and β - signals, while in d_8 -THF, differences in the chemical shift are diminished.

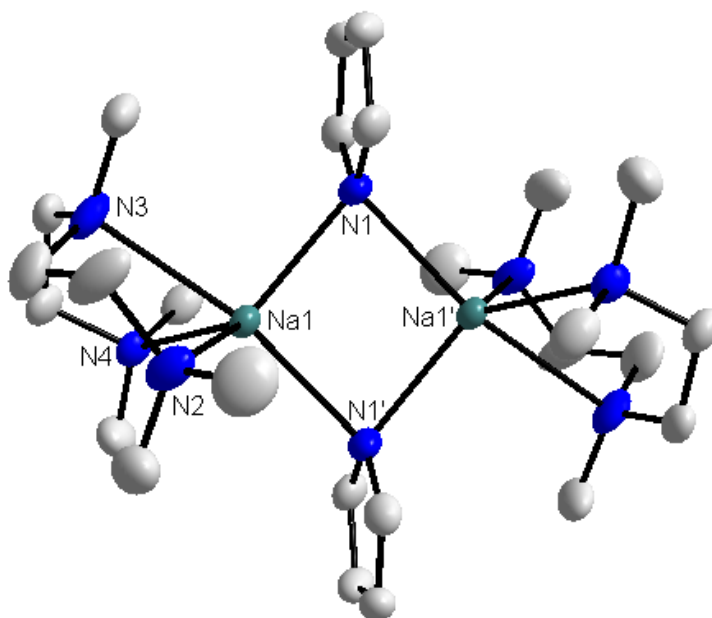


Figure 3.10 Molecular structure of **12** with thermal ellipsoids drawn at the 50% probability level and hydrogen atoms and minor disordered component omitted for clarity. Selected bond lengths (\AA) and bond angles ($^\circ$): Na1-N1, 2.4312(17); Na1-N1', 2.4803(15); Na1-N2, 2.62(4); Na1-N3, 2.61(3); Na1-N4, 2.487(14); N1-Na1-N1', 95.30(5); N1-Na1-N2, 116.7(6); N1-Na1-N3, 96.0(4); N1-Na1-N4, 102.8(2); N2-Na1-N3, 70.6(6); N2-Na1-N4, 112.6(7); N3-Na1-N4, 66.9(3); Na1-N1-Na1', 95.30(5).

Table 3.2: ^1H NMR Spectroscopic Data.

Compound	Chemical Shift (δ /ppm)				Solvent
	α -CH	β -CH	Difference (α -CH)	Difference (β -CH)	
Free Pyrrole	6.37	6.31	-	-	C_6D_6
$[\text{}^t\text{BuZn}(\text{NC}_4\text{H}_4)(\text{TMEDA})\cdot\text{HNC}_4\text{H}_4]$, 7 ^[a]	7.07	6.88	0.70	0.57	C_6D_6
$[\text{Zn}(\text{NC}_4\text{H}_4)_2(\text{TMEDA})]$, 8	7.10	6.92	0.73	0.61	C_6D_6
$[\{(\text{PMDETA})\cdot\text{Na}\}_2\text{Zn}(\text{NC}_4\text{H}_4)_4]$, 11	7.42	6.58	1.05	0.27	C_6D_6
$[\{(\text{PMDETA})\cdot\text{Na}(\text{NC}_4\text{H}_4)_2\}_2]$, 12	7.21	6.74	0.84	0.43	C_6D_6
Free Pyrrole	6.65	6.03	-	-	d_8 -THF
$[\{(\text{THF})_2\cdot\text{NaZn}(\text{THF})(\text{NC}_4\text{H}_4)_3\}_\infty]$, 9	6.94	6.05	0.29	0.02	d_8 -THF
$[\{(\text{TMEDA})\cdot\text{Na}\}_2\text{Zn}(\text{NC}_4\text{H}_4)_4]$, 10	6.72	6.04	0.07	0.01	d_8 -THF

a) ^1H signals arising due to the HNC_4H_4 pyrrole molecule are not considered within Table 3.2.

Table 3.3: $^{13}\text{C}\{\text{H}\}$ NMR Spectroscopic Data.

Compound	Chemical Shift (δ /ppm)				Solvent
	α -CH	β -CH	Difference (α -CH)	Difference (β -CH)	
Free Pyrrole	117.5	108.4	-	-	C_6D_6
$[\text{}^t\text{BuZn}(\text{NC}_4\text{H}_4)(\text{TMEDA})\cdot\text{HNC}_4\text{H}_4]$, 7 ^[a]	127.2	107.5	9.7	0.9	C_6D_6
$[\text{Zn}(\text{NC}_4\text{H}_4)_2(\text{TMEDA})]$, 8	126.9	108.4	9.4	0.0	C_6D_6
$[\{(\text{PMDETA})\cdot\text{Na}\}_2\text{Zn}(\text{NC}_4\text{H}_4)_4]$, 11	127.3	107.3	9.8	1.1	C_6D_6
$[\{(\text{PMDETA})\cdot\text{Na}(\text{NC}_4\text{H}_4)_2\}_2]$, 12	127.9	106.8	10.4	1.6	C_6D_6
Free Pyrrole	117.9	108.0	-	-	d_8 -THF
$[\{(\text{THF})_2\cdot\text{NaZn}(\text{THF})(\text{NC}_4\text{H}_4)_3\}_\infty]$, 9	127.0	106.7	9.1	1.3	d_8 -THF
$[\{(\text{TMEDA})\cdot\text{Na}\}_2\text{Zn}(\text{NC}_4\text{H}_4)_4]$, 10	126.9	107.4	9.0	0.6	d_8 -THF

a) $^{13}\text{C}\{\text{H}\}$ signals arising due to the HNC_4H_4 pyrrole molecule are not considered within Table 3.3

Variable temperature ^1H NMR analysis was performed on **11** in C_6D_6 solution. At ambient temperature, only two pyrrolyl signals (α -CH and β -CH) were observed (at 7.42 and 6.58 ppm, respectively) in the ^1H NMR spectrum indicating that the four pyrrolyl ligands are equivalent under these conditions. Even when the NMR experiment was repeated at low temperature ($-50\text{ }^\circ\text{C}$), no distinction was observed between the terminal pyrrole ligands and those π -bonded to sodium. It is also worthy of note that the NMR spectra of compounds **9-12** show the absence of ^tBu signals, indicating that no heteroanionic butyl-pyrrolyl products had formed.

3.4 Concluding Remarks on Metal Derivatives of Pyrrole

Applying a straightforward, mixed metal deprotonation strategy, we have successfully attached one, two, three or four *N*-deprotonated pyrrole ligands to a zinc centre. Within this set of zinc pyrrolyl compounds, three homoleptic sodium zincate formulations have been synthesised, isolated from solution and structurally characterised. Cross-coupling reactions represent one of the major applications of organozinc reagents within synthetic chemistry, and in this regard these homoleptic complexes present a potential advantage over their heteroleptic relatives, which can complicate cross-coupling reactions through the greater number of available by-products.

In all the neutral and anionic (ate) zinc complexes prepared in this work, the pyrrolyl ligands engage the Group 12 metal in a σ -fashion, in contrast to their predominately π -bonding engagement with the sodium cations completing the bimetallic zincate contacted ion-pair structures. Evidence from a zinc-free sodium pyrrolyl structure prepared for comparative purposes, which shows a large proportion of Na-N(pyrrolyl) σ -bonding, suggests the alkali metal is relegated to a subordinate bonding role when combined with the stronger Lewis acid zinc in pyrrolyl-zincate structures.

3.5 Future Work

Within this part of the PhD project, the non-substituted parent pyrrole ligand was successfully incorporated into homoleptic tri- and tetra-anionic sodium zincate formulations. In the future, the scope of this research should be extended to *N*-derivatised pyrrole substrates, such as *N*-methylpyrrole, which provide a more challenging metal-hydrogen exchange target owing to the greater strength of *C-H* bonds in comparison to their more acidic and hence more labile *N-H* counterparts.

Subsequently, the dimetallation of *N*-derivatised pyrrole substrates should also be investigated.

One of the most prevalent applications of organozinc chemistry is within cross-coupling reactions, where an organozinc reagent used in conjunction with an organic halide and a nickel or palladium catalyst facilitates the stereoselective formation of a carbon-carbon bond. Highlighting the synthetic importance of cross-coupling reactions, Negishi was awarded the Nobel Prize in 2010 (shared with Heck and Suzuki) for pioneering the development of this methodology. However, many existing sodium zincate systems are heteroleptic, involving a mixture of ligands which can complicate cross-coupling reactions as there are several potential homo and hetero-coupled by-products. In comparison, the homoleptic sodium zincate systems developed within this part of the PhD project offer a reduced number of cross-coupling by-products. Future work shall therefore be directed towards testing this family of compounds within cross-coupling reactions.

Pertinent to heterocyclic chemistry, oligomeric heterocyclic compounds are sought-after synthetic targets on account of their electronic and optoelectronic properties.^[222] Indeed, oligomeric thiophenes have previously been synthesised through the regioselective metallation of substituted thiophene substrates using the Knochel-Hauser base (TMPMgCl·LiCl), followed by cross-coupling with bromothiophene promoted by a nickel catalyst.^[223] Such chemistry should be explored with *N*-derivatised pyrrole compounds, in an attempt to build up oligomeric scaffolds. In addition, extending the scope of this chemistry to the synthesis of mixed thiophene-pyrrole and furan-pyrrole oligomers may prove interesting, as these highly conjugated organic materials have many potential applications, for example within photovoltaic cells and field-effect transistors.^[224]

Furthermore, the metallation of ring-substituted *N*-derivatised pyrrole ligands should be probed. Recently, through a combination of *ortho*-metallation and *alpha*-metallation, the dizincation of a substituted thiophene compound was achieved which led to the formation of a supramolecular, 16-membered metallocyclic ring structure

$[\{D_2Na[\mu-3,5-[2-C(O)NEt_2]-C_4H_1S]Zn(tBu)\}_4]$, where D represents the donor ligand (either didentate TMEDA or two monodentate THF ligands).^[225] Due to the similarity between isoelectronic pyrrole and thiophene, the dimetallation of substituted pyrrole and indole systems should also be investigated. More specifically, the metallation of pyrrole or indole substrates possessing a directing metallating group, therefore providing competitive *ortho*- and *alpha*-metallation sites, should be examined (Figure 3.11).

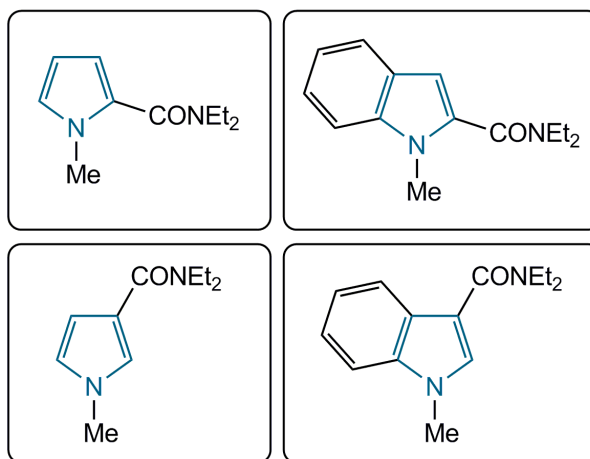


Figure 3.11 ChemDraw representation of example amide-substituted pyrrole substrates having potential competitive metallation sites.

Studies reported in Chapters 5 and 6 have shown that the incorporation of a multifunctional amine within a bimetallic environment can instigate novel molecular structures and promote unexpected reactivities. Future work could therefore probe the metallation of pyrrole substrates involving an additional amine functional group, such as the donor appended pyrrole substrate illustrated in Figure 3.12.^[226]

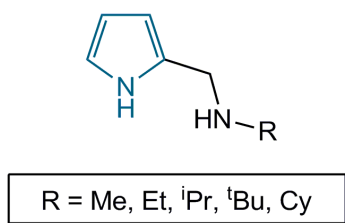


Figure 3.12 ChemDraw representation of an example substituted pyrrole substrate containing a donor appended amine arm.^[226]

3.6 Experimental

3.6.1 Synthesis of $[{}^t\text{BuZn}(\text{NC}_4\text{H}_4)(\text{TMEDA})\cdot\text{HNC}_4\text{H}_4]$, **7**

Under Ar atmosphere, TMEDA (0.30 mL, 2 mmol) was transferred *via* syringe to a solution of ${}^t\text{Bu}_2\text{Zn}$ (0.36 g, 2 mmol) in hexane (10 mL). The reaction mixture was allowed to stir for 10 minutes. Pyrrole (0.28 mL, 4 mmol) was then added, producing a yellow solution. A crop of colourless crystals (0.59 g, 80% yield) was formed upon gently agitating the flask.

${}^1\text{H}$ NMR (400.03 MHz, C_6D_6 , 300 K): δ = 7.07 (m, 2H, α -CH₂, ZnNC₄H₄), 6.88 (m, 2H, β -CH₂, ZnNC₄H₄), 6.39 [dd, ${}^3\text{J}(\text{H},\text{H}) = 4.1$ Hz, ${}^4\text{J}(\text{H},\text{H}) = 2.0$ Hz, 2H, α -CH₂, HNC₄H₄], 6.32 [dd, ${}^3\text{J}(\text{H},\text{H}) = 4.1$ Hz, ${}^4\text{J}(\text{H},\text{H}) = 2.1$ Hz, β -CH₂, HNC₄H₄], 1.79 (s, 12H, CH₃-TMEDA), 1.66 (br s, 4H, CH₂-TMEDA) and 1.43 ppm (s, 9H, ${}^t\text{Bu}$).
 ${}^{13}\text{C}\{\text{H}\}$ NMR (100.60 MHz, C_6D_6 , 300 K): δ = 127.2 (s, α -CH₂, ZnNC₄H₄), 117.5 (s, α -CH₂, HNC₄H₄), 108.3 (s, β -CH₂, HNC₄H₄), 107.5 (s, β -CH₂, ZnNC₄H₄), 57.1 (s, CH₃-TMEDA), 47.3 (s, CH₂-TMEDA) and 34.8 ppm (s, ${}^t\text{Bu}$).

Owing to traces of **8** present in the crystalline product, experimental microanalysis values did not match the theoretical values.

Crystal data for **7**: $\text{C}_{18}\text{H}_{34}\text{N}_4\text{Zn}$, $M_r = 371.86$, orthorhombic, space group $Pn2_1$, $a = 15.6099(2)$, $b = 9.6563(1)$, $c = 27.2685(4)$ Å, $V = 4110.29(9)$ Å³, $Z = 8$, $\mu = 1.200$ mm⁻¹, 48155 reflections, 10490 unique, $R_{int} = 0.0214$, final refinement to full-matrix least squares on F^2 gave $R = 0.0241$ (F , 9180 obs. data only) and $R_w = 0.0573$ (F^2 , all data), GOF = 1.010.

3.6.2 Synthesis of $[\text{Zn}(\text{NC}_4\text{H}_4)_2(\text{TMEDA})]$, **8**

TMEDA (0.15 mL, 1 mmol) was transferred *via* syringe to a solution of ${}^t\text{Bu}_2\text{Zn}$ (0.36 g, 1 mmol) in hexane (5 mL). The reaction mixture was allowed to stir for 10 minutes. Pyrrole (0.28 mL, 4 mmol) was then introduced, producing a yellow

solution. A crop of colourless crystals (0.28 g, 89% yield) was formed upon gently agitating the flask.

^1H NMR (400.03 MHz, C_6D_6 , 300 K): δ = 7.10 (m, 4H, α - CH_2 , ZnNC_4H_4), 6.92 (m, 4H, β - CH_2 , ZnNC_4H_4), 1.66 (s, 12H, CH_3 -TMEDA) and 1.48 ppm (s, 4H, CH_2 -TMEDA). $^{13}\text{C}\{\text{H}\}$ NMR (100.59 MHz, C_6D_6 , 300 K): δ = 126.9 (s, α - CH_2 , ZnNC_4H_4), 108.4 (s, β - CH_2 , ZnNC_4H_4), 56.7 (s, CH_2 -TMEDA) and 46.8 ppm (s, CH_3 -TMEDA).

Due to the extreme air- and moisture-sensitivity of this compound, satisfactory elemental microanalysis data could not be obtained.

Crystal data for **8**: $\text{C}_{14}\text{H}_{24}\text{N}_4\text{Zn}$, $M_r = 313.74$, orthorhombic, space group $Pn\bar{a}2_1$, $a = 15.4350(3)$, $b = 10.3607(2)$, $c = 9.7566(2)$ Å, $V = 1560.25(5)$ Å³, $Z = 4$, $\mu = 1.568$ mm⁻¹, 29629 reflections, 4140 unique, $R_{int} = 0.0300$, final refinement to full-matrix least squares on F^2 gave $R = 0.0239$ (F , 3913 obs. data only) and $R_w = 0.0582$ (F^2 , all data), GOF = 1.030.

3.6.3 Synthesis of $\{[(\text{THF})_2\text{NaZn}(\text{THF})(\text{NC}_4\text{H}_4)_3]_\infty\}$, **9**

$^n\text{Bu}_2\text{Zn}$ (2 mL of a 1.0 M solution in heptane, 2 mmol) was transferred *via* syringe to a suspension of freshly prepared $^n\text{BuNa}$ (0.16 g, 2 mmol) in hexane (10 mL), producing a pale-brown solution. Pyrrole (0.42 mL, 6 mmol) was then added *via* syringe to the mixture, forming a white suspension. The reaction mixture was allowed to stir for 30 minutes. THF (3 mL) was subsequently added *via* syringe. Approximately half of the solvent was removed *in vacuo*. Toluene (8 mL) was then added. The resulting pale brown solution was transferred to the freezer at -30°C . This solution deposited a crop of colourless crystals (0.28 g, 28% yield) after 48 hours.

^1H NMR (400.03 MHz, d_8 -THF, 300 K): δ = 6.94 (br. s, 6H, α - CH_2 , ZnNC_4H_4), 6.05 (m, 6H, β - CH_2 , ZnNC_4H_4), 3.62 (m, 3H, α - CH_2 , THF) and 1.77 ppm (m, 3H, β - CH_2 , THF). $^{13}\text{C}\{\text{H}\}$ NMR (100.60 MHz, d_8 -THF, 300 K): δ = 127.0 (s, α - CH_2 , ZnNC_4H_4), 106.7 (s, β - CH_2 , ZnNC_4H_4), 68.2 (s, α - CH_2 , THF) and 26.4 ppm (s, β - CH_2 , THF).

As labile THF is removed under vacuum upon isolation of crystalline **9**, satisfactory elemental microanalysis values could not be obtained.

Crystal data for **9**: C₂₄H₃₆N₃NaO₃Zn, M_r = 502.92, triclinic, space group P-1, *a* = 8.3429(2), *b* = 11.0909(3), *c* = 14.1002(3) Å, *α* = 94.178(2), *β* = 104.038(2), *γ* = 95.994(2)°, *V* = 1252.28(5) Å³, *Z* = 2, *μ* = 1.027 mm⁻¹, 14316 reflections, 6611 unique, *R*_{int} 0.0303, final refinement to full-matrix least squares on *F*² gave *R* = 0.0364 (*F*, 5404 obs. data only) and *R*_w = 0.0822 (*F*², all data), GOF = 1.037.

3.6.4 Synthesis of [(TMEDA)·Na]₂Zn(NC₄H₄)₄, **10**

ⁿBu₂Zn (2 mL of a 1.0 M solution in heptane, 2 mmol) was transferred *via* syringe to a suspension of ⁿBuNa (0.16 g, 2 mmol) in hexane (10 mL), giving a pale-brown solution. Pyrrole (0.14 mL, 2 mmol) was then added *via* syringe to the mixture, forming a white suspension. TMEDA (2.40 mL, 16 mmol) was injected into the reaction mixture *via* syringe and the resulting mixture was allowed to stir for 1 hour. The white solid produced was removed *via* filtration. A colourless solid began to precipitate. Toluene (15 mL) was added and the filtrate was heated, producing a solution which was then slowly cooled to room temperature. Colourless crystals [0.15 g, 12% yield based upon the pyrrole stoichiometry (i.e. with a maximum yield of 25%)] were formed from the filtrate after 18 hours.

¹H NMR (400.03 MHz, *d*₈-THF, 300 K): *δ* = 6.73 (br. s, 8H, α-CH₂, ZnNC₄H₄), 6.04 (m, 8H, β-CH₂, ZnNC₄H₄), 2.86 (s, 8H, CH₂-TMEDA) and 2.50 ppm (s, 24H, CH₃-TMEDA). ¹³C{¹H} NMR (100.60 MHz, *d*₈-THF, 300 K): *δ* = 126.9 (s, α-CH₂, ZnNC₄H₄), 107.4 (s, β-CH₂, ZnNC₄H₄), 58.2 (s, CH₂-TMEDA) and 47.7 ppm (s, CH₃-TMEDA).

Due to the extreme air- and moisture-sensitivity of this compound, satisfactory elemental microanalysis data could not be obtained.

Crystal data for **10**: C₂₈H₄₈N₈Na₂Zn, M_r = 608.09, tetragonal, space group P -4n2, *a* = 12.2787(6), *b* = 12.2787(6), *c* = 11.2091(9) Å, *V* = 1689.96(18) Å³, *Z* = 2, *μ* = 0.781 mm⁻¹, 4944 reflections, 1938 unique, *R*_{int} 0.0440, final refinement to full-

matrix least squares on F^2 gave $R = 0.0464$ (F, 1532 obs. data only) and $R_w = 0.0902$ (F^2 , all data), GOF = 1.058.

3.6.5 Synthesis of $[\{(PMDETA)\cdot Na\}_2Zn(NC_4H_4)_4]$, **11**

A solution of tBu_2Zn (0.18 g, 1 mmol) in hexane (5 mL) was transferred *via* syringe to a suspension of nBuNa (0.16 g, 2 mmol) in hexane (10 mL), to afford a pale brown solution. Next, pyrrole (0.28 mL, 4 mmol) was added *via* syringe to the mixture, forming a white suspension. PMDETA (0.42 mL, 2 mmol) was then injected *via* syringe forming a white oil. The reaction mixture was stirred for 30 minutes. Toluene (15 mL) was then added and the reaction mixture was briefly heated with a heat gun to form a colourless solution. The resulting solution was transferred to the refrigerator (4 °C) and colourless crystals (0.44 g, 61% yield) were obtained after 24 hours.

1H NMR (400.03 MHz, C_6D_6 , 300 K): $\delta = 7.42$ (s, 8H, α - CH_2 , $ZnNC_4H_4$), 6.58 (s, 8H, β - CH_2 , $ZnNC_4H_4$), 1.73 (s, 24H, $N(CH_3)_2$ -PMDETA), 1.61 (s, 6H, NCH_3 -PMDETA) and 1.52 ppm (s, 16H, CH_2 -PMDETA); ${}^{13}C\{H\}$ NMR (100.60 MHz, C_6D_6 , 300 K): $\delta = 127.3$ (s, α - CH_2 , $ZnNC_4H_4$), 107.3 (s, β - CH_2 , $ZnNC_4H_4$), 57.1 (s, CH_2 -PMDETA), 54.7 (s, CH_2 -PMDETA), 45.3 (s, $N(CH_3)_2$ -PMDETA) and 43.0 ppm (s, NCH_3 -PMDETA).

El. Microanalysis calc. for $[\{(PMDETA)\cdot Na\}_2Zn(NC_4H_4)_4]$ ($M_r = 722.29$) C, 56.54; H, 8.65; N, 19.39%; found: C, 56.63; H, 9.07; N, 19.37%.

Crystal data for **11**: $C_{34}H_{62}N_{10}Na_2Zn$, $M_r = 722.29$, monoclinic, space group $P 2_1/c$, $a = 9.0953(9)$, $b = 25.2534(13)$, $c = 17.1703(8)$ Å, $\beta = 102.034(5)^\circ$, $V = 8097.9(7)$ Å³, $Z = 8$, $\mu = 0.664$ mm⁻¹, 41267 reflections, 17641 unique, R_{int} 0.0378, final refinement to full-matrix least squares on F^2 gave $R = 0.0439$ (F, 12360 obs. data only) and $R_w = 0.0984$ (F^2 , all data), GOF = 1.015.

3.6.6 Synthesis of $[\{(PMDETA)\cdot Na(NC_4H_4)\}_2]$, **12**

Pyrrole (0.28 mL, 4 mmol) was added *via* syringe to a suspension of nBuNa (0.32 g, 4 mmol) in hexane (10 mL). The white suspension was subsequently stirred for 2 hours 30 minutes. Et_2Zn (2.0 mL of a 1.0M solution in heptane, 2 mmol) was then injected *via* syringe to the Schlenk tube. The reaction mixture was then stirred for 30 minutes. PMDETA (0.84 mL, 4 mmol) was transferred *via* syringe to the mixture. Toluene (15 mL) was then added to the yellow suspension that had formed. The resulting solution was transferred to the refrigerator (4 °C) where colourless crystals (0.56 g, 53% yield) grew over 24 hours.

1H NMR (400.03 MHz, C_6D_6 , 300 K): δ = 7.21 (br. s, 4H, α - CH_2 , $NaN(C_4H_4)$), 6.74 (br. s, 4H, β - CH_2 , $NaN(C_4H_4)$), 2.03 (s, 24H, $N(CH_3)_2$ -PMDETA), 1.87 and 1.84 [t, $^3J(H,H) = 2.8$ Hz, 8H, CH_2 -PMDETA] and 1.66 ppm (s, 6H, NCH_3 -PMDETA).
 $^{13}C\{H\}$ NMR (100.60 MHz, C_6D_6 , 300 K): δ = 127.9 (s, α - CH_2 , $NaN(C_4H_4)$), 106.8 (s, β - CH_2 , $NaN(C_4H_4)$), 57.2 (s, CH_2 -PMDETA), 55.0 (s, CH_2 -PMDETA), 45.3 (s, $N(CH_3)$ -PMDETA) and 41.3 ppm (s, $N(CH_3)_2$ -PMDETA).

El. Microanalysis calc. for $[\{(PMDETA)\cdot Na(NC_4H_4)\}_2]$ ($M_r = 524.75$) C, 59.51; H, 10.37; N, 21.35%; found: C, 58.64; H, 10.91; N, 21.40%.

Crystal data for **12**: $C_{26}H_{54}N_8Na_2$, $M_r = 524.75$, monoclinic, space group $P 2_1/n$, $a = 9.3617(5)$, $b = 9.6380(4)$, $c = 18.0907(8)$ Å, $\beta = 100.702(5)^\circ$, $V = 1603.90(13)$ Å³, $Z = 2$, $\mu = 0.090$ mm⁻¹, 8124 reflections, 38641 unique, R_{int} 0.0224, final refinement to full-matrix least squares on F^2 gave $R = 0.0595$ (F , 2857 obs. data only) and $R_w = 0.1589$ (F^2 , all data), GOF = 1.026.

Chapter 4

Ambient Temperature Zincation of *N*-Boc Pyrrolidine: Synthesis, Structure and Reactivity of a Sodium Pyrrolidide-Zincate Reagent

“I believe there is no philosophical high-road in science,
with epistemological signposts.
No, we are in a jungle and find our way by trial and error,
building our road behind us as we proceed.”

Max Born

German physicist

Nobel Prize for Physics, 1954

4.1 Summary

Sodium TMP-zincate, [(TMEDA)Na(μ -TMP)(μ -^tBu)Zn(^tBu)], can deprotonate *N*-Boc pyrrolidine cleanly at ambient temperature in hexane solution, whereas in toluene the captured α -carbanion of the heterocycle attacks the solvent setting off a cascade of reactions that ultimately produce a pyrrolidine-substituted enolate. Extending the scope of this sodium pyrrolidide-zincate base methodology towards ferrocene and anisole resulted in C-H bond cleavage and capture of the zincated substrates within a sodium TMP-zincate framework.

4.2 Introduction to Achieving the α -sp³ Functionalisation of Pyrrolidine

Pyrrolidines are an important class of nitrogen heterocycle which feature in many natural products and pharmaceutical agents. Treatments containing α -aryl-substituted pyrrolidines are known for many diseases including cancer,^[227] Parkinson's disease,^[228] and Alzheimer's disease.^[229] These heterocycles also play various roles in catalysis.^[230] Functionalisation at the α -sp³ carbon atom of the saturated, five-membered (NC₄) ring is often a key step in the synthesis of substituted pyrrolidines and this is usually done with prior protection of the nucleophilic N atom, often with the bulky *tert*-butyloxycarbonyl (Boc) group as it is inert to many nucleophiles and basic reagents. *N*-Boc derivatives can be readily formed using environmentally benign conditions that are solvent free and catalyst free.^[231] With related carbamate esters such as 1-phenylethyl diisopropylcarbamate, the α -OCH and α -NCH offer competitive deprotonation sites:^[232] advantageously the absence of α -OCH within Boc impedes such side-reactions.

Lithiation (C-*H* to C-*Li* exchange) can open the door to α -pyrrolidine functionalisation provided a sub-ambient temperature regime is strictly followed to

avoid the decomposition of the sensitive ester-carrying pyrrolidine. For example, to use ^sBuLi activated by TMEDA (*N, N, N', N'*-tetramethylethylenediamine) in Et₂O solution, the temperature must be lowered to -78 °C,^[233] while even in the absence of TMEDA the temperature can only be raised to -30 °C (in THF solution).^[234] Introduction of a chiral amine provides access to asymmetric *N*-Boc pyrrolidines as pioneered by Beak through a ^sBuLi/(-)-sparteine combination.^[235] Building on this foundation, Campos and O'Brien^[234] have developed an enantioselective deprotonative-lithiation/transmetallation/Negishi coupling tandem sequence to produce a series of Boc-protected α-arylated pyrrolidines. More recently, this methodology has been extended to enantioconvergent Negishi cross coupling reactions through the incorporation of a chiral Ni catalyst.^[236] Post lithiation [performed at -78 °C in *tert*-butyl methyl ether or Et₂O solvent], transmetallation *via* the salt ZnCl₂ generates an α-zincated pyrrolidine intermediate.^[234] However, this is not isolated from solution and so its exact composition and structure is unknown. Similarly, a recent patent^[227] detailing the synthesis of anti-cancer treatments which act as benzoxepin PI3K inhibitors, mentions zincated pyrrolidines [α-Zn(Cl)C₄H₇N-Boc] and [β-Zn(I)C₄H₇N-Boc] but does not give any characterisational details.

Here in this part of the project we report a new “low polarity” metallation methodology for the unprecedented room temperature deprotonation of *N*-Boc pyrrolidine and, also for the first time, provide detailed crystallographic and spectroscopic data on a metallated *N*-Boc pyrrolidine intermediate.^[73] Investigating the solvent dependency of this reaction, we also reveal explicit information about the destiny of the Boc protecting group when a metallated *N*-Boc pyrrolidine attacks the toluene solvent. Agami and Couty remarked upon the paucity of knowledge of such metal-mediated Boc decomposition processes in a review article.^[237] Furthermore, we reveal the contrasting outcomes of introducing alternative substrates, such as ferrocene or anisole, into the sodium pyrrolidide-zincate system.

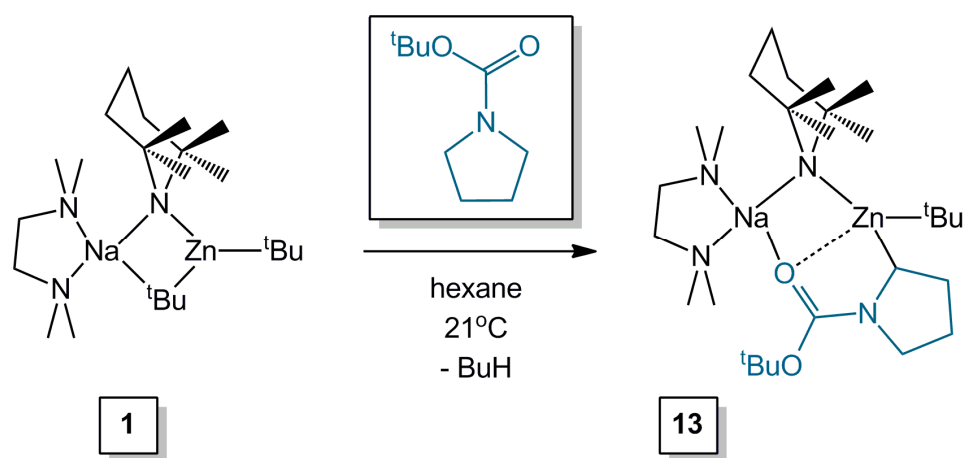
4.3 Results and Discussion

4.3.1 The Quest for Ambient Temperature Metallation

Our primary goal was to prepare a zincated *N*-Boc pyrrolidine through a room temperature direct (single step) hydrogen-zinc exchange reaction as a marked improvement on the low temperature two step lithiation/ ZnCl_2 -transmetallation protocol generally utilised for access to organozinc compounds. Alkylzinc reagents are weak bases incapable of executing C-H deprotonation on relatively non-acidic substrates (for completeness we checked and confirmed the failure of the reaction between *N*-Boc pyrrolidine and ${}^t\text{Bu}_2\text{Zn}$ in the presence of TMEDA) so we turned our attention to the heteroleptic alkyl-amido sodium zincate base $[(\text{TMEDA})\text{Na}(\mu\text{-TMP})(\mu\text{-}{}^t\text{Bu})\text{Zn}({}^t\text{Bu})]$, **1** (TMP = 2, 2, 6, 6-tetramethylpiperidide) developed previously by our group.^[140a; 148; 177d; 238] One of a new generation of reactivity-enhanced zincating reagents that work through co-operative effects (at the simplest level *via* anionic “ate” activation)^[136; 239] between their various components, **1** has previously succeeded in zincating a wide variety of organic substrates.^[143b-e; 147] Most relevant to this study, THF, the saturated, 5-membered O-heterocycle isoelectronic to pyrrolidine, was deprotonated using the sodium zincate base $[(\text{TMEDA})\text{Na}(\mu\text{-TMP})(\mu\text{-CH}_2\text{SiMe}_3)\text{Zn}(\text{CH}_2\text{SiMe}_3)]$.^[152] The salient feature of this precedent was not that THF could be deprotonated, but rather that its deprotonation could be achieved without any decomposition (ring opening) of the hypersensitive α -anion of THF as conventional lithiation methods have to be carried out at very low temperatures to avoid attack of THF.^[154]

The reaction between the cyclic amine and **1** (Scheme 4.1) was first performed in hexane solution. Though this reaction was carried out at room temperature (the reagents were stirred together for 15 minutes), in order to grow X-ray quality crystals of the product the reaction solution was cooled to $-70\text{ }^\circ\text{C}$. Obtained in an isolated yield of 65% (the filtrate NMR spectrum was convoluted but no further product

resonances were observed), these crystals were identified as the heterotrileptic alkyl-amido-pyrrolidide complex [(TMEDA)Na(TMP)(α -C₄H₇NBoc)Zn(^tBu)], **13**. Formally, **1** has been transformed into **13** by selective substitution of a *t*-butyl ligand by an *N*-Boc pyrrolidine ligand deprotonated at an α -C atom. X-ray crystallographic studies of **13** (Figure 4.1) reveal the structural consequences of this transformation with retention of the (TMEDA)Na(μ -TMP)Zn(^tBu) framework but replacement of the second bridging *t*-butyl ligand by a *N*-Boc pyrrolidine bridge that connects both metal atoms through α -C-Zn and (carbonyl)O-Na bonds leading to a 7-atom, 5-element (NaNZnCNCO) ring.



Scheme 4.1 Synthesis of sodium pyrrolidide-zincate **13**.

This dual metal-ligand bonding combined with the marked covalency of the α -C-Zn bond are presumably key factors in stabilising the electron-rich, anionic modification of the cyclic amine. Significantly, in contrast to the aforementioned metastable lithiated forms of *N*-Boc pyrrolidine, crystals of this zincated variant are stable for at least four months under an argon atmosphere. Preliminary electrophilic quenching studies of **13** appear promising, as the reaction of crystalline **13** with benzoylchloride generated 2-benzoylpyrrolidine-1-carboxylic acid *t*-butyl ester in a high yield of 87% (Scheme 4.2).

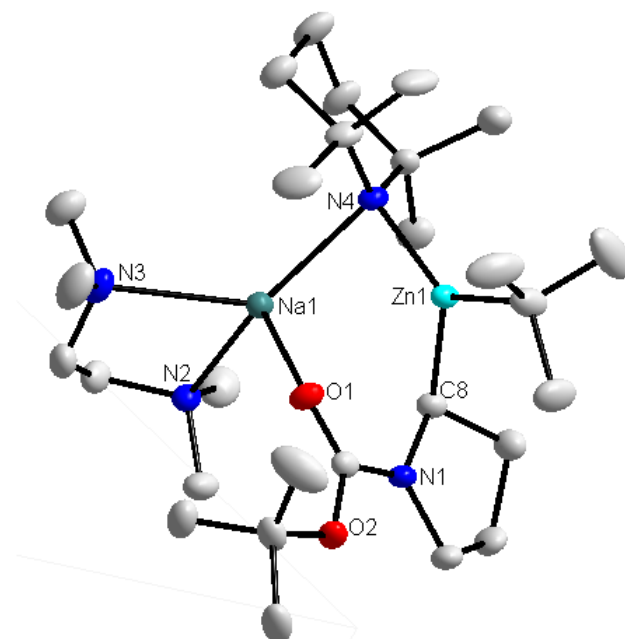
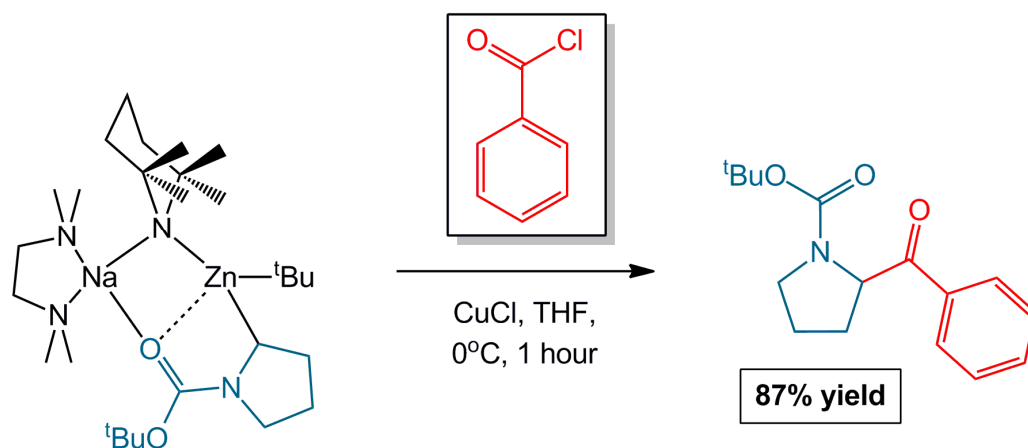
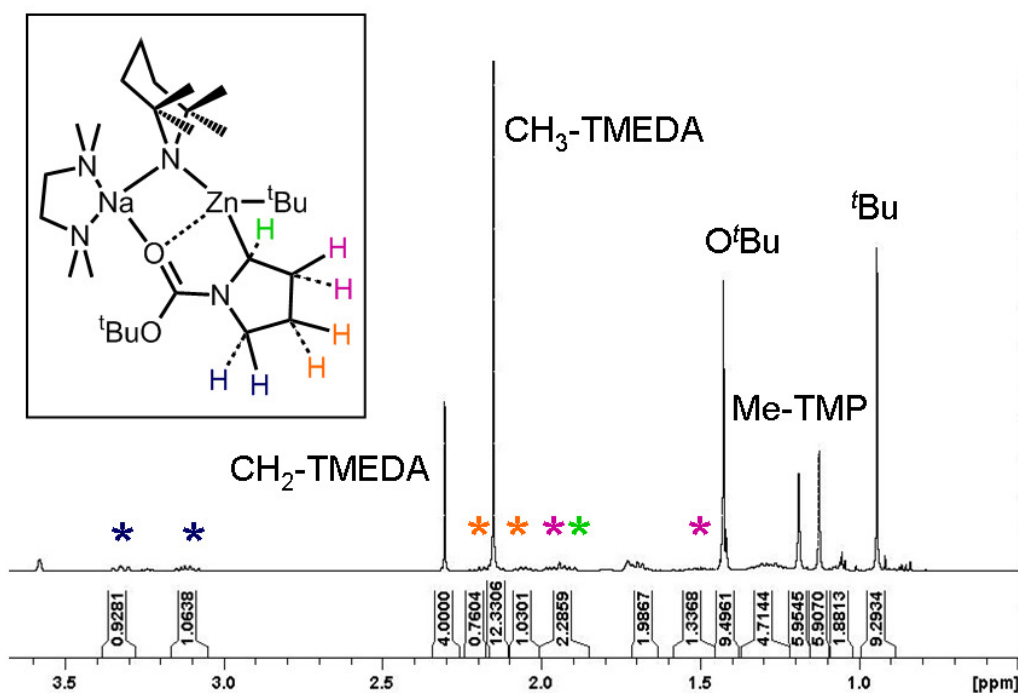


Figure 4.1 Molecular structure of **13** with thermal ellipsoids drawn at the 50% probability level and hydrogen atoms omitted for clarity. Selected bond lengths (Å) and bond angles (°): Na1-O1, 2.3063(16); Na1-N2, 2.4865(17); Na1-N3, 2.568(2); Na1-N4, 2.4498(17); Zn1-N4, 2.0354(17); Zn1-O1, 2.7959(14); Zn1-C1, 2.051(2); Zn1-C8, 2.086(2); Na1-N4-Zn1, 84.12(6); O1-Na1-N2, 104.92(6); O1-Na1-N3, 105.70(6); O1-Na1-N4, 99.15(6); N2-Na1-N3, 74.25(6); N2-Na1-N4, 140.19(7); N3-Na1-N4, 128.56(6); C1-Zn1-N4, 130.81(8); C1-Zn1-C8, 117.24(9); N4-Zn-C8, 111.87(7).

Though the synthesis of, for example, lithium,^[240] zinc,^[227] and tin^[241] complexes of substituent-free *N*-Boc pyrrolidine have been reported previously, a search of the CCDB revealed no hits for any metallated *N*-Boc pyrrolidine structure, making the structure of **13** unique.^[242] Analysis of **13** through multinuclear (¹H, ¹³C{H}) NMR spectroscopy in *d*₈-THF solution confirmed that mono-deprotonation of the pyrrolidine ring has taken place. The salient feature is the observation of seven NC₄H₇ resonances, highlighting the inequivalence of the axial and equatorial pyrrolidine ring protons (Spectrum 4.1). Consistent with the solid state structure, two Me-TMP resonances are observed in the ¹H NMR spectrum at 1.19 and 1.13 ppm, evidence that the bridging coordination mode of TMP is retained even in the Lewis donor solvent *d*₈-THF.



Scheme 4.2 Quenching of **13** with benzoyl chloride to produce 2-benzoylpyrrolidine-1-carboxylic acid *t*-butyl ester.



Spectrum 4.1 The ¹H NMR (400.03 MHz, 300 K) spectrum of [(TMEDA)Na(TMP)(α -C₄H₇NBoc)Zn(^tBu)] (**13**) in *d*₈-THF, highlighting the inequivalence of all seven NC₄H₇ resonances.

4.3.2 Uncovering the Solvent Dependency of the Reaction

Endeavours to reproduce the zincation reaction in a mixed hexane/toluene solution resulted in a different outcome. The surprising product obtained was the crystalline sodium enolate $[(\text{TMEDA})\text{Na}[\text{OC}(\text{NC}_4\text{H}_8)\text{CHPh}]_2]$, **14** (Figure 4.2, isolated yield, 18%; NMR spectroscopic analysis of the filtrate revealed no more of this product in solution).^[16] Thus the participation of toluene results at least in part in cleavage of the Boc “protecting group” through elimination of the alkoxide leaving group $^t\text{BuO}^-$. The formation of **14** implies that *N*-Boc pyrrolidine, having initially reacted as a Brønsted acid by surrendering a hydrogen atom to **1**, can then, in its α -carbanionic form, function as a Brønsted base by recapturing a hydrogen atom from toluene. Evidence that pyrrolidide deprotonates toluene comes through ^1H NMR monitoring of the reaction of **1** with *N*-Boc pyrrolidine in the presence of deuterated toluene. Carried out in d_8 -THF solution for optimum solubility, the ^1H NMR spectrum shows that the $\alpha:\beta$ ratio decreases to 3:4, consistent with a mono-deuterated $\text{C}_4\text{H}_7\text{D}$ derivative. Thus a mechanism can be postulated for the reaction between **13** and toluene (Scheme 4.3).

In the first step in this mechanism the α -carbanion of the heterocycle deprotonates toluene laterally to regenerate *N*-Boc pyrrolidine with concomitant generation of a benzyl group. Secondly the benzyl nucleophile attacks the carbonyl of the carbamate to form a carboxamide with concomitant elimination of a *t*-butoxide group. Although reports of the decomposition of the *N*-Boc group are rare,^[237] related work by Stanetty describes the nucleophilic attack of $^n\text{BuLi}$ upon *N*-Boc aniline, generating a mixture of secondary amine and amide products.^[243] Note that the amide (benzoyl pyrrolidine), $\text{PhCH}_2\text{C}(=\text{O})\text{NC}_4\text{H}_8$, is a known compound for which deprotonation at the PhCH_2 position has been observed.^[244] Given the propensity of reactions of **1** and similar ate reagents in non-polar solvents to involve both metals in intramolecular processes, these events probably occur through the putative intermediates **A** and **B** though alternative processes involving single metal complexes cannot be ruled out. The final step is likely to involve fragmentation of the bimetallic complex with elimination of the zinc component ZnRR' ($\text{R} = \text{O}^t\text{Bu}$

and R' = TMP or ^tBu) accompanied by deprotonation of the PhCH₂ via ^tBu⁻ to generate the sodium enolate **14** (and subsequently benzoyl pyrrolidine after an aqueous work up) and BuH or TMP(H). Since this PhCH₂ deprotonation leads to the formation of a resonance delocalised C⁻=C=O⁻ unit, the lateral methyl group of toluene has effectively been doubly deprotonated.

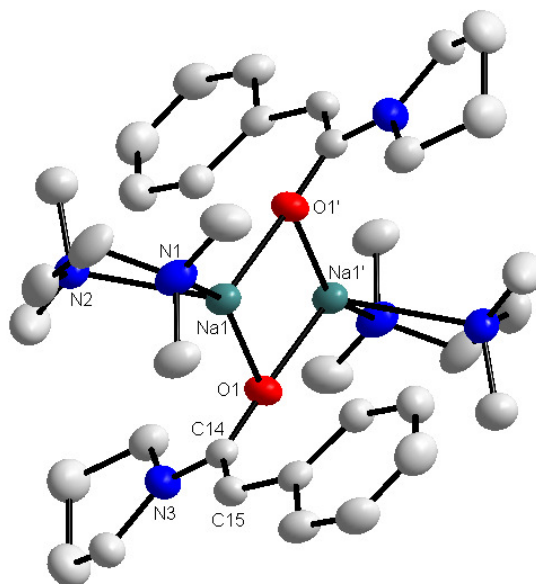
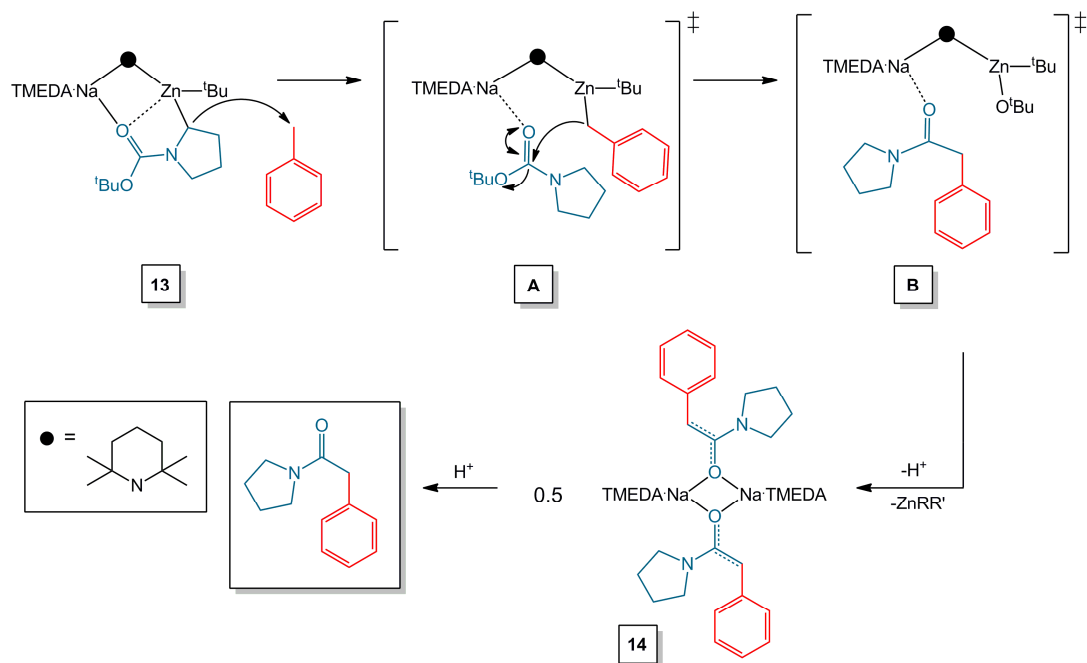


Figure 4.2 Molecular structure of **14** with thermal ellipsoids drawn at the 50% probability level and hydrogen atoms omitted for clarity. Selected bond lengths (Å) and bond angles (°): Na1-O1, 2.359(2); Na1-O1', 2.192(2); Na1-N1, 2.504(2); Na1-N2, 2.499(3); O1-C14, 1.282(3); C14-C15, 1.392(3); C14-N3, 1.382(4); O1-Na1-O1', 84.35(8); O1-Na1-N2, 109.88(9); O1-Na1-N1, 149.02(9); O1'-Na1-N1, 124.17(9); O1'-Na1-N2, 109.34(9); N1-Na1-N2, 74.43(9); Na1-O1-Na1', 95.65(8); C14-O1-Na1, 97.67(15); C14-O1-Na1', 165.02(17); O1-C14-C15, 124.8(3); O1-C14-N3, 116.1(2).

Note that in the absence of the pyrrolidine, as previously reported, the reaction between sodium zincate reagent **1** and toluene affords a statistical mixture of *meta*- and *para*-tolyl isomers, whilst surprisingly, no benzyl formation occurs.^[245] Additional DFT calculations affirmed that the *meta*- and *para*-isomers are the most energetically favourable products under these synergic bimetallic conditions. Whilst the α-C-Zn bond parameters are similar for each of the four potential deprotonation products; it is the engagement of Na with the π-system, perpendicular to the tolyl

ring, which plays a pivotal role in determining the most stable product. The preferential formation of the *meta*- and *para*-tolyl isomers rules out the participation of this reaction in producing **14**, unless some sophisticated rearrangement is in operation.



Scheme 4.3 Postulated mechanism for the surprising generation of enolate **14**.

Metal enolate compounds^[246] can be thought of as possible intermediates in Aldol reactions^[247] so their structures attract widespread attention though examples with amino functionalities are relatively rare. Therefore we decided to crystallographically characterise **14**. This determination revealed a centrosymmetric dimeric structure with a strictly planar (NaO)₂ ring (sum of endocyclic angles 360°). Of length 1.392(3) Å, the C(14)=C(15) bond lies towards the longest of such bonds in known alkali metal enolate structures (summarised in Table 4.1), while the C(14)-O(1) bond is concomitantly short at 1.282(3) Å, suggesting a resonance delocalised C⁻=C=O⁻ pattern.

Values found in the literature for other alkali metal enolates, bearing the general formula MOC(R)=CR', show little variation in the C-R bond length when R is an alkyl group (Table 4.1, entries A-H). Typical bond lengths range from 1.501(5)

within [(TMEDA)Na{OC(=CH₂)Mes}]₂ (where Mes is mesitylene)^[220] to 1.531(10) Å as found in [(LiBr·LiOC(ⁱPr)=CMe₂·(TMEDA))₂]^[248] similar to the perfect value for a single C-C bond (1.54 Å).^[249] Amino enolate **14** possesses a C-R bond length of 1.382(4) Å, which is shorter than that observed within related structurally characterised amino enolate compounds (that is, where R represents an amine) such as [(TriMEDA)Li{OC(=CHCH₃)NMe₂}] (where TriMEDA is *N,N,N'*-trimethylethylenediamine),^[250] where the corresponding C-R bond length is 1.441(1) Å (Table 4.1, entry J).

Table 4.1: Comparative bond length data for literature enolate compounds.

Entry	Bond Length (Å)			
	M-O	O-C	C=C in (O)C(R)=CR'	C-R in (O)C(R)=CR'
A ^[220]	2.225(3) ^b	1.317(5)	1.338(6)	1.501(5) ^d
B ^[251]	2.528(6) ^c	1.278(9)	1.362(11)	1.526(11) ^d
C ^[248]	1.85(2) ^a	1.347(9)	1.360(11)	1.531(10) ^d
D ^[248]	1.883(9) ^a	1.335(6)	1.338(7)	1.520(7) ^d
E ^[252]	2.03(1) ^a	1.359(8)	1.37(1)	1.53(1) ^d
F ^[253]	1.918 ^{a,f}	1.342(6)	1.330(6)	1.526(8) ^d
G ^[253]	2.301 ^{b,f}	1.308(4)	1.358(6)	1.514(8) ^d
H ^[253]	2.626 ^{c,f}	1.306(4)	1.350(4)	1.501(6) ^d
I ^[254]	1.920(7) ^a	1.300(5)	1.337(7)	1.443(6) ^e
J ^[250]	1.896(2) ^{a,g}	1.306(1)	1.355(2)	1.444(1) ^e
14	2.359(2) ^b	1.282(3)	1.392(3)	1.382(4) ^e

a) M = Li; b) M = Na; c) M = K; d) R = C; e) R = N; f) structure is an aggregate and the average M-O bond length has been given; g) structure involves a pentacoordinate M.

Ruling out the possibility that enolate **14** requires a mixed-metal system for its preparation, we prepared it rationally *via* a 1:1:1 mixture of benzylna, *N*-Boc pyrrolidine, and TMEDA in a hexane/toluene medium. A reaction pathway involving carbonyl-nucleophilic addition of a benzyl anion to the *N*-Boc group, coupled with loss of the *t*-butoxide anion, was proposed (Scheme 4.4). Subsequent deprotonation at the CH₂-benzylic position could then be executed by either sodium *t*-butoxide or benzyl sodium. By assuming the latter is consumed completely in the first step of the reaction then the former is the most likely deprotonation agent.

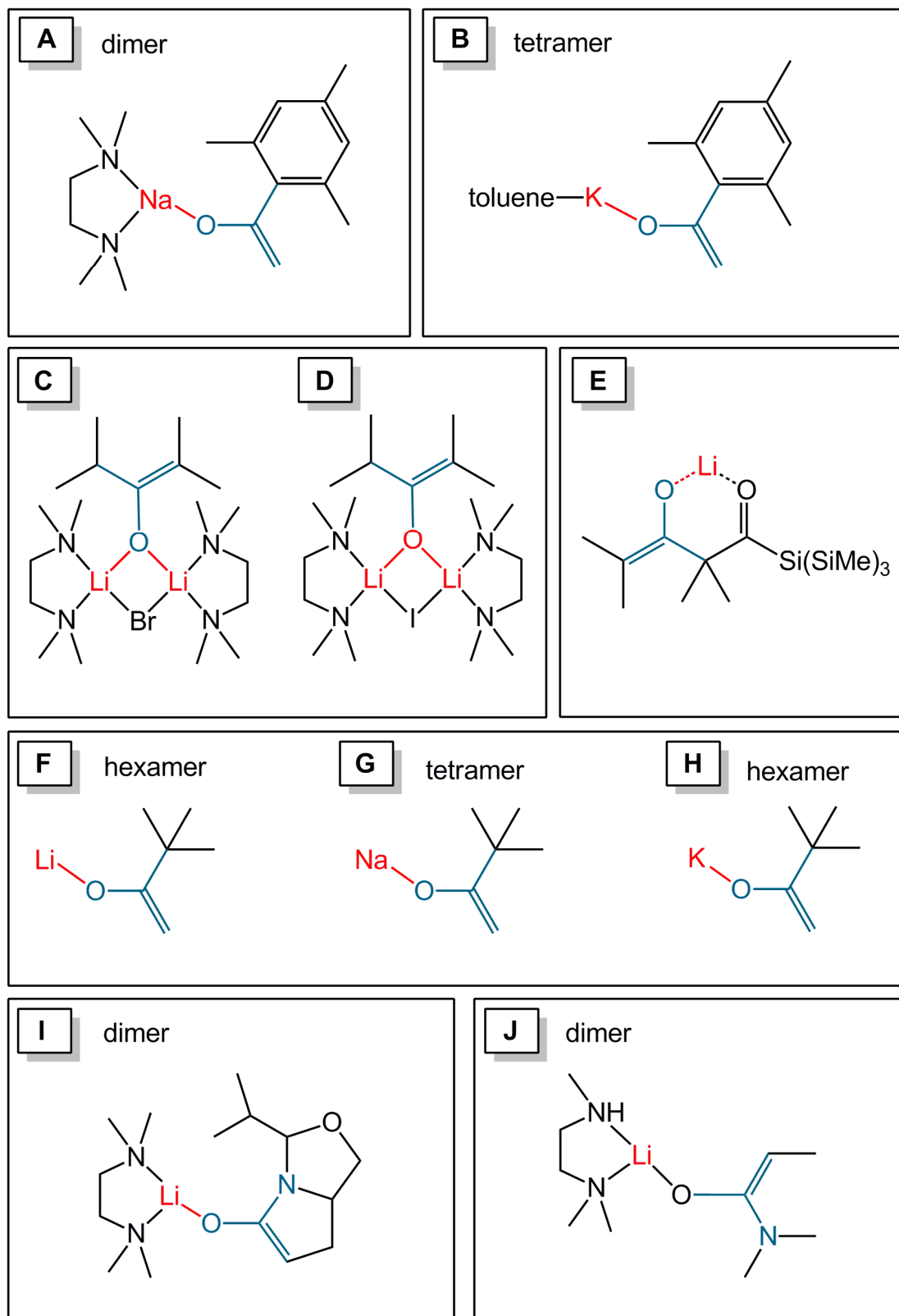
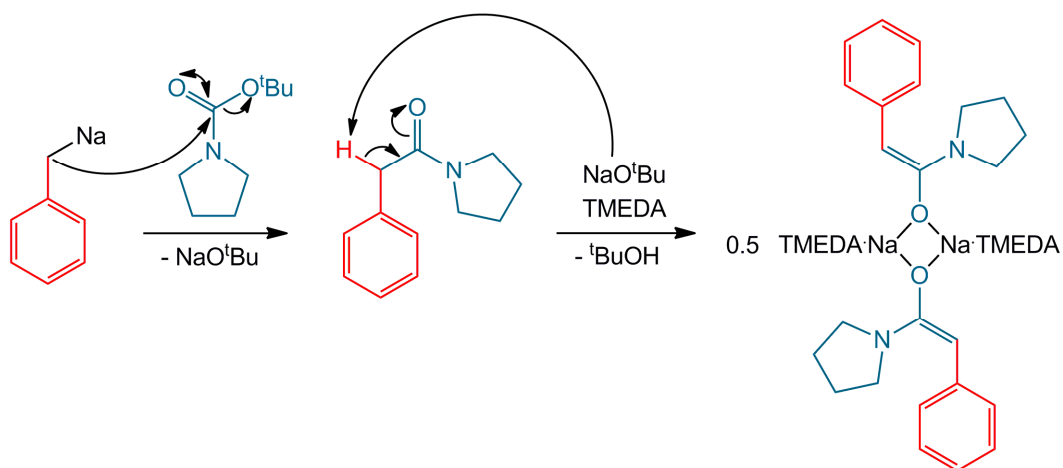


Figure 4.3 Molecular structures of alkali metal enolates listed in Table 4.1.



Scheme 4.4 Rational synthesis of **14** *via* reaction of benzyl sodium with *N*-Boc pyrrolidine in the presence of TMEDA.

4.3.3 Examining the Alkyl Analogue: Reactivity Studies of the Related Sodium Methyl Zincate

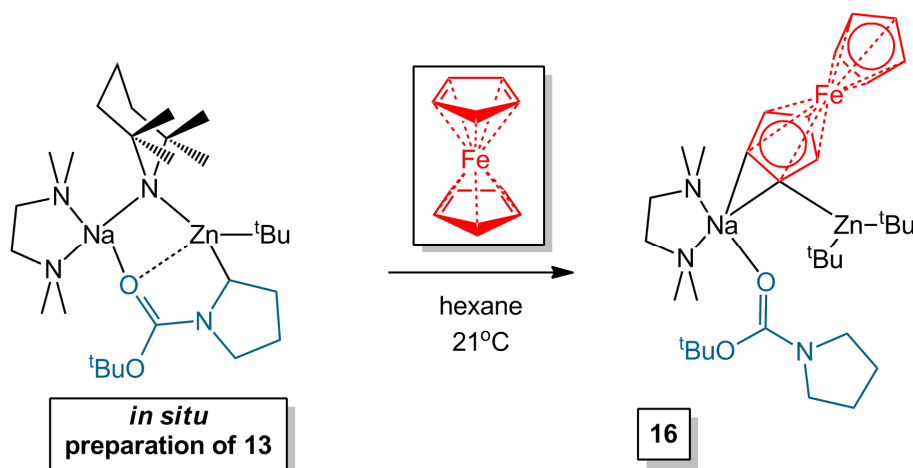
For comparative purposes, the methyl analogue of **1**, [(TMEDA)Na(μ -TMP)(μ -Me)Zn(Me)] (**15**), was synthesised by simple co-complexation of the sodium amide with dimethylzinc, in the presence of a molar equivalent of TMEDA in hexane solvent. Reflecting in part the weaker Brønsted basicity of methyl ligands in comparison to *t*-butyl ligands, **15** exhibits no reactivity towards toluene, in contrast to the *meta*- and *para*-deprotonation achieved using the *t*-butyl base **1**.^[245] These reactions usually operate by a kinetic TMP deprotonation so in theory both the *t*-butyl and the methyl bases should behave similarly.^[148] However, in the latter case the strength of the Zn-Me bond prohibits its breaking in favour of TMP^- replacing the zincated substrate. Thus in the case of the methyl base the deprotonation could be happening, followed by a retro-reaction with regeneration of the toluene. However, ^1H NMR monitoring of the reaction of **15** with both toluene and *N*-Boc pyrrolidine in C_6D_6 solution, revealed resonances corresponding to enolate **14** after just 30 minutes. Incorporation of *N*-Boc pyrrolidine into the reaction system can therefore promote the reactivity of **15** towards toluene, facilitating a sequence of reactions that

culminate in the formation of **14**. Although the origin of this reactivity enhancement could lie with the initial deprotonation of *N*-Boc pyrrolidine by **15**, attempts to crystallise the methyl analogue of **13** were unsuccessful and only crystalline **15** was recovered from solution. Alternatively, *N*-Boc pyrrolidine could boost the reactivity of **15** through Lewis donor coordination towards the sodium centre (*vide infra*).

4.3.4 Exploring the Scope of the Methodology: Reactivity towards Alternative Aromatic Substrates

An intriguing question arising from these results asked whether heteroleptic **13** was capable of the deprotonation of non-activated aromatic substrates other than toluene. Endeavouring to explore the generality of this reaction, the related alkyl-substituted aromatic substrates ethylbenzene, cumene and mesitylene were selected for initial investigation. Accordingly, each substrate was combined with **13** (prepared *in situ*) in a 1:1 ratio in a hydrocarbon medium. In all three cases, a crop of X-ray quality crystals was deposited after 24 hours at -30 °C. Analysis of the crystalline materials through X-ray crystallography and multinuclear (¹H, ¹³C{H}) NMR spectroscopy revealed that each product was simply recovered **13**. However, moving to more reactive substrates such as ferrocene and anisole generated a more positive outcome as now outlined.

Addition of ferrocene to a hexane solution of **13** (again prepared *in situ*) instantaneously produced a vivid orange solution which furnished crystals of [(TMEDA)(Boc-NC₄H₈)Na{(η²-C₅H₄)Fe(C₅H₅)}Zn(^tBu)₂] (**16**) (Scheme 4.5) after 24 hours at -30 °C (yield 0.12 g, 18%). The molecular structure of **16** in the solid state was determined by X-ray crystallography. Complex **16** was also characterised in the solution state by multinuclear NMR spectroscopy. Although the best yield of isolated crystalline material was a modest 18%, NMR spectroscopic analysis of the filtrate revealed no further product was present in solution: only resonances pertaining to free ferrocene and **13** were observed.



Scheme 4.5 Application of an *in situ* preparation of **13** for the synthesis of sodium ferrocenyl-zincate **16**.

In the solid state structure of **16**, *N*-Boc pyrrolidine coordinates to Na as a neutral Lewis donor, having an elongated Na-O bond in comparison to that within **13** [Na1-O1, 2.240(6) Å in **15**; Na1-O1, 2.3063(16) Å in **13**] (Figure 4.4). To the best of our knowledge, this is the first crystallographically characterised example of *N*-Boc pyrrolidine acting as a carbonyl (C=O) donor towards a metal centre. Within **16**, a mono-deprotonated ferrocene unit forms an asymmetrical bridge between Na and Zn, [Na1-C16, 2.634(7); Na1-C17, 2.834(8); Zn1-C16, 2.053(7) Å], interacting with Na in a η^2 -fashion, whilst bonding to Zn through a η^1 -coordination mode. The pentacoordinated Na is further stabilised through dative bonding from the didentate Lewis donor TMEDA. In comparison to the precursor sodium zincate **1**, the increased steric congestion at Na resulting from the additional *N*-Boc pyrrolidine donor molecule is evidenced by the more open, curved $\text{NaC}_{\text{Cp}}\text{ZnC}_{\text{Me}}$ backbone of **16**. Unlike **1**, there is no significant Na-C_{Me} interaction within **16**; the shortest Na-C_{Me} contact distance being Na1...C27 [3.1543(3) Å], in contrast to the Na...C_{Me} bond length of 2.750(10) Å within **1**. Possessing a distorted trigonal planar geometry, Zn also bonds to two terminal ^tBu ligands, with the sum of the Zn1-C16-C26-C30 angles around Zn totalling 359.8°. Indeed, the two ^tBu ligands are equivalent on the NMR timescale, as only one ^tBu singlet is present at 1.32 ppm (when analysed in C₆D₆ solvent at 300 K).

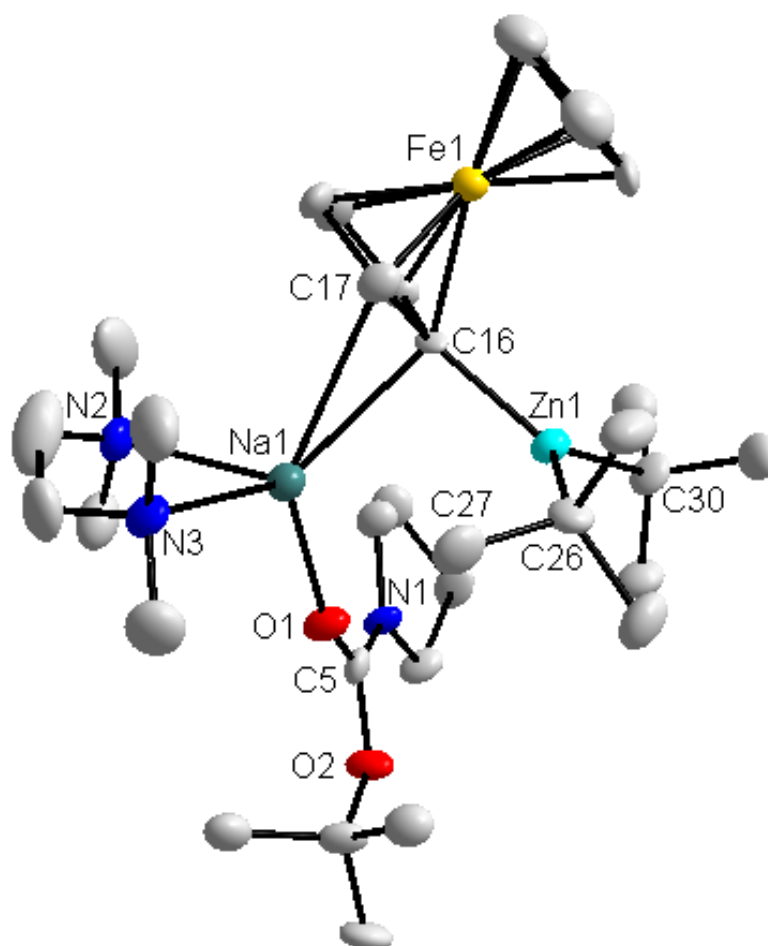
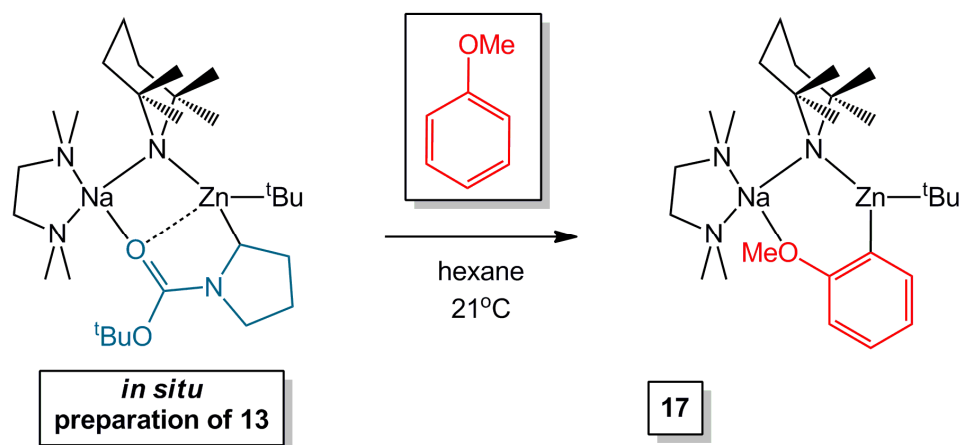


Figure 4.4 Molecular structure of **15** with thermal ellipsoids drawn at the 50% probability level and hydrogen atoms omitted for clarity. Selected bond lengths (Å) and bond angles (°): Na1-O1, 2.240(6); Na1-N2, 2.471(7); Na1-N3, 2.518(6); Na1-C16, 2.634(7); Na1-C17, 2.834(8); Zn1-C16, 2.053(7); Zn1-C26, 2.061(7); Zn1-C30, 2.062(7); O1-C5, 1.214(8); O2-C5, 1.363(8); N1-C5, 1.336(8); O1-Na1-N2, 102.3(2); O1-Na1-N3, 112.5(2); O1-Na1-C16, 109.9(2); O1-Na1-C17, 139.3(2); N2-Na1-N3, 74.4(2); N2-Na1-C16, 115.4(2); N2-Na1-C17, 105.2(2); N3-Na1-C16, 132.9(2); N3-Na1-C17, 103.6(2); C16-Na1-C17, 30.18(19); C16-Zn1-C26, 114.3(3); C16-Zn1-C30, 124.5(3); C26-Zn1-C30, 121.0(3); Zn1-C16-Na1, 93.5(3); Na1-C16-Fe1, 145.4(3); Na1-C17-Fe1, 137.0(3); Zn1-C16-Fe1, 116.8(3); O1-C5-O2, 125.9(7); O1-C5-N1, 124.1(7); N1-C5-O2, 110.0(6).

Previously, the metallation of ferrocene was achieved using the related lithium zincate base [(TMEDA)Li(μ -TMP)(μ -ⁿBu)Zn(ⁿBu)]. Crystalline products involving a ferrocenyl ligand (Fc*, C₅H₅FeC₅H₄) included the neutral zinc compound [(TMEDA)Zn(Fc*)₂] and the THF solvent separated lithium zincate [Li(THF)₄][(Fc*)₃Zn].^[255] In addition, studies have shown that reaction of the related potassium zincate base [(PMDETA)K(μ -TMP)(μ -Me)Zn(Me)] with ferrocene yielded crystalline [{(PMDETA)K(μ -Me)₂Zn(Fc*)}_∞].^[256] In contrast to monomeric **16**, this potassium ferrocenyl zincate adopts a polymeric structure, reflecting the reduced steric bulk of the methyl ligands and the larger coordination capacity of potassium (versus that of sodium) as propagation occurs through two K-Me-Zn bridges. Furthermore, the ferrocenyl unit forms an asymmetric bridge, with η^1 -(C₅H₄)Zn and η^5 -(C₅H₄)K coordination modes highlighting the predilection of potassium to form multihapto π -system interactions.^[257] Exemplifying the remarkable chemistry that can be obtained using cooperative bimetallic systems, the four-fold deprotonation of ferrocene has previously been achieved using a synergic sodium amido magnesiate base.^[258]

A popular test substrate for evaluating the effectiveness of directed *ortho*-metallation,^[42; 158-163] anisole is activated towards deprotonation in a two-fold manner. Firstly and most significantly, activation occurs through inductive acidification of the *ortho*-hydrogens by the electron withdrawing oxygen of the methoxy group. Secondly, the lone pairs of the methoxy group provide a potential Lewis basic coordination point for an incoming organometallic reagent, although previous studies have suggested that methoxy-lithium interactions have a negligible impact upon the promotion of directed *ortho*-metallation.^[33] Endeavouring to deprotonate anisole with **13**, the reaction between the aromatic ether and the pyrrolidide-zincate (prepared *in situ*) was initially performed at ambient temperature in hexane solvent (Scheme 4.6). Cooling the resultant colourless solution (to -30 °C) enabled the isolation of crystalline [(TMEDA)Na(μ -TMP)(μ -C₆H₄OMe)Zn(^tBu)] (**17**, yield 0.21 g, 41%). X-ray crystallographic studies of **17** revealed that the sodium TMP-zincate backbone is retained, with the incorporation of an *ortho*-deprotonated anisole fragment.



Scheme 4.6 Synthesis of sodium anisyl-zincate **17** from an *in situ* preparation of **13**.

Disordered over two positions, the ^tBu group bears a coincident branched carbon atom [major occupancy = 83.0(9)%], whilst the anisole fragment is disordered over two positions but bears no coincident atoms [major occupancy = 53.4(6)%]. With a strong resemblance to **13**, sodium TMP-zincate **17** can be viewed as a dinuclear, six-membered [NaZnCCO] ring system, in which sodium and zinc are linked through a bridging TMP unit [Na1-N1, 2.415(7) Å; Zn1-N1, 2.003(6) Å], and a bridging anisyl unit which bonds asymmetrically through *ortho*-C-Zn and MeO-Na interactions [Zn1-C2, 2.114(14) Å; Na1-O1, 2.456(13) Å]. With further stabilisation provided by the chelation of didentate TMEDA, the tetrahedral coordination environment surrounding the sodium centre is highly distorted [range of bond angles from 74.9° to 133.3°, mean: 108.7°].^[213] Furthermore, a terminal ^tBu ligand completes the coordination sphere of the distorted trigonal planar zinc centre [sum of Zn-N1-C2-C23 angles is 359.4°]. In comparison to pyrrolidide-zincate **13**, the Na-O bond within **17** is elongated [Na1-O1, 2.456(13) Å in **17**, Na1-O1, 2.3063(16) Å in **13**]. The heterocyclic amine *N*-Boc pyrrolidine is absent from **17**, which could be a consequence of Lewis donor competition from the methoxy group, which is brought into close proximity with sodium upon the *ortho*-zincation of anisole. The *ortho*-deprotonated anisole fragment lies almost perpendicular to the Na-N_{TMP}-Zn backbone, with a dihedral angle of 87.93° between the phenyl ring plane and the Na-N_{TMP}-Zn plane (Figure 4.5).

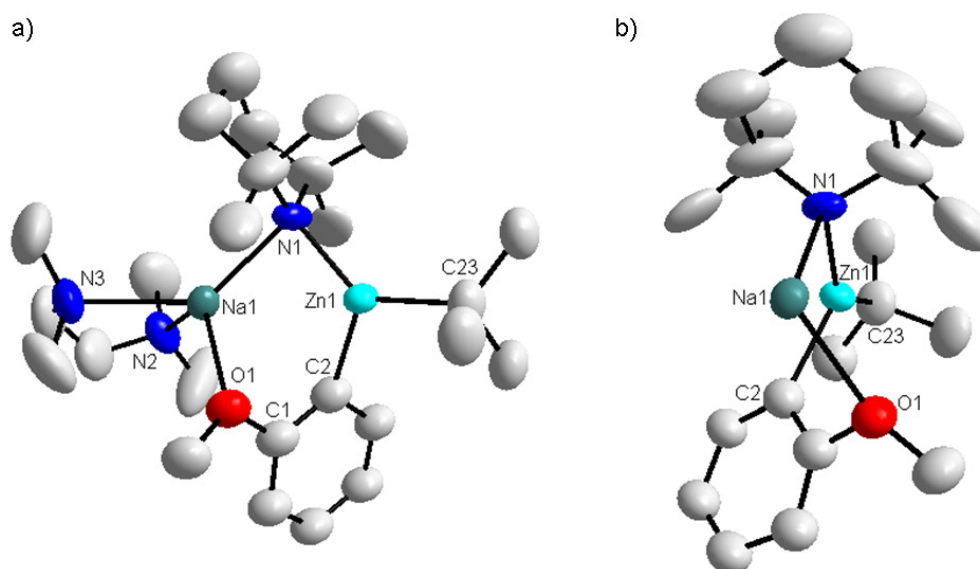


Figure 4.5 a) Molecular structure of **17** with thermal ellipsoids drawn at the 50% probability level. Hydrogen atoms and the minor disorder component have been omitted for clarity. Selected bond lengths (Å) and bond angles (°): Na1–O1, 2.456(13); Na1–N1, 2.415(7); Na1–N2, 2.488(8); Na1–N3, 2.553(9); Zn1–N1, 2.003(6); Zn1–C2, 2.114(14); Zn1–C23, 2.036(8); O1–C1, 1.389(14); C1–C2, 1.370(11); O1–Na1–N1, 101.1(4); O1–Na1–N2, 114.6(4), O1–Na1–N3, 98.2(4); N1–Na1–N2, 133.3(3); N1–Na1–N3, 130.3(3), N2–Na1–N3, 74.9(3); N1–Zn1–C2, 114.2(5); N1–Zn1–C23, 132.8(3); C2–Zn1–C23, 112.4(5); Na1–O1–C1, 96.5(11); b) Alternative view of **17** (TMEDA omitted for clarity) highlighting the angle between the Na–N_{TMP}–Zn backbone and the C₆H₄–OMe unit.

Observation of four multiplets in the aromatic region of the ¹H NMR spectrum of **17** confirmed the mono-deprotonation of anisole. As a consequence of metallation, there is a significant shift of the C₆H₄OMe resonances with respect to those of the parent ether. Most notably, the resonance assigned to the *meta*-H of **17** (positioned adjacent to the site of metallation), experiences a downfield shift of 0.59 ppm, from 7.12 ppm in anisole to 7.71 ppm in **17**. It appears that the bulky amido unit, TMP, retains its bridging position in C₆D₆ solvent, as highlighted by the inequivalence of the Me–TMP groups observed (1.59 and 1.54 ppm in the ¹H NMR spectrum; 35.3 and 34.9 ppm in the ¹³C{H} NMR spectrum). In related work, the direct zincation of anisole

was achieved using the lithium zincate [(THF)Li(μ -TMP)(μ -^tBu)Zn(^tBu)], where variation of the THF and anisole stoichiometry led to the formation of three novel lithium anisyl-zincate species including heterotrileptic [(THF)Li(μ -TMP)(μ -*o*-C₆H₄OMe)Zn(^tBu)].^[259]

4.4 Concluding Remarks on the Synergic Metallation of *N*-Boc Pyrrolidine

In conclusion, the temperature threshold at which the metallation of *N*-Boc pyrrolidine can occur without decomposition has been raised substantially by using a synergically operative sodium TMP-zincate base. Indeed, there are significant cost-saving implications associated with the preclusion of sub-ambient temperature regimes. Recent values from Chemical Development at GSK have indicated that utilising temperatures below -40 °C increases the annual production cost by at least £250,000 per batch tonne.^[260] However, a complication is that the reaction is solvent dependent, working well in hexane, but failing in toluene due to the substantial Brønsted basicity of the α -carbanion of the heterocycle, which sets off a cascade of reactions leading ultimately to a pyrrolidine-substituted enolate. Further probing the reactivity of sodium pyrrolidide-zincate **13** (prepared *in situ* rather than isolated) showed failure to metallate the other alkyl-substituted aromatic substrates ethylbenzene, cumene and mesitylene. In contrast, the deprotonation of both ferrocene and anisole was successfully achieved. Intriguingly, the destination of *N*-Boc pyrrolidine significantly differs between the toluene, ferrocene and anisole systems. Whilst formation of a benzyl ligand from toluene subjects the *N*-Boc group to subsequent nucleophilic attack, deprotonation of ferrocene demonstrates the alternative capability of *N*-Boc pyrrolidine to act simply as a novel Lewis donor ligand towards sodium, which presents the first crystallographic evidence where this *N*-protected heterocycle coordinates to any metal centre. In marked contrast, the incorporation of a deprotonated anisole fragment within the sodium TMP-zincate framework reveals the absence of *N*-Boc pyrrolidine from the solid state molecular structure.

4.5 Future Work

Given the importance and widespread use of the pyrrolidine scaffold within pharmaceutical products, which often involve a chiral α -sp³ carbon centre, it would be highly desirable to upgrade this deprotonation system to achieve enantioselective metallation. Incorporation of a chiral ligand such as TMCDA or (-)-sparteine in place of TMEDA should be investigated, as related monometallic precedents have shown excellent promise towards enantioselective deprotonation.^[235] In this regard, alternative electrophilic quenching reactions should also be trialled, to expand the scope of the α -C functionalisation. Furthermore, the reaction could be improved through the development of an atom economical base in which all of the arms of the reagent function as base ligands.

Sodium zincate **13** represents an unusual example of a heterotrileptic formulation where, having sacrificed a proton as a Brønsted acid, the resultant pyrrolidyl anion subsequently proves itself to be capable of Brønsted basic behaviour. To explore the possibility that this *N*-Boc pyrrolidyl system could be more widely utilised as an unusual base, the reactivity of **13** with an extensive range of substrates should therefore be tested.

4.6 Experimental

4.6.1 Synthesis of [(TMEDA)Na(TMP)(α -NC₄H₇NBoc)Zn(^tBu)], **13**

TMP(H) (0.17 mL, 1 mmol) was transferred *via* syringe to a suspension of freshly prepared ⁿBuNa (0.08 g, 1 mmol) in hexane (5 mL). The colourless suspension was allowed to stir for 1 hour at ambient temperature. A solution of ^tBu₂Zn (0.18 g in 5 mL hexane, 1 mmol) was transferred to the reaction mixture *via* cannula, followed by TMEDA (0.15 mL, 1 mmol). Gentle heating produced a pale yellow solution, to which *N*-Boc pyrrolidine (0.18 mL, 1 mmol) was added *via* syringe to form a brown

oil. The reaction mixture was transferred to the freezer at $-70\text{ }^{\circ}\text{C}$ and colourless crystals were obtained after 4 hours (0.37 g, 65% yield).

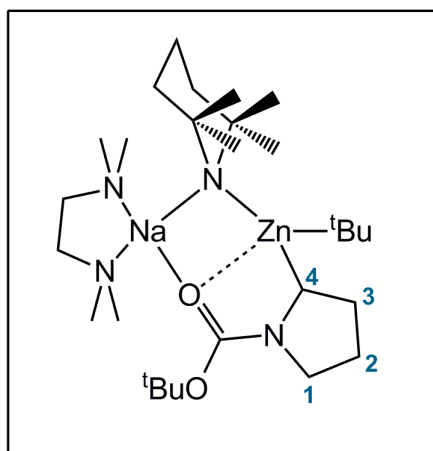


Figure 4.6 Labelling scheme for sodium zincate **13**.

^1H NMR (400.03 MHz, d_8 -THF, 300 K) δ = 3.32 (m, 1H, 1-NC₄H₇), 3.12 (m, 1H, 1-NC₄H₇), 2.30 (s, 4H, CH₂-TMEDA), 2.19 (m, 1H, 3-NC₄H₇), 2.15 (s, CH₃-TMEDA), 2.05 (m, 1H, 3-NC₄H₇), 1.94 (m, 2H, overlapping signals for 2-NC₄H₇ and 4-NC₄H₇), 1.69 (m, 2H, γ -TMP), 1.51 (m, 1H, 2-NC₄H₇), 1.43 (s, 9H, O^tBu), 1.28 (m, 4H, β -TMP), 1.19 and 1.13 (s, 6H, Me-TMP) and 0.94 ppm (s, 9H, ^tBu). $^{13}\text{C}\{^1\text{H}\}$ NMR (100.60 MHz, d_8 -THF, 300 K) δ = 156.7 (s, CO), 78.2 (O^tBu quaternary), 58.9 (s, CH₂-TMEDA), 56.7 (s, 4-NC₄H₇), 53.7 (s, α -TMP quaternary), 47.5 (1-NC₄H₇), 46.2 (s, CH₃-TMEDA), 42.6 (s, β -TMP), 36.3 (br s, Me-TMP), 36.0 (s, ^tBu), 31.8 (s, 3-NC₄H₇), 30.2 (s, 2-NC₄H₇), 29.1 (s, O^tBu), 21.6 (s, ^tBu quaternary) and 20.7 ppm (s, γ -TMP).

Due to the acute air sensitivity of **13**, satisfactory C, H, N analyses could not be obtained.

Crystal data for **13**, C₂₈H₅₉N₄Na₁O₂Zn₁, M_r = 572.15, orthorhombic, space group Pbca, a = 16.8528(6), b = 19.2437(5), c = 20.3447(5) Å, V = 6598.0(3) Å³, Z = 8, μ = 0.785 mm⁻¹; 26669 reflections, 7941 unique, R_{int} 0.0568, final refinement to full-matrix least squares on F^2 gave R = 0.0425 (F , 5320 obs. data only) and R_w = 0.0949 (F^2 , all data), GOF = 1.026.

4.6.2 Reaction of **13** with benzoylchloride: synthesis of 2-benzoylpyrrolidine-1-carboxylic acid *t*-butyl ester

To a suspension of NaTMP, synthesised from freshly prepared ⁿBuNa (0.16 g, 2 mmol) and TMP(H) (0.34 mL, 2 mmol) in hexane (10 mL), a solution of ^tBu₂Zn (0.36 g, 2 mmol in 10 mL hexane) was added. Addition of TMEDA (0.30 mL, 2 mmol) to the colourless precipitate produced a pale yellow solution upon gentle heating. Crystalline sodium zincate [(TMEDA)Na(μ-TMP)(μ-^tBu)Zn(^tBu)] (**1**) was deposited after 1 hour upon cooling the solution to -30 °C. Crystalline **1** (0.46 g, 1 mmol) was dissolved in hexane (10 mL) and *N*-Boc pyrrolidine (0.18 mL, 1 mmol) was added to the pale yellow solution. The reaction was allowed to stir at ambient temperature for 24 hours. All volatiles were then removed *in vacuo*, THF (10 mL) was added and the resultant solution was cooled to 0 °C. CuCl (0.05 g, 0.5 mmol) was added and the black solution formed was allowed to stir for 5 mins. Following this, benzoylchloride (0.48 mL, 4 mmol) was added slowly under stirring.^[152] After 30 minutes the ice bath was removed and after a further 30 minutes, deionised water (20 mL) and hexane (20 mL) were added. The organic layer was separated from the aqueous layer and the aqueous layer was washed with hexane (3 x 10 mL). Magnesium sulfate was used to dry the combined organic layers. Solvent was removed *in vacuo* and the resultant colourless oil was purified using flash column chromatography on silica with a 19:1 hexane-EtOAc eluent (increased to pure EtOAc over a period of 35 minutes). 2-Benzoylpyrrolidine-1-carboxylic acid *t*-butyl ester (0.21 g, 76.3%) was obtained as a colourless oil; R_F 4:1 (hexane-EtOAc) 0.4. When a crystalline sample of **13** was dissolved in THF (10 mL) and immediately used in a similar reaction, an improved yield of 2-benzoylpyrrolidine-1-carboxylic acid *t*-butyl ester (0.24 g, 87.2%) was achieved.

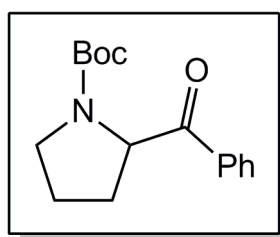


Figure 4.7 Quench product 2-benzoylpyrrolidine-1-carboxylic acid *t*-butyl ester.

^1H NMR (400.03 MHz, CDCl_3 , 300 K) (60:40 mixture of rotamers): δ = 8.01-7.95 (m, 2H, *m*-Ph), 7.59-7.54 (m, 1H, *p*-Ph), 7.51-7.44 (m, 2H, *o*-Ph), 5.35 [dd, $^3J(\text{H,H})$ = 9.4, 3.4 Hz, 0.4H, NCH], 5.19 [dd, $^3J(\text{H,H})$ = 8.8, 3.9 Hz, 0.6H, NCH], 3.70-3.50 (m, 2H, NCH₂), 2.34-2.30 (m, 1H, CH₂), 1.97-1.91 (m, 3H, CH₂), 1.48 (s, 3.9H, ^tBu) and 1.27 ppm (s, 5.6H, ^tBu). $^{13}\text{C}\{\text{H}\}$ NMR (100.60 MHz, CDCl_3 , 300 K) (rotamers): δ = 198.9 (PhC=O), 198.4 (PhC=O), 154.5 (C=O, Boc), 153.8 (C=O, Boc), 135.3 (*ipso*-Ph), 135.1 (*ipso*-Ph), 128.7 (Ph), 128.6 (Ph), 128.6 (Ph), 128.5 (Ph), 128.2 (Ph), 79.8 (^tBu quaternary), 79.6 (^tBu quaternary), 61.4 (NCH), 61.1 (NCH), 46.8 (NCH₂), 46.6 (NCH₂), 30.9 (CH₂), 29.7 (CH₂), 28.5 (^tBu), 28.2 (^tBu), 24.2 (CH₂) and 23.6 (CH₂). Spectroscopic data are consistent with those reported in the literature.^[234]

4.6.3 Control Reaction between *N*-Boc pyrrolidine and ^tBu₂Zn

TMEDA (0.05 mL, 0.3 mmol) was added to a colourless solution of ^tBu₂Zn (0.06 g, 0.3 mmol) in hexane (5 mL). *N*-Boc pyrrolidine (0.06 mL, 0.3 mmol) was subsequently added and the reaction mixture was allowed to stir for 15 minutes prior to transfer to the freezer at -30 °C. After 1 week, the colourless solution was analysed via ^1H NMR spectroscopy, which revealed signals corresponding to free *N*-Boc pyrrolidine, free TMEDA and hexane. The highly volatile dialkylzinc compound ^tBu₂Zn is likely to have been removed under vacuum.

4.6.4 Synthesis of $\{[(\text{TMEDA})\text{Na}[\text{OC}(\text{NC}_4\text{H}_8)\text{CPh}]]_2\}$, **14**

The heterotri-anionic zincate $[(\text{TMEDA})\text{Na}(\text{TMP})(\alpha\text{-NC}_4\text{H}_7\text{NBoc})\text{Zn}(\text{tBu})]$ (**13**) was prepared on a 2 mmol scale via the preparation method detailed above. Toluene (10 mL) was subsequently added, producing a yellow-brown solution that was stirred for 10 minutes at ambient temperature. The resultant solution was transferred to the refrigerator (at 4 °C) and pale yellow crystals (0.12 g, 18%) were obtained after 24 hours.

Alternative rational synthesis: *N*-Boc pyrrolidine (0.35 mL, 2 mmol) was transferred *via* syringe to an orange suspension of benzyl sodium (0.23 g, 2 mmol) in hexane (10 mL), producing a pale brown solution. TMEDA (0.30 mL, 2 mmol) was subsequently added *via* syringe to the mixture, forming an orange suspension. Toluene (10 mL) was added and the reaction mixture was heated, producing an orange solution that was transferred to the refrigerator (at 4 °C). A crop of pale yellow crystals (0.10 g, 15%) was deposited after 72 hours.

^1H NMR (400.03 MHz, d_8 -THF, 300 K): δ = 7.30 [d, $^3\text{J}(\text{H,H})$ = 7.6 Hz, 2H, *o*-C₆H₅], 6.83 [t, $^3\text{J}(\text{H,H})$ = 7.6 Hz, 2H, *m*-C₆H₅], 6.24 [t, $^3\text{J}(\text{H,H})$ = 7.1 Hz, 1H, *p*-C₆H₅], 4.00 (s, 1H, =CH), 3.32 [t, $^3\text{J}(\text{H,H})$ = 6.4 Hz, 4H, α -NC₄H₈], 2.30 (s, 4H, CH₂-TMEDA), 2.15 (s, 12H, CH₃-TMEDA), 1.83 (m, 4H β -NC₄H₈). $^{13}\text{C}\{\text{H}\}$ NMR (100.60 MHz, d_8 -THF, 300 K): δ = 167.5 (s, CO), 148.2 (s, *i*-C₆H₅), 128.6 (s, *m*-C₆H₅), 121.4 (s, *o*-C₆H₅), 114.8 (s, *p*-C₆H₅), 72.4 (s, =CH), 58.9 (s, CH₂-TMEDA), 46.7 (s, α -NC₄H₈), 46.2 (s, CH₃-TMEDA) and 26.6 (s, β -NC₄H₈).

Due to the acute air sensitivity of **14**, satisfactory C, H, N analyses could not be obtained.

Crystal data for **14**, C₃₆H₆₀N₆Na₂O₂, M_r = 654.88, triclinic, space group P-1, a = 8.541(3), b = 11.032(3), c = 11.358(3) Å, α = 69.33(3), β = 76.16(3), γ = 72.49(3)°, V = 944.2(5) Å³, Z = 1, μ = 0.092 mm⁻¹; 4600 reflections, 3341 unique, R_{int} 0.0476, final refinement to full-matrix least squares on F^2 gave R = 0.0591 (F , 2312 obs. data only) and R_w = 0.1954 (F^2 , all data), GOF = 1.071.

4.6.5 Synthesis and reactivity of [(TMEDA)Na(μ -TMP)(μ -Me)Zn(Me)], **15**

TMP(H) (0.17 mL, 1 mmol) was transferred *via* syringe to a suspension of freshly prepared ⁿBuNa (0.08 g, 1 mmol) in hexane (5 mL) and the white suspension was allowed to stir for 1 hour at ambient temperature. A solution of Me₂Zn (1 mL of a 1.0 M heptane solution, 1 mmol) was transferred to the reaction mixture *via* cannula, followed by TMEDA (0.15 mL, 1 mmol), which generated a beige precipitate (**15**). Monitoring the reaction of isolated **15** (0.02 g, 0.05 mmol) with *N*-Boc pyrrolidine (0.009 mL, 0.05 mmol) and toluene (0.005 mL, 0.05 mmol) in C₆D₆ solution at 300

K by ^1H NMR spectroscopy revealed resonances corresponding to enolate **14** after 30 minutes.

4.6.6 Reaction of **13** with aromatic substrates: general experimental procedure

A hexane solution of the heterotri-anionic zincate [(TMEDA)Na(TMP)(α -NC₄H₇NBoc)Zn(^tBu)] (**13**) was prepared on a 1 mmol scale *via* the experimental method detailed above. Subsequently, an aromatic substrate (either mesitylene, 0.14 mL, 1 mmol; ethylbenzene, 0.12 mL, 1 mmol; or cumene, 0.14 mL, 1 mmol) was introduced. After 10 minutes of stirring at ambient temperature, followed by cooling to -30 °C, each reaction mixture deposited a crop of colourless crystals after 24 hours. Analysis by X-ray crystallography and NMR spectroscopy confirmed the crystalline material to be recovered **13**.

4.6.7 Synthesis of [(TMEDA)(Boc-NC₄H₈)Na{(η^2 -C₅H₄)Fe(C₅H₅)}Zn(^tBu)₂], **16**

To a hexane solution of zincate **13** (prepared *in situ* on a 1 mmol scale *via* the preparation method detailed above), ferrocene (0.186 g, 1 mmol) was added *via* solid addition tube, which instantly produced an orange solution. After 10 minutes of gentle heating, the orange solution was cooled to -30 °C. Colourless crystals (0.12 g, 18% yield) were deposited from solution after 24 hours.

^1H NMR (400.03 MHz, C₆D₆, 300 K): δ = 4.47 and 4.45 (s and m, 1H, C₅H₄), 4.43 (s, 5H, Cp), 4.42 and 4.26 (m, 1H, C₅H₄), 3.08 and 2.97 [q, $^3\text{J}(\text{H},\text{H}) = 5.9$ Hz, and t, $^3\text{J}(\text{H},\text{H}) = 6.6$ Hz, 2H, α -NC₄H₈], 1.81 (s, 9H, O^tBu), 1.77 (s, 12H, CH₃-TMEDA), 1.64 (s, 4H, CH₂-TMEDA), 1.39 and 1.32 (m, 2H, β -NC₄H₈) and 1.32 (s, 18H, ^tBu). $^{13}\text{C}\{\text{H}\}$ NMR (100.60 MHz, C₆D₆, 300 K): δ = 79.0, 71.2 and 70.5 (s, C₅H₄), 68.2 (s, Cp), 67.9 (s, C₅H₄), 56.8 (s, CH₂-TMEDA), 46.3 and 45.9 (s, α -NC₄H₈), 45.9 (s,

CH₃-TMEDA), 36.5 (s, O^tBu), 28.6 (s, ^tBu), 25.5 and 24.9 (s, β-NC₄H₈) and 22.9 (s, ^tBu quaternary). Signals for C=O, Zn-C_{Cp} and O^tBu (quaternary) were not detected. Due to the acute air sensitivity of **16**, satisfactory C, H, N analyses could not be obtained.

Crystal data for **16**, C₃₃H₆₀FeN₃NaO₂Zn, M_r = 675.05, monoclinic, space group P2₁, *a* = 9.7379(10), *b* = 19.3823(17), *c* = 9.9895(11) Å, β = 104.439(11)°, *V* = 1825.9(3) Å³, *Z* = 2, μ = 1.096 mm⁻¹; 16563 reflections, 6953 unique, *R*_{int} 0.0972, final refinement to full-matrix least squares on *F*² gave *R* = 0.0775 (*F*, 4571 obs. data only) and *R*_w = 0.1398 (*F*², all data), GOF = 1.016.

4.6.8 Synthesis of [(TMEDA)Na(μ-TMP)(μ-C₆H₄OMe)Zn(^tBu)], **17**

Upon the introduction of anisole (0.11 mL, 1 mmol) to a hexane solution of zincate **13** (prepared *in situ* on a 1 mmol scale, *vide supra*), a colourless solution formed. Subsequent cooling to -30 °C furnished a crop of colourless crystals after 24 hours (0.21 g, 41% yield).

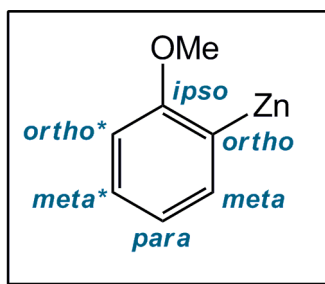


Figure 4.8 Labelling scheme for **17**.

¹H NMR (400.03 MHz, C₆D₆, 300 K): δ = 7.71 [dt, ³J(H,H) = 6.77 Hz, ⁴J(H,H) = 1.77 Hz, 1H, *m*-C₆H₄], 7.12 [td, ³J(H,H) = 7.51 Hz, ⁴J(H,H) = 1.79 Hz, 1H, *m**-C₆H₄], 7.04 [t, ³J(H,H) = 6.77 Hz, 1H, *p*-C₆H₄], 6.58 [d, ³J(H,H) = 7.86 Hz, 1H, *o**-C₆H₄], 3.40 (s, 3H, OMe), 2.01 and 1.90 (m, 1H, γ-TMP), 1.86 (m, 2H, β-TMP), 1.59 and 1.54 (s, 6H, Me-TMP), 1.55 (s, 12H, CH₃-TMEDA), 1.54 (s, 4H, CH₂-TMEDA), 1.34 (m, 2H, β-TMP) and 1.23 (s, 9H, ^tBu). ¹³C{¹H} NMR (100.60 MHz, C₆D₆, 300 K): δ = 165.8 (s, C_{ipso}), 155.2 (s, C_{Zn}), 140.8 (s, C_{meta}), 126.6 (s, C_{meta*}), 122.6 (s,

C_{para}), 110.8 (s, C_{ortho}^*), 56.9 (s, CH₂-TMEDA), 56.4 (s, OMe), 53.0 (s, α -TMP quaternary), 45.6 (s, CH₃-TMEDA), 40.8 (s, β -TMP), 36.2 (s, ^tBu), 35.3 and 34.9 (s, Me-TMP), 20.4 (s, γ -TMP) and 20.1 (s, ^tBu quaternary).

Due to the acute air sensitivity of **17**, satisfactory C, H, N analyses could not be obtained.

Crystal data for **17**, C₂₆H₅₀N₃NaOZn, $M_r = 509.05$, orthorhombic, space group P2₁2₁2₁, $a = 10.9980(12)$, $b = 14.644(3)$, $c = 18.434(3)$ Å, $V = 2968.8(8)$ Å³, $Z = 4$, $\mu = 0.862$ mm⁻¹; 25876 reflections, 5160 unique, R_{int} 0.0760, final refinement to full-matrix least squares on F^2 gave $R = 0.0903$ (F , 3771 obs. data only) and $R_w = 0.1966$ (F^2 , all data), GOF = 1.114.

Chapter 5

Modifying Alkylzinc Chemistry with 2, 2'-Dipyridylamide: Activation of ^tBu-Zn Bonds Towards *Para*-Alkylation of Benzophenone

“The scientist is not a person who gives the right answers,
he is one who asks the right questions.”

Claude Lévi-Strauss
French anthropologist

5.1 Summary

Carried out with the intention of designing new sodium zincate structural motifs, this part of the PhD project utilised 2,2'-dipyridylamine [dpa(H)], a secondary amine equipped with two pyridyl appendages, as a structural template-changing coligand. Turning away from the commonly employed monofunctional amide ligand TMP (2,2,6,6-tetramethylpiperidide), to multifunctional dpa enabled the synthesis of a set of alkylzinc-based compounds with unprecedented molecular structures. This remarkable set of structures incorporates dpa in either neutral zinc, sodium zincate or potassium zincate modifications. Among the middle category is the special sodium-zinc compound, [(TMEDA)₂Na₂(μ-dpa)₂Zn(^tBu)₂], which though formally a zincate, masquerades as a simple donor-acceptor adduct. Investigating the reactivity of these new compounds, most intriguingly it is found that sub-stoichiometric amounts of the sodium amide metalloligand [(TMEDA)Na(dpa)]₂ can activate ^tBu₂Zn towards the *t*-butylation of benzophenone at the challenging 1, 6-position, that is, *para* to the carbonyl substituent. In marked contrast, in the absence of this metalloligand ^tBu₂Zn is wholly inactive towards this ketone.

Exploring the consequence of altering the components within this sodium dipyridylamide metalloligand has revealed that the nature of the donor ligand and the alkali metal dictate the reaction outcome, exhibiting a strong influence on the alkylation yields and the reaction selectivity. Indeed, varying the donor ligand led to the synthesis and structural elucidation of three novel sodium dipyridylamide formulations, each of which can function as a metalloligand to generate a co-complex with ^tBu₂Zn. Also playing a key role in the reaction outcome is the choice of solvent, as whilst the reaction works well in hexane, the yields are significantly lowered upon changing to the Lewis donor solvent THF.

5.2 Introduction to Polar Metal Amides

Derived from sterically imposing secondary amines (R_2NH), polar metal amides have a long successful track record as important reagents in synthesis, with several recent reviews confirming that their popularity continues to be high.^[8; 73; 130c; 130d; 131; 261] Although in this category monometallic amides are well-established components of the synthetic chemist's toolbox, current research has brought heterobimetallic amides into the limelight. The synergic combination of two metals within an organoamide-ligand environment has often led to unexpected and unprecedented chemistry, which cannot be reproduced by either metal acting in isolation. Sophisticated bimetallic bases have been developed, where perhaps counter intuitively, it is the softer polyvalent metal (such as Zn,^[75; 147; 202; 255; 262] Mg,^[65; 74; 263] Al,^[128; 153; 155; 173; 198; 264] Cd,^[129; 199b; 199c] or Mn^[265]) that executes metallo-deprotonation (conversion of an inert C-H bond to a labile, more synthetically flexible C-metal bond), assisted by the presence of a reactivity enhancing alkali metal.

The vast majority of the recent eye-catching advances in zincate executed metallation chemistry have centred on the cyclic secondary monoamide TMP (2,2,6,6-tetramethylpiperidide). Developed by Kondo and Uchiyama, the original TMP zincate reagent “LiZn(TMP)^tBu₂” is an effective base for both aromatic and heteroaromatic substrates encompassing a wide range of functionality.^[128] Knochel has since compiled a portfolio of new TMP based metallating agents including most recently the zinc pivalate “(TMP)Zn(OPiv)·LiCl” (OPiv = pivalate) which like “LiZn(TMP)^tBu₂” displays strong deprotonating power and exceptional functional group tolerance but has the added advantage that its arylzincated derivatives boast prolonged air stability.^[266] The area of zincate metallation chemistry with most well-defined structural information is that involving the TMEDA-supported sodium TMP reagent [(TMEDA)Na(μ-TMP)(μ-^tBu)Zn(^tBu)], **1**, (TMEDA = *N,N,N',N'*-tetramethylethylenediamine). This reagent, which exhibits enhanced reactivity over the aforementioned lithium zincates, and many of its arylzincated derivatives adopt similar structures designed on an architectural template of a Na-anion-Zn-anion ring

carrying terminal ligands. A neutral donor binds terminally to Na, whereas an anion binds terminally to Zn (Figure 5.1).

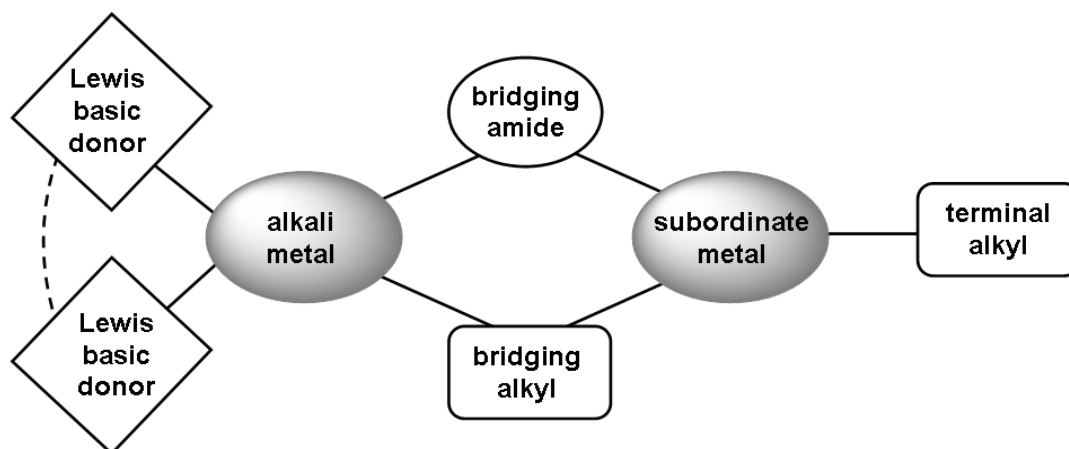


Figure 5.1 General structural motif observed for heteroleptic alkali metal zincate bases.

To attempt to break this template and develop new structural motifs that could stimulate new reactivity we have investigated replacing monofunctional TMP with multifunctional 2,2'-dipyridylamide [dpa, (2-NC₅H₄)₂N] (Figure 5.2). Offering three potential ligating N sites, one anionic and the other two neutral, this *N*-bridged bis-*N*-heterocycle finds utility in a diverse range of applications including most significantly medicine,^[267] catalysis,^[268] photoluminescence^[269] and supramolecular chemistry.^[270]

In this chapter we report a set of novel structures incorporating dpa in neutral zinc, sodium zincate and potassium zincate modifications all containing *t*-butyl ligands. Preliminary reactivity studies, in revealing that the mixed sodium-zinc dpa complexes can *t*-butylate the ketone benzophenone in the challenging *para* (1, 6-addition) position, hint that the reaction can be made sub-stoichiometric in the sodium component.

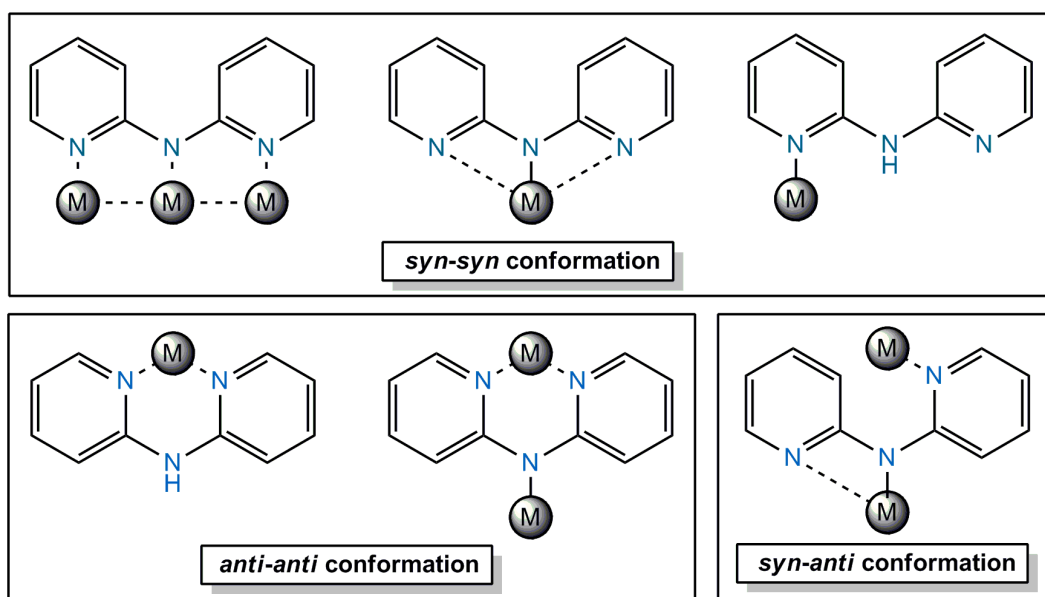


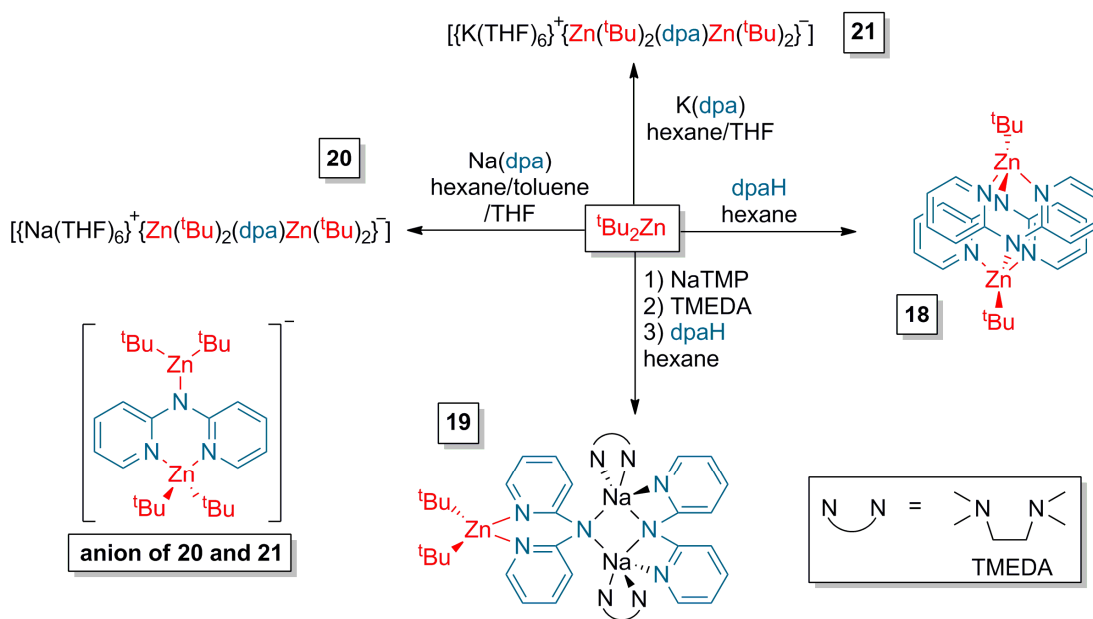
Figure 5.2 Potential ligating modes of neutral dpa(H) and anionic dpa⁻ towards a metal centre “M”, displaying either *syn* [N(pyridyl) is directed the same way as N(amido)] or *anti* [N(pyridyl) is directed towards the neighbouring pyridyl ring] bonding conformations.

5.3 Results and Discussion

5.3.1 Synthesis and Characterisation of Alkylzinc and Alkali Metal Zincate Compounds with Unprecedented Structural Motifs

Neutral, heteroleptic zinc complex $\{[(\text{dpa})\text{Zn}(\text{tBu})]_2\}$, **18**, was synthesised in a straightforward way through the 1:1 stoichiometric combination of tBu_2Zn and the amine dpa(H) in hexane solution (Scheme 5.1). NMR spectroscopic studies of the filtrate revealed the absolute yield was higher than the 70% yield of isolated crystals; only traces of unreacted dpa(H) were observed. Possessing an attractive “hour-glass” shaped core, the centrosymmetric molecular structure of **18** (Figure 5.3) is dimeric with the distorted tetrahedral zinc atom^[213] bonded to the deprotonated N of

one amido unit, occupying the di-pyridyl pocket of the other, and completing its coordination *via* a terminal ^tBu ligand. In the hour-glass description (Figure 5.3b), each bulb comprises a puckered, 6-atom (NCNCNZn) ring with Zn situated 1.0991(3) Å from the nearest NCNCN plane and 1.7143(3) Å from the second NCNCN plane (Figure 5.3c). This motif bears a strong resemblance to that of the isoelectronic neutral zinc dimer [MeZnC(H)Py₂]₂ (Py = 2-pyridyl).^[271] To our knowledge, **18** represents the first crystallographically characterised Zn-dpa complex showing a Zn-(bridgehead) N bond, although it has been noted in alkylated dimeric derivatives, though their mode of dimerization is distinct from that in **18**. For example, the dimeric compound [Zn(dpa*)(Et)]₂ [where dpa* is 6,6'-di-*tert*-butyl(dpa)] involves dpa* ligands with a *syn-anti* conformation and possesses a central, 4-membered (ZnN)₂ ring supplemented by dative Zn-N bonding.^[272] The *anti-anti* conformation^[273] within **18** also contrasts with the *syn-anti* conformations found in all three polymorphs of dpa(H).^[274]



Scheme 5.1 Synthesis of neutral zinc dimer **18**, disodium zincate **19**, sodium zinczincate **20** and potassium zinczincate **21**.

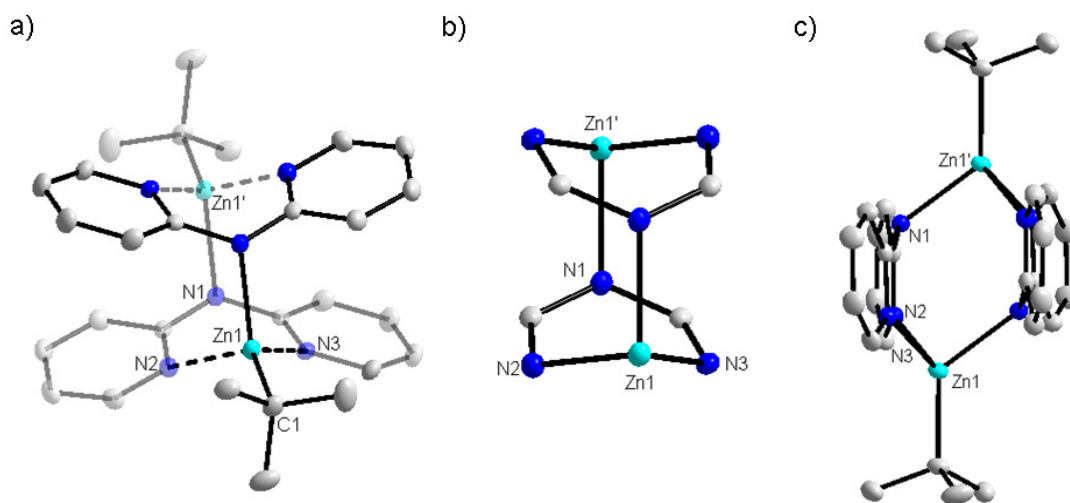
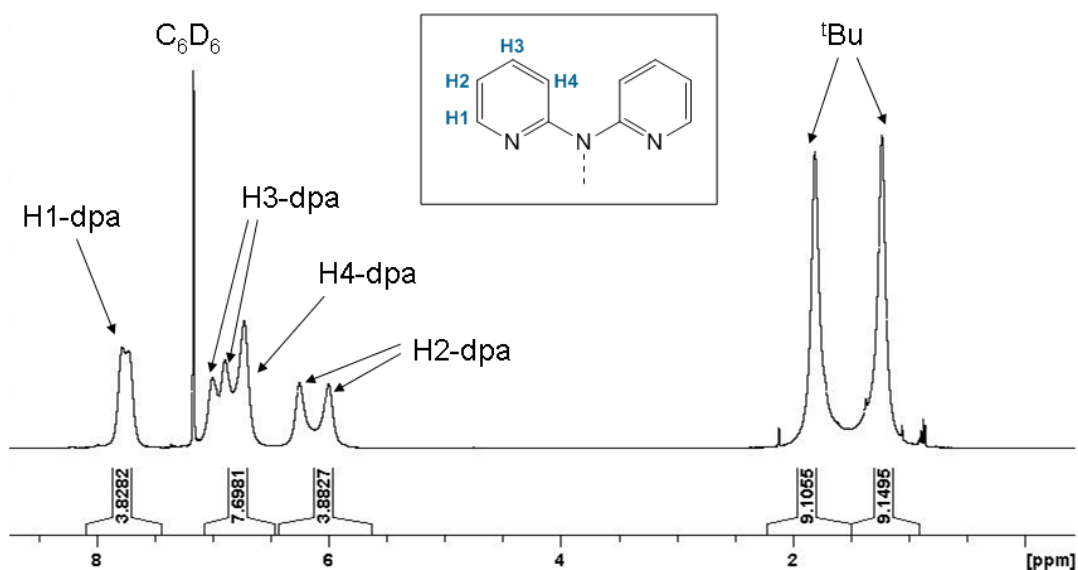


Figure 5.3 a) Molecular structure of heteroleptic **18** with thermal ellipsoids at 50% probability level and hydrogen atoms omitted for clarity. Selected bond lengths (Å) and bond angles (°): Zn1-N1, 2.116(2); Zn1-N2, 2.079(2); Zn1-N3, 2.070(2); Zn1-C1, 2.005(3); C1-Zn1-N1, 126.47(10); C1-Zn1-N2, 122.61(10); C1-Zn1-N3, 123.80(10); N1-Zn1-N2, 94.13(8); N1-Zn1-N3, 93.25(8); N2-Zn1-N3, 85.99(8); b) fragment of **18** highlighting the "hourglass" shaped (NCNCNz)₂ core; c) side-on perspective of **18**.

At ambient temperature, the ¹H and ¹³C{H} NMR spectra of **18** in C₆D₆ solution display two sets of pyridyl resonances and two ^tBu resonances (Spectrum 5.1), where one set may be expected due to the centre of symmetry of **18** in the solid state. Variable temperature ¹H NMR analysis revealed that these resonances coalesce at 320K, whilst cooling to subambient temperature enhances their separation. A variable concentration study, alongside a DOSY NMR experiment (Figure 5.4), suggest the two sets of resonances belong to the same species, hence this effect is likely to be a result of conformational isomerism as opposed to any dimer/monomer equilibrium.

DFT calculations revealed that there is a low energy conformational isomer of **18**, **18_{calc-A}**, arising chiefly from the rotation of one N(amino)-C(pyridyl) bond of each dpa ligand, which is more stable than model **18_{calc}** by 5.35 kcal mol⁻¹ (Figure 5.5). It seems plausible that these conformational isomers could be responsible for the two

sets of distinct ^1H NMR resonances observed at low temperatures. Two additional conformational isomers, **18_{calc}-B** and **18_{calc}-C** were also investigated theoretically (Figure 5.5). Isomer **18_{calc}-B**, arising from rotation of both ^tBu groups about 180° , is less stable than model **18_{calc}** by $1.69 \text{ kcal mol}^{-1}$. Thus it cannot be unequivocally ruled out that **18_{calc}-B** is responsible for the second set of resonances observed in the ^1H NMR spectrum. Model **18_{calc}-C**, a dimer having a 4-membered $(\text{ZnN})_2$ ring supplemented by dative Zn-N bonding was also probed theoretically. This alternative structure bears a strong resemblance to that of the reported compound $[\text{Zn}(\text{dpa}^*)(\text{Et})_2]$.^[272] DFT calculations revealed this structure to be $10.80 \text{ kcal mol}^{-1}$ less stable than **18_{calc}**. At first glance the pyridine rings of **18_{calc}-C** appear to be non-equivalent. However, in the related complex $[\text{Zn}(\text{dpa}^*)(\text{Et})_2]$, only one set of pyridyl NMR resonances is observed, suggesting that the pyridyl rings interconvert too rapidly to observe two sets of resonances on the NMR timescale.



Spectrum 5.1 The ^1H NMR (400.03 MHz, 300 K) spectrum of $[(\text{dpa})\text{Zn}(^t\text{Bu})_2]$ (**18**) in C_6D_6 .

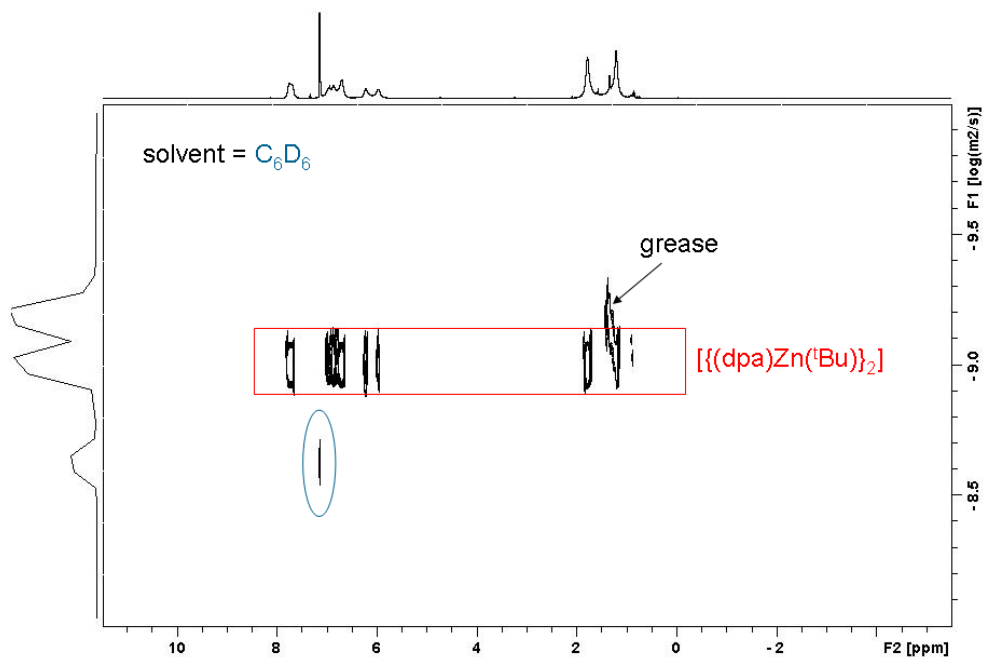


Figure 5.4 DOSY NMR Spectrum of $[(\text{dpa})\text{Zn}(\text{tBu})_2]$ (**18**).

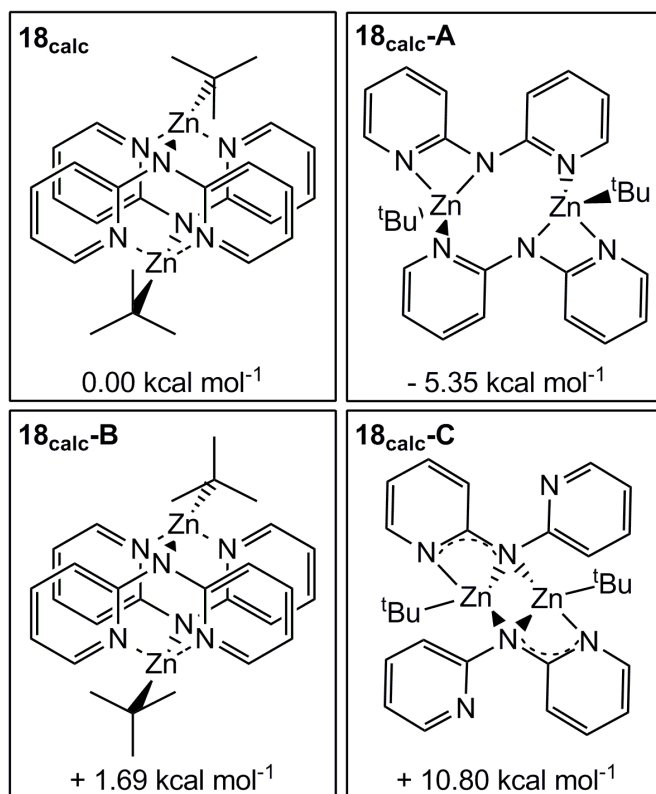


Figure 5.5 Structure and relative energies of model **18_{calc}** and its conformational isomers **18_{calc}-A**, **18_{calc}-B**, and **18_{calc}-C**.

On reacting TMP-zincate **1** with dpa(H) in hexane solution we expected to observe a straightforward transamination reaction.^[275] In fact the isolated crystalline product turned out to be the disodium-monozinc species $[(\text{TMEDA})_2\text{Na}_2(\mu\text{-dpa})_2\text{Zn}(\text{tBu})_2]$, **19** [yield, 70% based on the dpa(H) stoichiometry]. In generating this product, formally transamination has occurred but the 2:1, Na:Zn stoichiometry of **19** is inconsistent with the 1:1 stoichiometry employed in the reaction. The molecular structure of **19** (Figure 5.6) can be viewed as a cocomplex between a TMEDA-complexed sodium amide dimer and a bisalkyl zinc monomer, the connecting junctions being two dative Zn-N(pyr) bonds that complete a distorted tetrahedral (C_2N_2) zinc environment. To bind to Zn, one dipyrindylamide must adopt an *anti-anti* disposition with its pyridyl N atoms oriented away from the $[\text{Na}(\text{amido})\text{N}]_2$ ring, while the second has a *syn-syn* conformation with each Na bonded to the amido N and one or the other of the pyridyl N atoms.

Resonance delocalisation within the dipyrindylamide scaffold is usually associated with shorter C-(amido)N-C bridges (for example, about 1.34 Å each), longer C-(pyr)N bonds (for example, about 1.38 Å), and a dihedral angle between the two pyr ring planes approaching 0° as ascertained by data from several neutral dpa(H) and anionic dpa complexes.^[274; 276] By comparison the corresponding dimensions within **19** [e.g., C(10)-N(1), 1.371(2) Å; C(15)-N(1), 1.373(2) Å; C(10)-N(2), 1.347(2) Å; C(15)-N(3), 1.346(2) Å; dihedral angle of unit bonded to Zn, 22.9°] suggest the degree of delocalisation is small. This prompts the thought that though formally a higher order zincate (conforming to the empirical formula $\text{Na}_2\text{ZnR}_2\text{R}'_2$), **19** is best interpreted as a neutral donor-acceptor bisalkylzinc complex with a metalloligand as donor. Supporting this interpretation, the structure of **19** is novel as it bears little resemblance to the common “Weiss” motif of di-alkali-metal zincate and related ate structures^[130b; 177d; 216b] (Figure 5.7) but shows more in common with homonuclear zinc complexes such as the alkyl amides $[\text{tBu}_2\text{Zn}\{(\text{iPrN}(\text{H})\text{CH}_2\text{CH}_2\text{N}(\text{H})\text{iPr})\}]$ ^[277] or $[(\text{tBu}_2\text{Zn})_3(\text{C}_4\text{H}_4\text{N}_2)_4]$.^[278]

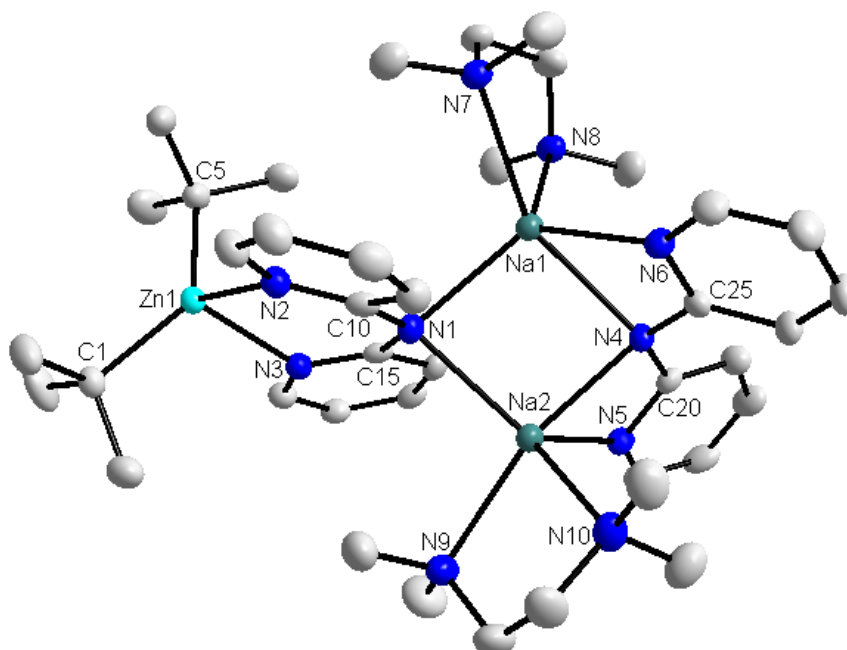
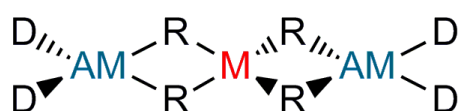


Figure 5.6 Molecular structure of **19** with thermal ellipsoids at 50% probability level and hydrogen atoms omitted for clarity. Selected bond lengths (Å) and bond angles (°): Zn1-C1, 2.048(2); Zn1-C5, 2.044(2); Zn1-N2, 2.185(2); Zn1-N3, 2.157(2); N1-C10, 1.371(2); N1-C15, 1.373(2); N2-C10, 1.347(2); N3-C15, 1.346(2); C1-Zn1-C5, 130.31(7); C1-Zn1-N2, 111.19(6); C1-Zn1-N3, 110.41(6); N2-Zn1-N3, 82.42(6); N2-Zn1-C5, 108.19(6); N3-Zn1-C5, 103.65(7); N7-Na1-N8, 74.63(5); N9-Na2-N10, 74.18(6); C10-N1-C15, 125.1(2).



AM = alkali metal
M = divalent metal
R = alkyl/amido/ether ligand
D = donor ligand

Figure 5.7 Graphical representation of a Weiss motif structure.

Surprisingly when the same metal components in **19** were mixed together in the presence of THF but absence of TMEDA the structural outcome was remarkably different (Scheme 5.1). In general replacing TMEDA by THF can be rather trivial in organoalkali-metal chemistry with one bidentate TMEDA substituted by two monodentate THF molecules without altering the basic structure of the complex

though reactivity may be changed^[46] but here the structural effect is much more discriminating. In contrast to contacted ion pair **19** with its 2:1 Na:Zn stoichiometry, the isolated product from the THF containing solution is the solvent-separated monosodium-dizinc complex $[\{\text{Na}(\text{THF})_6\}^+\{\text{Zn}(\text{tBu})_2(\text{dpa})\text{Zn}(\text{tBu})_2\}^-]$, **20**. The octahedrally coordinated cation of **20** is known,^[279] for example in the solvent separated sodium zincate $[\text{Na}(\text{THF})_6]^+[\text{Zn}(\text{C}_5\text{H}_5)_3]^-$,^[211] but its anionic moiety (Figure 5.8) is to the best of our knowledge unprecedented.^[178] This anion contains two tBu_2Zn monomers which connect through one dpa anion which, lying flat in an *anti-anti* conformation, presents a chelating pyridyl pocket to one Zn atom making it 4 coordinate and the bridgehead amido N to the other Zn making it 3 coordinate. Unfortunately, the anion lies on a crystallographic centre of symmetry – and as this symmetry can only be approximately satisfied by the dpa ligand, the structure is disordered over two sites. This prevents any discussion of dimensions, though the atomic connectivity is definite.

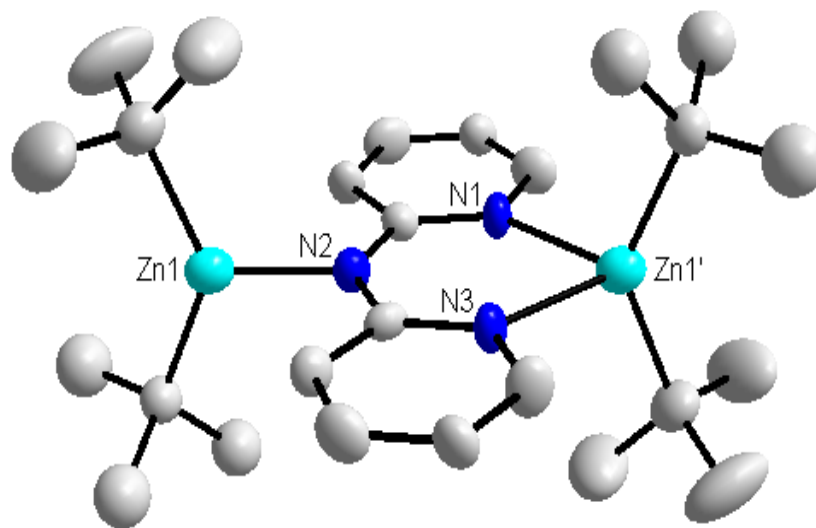


Figure 5.8 Anion of solvent separated ion pair structure of **20** with thermal ellipsoids at 50% probability level and hydrogen atoms and disorder components omitted for clarity. The anionic moiety of **21** is effectively identical.

We therefore turned to a DFT study using the B3LYP^[190] method and the 6-311G (d,p)^[191] basis set in which the anionic moiety of **20** was modelled (**20_{calc}**). Its dimensions revealed slightly more delocalisation than that implied in **19**. Key

indicators are the (amido)N-C(H) bond lengths [1.363 Å; cf, 1.372 Å, mean, in **19**] and the dihedral angle between the (pyr)N-C(H) bonds [C-N...N-C is 3.9° in **20**_{calc}, cf, 26.0° in **19**]. Also within the pyridyl rings there are long C-N bonds and two relatively short C-C bonds akin to a N-C=C-C=C-C-N pattern (bond lengths 1.345/1.345, 1.380/1.380, 1.401/1.401, 1.374/1.374, 1.429/1.428, and 1.360/1.359 Å, Figure 5.9) similar to that found in a series of [Me₂MPy₂N]_n complexes, where M is Al, Ga, In or Tl.^[276b] Formally **20** could be considered a sodium zinczincate^[280] in that it combines a neutral ^tBu₂Zn unit with a [Zn(dpa)^tBu₂]⁻ ate, though the true electronic distribution as reflected by the theoretical calculations lies between these two extremes.

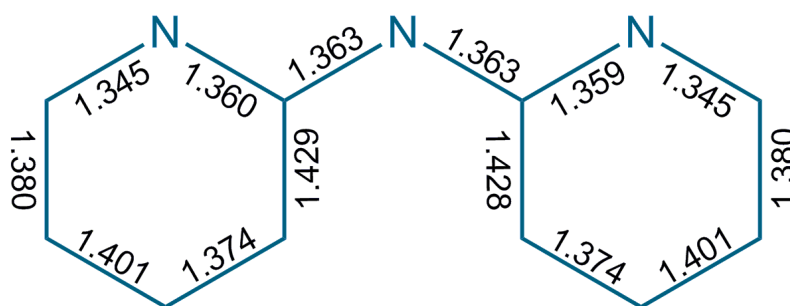


Figure 5.9 Bond lengths (Å) within the dpa fragment of **20**_{calc}.

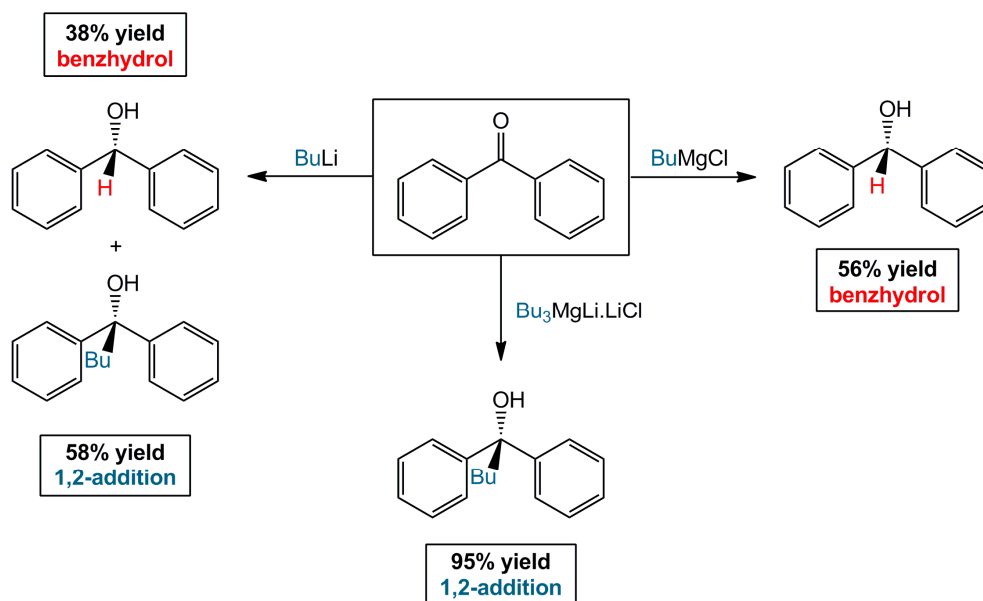
We also successfully prepared the potassium congener of **20** [$\{K(THF)_6\}^+ \{Zn(^tBu)_2(dpa)Zn(^tBu)_2\}^-$], **21**, through the combination of KR (where R is CH₂SiMe₃), dpa(H) and ^tBu₂Zn in a hexane/THF solvent system (Scheme 5.1). Unfortunately, disorder of the dpa ligand in **21** limits the discussion of the structure although the connectivity is definite. Matching the anion of **20**, the anion of potassium zinczincate **21** has retained both *tert*-butyl ligands on its zinc centres, whilst each dpa(H) ligand has been deprotonated and bridges the two chemically distinct Zn centres to form an asymmetrical dinuclear structure. Meanwhile, the potassium counter ion is coordinatively saturated through dative bonding from six THF ligands. This cation has previously been observed,^[281] for example within the potassium zincate [K(THF)₆]⁺[Zn(O-2,6-^tBu₂C₆H₃)₃]⁻.^[282] Reflecting on the reaction, it is likely that the more reactive potassium reagent performs the initial deprotonation of dpa(H), followed by a subsequent transmetalation. Supporting this thought, note

that in the absence of ${}^t\text{Bu}_2\text{Zn}$ the reaction of KR with dpa(H) in THF solvent produces the polymer $[\text{K}^+\text{dpa}^-]_\infty$.^[283]

5.3.2 Reactivity Studies: Initial Investigation into the Alkylation of Benzophenone

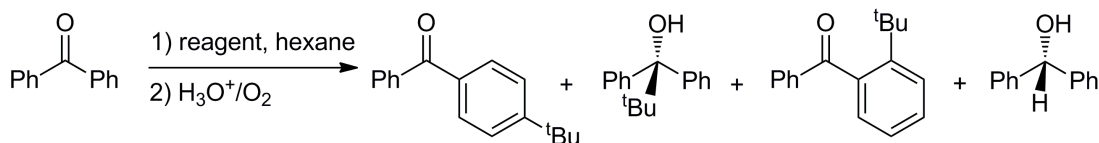
Alkylselective addition to ketones *via* Grignard reagents has been much studied with benzophenone often used as a benchmark ketone as its reactions can have several potential outcomes (Scheme 5.2).^[284] Monometallic reagents generally produce significantly greater proportions of the hydride reduction product benzhydrol (BuMgCl: 56%, BuLi: 38%); whereas bimetallic combinations can offer superior selectivity, with the use of the synergic lithium magnesiate base $\text{Bu}_3\text{MgLi}\cdot\text{LiCl}$ leading to exclusive carbonyl (1, 2-) addition in an impressive 95% yield.^[285] Excellent progress has been made in carbonyl (1, 2-) addition most recently by Ishihara who showed that catalytic amounts of ZnCl_2 (generating “ R_3ZnMgCl ” intermediates) can greatly enhance such reactions.^[285b] Hevia also reported that introducing a mere 10 mol% of the magnesium-zinc “hybrid” $[(\text{THF})_6\text{Mg}_2\text{Cl}_3]^+[\text{Zn}_2\text{Et}_5]^-$ to the reaction of the alkyl Grignard reagent EtMgCl and benzophenone gave 1, 2-addition in 90% yield.^[284f] These bimetallic zinc-mediated successes inspired us to test the *t*-butylation performance of sodium zincates **19** and **20** in hexane solution noting that **1** had previously delivered a ${}^t\text{Bu}$ nucleophile to the *para* (1, 6-) position of benzophenone albeit on the sole evidence of an isolated crystalline enolato intermediate.^[144]

Table 5.1 reveals that the three sodium zincates **1**, **19**, and **20** give competitive yields of the challenging *para* addition product 4-*t*-butylbenzophenone in contrast to the near 0% yields witnessed for the homonuclear zinc species. Unreacted benzophenone was also recovered. A striking comparison is that the metalloligand solvated ${}^t\text{Bu}_2\text{Zn}$ produces 40 times as much *para* product as unsolvated ${}^t\text{Bu}_2\text{Zn}$ or its pyridine and TMEDA solvates.



Scheme 5.2 Competitive 1,2-addition and reduction (benzhydrol) products obtained from the reaction of benzophenone with monometallic organolithium (left) and organomagnesium (right) reagents, and with a bimetallic lithium magnesiate (centre).

In a very early study Olah reported that reacting ^tBuLi with benzophenone in THF solvent gave a 52% yield of ring alkylation products (1:9, *ortho:para* ratio), but this was accomplished only at -100°C using toxic thionyl chloride as oxidant as an aqueous work-up dropped the combined yield to 28% and running the reaction in hexane at ambient temperature switched the major product to that of 1, 2-addition.^[284e] Clearly the zincate systems are advantageous since they give comparable yields at ambient temperature using a mild aqueous work-up. The most intriguing result came when a 1:1 mixture of ^tBu₂Zn and benzophenone was treated with only 10 mol% of sodium amide [(TMEDA)Na(dpa)]₂, presumably generating 10 mol% of **19** *in situ* in hexane solution. At ambient temperature, 4-*t*-butylbenzophenone was obtained in a low yield of 11% but impressively this increased to 52% under reflux conditions, implying that the substoichiometric sodium amide is recycling in some way.

Table 5.1: Reaction of zinc reagents with benzophenone in hexane solution for 18 hrs.

Entry	Reagent	Product Yield (%) ^[a]				Total
		<i>para</i> - addition (1, 6)	carbonyl- addition (1, 2)	<i>ortho</i> - addition (1, 4)	Benzhydrol (H ⁻ addition)	
Stoichiometric^[b]						
1	^t Bu ₂ Zn (1 equiv)	1	0	0	0	1
2	^t Bu ₂ Zn.2 pyridine (1 equiv)	1	0	0	0	1
3	^t Bu ₂ Zn.TMEDA (1 equiv)	1	1	0	0	2
4	1 (1 equiv)	58	14	3	0	75
5	19 (1 equiv)	40	6	0	11	57
6	20 (1 equiv)	42	13	0	3	58
Sub-stoichiometric^[c]						
7	^t Bu ₂ Zn (1 equiv)	11	1	0	8	20
8	^t Bu ₂ Zn (1 equiv) + [(TMEDA)Na(TMP)] (0.1 equiv)	33	8	0	6	47
9	^t Bu ₂ Zn (1 equiv) + [(TMEDA)Na(dpa)] ₂ (0.1 equiv)	52	12	0	7	71
10	^t Bu ₂ Zn (1 equiv) + [Na(THF) ₆][Zn(dpa) ^t Bu ₂] (0.1 equiv)	33	7	0	9	49

a) Yields determined by ¹H NMR spectroscopy using hexamethylbenzene (10 mol%) as an internal standard; b) Conditions: ^tBu₂Zn (1 mmol) and donor amine (none; pyridine, 2 mmol; TMEDA, 1 mmol); or sodium zincate reagent (**1**, [(TMEDA)Na(μ-TMP)(μ-^tBu)Zn(^tBu)]; **19**, [(TMEDA)₂Na₂(μ-dpa)₂Zn(^tBu)₂] or **20**, [{Na(THF)₆}⁺{Zn(^tBu)₂(dpa)Zn(^tBu)₂}⁻]; 1 mmol), PhC(=O)Ph (1 mmol), hexane (8 mL) for 18 hours at ambient temperature; c) Conditions: sodium reagent [none; {(TMEDA)Na(TMP)}, 0.5 mmol; {(TMEDA)Na(dpa)}₂, 0.5 mmol; {Na(THF)₆}{Zn(dpa)^tBu₂}, 0.5 mmol], ^tBu₂Zn (5 mmol), PhC(=O)Ph (5 mmol), hexane (40 mL) for 18 hours at 75 °C.

5.3.3 Extending the Scope of Synergic Alkali-Metal Zinc Mediated Alkylation Chemistry

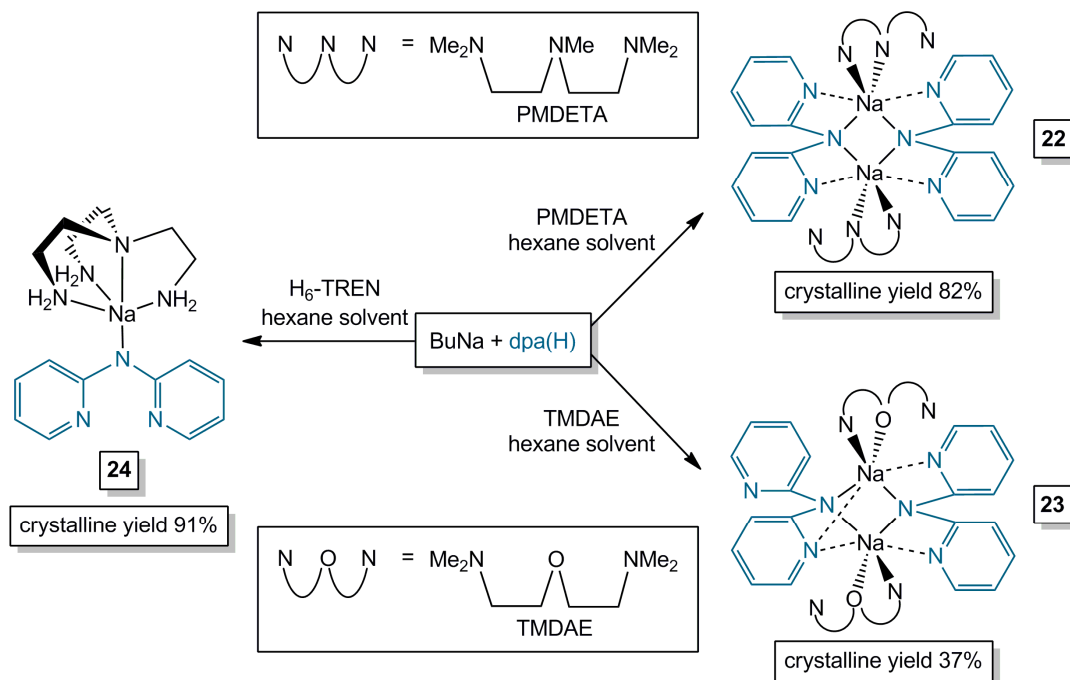
These intriguing results with benzophenone prompt various questions. Would changing the constituents of the [(TMEDA)Na(dpa)]₂ metalloligand allow us to tune

the reactivity and selectivity towards the alkylation of benzophenone? Is the coordination of TMEDA to sodium within the metalloligand structure important to the outcome of these addition reactions? Can we extend this methodology to the nearest neighbours of sodium; lithium and potassium? The studies reported forthwith aimed to find answers to these important questions. Thus, a range of alkali metal dipyridylamide metalloligands was applied to the alkylation of benzophenone, using ${}^t\text{Bu}_2\text{Zn}$ as the alkyl transfer reagent. Through the combination of spectroscopic and structural characterisation studies with theoretical calculations, this work sheds insight upon the impact of changing parameters such as the Lewis donor, alkali metal and solvent polarity upon the yields and product distribution.

5.3.4 Modification of the Donor Ligand: Synthesis of a Series of Sodium Dipyridylamide Metalloligands

Striving to establish the importance or otherwise of the donor employed within the $[(\text{TMEDA})\text{Na}(\text{dpa})]_2$ metalloligand, we prepared a series of sodium amide compounds with the general formula $[(\text{donor})\text{Na}(\text{dpa})]_x$. Accordingly, alternative Lewis donors PMDETA (*N,N,N',N'',N''*-pentamethyldiethylenetriamine), TMDAE (*N,N,N',N'*-tetramethyldiaminoethylether) and $\text{H}_6\text{-TREN}$ [*N',N'*-bis(2-aminoethyl)ethane-1,2-diamine] were selected for investigation (Scheme 5.3). We began by deprotonating $\text{dpa}(\text{H})$ with *n*-butylsodium in hexane solvent. This reaction produced a white suspension, which was subsequently treated with the appropriate donor amine. For the trifunctional donors PMDETA and TMDAE, two molar equivalents (on a 1 mmol scale reaction) were required to achieve solubility. Initially performed at ambient temperature, the reaction solutions were cooled to $-30\text{ }^\circ\text{C}$ in order to grow X-ray quality crystals of $[(\text{PMDETA})\text{Na}(\text{dpa})]_2$ [**22**, 82% isolated yield (reported yields are based upon the $\text{dpa}(\text{H})$ stoichiometry)] and $[(\text{TMDAE})\text{Na}(\text{dpa})]_2$, [**23**, 37% yield]. Upon moving to tetrafunctional $\text{H}_6\text{-TREN}$ (one molar equivalent), addition of toluene and gentle heating produced a pale yellow solution, which afforded a crop of colourless crystals of $[(\text{H}_6\text{-TREN})\text{Na}(\text{dpa})]$

(**24**) in an isolated yield of 91% upon gradual cooling to ambient temperature. New sodium amides **22-24** were characterised in solution using multinuclear (^1H , $^{13}\text{C}\{^1\text{H}\}$) NMR spectroscopy, and the molecular structures of **22** and **23** were elucidated by X-ray crystallographic studies as now discussed in detail.



Scheme 5.3 Synthesis of sodiated dipyridylamine dimers **22** and **23**, and the monomer **24**.

5.3.5 Structural Insights into Sodium Dipyridylamides 22-24

Unfortunately, severe disorder in the molecular structure of **22** prevents any discussion of its dimensions, although the connectivity is definite (Figure 5.10). A commonly observed motif within alkali metal chemistry,^[177a; 177b] and most pertinently for sodium amides^[177c; 177d; 286] such as $[\{(\text{TMEDA})\text{Na}(\text{NPh}_2)\}_2]$ ^[177c] and $[\{(\text{THF})\text{Na}(\text{HMDS})\}_2]$,^[286b] **22** adopts a dimeric, cyclic arrangement, where each Na centre is coordinated by two bridging dipyridylamide units and a chelating PMDETA. An unusual feature is the incomplete chelation of triamine donor

PMDETA, which engages Na in a bidentate rather than in its common full tridentate capacity. ^1H NMR spectroscopic analysis suggests that this bidentate bonding mode is not retained in C_6D_6 solution (*vide infra*). A search of the CCDB revealed only 11 structurally characterised compounds display this rare bidentate bonding mode, in comparison to 425 that involve tri-coordination of PMDETA to a metal centre.^[242] Most relevant to **22** is the structurally related phenyl complex $[(\text{PMDETA})\text{Na}\{\text{Ph}(2\text{-NC}_5\text{H}_4\text{N})\}]_2$.^[287] Both possess a planar $[\text{NaNNa}]\text{N}$ core; with hexa-coordinate Na adopting a distorted octahedral geometry; and with two amido bridges connecting the two Na centres. However, a key distinction between the two structures is the bonding mode of the bridging amide unit. Within $[(\text{PMDETA})\text{Na}\{\text{Ph}(2\text{-NC}_5\text{H}_4\text{N})\}]_2$, each amide unit forms both a Na-N(pyridyl)-Na and Na-N(amido)-Na bridge. In contrast replacing the phenyl ring with a second pyridyl ring in **22** results in loss of the N(pyridyl) bridge in exchange for two dative Na-N(pyridyl) interactions with a terminally attached, *syn-syn* dpa ligand (Figure 5.10).

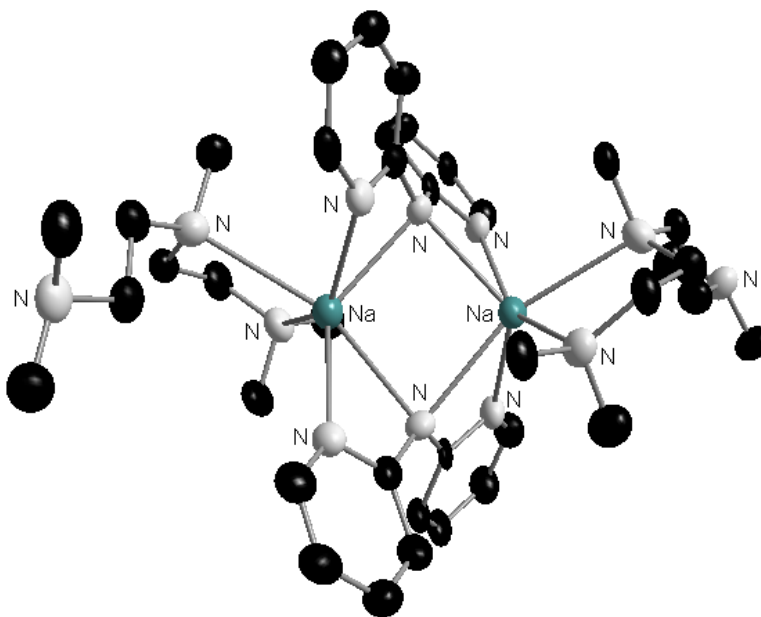


Figure 5.10 Molecular structure of **22** with thermal ellipsoids at 50% probability level and hydrogen atoms and disorder components omitted for clarity.

In view of the disorder problems with the crystal structure of **22** we turned to a DFT study in which the molecular structure of **22** was modelled (**22_{calc}**, Figure 5.11), first

utilising the B3LYP functionals^[190] and the 6-311G (d,p) basis set.^[191] The resultant optimised geometries were subjected to a frequency analysis, and the total energy computed by the DFT calculation was adjusted by inclusion of the zero-point energy contribution.

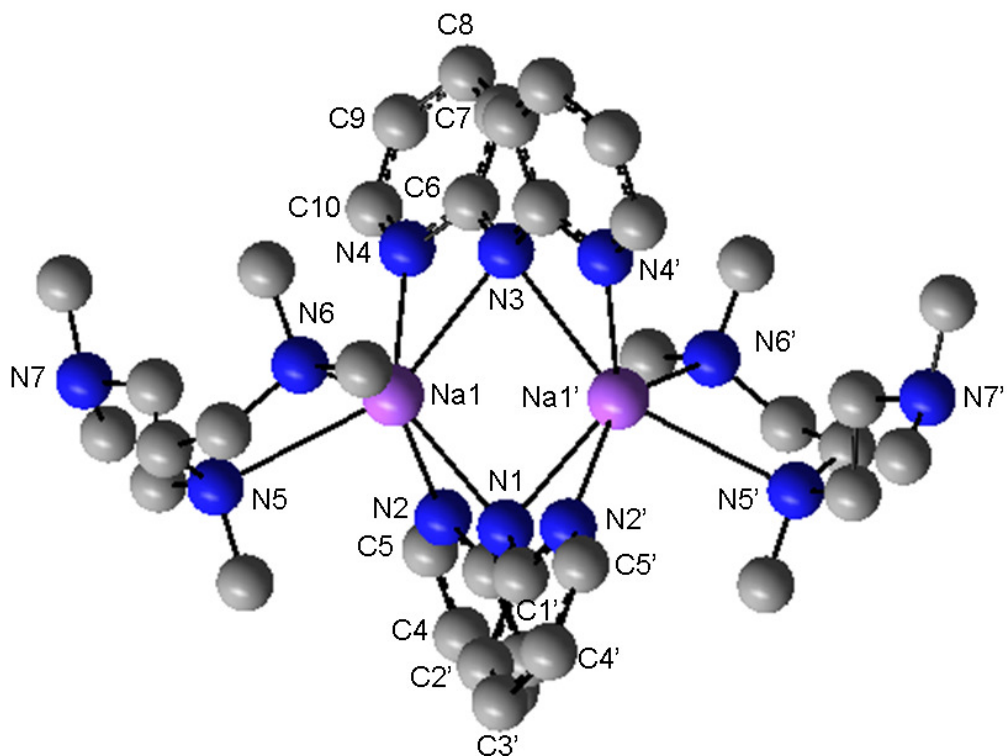


Figure 5.11 DFT model of **22_{calc}** with hydrogen atoms omitted for clarity. C1, C2 and C3 are partly shielded from view by C1', C2' and C3'. Selected bond lengths (Å) and bond angles (°): Na1-N1, 2.541; Na1-N2, 2.511; Na1-N3, 2.704; Na1-N4, 2.451; Na1-N5, 2.877; Na1-N6, 2.612; N1-C1, 1.363; N2-C1, 1.364; N2-C5, 1.335; N3-C6, 1.362; N4-C6, 1.365; N4-C10, 1.337; C1-C2, 1.424; C2-C3, 1.382; C3-C4, 1.399; C4-C5, 1.389; C6-C7, 1.426; C7-C8, 1.380; C8-C9, 1.400; C9-C10, 1.387; N1-Na1-N2, 54.0; N1-Na1-N3, 98.9; N1-Na1-N4, 52.9; N5-Na1-N6, 67.8; Na1-N1-Na1', 84.0; Na1-N1'-Na1', 77.9.

Within dimeric **22_{calc}**, a C_2 axis of symmetry runs through N1 and N3. Thus each *syn-syn* dpa unit forms a symmetrical bridge between the two Na centres, although there are slight differences in their coordination towards Na. The first dpa unit

displays similar (amido)N-Na and (pyridyl)N-Na bond lengths (Na1-N1, 2.541 Å and Na1-N2, 2.511 Å, respectively). In contrast, Na draws considerably closer to the terminal, (pyridyl)N arm (Na1-N4, 2.451 Å) of the second dpa fragment than it does to the (amido)N centre (Na1-N3, 2.704 Å). Accordingly, the central, 4-membered [NaN]₂ core of **22_{calc}** deviates from planarity, as the sum of the endocyclic angles is 323.8°. Inspection of the bond lengths of **22_{calc}** reveals that resonance delocalisation of the anionic charge occurs within both dpa units. In comparison to bond length data from related neutral dpa(H) and anionic dpa complexes, the (amido)N-C bond lengths of **22_{calc}** are short (N1-C1, 1.363 Å; N2-C6, 1.362 Å), whilst the (pyridyl)N-C bonds of **22_{calc}** are elongated due to the loss of aromaticity (N2-C1, 1.364 Å; N4-C6, 1.365 Å).^[274; 276] This contrasts with the bonding pattern observed within the neutral dpa(H) cobalt species [Co{dpa(H)}Cl₂], where the (amino)N-C bond lengths are long [1.373(4) and 1.382(4) Å] in comparison to the (pyridyl)N-C bonds [1.351(4) and 1.348(4) Å].^[276a]

Although **19** and **22_{calc}** differ in their Lewis donor components, the didentate coordination mode of PMDETA within **22_{calc}** mimics that of TMEDA within **19**. Thus the similarity between the sodium amide component of **19** and **22_{calc}** allows for tentative comparisons to be made. Within **22_{calc}**, the steric congestion at Na is reflected by the narrow N-Na-N bite angle of 67.8° for PMDETA, which is considerably smaller than the corresponding TMEDA bite angles within **19** [N7-Na1-N8, 74.63(5)°; N9-Na1-N10, 74.18(6)°]. It therefore seems logical that in **19**, coordination of the metalloligand {(TMEDA)Na(dpa)}₂ towards ^tBu₂Zn relieves the steric strain at the Na centre, as one dpa unit welcomes ^tBu₂Zn into its pyridyl pocket by switching its coordination mode from *syn-syn* to *anti-anti*.

As perhaps would be anticipated according to the close similarity between isoelectronic PMDETA and TMDAE, sodium amide **23** exhibits a dimeric arrangement (Figure 5.12a) akin to that of **22**. With no crystallographically imposed symmetry, the structure of **23** contains two distinct Na centres, each of which engages in a bidentate fashion with chelating TMDAE. A consideration of the space filling representation of **23** (Figure 5.12b) reveals that there is significant steric

congestion at the Na centre and accordingly, one terminal NMe₂ arm of each TMDAE waves freely. Each hexacoordinate Na also interacts with two bridging dpa units, both in a bidentate fashion, although the coordination mode differs. The first dpa ligand adopts a *syn-syn* conformation equivalent to that observed in **22**, where N(amido) bridges between two Na centres with two terminal N(pyridyl)-Na interactions providing further stabilisation. In contrast, the second dpa unit occupies a *syn-anti* conformation, with N(amido) and N(*syn*-pyridyl) forming an unsymmetrical bridge [where the bridging Na1-N8, Na1-N9, Na2-N8 and Na2-N9 bond lengths are 2.680(4), 2.538(3), 2.752(4) and 2.496(3) Å, respectively]. As a result, **23** contains two central four-membered [NaNNaN] rings at its core, each deviating from planarity with torsion angles of 15.281(2)° (Na2-N6-Na1-N9), and 35.359(2)° (Na1-N6-Na2-N8). Indicative of a small degree of resonance delocalisation within the dpa units (*vide supra*), the dihedral angles between the pyridyl ring planes are relatively large [48.216° between the N5 and N7 pyridyl ring planes; 27.787° between the N8 and N10 pyridyl ring planes].

The chemistry of the trifunctional, mixed N and O donor TMDAE is underdeveloped in comparison to that of its triamine counterpart, PMDETA.^[288] In this regard, **23** represents a rare example of a structurally characterised compound containing a non-substituted TMDAE donor. A search of the CCDB^[242] surprisingly revealed that only one other compound involving a non-substituted TMDAE ligand has been structurally characterised,^[178] namely the solvated copper salt [(TMDAE)CuCl₂].^[289] In this example, TMDAE binds to Cu in a tridentate fashion. Illustrating the capability of TMDAE to act alternatively as a bidentate donor, the lithium aluminate [Li(μ-Me₂NCH₂CH₂OCHCH₂NMe₂)(μ-TMP)Al(^tBu)₂] has also been structurally characterised,^[290] although in this case, TMDAE has also been subjected to deprotonation on a CH₂ unit adjacent to the O atom.

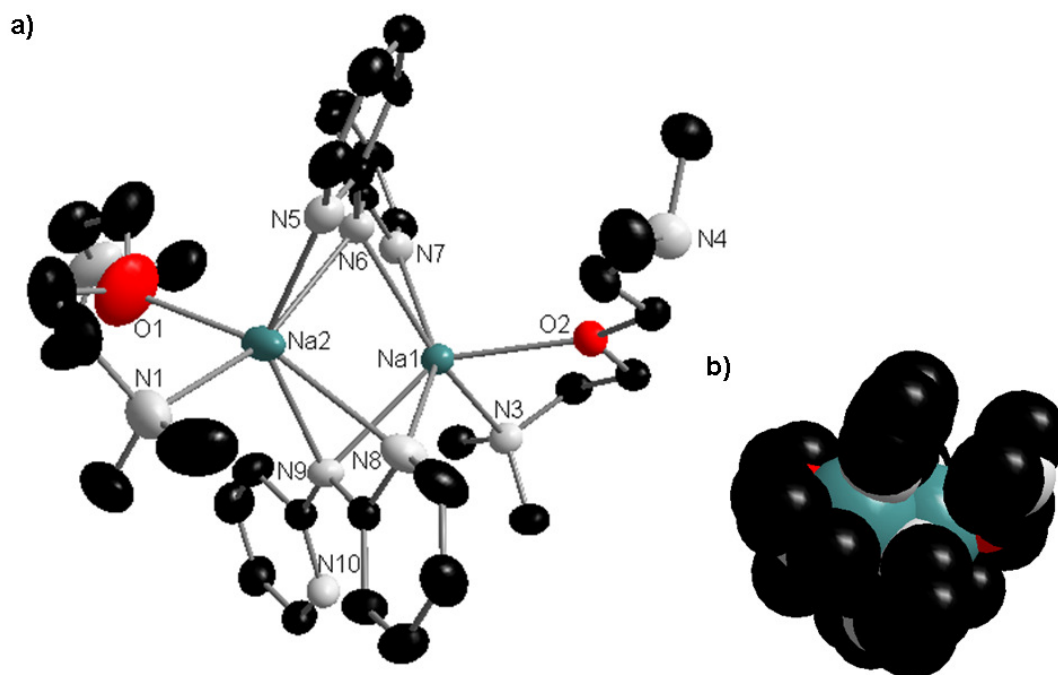


Figure 5.12 a) Molecular structure of **23** with thermal ellipsoids at 50% probability level. Hydrogen atoms and minor disordered components of TMDAE have been omitted for clarity. Selected bond lengths (Å) and bond angles (°): Na1-O2, 2.430(3); Na1-N3, 2.501(3); Na1-N6, 2.488(3); Na1-N7, 2.535(4); Na1-N8, 2.680(4); Na1-N9, 2.538(3); Na2-O1, 2.326(16); Na2-N1, 2.434(4); Na2-N5, 2.470(4); Na2-N6, 2.454(3); Na2-N8, 2.752(4); Na2-N9, 2.496(3); O2-Na1-N3, 71.06(10); O2-Na1-N6, 111.63(11); O2-Na1-N7, 102.93(11); O2-Na1-N8, 100.24(11); O2-Na1-N9, 139.81(11); N3-Na1-N6, 149.14(12); N3-Na1-N7, 94.91(12); N3-Na1-N8, 113.85(12); N3-Na1-N9, 93.47(11); N6-Na1-N7, 54.23(11); N6-Na1-N8, 96.23(12); N6-Na1-N9, 100.53(11); N7-Na1-N8, 147.69(12); N7-Na1-N9, 115.49(11); N8-Na1-N9, 51.39(10); O1-Na2-N1, 72.9(4); O1-Na2-N5, 101.4(4); O1-Na2-N6, 101.0(4); O1-Na2-N8, 163.7(4); O1-Na2-N9, 122.0(4); N1-Na2-N5, 100.85(14); N1-Na2-N6, 154.53(15); N1-Na2-N8, 93.33(14); N1-Na2-N9, 101.32(13); N5-Na2-N6, 55.34(12); N5-Na2-N8, 89.66(12); N5-Na2-N9, 135.37(13); N6-Na2-N9, 102.68(11); N6-Na2-N8, 95.21(12); N8-Na2-N9, 50.87(10); b) Space filling diagram of **23**, highlighting the considerable steric congestion at the sodium centres.

Severe disorder made it impossible to accurately refine the molecular structure of **24**, hence no structural data can be presented here. We therefore turned again to a DFT study using the B3LYP method^[190] and the 6-311G (d,p) basis set^[191] to facilitate the modelling of the molecular structure of **24**. Computations were performed to probe the relative energies of the conformational isomers of **24**, where dpa adopts either a *syn-syn* (model **24_{calc-A}**), *syn-anti* (model **24_{calc-B}**) or *anti-anti* (model **24_{calc-C}**) arrangement (Figure 5.13). As the common behavioural pattern of H₆-TREN is to act as a monomerisation agent, **24_{calc-A-C}** were modelled as monomeric species.^[257; 291] Surprisingly, comparison of these model isomers revealed only a small difference in the relative energies of the three conformers, spanning only 9.00 kcal mol⁻¹. Although model **24_{calc-A}** is the energy minimum structure, the difference between **24_{calc-A}** and **24_{calc-B}** is very low at only 3.19 kcal mol⁻¹. However, for brevity, only the bond parameters of the thermodynamically favourable model **24_{calc-A}** shall be discussed herein.

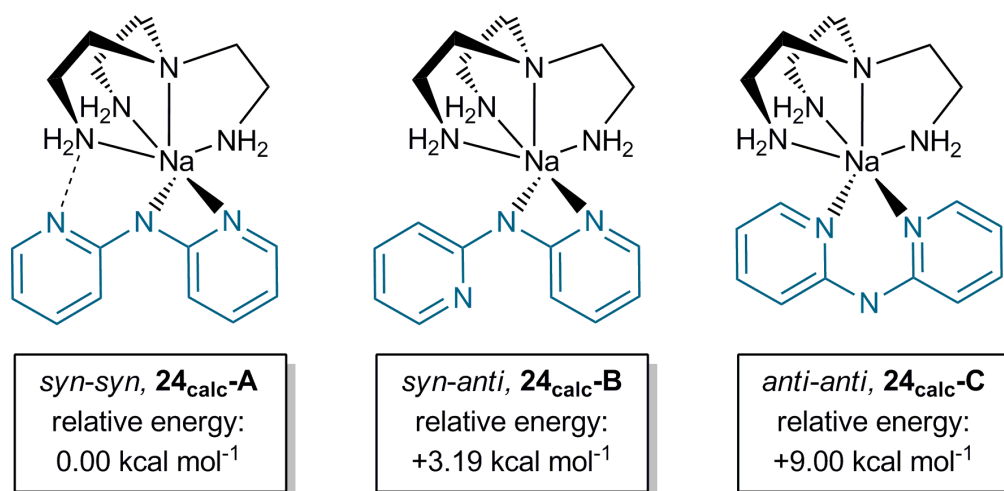


Figure 5.13 Relative energies of DFT-models **24_{calc-A-C}**, representative of the regioisomers of complex **24**.

Within **24_{calc-A}**, sodium engages *syn-syn* dpa in an asymmetric fashion (Na1-N1, 2.388 Å; Na1-N3, 2.539 Å, Na1...N2, 3.720 Å) and additional chelation by tetradentate H₆-TREN completes the highly congested, distorted octahedral coordination sphere [N-Na-N bond angles range from 55.1° to 159.2°]. Akin to the anion of sodium zinczincate **20**, the short C-(amido)N bond lengths of dpa [1.351

and 1.353 in **24_{calc}-A** cf, 1.363 Å in **20**] are indicative of resonance delocalisation within the dpa scaffold. Furthermore, the N-C=C-C-C-N pyridyl pattern observed within **20** is repeated in **24_{calc}-A** (bond lengths 1.334/1.333, 1.389/1.389, 1.399/1.400, 1.381/1.380, 1.427/1.428, 1.368/1.373 Å). With steric congestion about the Na centre blocking a second Na-N(pyr) interaction, the non-coordinated pyridyl N2 is stabilised through the formation of a hydrogen bond with H₆-TREN [N2...HN4, 2.068 Å].

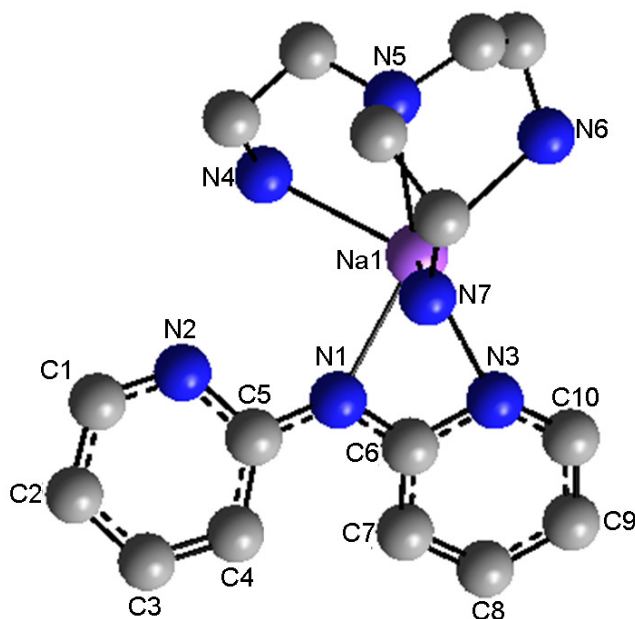


Figure 5.14 DFT model of **24_{calc}-A** with hydrogen atoms omitted for clarity. Selected bond lengths (Å) and bond angles (°): Na1-N1, 2.388; Na1...N2, 3.720; Na1-N3, 2.539; Na1-N4, 2.516; Na1-N5, 2.756; Na1-N6, 2.526; Na1-N7, 2.510; N1-C5, 1.353; N1-C6, 1.351; N2-C1, 1.334; N2-C5, 1.368; N3-C6, 1.373; N3-C10, 1.333; C1-C2, 1.389; C2-C3, 1.399; C3-C4, 1.381; C4-C5, 1.427; C6-C7, 1.428; C7-C8, 1.380; C8-C9, 1.400; C9-C10, 1.389; N1-Na1-N3, 55.1; N1-Na1-N4, 86.3; N1-Na1-N5, 138.8; N1-Na1-N6, 151.6; N1-Na1-N7, 91.9; N3-Na1-N4, 131.1; N3-Na1-N5, 159.2; N3-Na1-N6, 99.1; N3-Na1-N7, 99.5; N4-Na1-N5, 69.7; N4-Na1-N6, 107.2; N4-Na1-N7, 111.8; N5-Na1-N6, 69.5; N5-Na1-N7, 68.4; N6-Na1-N7, 105.3.

Although the application of either H₆- or Me₆-TREN as a highly chelating Lewis donor has been studied extensively within the context of transition metal chemistry,

similar studies within s-block chemistry are less well evolved. Nonetheless, more recently structural studies of alkali metal-TREN complexes have been forthcoming (Figure 5.15).^[257; 291-292]

5.3.6 Solution State Characterisation of Sodium Amides 22-24

Multinuclear [^1H , $^{13}\text{C}\{\text{H}\}$] NMR spectroscopic analysis of sodium amide complexes **22-24** in d_8 -THF solution confirmed that in each case, mono-deprotonation of dpa(H) has occurred with the loss of the N-H resonance at 8.87 ppm. As a consequence of dpa(H) metallation, the four aromatic resonances (labelled H1-H4) experience a significant low frequency shift (Table 5.2). For example, the H4-dpa resonance deviates upfield from 7.72 ppm in the parent amine, by 0.60 ppm in **22**, 0.42 ppm in **23** and 0.57 ppm in **24**. On the basis of this information it appears that aggregation (in **22** and **23**) has less bearing on these chemical shifts than the local coordination environment of the Na centre. Within the $^{13}\text{C}\{\text{H}\}$ NMR spectra, metallation of dpa translates as a downfield shift of the C_{ipso} resonance, by 11.4 ppm in **22**, 7.4 ppm in **23** and 11.2 ppm in **24**.

Comparison of the ^1H NMR spectroscopic resonances attributed to PMDETA in **22** with those of non-coordinated PMDETA give good agreement in d_8 -THF solvent [NCH_2 , 2.42 and 2.31 ppm; NCH_3 , 2.18 ppm; $\text{N}(\text{CH}_3)_2$, 2.14 ppm]. Thus, the bulk Lewis donor solvent d_8 -THF is exposed as a non-innocent solvent medium, which displaces the trifunctional amine from coordination to the electropositive Na centre in solution. Moreover, this finding is mirrored by the resonances ascribed to TMDAE and H_6 -TREN within **23** and **24** respectively, which are in close agreement with those of non-coordinated TMDAE and H_6 -TREN in d_8 -THF solution.

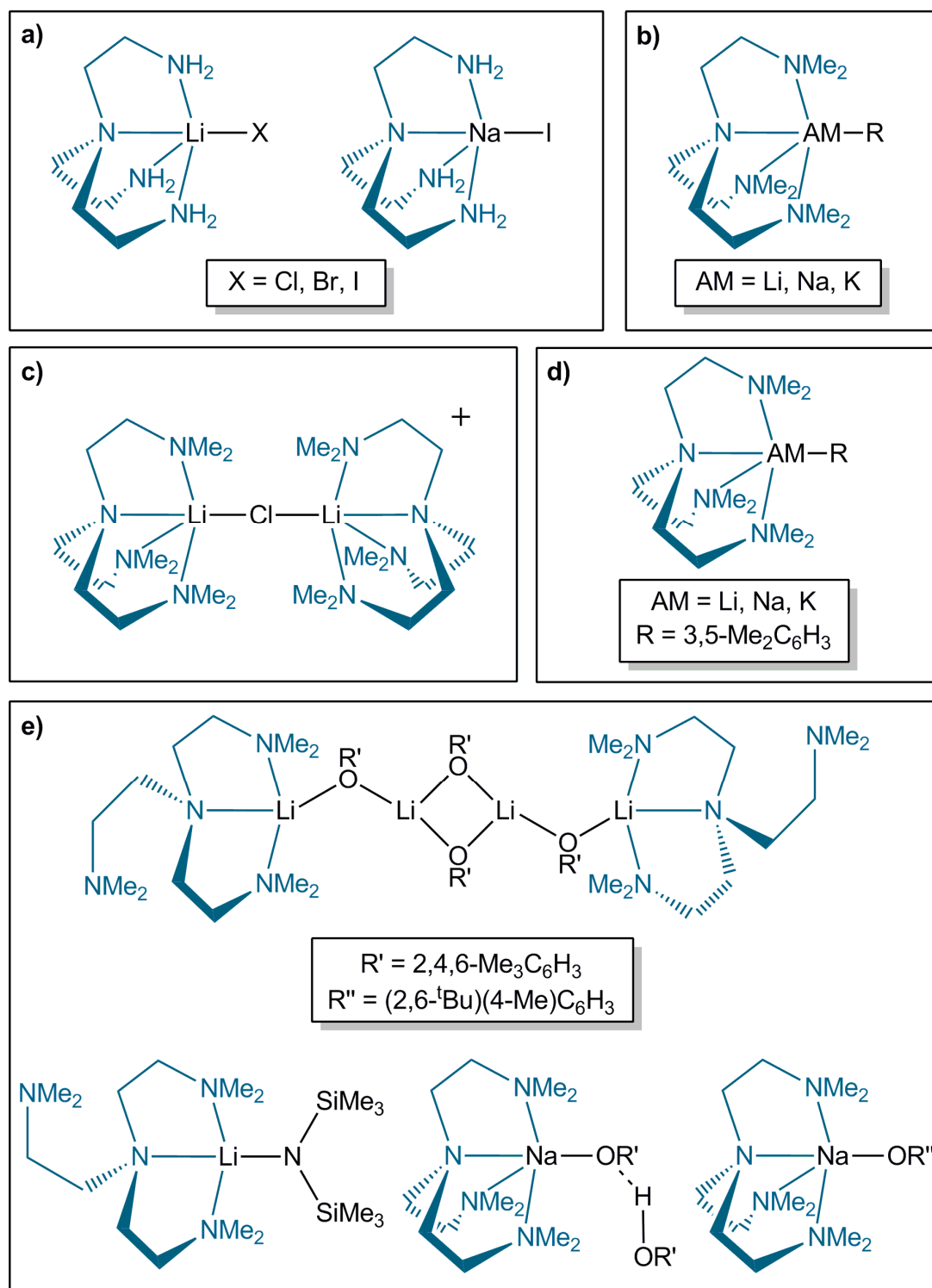
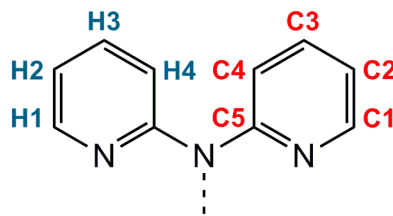


Figure 5.15 ChemDraw representation of the molecular structures of s-block-TREN complexes a) ^[291a] b) ^[257] c) ^[292a] d) ^[291b] e) ^[292b]

Table 5.2: Comparison of ^1H (400.03 MHz, 300 K) and $^{13}\text{C}\{\text{H}\}$ (100.59 MHz, 300 K) NMR shifts in d_8 -THF solution for dpa(H) and its sodium derivatives [(PMDETA)Na(dpa)]₂ (**22**), [(TMDAE)Na(dpa)]₂ (**23**), [(H₆-TREN)Na(dpa)] (**24**).



Atom Assignment	dpa(H)	Chemical Shift (ppm)		
		22	23	24
H1	8.16	7.91	7.99	7.92
H2	6.75	6.19	6.38	6.22
H3	7.53	7.12	7.30	7.15
H4	7.72	7.12	7.30	7.15
C1	148.3	149.1	148.8	149.0
C2	116.3	110.3	112.3	109.8
C3	137.7	136.5	136.9	136.3
C4	112.5	112.5	112.6	113.0
C5	155.8	167.2	163.2	167.0

5.3.7 Evaluating the Formation of a Bimetallic Sodium-Zinc Product upon Co-Complexation of $^t\text{Bu}_2\text{Zn}$ with Sodium Amides **22**, **23** or **24**

Evidence that combining metalloligand [(TMEDA)Na(dpa)]₂ with $^t\text{Bu}_2\text{Zn}$ results in the formation of a co-complex comes in the form of the donor-acceptor sodium-zinc compound **19** (Figure 5.6).^[293] Attempts to ascertain whether **22**, **23** and **24** can also behave as metalloligands towards $^t\text{Bu}_2\text{Zn}$ were carried out through the 1:1 equimolar combination of each sodium amide with $^t\text{Bu}_2\text{Zn}$, whereupon each reaction mixture was studied *via* ^1H NMR spectroscopy in C_6D_6 solution (Table 5.3). Unfortunately, repeated attempts to grow crystals of these putative co-complexes suitable for X-ray diffraction analysis were unsuccessful. Detection of resonances attributed to **22**, **23** or **24**, and $^t\text{Bu}_2\text{Zn}$ in a 1:1 ratio infers the formation of a sodium-zinc co-complex. Non-coordinated $^t\text{Bu}_2\text{Zn}$ is highly volatile under reduced pressure at ambient

temperature. Henceforth, it would have been removed *in vacuo* on preparing the solution samples. Examination of the $^1\text{Bu}_2\text{Zn}$ resonances, which are different in each case (1.58 ppm in **22**; 1.53 ppm in **23**; 1.66 ppm in **24**) confirms there is a considerable shift towards higher frequency in comparison to non-coordinated $^1\text{Bu}_2\text{Zn}$ (1.08 ppm). Incorporation of $^1\text{Bu}_2\text{Zn}$ also significantly alters the resonances associated with the sodium amide moieties **22-24** (Table 5.3). For example, upon addition of $^1\text{Bu}_2\text{Zn}$ to **22**, H3-dpa experiences an upfield shift of 0.16 ppm, whilst the PMDETA-N(CH_3)₂ resonance moves upfield by 0.19 ppm.

Table 5.3: Comparison of ^1H NMR data (400.03 MHz, 300 K, C_6D_6 solvent) for sodium amides **22**, **23** and **24**, in the absence and presence of $^1\text{Bu}_2\text{Zn}$.

Signal	Chemical Shift (ppm)					
	22		23		24	
	[(PMDETA)Na(dpa)] ₂ without $^1\text{Bu}_2\text{Zn}$	[(PMDETA)Na(dpa)] ₂ with $^1\text{Bu}_2\text{Zn}$	[(TMDAE)Na(dpa)] ₂ without $^1\text{Bu}_2\text{Zn}$	[(TMDAE)Na(dpa)] ₂ with $^1\text{Bu}_2\text{Zn}$	[(TREN)Na(dpa)] without $^1\text{Bu}_2\text{Zn}$	[(TREN)Na(dpa)] with $^1\text{Bu}_2\text{Zn}$
H1-dpa	8.12	8.04	8.04	7.99	8.18	8.18
H2-dpa	6.31	6.30	6.26	6.26	6.34	6.33
H3-dpa	7.27	7.11	7.18	7.08	7.30	7.16
H4-dpa	7.15	7.11	7.09	7.07	7.20	7.05
$^1\text{Bu}_2\text{Zn}$	-	1.58	-	1.53	-	1.66
donor ^[a]	2.24	2.03	2.16	2.06	1.91	1.76
N(CH_2)						
donor ^[a]	2.13	1.97	3.16	2.98	2.27	2.14
X(CH_2) ^[b]						
donor ^[a]	2.11	1.92	2.01	1.92	0.78	0.58
NR ₂ ^[c]						
donor ^[a]	1.99	1.86	-	-	-	-
N(CH_3)						

a) For **22**, donor = PMDETA; for **23**, donor = TMDAE; for **24**, donor = H₆-TREN; b) for **22** and **24**, X = N, for **23**, X = O; c) for **22** and **23**, R = (CH_3), for **24**, R = H.

To glean further insight into the solution state structures, we next analysed these reaction systems by diffusion-ordered spectroscopy (DOSY) experiments.^[294] A powerful and increasingly popular technique for the analysis of chemical mixtures,^[75; 129; 284f; 295] DOSY can shed light on the different species present in a multi-component solution, which are separated according to their diffusion coefficients. DOSY analysis of sodium amides **22-24** in the presence of $^1\text{Bu}_2\text{Zn}$ establishes that the resonances attributed to dpa and $^1\text{Bu}_2\text{Zn}$ possess similar diffusion

coefficients (Table 5.4). For example, the resonances attributed to dpa-H4 and ${}^t\text{Bu}_2\text{Zn}$ within **24** possess respective diffusion coefficients of $5.632 \times 10^{-10} \text{ m}^2 \text{ s}^{-1}$ and $5.580 \times 10^{-10} \text{ m}^2 \text{ s}^{-1}$, which points towards the coordination of **24** to ${}^t\text{Bu}_2\text{Zn}$ in C_6D_6 solution. However, it is of note that the diffusion coefficients of donor ligands PMDETA, TMDAE and H_6 -TREN differ significantly to those of dpa and ${}^t\text{Bu}_2\text{Zn}$. To demonstrate, the resonances of **24** assigned to H_6 -TREN have diffusion coefficients ranging from 7.759 to $7.910 \times 10^{-10} \text{ m}^2 \text{ s}^{-1}$. As d_8 -THF solvent has proven capable of displacing the donor ligands of **22**, **23** and **24** in solution (*vide supra*), it seems likely that this difference in diffusion coefficients could result from competitive equilibrium between donor ligand coordination and C_6D_6 coordination to Na. The capacity of benzene to act as a neutral π -donor towards sodium in the solid state has previously been observed through structural elucidation of the bimetallic complexes $[(\text{C}_6\text{H}_6)\text{NaCr}\{\text{O-Si}({}^t\text{Bu})_3\}_3]^{[296]}$ and $[(\text{C}_6\text{H}_6)\text{NaAl}(\text{dpp-BIAN})\text{Me}_2]$ (where dpp-BIAN is 1,2-bis[(2,6-diisopropylphenyl)imino]acenaphthene).^[297]

Table 5.4: Diffusion coefficients obtained from ${}^1\text{H}$ DOSY NMR experiments for sodium amides $[(\text{PMDETA})\text{Na}(\text{dpa})]_2$ (**22**), $[(\text{TMDAE})\text{Na}(\text{dpa})]_2$ (**23**) or $[(\text{H}_6\text{-TREN})\text{Na}(\text{dpa})]$ (**24**) in combination with ${}^t\text{Bu}_2\text{Zn}$ in C_6D_6 solution.

Signal	22 and ${}^t\text{Bu}_2\text{Zn}$		23 and ${}^t\text{Bu}_2\text{Zn}$		24 and ${}^t\text{Bu}_2\text{Zn}$	
	δ (ppm)	Diffusion Coefficient (10^{-10}) $\text{m}^2 \text{ s}^{-1}$	δ (ppm)	Diffusion Coefficient (10^{-10}) $\text{m}^2 \text{ s}^{-1}$	δ (ppm)	Diffusion Coefficient (10^{-10}) $\text{m}^2 \text{ s}^{-1}$
dpa-H1	8.04	6.354	7.97	6.661	8.16	5.912
dpa-H2	6.28	6.097	6.25	6.655	6.33	5.766
dpa-H3	7.09	6.262	7.06	6.478	7.13	6.159
dpa-H4	7.09	6.262	7.06	6.478	7.03	5.632
${}^t\text{Bu}_2\text{Zn}$	1.52	6.856	1.51	7.152	1.66	5.580
donor ^[a]	2.01	7.681	2.03	7.779	1.71	7.759
N(CH_2)						
donor ^[a]	1.95	8.142	2.95	7.864	2.09	7.839
X(CH_2) ^[b]						
donor ^[a]	1.89	7.821	1.90	8.135	0.58	7.910
NR ₂ ^[c]						
donor ^[a]	1.82	7.515	-	-	-	-
N(CH_3)						

a) For **22**, donor = PMDETA, for **23**; donor = TMDAE; for **24**, donor = H_6 -TREN; b) for **22** and **24**, X = N; for **23**, X = O; c) for **22** and **23**, R = (CH_3); for **24**, R = H.

5.3.8 Reactivity Studies: Investigating the Outcome of Varying the Lewis Donor upon the Alkylation of Benzophenone

It has long been known that the addition of Lewis donors to polar organometallic reagents can significantly alter their structures^[34-35] leading to changes in their reactivity.^[298] In the case of organoalkali metal compounds this change can normally be an enhancement; whereas with organoaluminium compounds it can have a detrimental effect on the reaction. We therefore decided to investigate the effect of modifying the Lewis donor within our metalloligand system (Table 5.5). A range of donor ligands were investigated, including the mixed O/N donors TEMPO (2,2,6,6-tetramethylpiperidine-N-oxyl radical) and TMDAE, and N donors DMAP, TMEDA, PMDETA, H₆-TREN and Me₆-TREN (Figure 5.16).

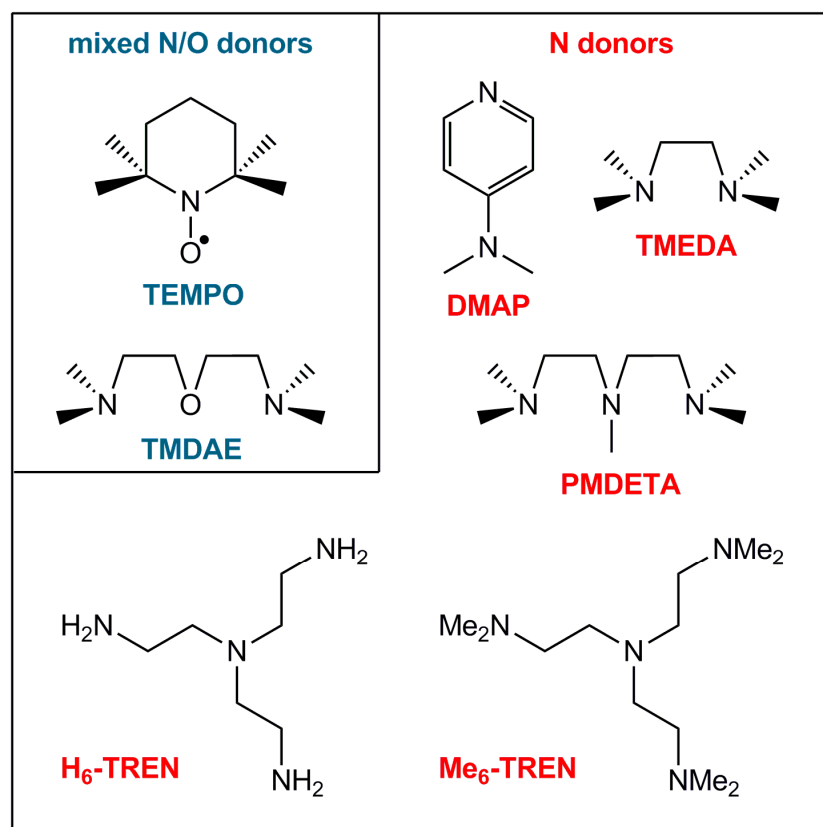


Figure 5.16 ChemDraw representation of the molecular structures of mixed O/N Lewis donors TEMPO and TMDAE and N Lewis donors DMAP, TMEDA, PMDETA, H₆-TREN and Me₆-TREN.

Using the homometallic zinc reagent ${}^t\text{Bu}_2\text{Zn}$ without a supporting sodium amide, a miserable 1% yield of the 1, 6-(*para*)-addition product was obtained at ambient temperature, with no other addition products detected, but only unreacted benzophenone. However, introduction of the sodium dipyridylamide metalloligand with DMAP, TMEDA or PMDETA as the Lewis donor boosted the reactivity of ${}^t\text{Bu}_2\text{Zn}$, leading to moderate *para*-alkylation yields of 24% (entry 2), 40% (entry 4) and 48% (entry 5), respectively. In each case, *para*-addition was obtained as the major product. In contrast, using TEMPO, TMDAE, $\text{H}_6\text{-TREN}$ or $\text{Me}_6\text{-TREN}$ as the Lewis donor gave no significant reactivity enhancement over ${}^t\text{Bu}_2\text{Zn}$ (entries 3 and 6-8). It is noteworthy that using the TMDAE metalloligand under reflux conditions led to a sizeable improvement of the *para*-alkylation yield, from 2% to 42% (compare entries 6 and 13). This surprising result was mirrored by $\text{Me}_6\text{-TREN}$, as moving to reflux conditions increased the *para*-alkylation yield by 33% (entries 8 and 15). As aforementioned, using sub-stoichiometric quantities (10 mol%) of $[(\text{TMEDA})\text{Na}(\text{dpa})]_2$ gives a 52% yield of the *para*-addition product. This enhanced ${}^t\text{Bu}_2\text{Zn}$ reactivity is successfully reflected when using sub-stoichiometric quantities of PMDETA-containing metalloligand **22**, culminating in a 53% yield of *para*-addition (entry 18) and suggesting that the metalloligand can be recycled to a modest degree within this reaction system.^[293]

Selection of PMDETA as the Lewis donor gives competitive *para*-addition yields to those obtained using TMEDA (respective yields of 48% and 40% at ambient temperature, entries 4-5). This is understandable, as the molecular structure of **22** (Figure 5.10) illustrates how PMDETA mimics TMEDA by acting as a didentate donor towards sodium. It seems unlikely that this asymmetric bonding mode is retained in C_6D_6 solution, as spectroscopic analysis of **22** in this medium reveals only one set of resonances corresponding to PMDETA. Alternatively, the triamine could be undergoing a fast exchange process. Furthermore, DOSY NMR spectroscopic analysis of **22** with ${}^t\text{Bu}_2\text{Zn}$ in C_6D_6 solvent suggests that C_6D_6 , which can act as a Lewis donor, is in competitive equilibrium with PMDETA. However, as **22** is crystallised from the non-polar solvent hexane, it seems plausible that the hexane solution state structure of **22** mirrors that of the solid-state structure.

Table 5.5: Reaction of zinc reagents with benzophenone in hexane solvent.

Entry	Donor	Reaction Temp. (°C)	Product Yield (%) ^[a]				Total
			<i>para</i> -Addition (1, 6-)	carbonyl-Addition (1, 2-)	<i>ortho</i> -Addition (1, 4-)	Benzhydrol (H ⁻ Addition)	
stoichiometric conditions^[b]							
1	None ^{[c], [293]}	25	1	0	0	0	1
2	DMAP	25	24	6	0	5	35
3	TEMPO	25	0	0	0	1	1
4	TMEDA ^[293]	25	40	6	1	8	55
5	PMDETA	25	48	2	0	8	58
6	TMDAE	25	2	1	0	0	3
7	H ₆ -TREN	25	1	1	0	1	3
8	Me ₆ -TREN	25	1	1	0	1	3
9	None ^{[c], [293]}	75	11	1	0	8	20
10	DMAP	75	25	14	0	8	47
11	TMEDA	75	33	11	0	14	58
12	PMDETA	75	46	3	1	10	60
13	TMDAE	75	42	11	6	2	61
14	H ₆ -TREN	75	5	4	0	7	16
15	Me ₆ -TREN	75	34	13	0	12	59
sub-stoichiometric conditions^[d]							
16	DMAP	75	26	8	0	7	41
17	TMEDA ^[293]	75	52	12	0	7	71
18	PMDETA	75	53	6	0	6	65
19	TMDAE	75	25	7	0	3	35

a) Yields determined by ¹H NMR spectroscopy using hexamethylbenzene (10 mol%) as an internal standard; b) Conditions: Nadpa (2 mmol), donor (2 mmol), ^tBu₂Zn (1 mmol), PhC(=O)Ph (1 mmol), hexane (8 mL) for 18 hours; c) ^tBu₂Zn alone was used as the reagent; d) Conditions: Nadpa (1 mmol), donor (1 mmol), ^tBu₂Zn (5 mmol), PhC(=O)Ph (5 mmol), hexane (40 mL) for 18 hours.

Despite their close similarity, exchanging PMDETA for isoelectronic TMDAE markedly reduces the yield of the *para* product (most noticeably from 48% to 2% at ambient temperature, entries 5 and 6). As could be expected based on the likeness of PMDETA and TMDAE, precursor complexes **22** and **23** adopt similar solid state structures: both are dimeric, each trifunctional Lewis donor bonds to sodium in a didentate fashion, and the two Na centres of each dimer are bridged *via* the amido N of deprotonated dpa. However, there are two key distinctions between **22** and **23**.

The donor chelation in **22** is *via* two N atoms, whereas in **23** it is *via* one O and one N atom. Also, within **22**, both dpa units adopt a *syn-syn* conformation, whilst in contrast the two dpa units within **23** differ in their conformation. The first mirrors the *syn-syn* bonding observed within **22**, whilst the second adopts a *syn-anti* conformation, connecting the two Na centres *via* two Na-N(amido) and two Na-N(*syn*-pyridyl) interactions.

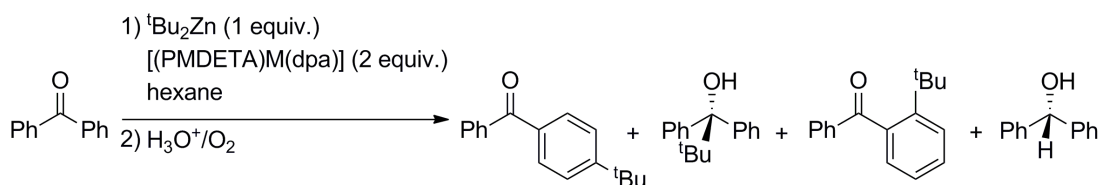
Functioning as a protective ligand shield to partly cover an alkali metal cation (Figure 5.15), tetradentate H₆-TREN has the capacity to act as a monomerisation agent towards organometallic species including alkali metal benzyl^[257] and 3,5-dimethylbenzyl^[291b] salts, where the alkali metal is lithium, sodium or potassium. This ability is again reflected in the molecular structure of crystalline **24** (Figure 5.14). The detrimental effect of H₆-TREN (and Me₆-TREN) upon reactivity could therefore be an artefact of too much steric shielding of the Na centre. These findings show that careful selection of the donor ligand is crucial to ensure that the reaction yields are not compromised.

5.3.9 Evaluating the Reaction Dependency of the Alkali Metal

As the best *para*-alkylation yields were obtained using PMDETA as the donor, this system was chosen to probe the effect of changing the alkali metal component of the metalloligand. Remarkably, simply substituting Na by Li destroyed the regioselectivity of the reaction, giving a mixture of *para*-addition, carbonyl-addition and benzhydrol in a relative ratio of 21:19:18 (Table 5.6, entry 1). Surprisingly, the reaction was suppressed when K was employed as the alkali metal, with an insignificant 2% yield of *para* product obtained (Table 5.6, entry 3) along with unreacted benzophenone. Thus the size and Lewis acidity of the alkali metal significantly impacts upon the yield and regioselectivity of the reaction, with the optimum results obtained using the intermediately sized Na. These findings bear some comparison to previous studies by Ishihara, where moving from the

organolithium reagent BuLi, to the corresponding Grignard reagent BuMgCl, changed the major product from carbonyl-addition (in a 58% yield) to benzhydrol (in a 56% yield), but significantly no *para*-addition was evident in either case.^[285d]

Table 5.6: Reaction of alkali metal dipyridylamide, PMDETA, ^tBu₂Zn and benzophenone in hexane solvent for 18 hours at ambient temperature.



Entry	Metal, M	Product Yield (%) ^{[a], [b]}				Total
		<i>para</i> -Addition (1, 6-)	carbonyl-Addition (1, 2-)	<i>ortho</i> -Addition (1, 4-)	Benzhydrol (H ⁻ Addition)	
1	Li	21	19	0	18	58
2	Na	48	2	0	8	58
3	K	2	2	0	0	4

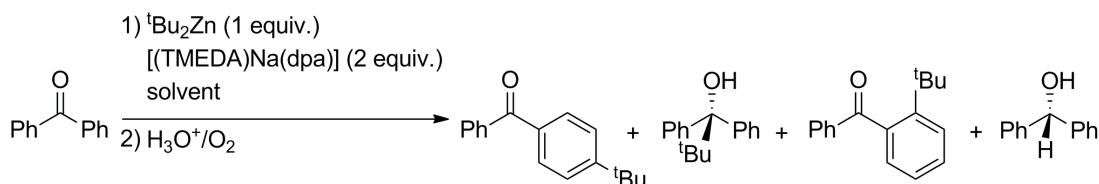
a) Yields determined by ¹H NMR spectroscopy using hexamethylbenzene (10 mol%) as an internal standard; b) Conditions: Mdpa (2 mmol, M = Li, Na or K), PMDETA (2 mmol), ^tBu₂Zn (1 mmol), PhC(=O)Ph (1 mmol), hexane (8 mL) for 18 hours at ambient temperature.

5.3.10 Exploring the Reaction Dependency on the Solvent

Curious to find out whether or not increasing the solvent polarity would improve the reaction yield, we next investigated Lewis basic THF as the bulk solvent in the reaction of **19** with benzophenone. However, a significant diminution of the *para*-addition yield was observed, from 40% in hexane solvent to 11% in neat THF solution (Table 5.7, respective entries 1 and 3). Analysis of crystalline **19** in C₆D₆ solvent suggests that TMEDA coordinates to Na in this medium, as a significant upfield shift is observed for the CH₂-TMEDA and CH₃-TMEDA resonances (by 0.66 and 0.38 ppm respectively from their values in free TMEDA, Table 5.8, entries 1 and

2). In contrast, when lone pair coordinating d_8 -THF was used as the solvent, the resonances attributed to TMEDA within **19** give close agreement with those of non-coordinated TMEDA (Table 5.8, entries 3 and 4). It has long been recognised in organoalkali metal chemistry that the solution state structure does not always reflect the solid state structure as the former is often more complicated involving multiple species and dynamic processes.^[32b; 33; 131; 299] Far from being an idle spectator, d_8 -THF participates through the displacement of TMEDA within **19**, which is accompanied by low reaction yields. It therefore seems logical that the microscopic coordination at the sodium centre is key, and that the coordination of stoichiometric TMEDA in comparison to the effect of using bulk THF plays a pivotal role in the extent and selectivity of the alkylation reaction. Indeed, it could in fact be the decoordination of TMEDA, which is paramount to the success of the nucleophilic addition, through creating a vacant site at the Lewis acidic sodium centre. It follows that this could facilitate the coordination of the Lewis donor benzophenone towards sodium, hence bringing it into close proximity with the activated $t\text{Bu}_2\text{Zn}$ fragment.

Table 5.7: Reaction of zincate $[(\text{TMEDA})_2\text{Na}_2(\mu\text{-dpa})_2\text{Zn}(t\text{Bu})_2]$ (**19**) with benzophenone for 18 hours at ambient temperature.



Entry	Solvent	Product Yield (%) ^{[a], [b]}				Total
		<i>para</i> - Addition (1, 6-)	carbonyl- Addition (1, 2-)	<i>ortho</i> - Addition (1, 4-)	Benzhydrol (H ⁻ Addition)	
1	hexane	40	6	1	8	55
2	hexane/THF	7	3	0	1	11
3	THF	11	3	0	1	15

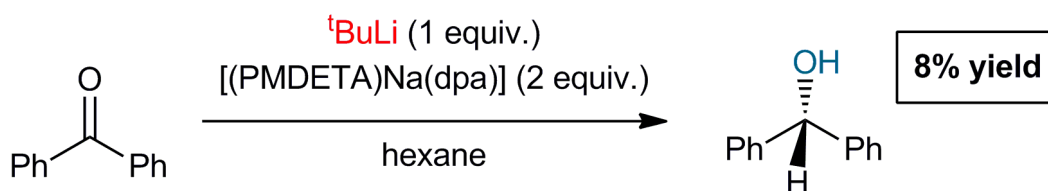
a) Yields determined by ^1H NMR spectroscopy using hexamethylbenzene (10 mol%) as an internal standard; b) Conditions: Nadpa (2 mmol), TMEDA (2 mmol), $t\text{Bu}_2\text{Zn}$, (1 mmol), PhC(=O)Ph (1 mmol), solvent (8 mL) for 18 hours at ambient temperature.

Table 5.8: Comparison of ^1H NMR data (400.03 MHz, 300 K) for non-coordinated TMEDA and TMEDA-coordinated zincate $[(\text{TMEDA})_2\text{Na}_2(\mu\text{-dpa})_2\text{Zn}(\text{tBu})_2]$ (**19**).

Entry	Compound	Solvent	Chemical Shift (ppm)	
			CH ₂ -TMEDA	CH ₃ -TMEDA
1	TMEDA	C ₆ D ₆	2.35	2.12
2	$[(\text{TMEDA})_2\text{Na}_2(\mu\text{-dpa})_2\text{Zn}(\text{tBu})_2]$ (19)	C ₆ D ₆	1.69	1.74
3	TMEDA	<i>d</i> ₈ -THF	2.30	2.15
4	$[(\text{TMEDA})_2\text{Na}_2(\mu\text{-dpa})_2\text{Zn}(\text{tBu})_2]$ (19)	<i>d</i> ₈ -THF	2.30	2.15

5.3.11 Evaluating the Effect of Substituting tBu_2Zn by tBuLi as the *tert*-Butyl Source

It was found that turning from tBu_2Zn to tBuLi as the *tert*-butyl ligand source in combination with $[(\text{PMDETA})\text{Na}(\text{dpa})]$ shuts down any *para*-addition, with the yield falling from 48% to 0%. Moreover, no other *tert*-butylation products were observed. Only the hydride addition product benzhydrol was observed and even that was obtained in a low yield of 8% (Scheme 5.4). Previously, the reaction of tBuLi with benzophenone was investigated by Yamataka and carbonyl-addition was observed as the major product (65% yield), alongside a significant quantity of *para*-addition (28% yield).^[300] It therefore seems that the presence of metalloligand **22** could impede the reactivity of tBuLi towards benzophenone.

**Scheme 5.4** Reaction of metalloligand **22** with tBuLi and benzophenone.

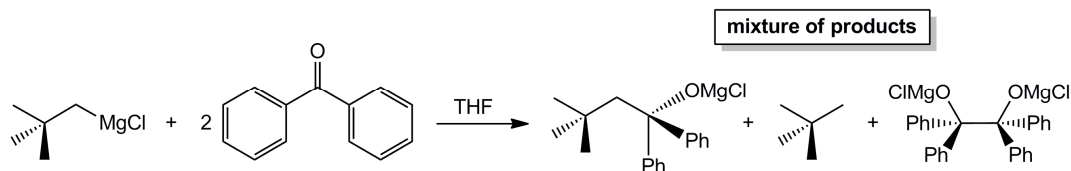
5.3.12 Evaluating the Addition of TEMPO to the Reaction System

Described recently as a “chameleonic ligand” due to its different forms,^[301] TEMPO can perform as a Lewis base either in its native radical form, or its reduced, anionic form (TEMPO*). Often exploited as a radical trapping reagent,^[302] TEMPO can also be used to provide insight into a postulated reaction mechanism.^[303] For instance, [(TMEDA)Na(μ -TMP)(μ -^tBu)Zn^tBu] (**1**), which can regioselectively *tert*-butylate benzophenone at the *para*-position,^[144] reacts with TEMPO to give the crystalline sodium zincate [(TMEDA)Na(μ -TMP)(μ -TEMPO*)Zn^tBu]. Accordingly, TEMPO has been reduced to its anion TEMPO* with concomitant formation of a ^tBu radical, thus providing evidence that **1**, normally thought to be an anionic base source, can also react through a single electron transfer (SET) mechanism.^[303] To compare with these findings, we incorporated TEMPO into our alkylation system, to probe the effect upon the yield and the regioselectivity. It transpired that the addition of TEMPO to metalloligand **22**, ^tBu₂Zn and benzophenone completely altered the course of the reaction, producing just a trace of the *para* product (1% yield *cf* 48% in the absence of TEMPO). Multinuclear (¹H, ¹³C{¹H}) NMR spectroscopic analysis of the crude reaction mixture confirmed that the known compound TEMPO-^tBu was present, alongside unreacted benzophenone.^[304] Diagnostic of TEMPO-^tBu, two distinctive singlets arising from the two inequivalent methyl groups of the nitroxide are observed at 1.15 and 1.10 ppm. A sharp singlet attributed to the ^tBu group is also present at 1.28 ppm. Completing the assignment, multiplets corresponding to β -TEMPO and γ -TEMPO hydrogen atoms were observed respectively at 1.48 and 1.30 ppm.

5.3.13 Mechanistic Insights

The nature of the mechanism for the addition of polar organometallic reagents to ketones has posed a long standing question, where the two major contending mechanisms involve a SET reaction pathway, or a polar reaction mechanism. Evidence to support a SET pathway for the alkylation of benzophenone has been

accrued,^[284d; 305] including the observation of the homo-coupled side-product benzopinacol (Scheme 5.5).^[306] Furthermore, Ashby and Bowers observed the cyclisation of a radical probe incorporated into a Grignard reagent, which infers that an alkyl radical species was formed prior to addition to benzophenone.^[284c]



Scheme 5.5 Example of a homo-coupling side product (benzopinacol) obtained upon the reaction of a Grignard reagent (neopentylmagnesium chloride) with benzophenone.^[306]

The inhibition of our alkylation reaction by TEMPO, combined with the interception of a ^tBu radical in the formation of TEMPO-^tBu, initially implied that this reaction could follow a SET reaction pathway. To gain further insight into the reaction system, TEMPO was added to a hexane solution of ^tBu₂Zn, upon which the characteristic red-orange colour associated with the TEMPO radical disappeared. Cooling the resultant colourless solution to -30 °C afforded a crystalline solid after 24 hours. Unfortunately, severe disorder in the crystallographic structure made it impossible to refine the molecular structure satisfactorily; hence no structural data can be presented. However, NMR spectroscopic analysis of the crystalline material in C₆D₆ solution confirmed the presence of anionic TEMPO*, in addition to *tert*-butyl ligands, in a 1:1 ratio and so its formula therefore appears to be [(TEMPO*)Zn(^tBu)] (yield 0.08 g; 29%). Carmona has previously reported the structural characterisation of the related heteroleptic dimer, [(TEMPO*)Zn(Et)]₂.^[121] Present in the filtrate, TEMPO-^tBu was also produced from the reaction of ^tBu₂Zn with TEMPO, as evidenced through NMR spectroscopy.

Given the propensity of TEMPO to act as a Lewis base ligand towards a metal centre, it cannot be ruled out that TEMPO shuts down the alkylation reaction by sequestering Zn from the sodium zinc co-complex. Henceforth, sodium amide **22**,

${}^t\text{Bu}_2\text{Zn}$ and TEMPO were combined in a 1:1:1 stoichiometric ratio in hexane solvent and the reaction mixture was analysed by NMR spectroscopy, which revealed resonances corresponding to TEMPO- ${}^t\text{Bu}$.^[304] This suggests that TEMPO breaks up the synergic, sodium metalloligand/*tert*-butylzinc partnership by extracting a butyl radical from the zinc centre, which could be a factor in the reduced alkylation yields observed. For comparative purposes, the failure of the neutral heteroleptic zinc complex $[(\text{TEMPO}^*)\text{Zn}{}^t\text{Bu}]$ to *tert*-butylate benzophenone, at any position, was tested and confirmed. It is also possible that TEMPO sequesters the alkali metal from the metalloligand complex. Most TEMPO coordination chemistry has been studied with d block,^[121; 307] p block^[308] and f block elements,^[309] however more recently, structural studies of s block element-TEMPO structures have been forthcoming,^[301; 303] including the alkali metal complexes $(\text{THF})_2\cdot[\text{Li}(\text{TEMPO}^*)]_4$ and $[(\text{THF})\text{Na}(\text{TEMPO}^*)]_4$.^[301b] Within our work, it is therefore impossible to unequivocally state that the reaction follows a radical pathway. Although TEMPO- ${}^t\text{Bu}$ was detected in the reaction mixture, this could either be produced from the interception of a ${}^t\text{Bu}$ radical prior to its reaction with benzophenone, or generated as a side product from reaction of TEMPO with ${}^t\text{Bu}_2\text{Zn}$.

Although the reaction mechanism/s appear/s convoluted and is/are not yet well understood, it is clear that the choice of ligand has a considerable impact upon the reaction yield. For instance, highly coordinating ligands such as $\text{H}_6\text{-TREN}$ have an adverse effect upon the reaction yield, which could be an artefact of too much steric shielding of the Na centre. Changing the bulk solvent medium from non-polar hexane to Lewis donor THF, which displaces the donor ligands TMEDA, PMDETA, TMDAE and $\text{H}_6\text{-TREN}$ in the solution state, leads to a significant decrease in the alkylation yields. It is therefore likely that coordination of the donor ligand to Nadpa is a dominant factor in preserving the synergic reactivity of the attacked ${}^t\text{Bu}_2\text{Zn}$ moiety.

5.4 Concluding Remarks on Dipyridylamine Chemistry

To conclude, this study has uncovered a set of alkylzinc-based compounds with unprecedented structures by utilising a secondary amide equipped with two pyridyl appendages as a structural template-changing coligand. Unlike conventional alkylzinc reagents, which are generally wholly unreactive, these heteroleptic derivatives can directly alkylate (*t*-butylate) benzophenone in the challenging remote *para* position. Most intriguingly, sub-stoichiometric amounts of sodium amide [(TMEDA)Na(dpa)]₂ can activate ^tBu₂Zn towards this *t*-butylation apparently through the mediacy of zincate **19**, the structure of which masquerades as a neutral donor-acceptor complex.

Extending the scope of this reaction has established that not only is the nature of the donor ligand used within the [(donor)Na(dpa)] metalloligand pivotal to the success of the alkylation, but also its coordination to Nadpa in the solution state, as displacement of TMEDA by the bulk Lewis donor solvent THF when in vast excess markedly decreases the reaction yields. Of the three metals investigated, it is Na, sandwiched between Li and K within Group 1, which comprises the optimum steric and electronic properties to achieve regioselective *para* alkylation in good yields. This pattern in particular is intriguing.

5.5 Future Work

Having established the principle of using sub-stoichiometric sodium amides in the alkylation of benzophenone, the next challenge is to investigate the limits to which this system can be extended. To further develop this chemistry, alternative multifunctional organo-amide ligands could be investigated as structural template changing co-ligands within sodium zincate systems to probe the effect upon structure and reactivity (Figure 5.17).

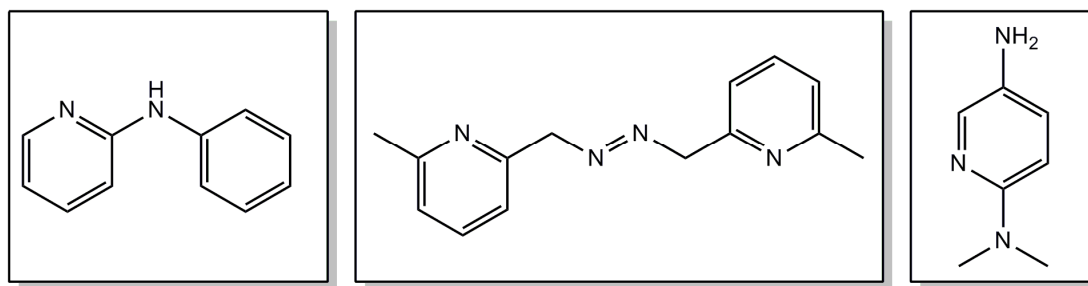


Figure 5.17 Structural representation of example multifunctional amines.

Different alkyl transfer reagents could be screened using the nucleophilic methodology outlined in this Chapter. For example, alternative zinc reagents such as Me_2Zn , Et_2Zn , ${}^i\text{Pr}_2\text{Zn}$ and Ph_2Zn , magnesium reagents including Me_2Mg and ${}^n\text{Bu}_2\text{Mg}$, and aluminium reagents such as Me_3Al , Et_3Al and ${}^n\text{Pr}_3\text{Al}$ should be investigated. Furthermore, the scope of substrates could be widened to include other conjugated ketones, for example fluorenone, benzoyl pyridine and chalcone (Figure 5.18). In addition, substrates containing other carbonyl functionalities, namely aldehydes and esters, would be prime for investigation. The ultimate goal of this chemistry is to achieve a widely applicable, atom efficient system, which can alkylate conjugated carbonyl substrates with high yields and selectivity, ideally with a catalytic sodium amide component that has a high turnover number and turnover frequency.

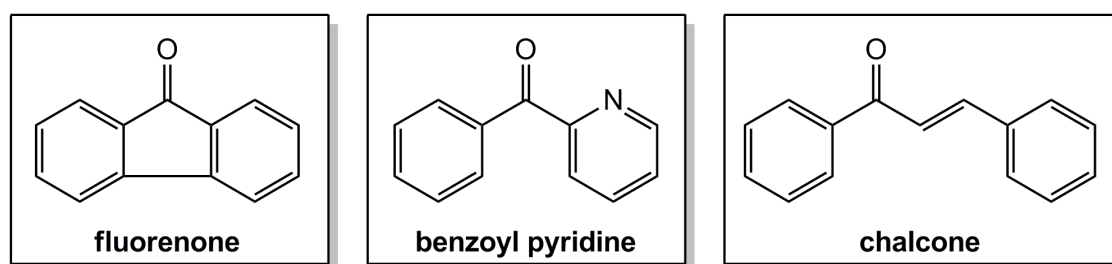


Figure 5.18 Structural representation of example aromatic ketone substrates.

5.6 Experimental

5.6.1 Synthesis of $\{[(\text{dpa})\text{Zn}(\text{tBu})]_2\}$, **18**

Dpa(H) (0.34 g, 2 mmol) was dissolved in a mixed hexane (10 mL)/toluene (20 mL) solvent system and was slowly added to a solution of freshly prepared tBu_2Zn (0.36 g, 2 mmol) in hexane (10 mL). The resultant pale yellow solution deposited a crop of colourless crystals after 18 hours [yield 0.41 g; based upon the dpa(H) stoichiometry, 70%].

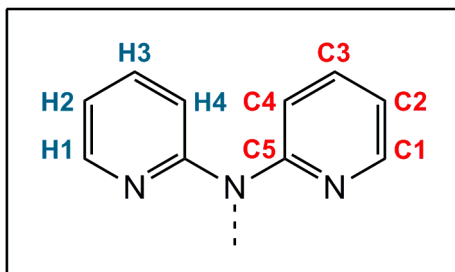


Figure 5.19 Labelling scheme for dpa.

^1H NMR (400.03 MHz, C_6D_6 , 300 K): δ = 7.77 and 7.72 (br. s, 2H, H1-dpa), 7.00 and 6.89 (br. s, 2H, H3-dpa), 6.72 (br. s., 4H, H4-dpa), 6.25 and 5.99 (br. s, 8H, H2-dpa), 1.80 and 1.23 ppm (br. s, 9H, tBu). $^{13}\text{C}\{\text{H}\}$ NMR (100.59 MHz, C_6D_6 , 300 K): δ = 163.1 (C5-dpa), 146.6 and 145.5 (C1-dpa), 139.3 (C3-dpa), 137.6 and 122.6 (C4-dpa), 113.9 (C2-dpa), 111.3 (C3-dpa), 35.4 and 33.6 ppm (tBu).

Due to the acute air sensitivity of **18**, satisfactory C, H, N analyses could not be obtained.

Crystal data for **18**: $\text{C}_{28}\text{H}_{34}\text{N}_6\text{Zn}_2$, M_r = 585.35, monoclinic, space group $\text{P}2_1/c$, a = 9.4833(3), b = 10.4377(4), c = 14.0888(5) Å, β = 105.844(4)°, V = 1341.58(8) Å³, Z = 2, μ = 1.816 mm⁻¹, 7483 reflections, 3451 unique, R_{int} 0.0284, final refinement to full-matrix least squares on F^2 gave R = 0.0413 (F , 2840 obs. data only) and R_w = 0.1039 (F^2 , all data), GOF = 1.065.

5.6.2 Synthesis of [(TMEDA)₂Na₂(μ-dpa)₂Zn(^tBu)₂], 19

TMP(H) (0.34 mL, 2 mmol) was transferred *via* syringe to a suspension of freshly prepared BuNa (0.16 g, 2 mmol) in hexane (10 mL). The colourless suspension was allowed to stir for 1 hour at ambient temperature. A solution of ^tBu₂Zn (0.36 g, 2 mmol) in hexane (10 mL) was added to the suspension *via* cannula, followed by 0.30 mL of TMEDA. Gentle heating produced a pale yellow solution, to which dpa(H) (0.34 g, 2 mmol) was added. This immediately produced a vivid orange solution. The reaction mixture was transferred to the refrigerator (4 °C) where a crop of orange crystals [yield 0.56 g; based upon the dpa(H) stoichiometry, 70%] were deposited after 18 hours.

¹H NMR (500.13 MHz, C₆D₆, 300 K): δ = 8.09 (br s, 4H, H1-dpa), 7.10-6.96 (br. m, 8H, H3-dpa and H4-dpa), 6.30 (br. m, 4H, H2-dpa), 1.74 (s, 24H, CH₃-TMEDA), 1.69 (s, 8H, CH₂-TMEDA) and 1.57 ppm (br. s, 18H, ^tBu). ¹³C{¹H} NMR (125.76 MHz, C₆D₆, 300 K): δ = 165.1 (C5-dpa), 148.9 (C3-dpa), 137.2 (C4-dpa), 113.5 (C1-dpa), 111.2 (C2-dpa), 56.9 (CH₂-TMEDA), 45.5 (CH₃-TMEDA), 35.8 (^tBu) and 20.7 ppm (quat. ^tBu).

Due to the acute air sensitivity of **19**, satisfactory C, H, N analyses could not be obtained.

Crystal data for **19**: C₄₀H₆₆N₁₀Na₂Zn, M_r = 798.38, monoclinic, space group P2₁/n, *a* = 11.5137(3), *b* = 21.6403(4), *c* = 18.3837(3) Å, β = 93.636(2)°, *V* = 4571.26(16) Å³, *Z* = 4, μ = 0.594 mm⁻¹, 23176 reflections, 10516 unique, *R*_{int} 0.0243, final refinement to full-matrix least squares on *F*² gave *R* = 0.0388 (*F*, 8121 obs. data only) and *R*_w = 0.0864 (*F*², all data), GOF = 1.032.

5.6.3 Synthesis of [{Na(THF)₆}⁺{Zn(^tBu)₂(dpa)Zn(^tBu)₂}⁻], 20

A solution of ^tBu₂Zn (0.36 g, 2 mmol) in hexane (10 mL) was added to a suspension of freshly prepared BuNa (0.16 g, 2 mmol) in hexane (10 mL) *via* cannula. Dpa(H) (0.34 g, 2 mmol) was added to the resultant solution, producing an orange suspension

that was allowed to stir for 20 minutes at ambient temperature. Upon addition of toluene (5 mL) and THF (1.5 mL) an orange solution was produced. Approximately half of the solvent was removed in vacuo and the solution was transferred to the refrigerator (4 °C). A crop of orange crystals (yield, 0.37 g; 19% out of a maximum of 50% based upon the ${}^t\text{Bu}_2\text{Zn}$ stoichiometry) was deposited after 18 hours. Labile THF is lost from the crystalline solid upon isolation, which is reflected in low integration values in NMR spectroscopic analyses.

Alternative rational synthesis: Dpa(H) (0.34 g, 2 mmol) was added to a freshly prepared suspension of BuNa (0.16 g, 2 mmol) in hexane (10 mL) and the reaction mixture was allowed to stir for 1 hour. A hexane (10 mL) solution of ${}^t\text{Bu}_2\text{Zn}$ (0.72 g, 4 mmol) was injected, followed by toluene (5 mL) and THF (1.5 mL), producing an orange solid (yield, 0.41 g; 42% out of a maximum of 100% based on the ${}^t\text{Bu}_2\text{Zn}$ stoichiometry).

${}^1\text{H}$ NMR (500.13 MHz, C_6D_6 , 300 K): δ = 7.92 (br. s, 2H, H1-dpa), 7.05 (br. s, 2H, H3-dpa), 6.92 (br. s, 2H, H4-dpa), 6.25 (br. s, 2H, H2-dpa), 3.51 (m, 16H, α -THF), 1.39 (m, 16H, β -THF) and 1.25 ppm (br. s, 36H, ${}^t\text{Bu}$). ${}^{13}\text{C}\{\text{H}\}$ NMR (125.76 MHz, C_6D_6 , 300 K): δ = 148.3 (C1-dpa), 137.7 (C3-dpa), 113.3 (C4-dpa), 111.7 (C2-dpa), 67.8 (α -THF), 32.8 (${}^t\text{Bu}$), 25.7 (β -THF) and 24.8 ppm (${}^t\text{Bu}$ quaternary).

Due to the acute air sensitivity of **20**, satisfactory C, H, N analyses could not be obtained.

Crystal data for **20**: $\text{C}_{50}\text{H}_{92}\text{N}_3\text{NaO}_6\text{Zn}_2$, $M_r = 985.00$, triclinic, space group P-1, $a = 10.0075(11)$, $b = 11.1283(9)$, $c = 13.3084(15)$ Å, $\alpha = 69.353(9)$, $\beta = 85.491(9)$, $\gamma = 84.723(8)^\circ$, $V = 1379.3(2)$ Å³, $Z = 1$, $\mu = 0.922$ mm⁻¹, 16565 reflections, 6820 unique, $R_{int} 0.0346$, final refinement to full-matrix least squares on F^2 gave $R = 0.0606$ (F , 5614 obs. data only) and $R_w = 0.1679$ (F^2 , all data), GOF = 1.037.

Compounds **20** and **21** are structurally closely related. Both contain a large number of disordered groups (butyl, THF and dipyridylamide) that required restraints and constraints to be applied to both bond lengths and displacement ellipsoids. Of particular relevance to the structural discussion is that the dipyridylamide ligands are disordered about the crystallographic centre of symmetry.

5.6.4 Synthesis of $[\{K(THF)_6\}^+\{Zn(tBu)_2(dpa)Zn(tBu)_2\}^-]$, **21**

Dpa(H) (0.34 g, 2 mmol) was added to a freshly prepared suspension of $K(CH_2SiMe_3)$ (0.25 g, 2 mmol) in hexane (10 mL). After 1 hour of stirring at ambient temperature, TMEDA (0.60 mL, 4 mmol) was added to this beige suspension. Approximately half of the solvent was removed in vacuo and THF (10 mL) was added to produce a yellow-orange solution. tBu_2Zn (0.36 g, 2 mmol) in hexane (10 mL) was introduced and the resultant orange solution was transferred to the freezer (at -30 °C), where a crop of orange crystals (yield 0.27 g; 14% out of a maximum of 50% based upon the tBu_2Zn stoichiometry) was deposited after 72 hours. Labile THF is lost from the crystalline solid upon isolation, which is reflected in low integration values in NMR spectroscopic analyses.

1H NMR (400.03 MHz, C_6D_6 , 300 K): δ = 8.04 (br. s, 2H, H1-dpa), 7.05 (br. t, 2H, H3-dpa), 6.76 (br. d, 2H, H4-dpa), 6.27 (br. t, 2H, H2-dpa), 3.45 (br. s, 15H, α -THF), 1.39 (m, 15H, β -THF) and 1.36 (br. s, 36H, tBu). $^{13}C\{H\}$ NMR (100.59 MHz, C_6D_6 , 300 K): δ = 148.1 (C1-dpa), 137.6 (C3-dpa), 115.1 (C4-dpa), 111.7 (C2-dpa), 67.8 (α -THF), 34.2 (tBu), 25.7 (β -THF) and 23.0 ppm (quat. tBu).

Due to the acute air sensitivity of **21**, satisfactory C, H, N analyses could not be obtained.

Crystal data for **21**: $C_{50}H_{92}KN_3O_6Zn_2$, $M_r = 1001.11$, triclinic, space group P-1, $a = 9.8787(6)$, $b = 11.2247(7)$, $c = 13.5206(7)$ Å, $\alpha = 72.296(5)$, $\beta = 83.032(5)$, $\gamma = 84.558(5)^\circ$, $V = 1415.02(14)$ Å³, $Z = 1$, $\mu = 0.965$ mm⁻¹, 15934 reflections, 7408 unique, $R_{int} 0.0309$, final refinement to full-matrix least squares on F^2 gave $R = 0.0642$ (F , 5590 obs. data only) and $R_w = 0.1874$ (F^2 , all data), GOF = 1.027.

5.6.5 Synthesis of $[(PMDETA)Na(dpa)]_2$, **22**

BuNa (0.08 g, 1 mmol) was suspended in hexane (15 ml). To this white suspension, dpa(H) (0.17 g, 1 mmol) was added and the resultant suspension was left to stir for 45 minutes. Subsequent addition of PMDETA (0.42 ml, 2 mmol) generated a pale grey

solution which, upon transferral to the refrigerator at -30 °C, deposited colourless crystalline material after 24 hours [yield 0.30 g; 82% yield based upon the dpa(H) stoichiometry].

^1H NMR (400.03 MHz, d_8 -THF, 300 K): δ = 7.91 [ddd, $^3\text{J}(\text{H,H})$ = 5.0 Hz, $^4\text{J}(\text{H,H})$ = 2.0 Hz, $^5\text{J}(\text{H,H})$ = 1.0 Hz, 2H, H1-dpa], 7.12 [ddd, $^3\text{J}(\text{H,H})$ = 8.4, 6.3 Hz, $^4\text{J}(\text{H,H})$ = 2.0 Hz, 2H, H3-dpa] and [ddd, $^3\text{J}(\text{H,H})$ = 8.4 Hz, $^4\text{J}(\text{H,H})$ = 1.5 Hz, $^5\text{J}(\text{H,H})$ = 1.0 Hz, 2H, H4-dpa], 6.19 [ddd, $^3\text{J}(\text{H,H})$ = 6.3, 5.0 Hz, $^4\text{J}(\text{H,H})$ = 1.5 Hz, 2H, H2-dpa], 2.42 and 2.31 [t, $^3\text{J}(\text{H,H})$ = 7.5 Hz, 4H, NCH_2 -PMDETA], 2.18 (s, 3H, NCH_3 -PMDETA) and 2.14 (s, 12H, $\text{N}(\text{CH}_3)_2$ -PMDETA). $^{13}\text{C}\{\text{H}\}$ NMR (100.59 MHz, C_6D_6 , 300 K): δ = 167.2 (C5-dpa), 149.1 (C1-dpa), 136.5 (C3-dpa), 112.5 (C4-dpa), 110.3 (C2-dpa), 58.9 and 57.4 (NCH_2 -PMDETA), 46.2 ($\text{N}(\text{CH}_3)_2$ -PMDETA) and 43.3 ppm (NCH_3 -PMDETA).

Due to time restrictions, satisfactory C, H, N analyses were not obtained for **22**.

Crystal data for **22**: $\text{C}_{38}\text{H}_{62}\text{N}_{12}\text{Na}_2$, M_r = 732.98, triclinic, space group P-1, a = 10.3495(13), b = 11.0583(11), c = 18.5966(18) Å, α = 101.113(8), β = 96.726(9), γ = 90.084(9)°, V = 2073.4(4) Å³, Z = 2, μ = 0.754 mm⁻¹, 17153 reflections, 17153 unique, R_{int} 0.0000, final refinement to full-matrix least squares on F^2 gave R = 0.1516 (F, 8270 obs. data only) and R_w = 0.4460 (F^2 , all data), GOF = 1.170.

After initial refinement, the program Rotax suggested the presence of twinning for **22**. A matrix corresponding to a 180° rotation about 1 0 0 was applied to give a new hklf5 formatted dataset. Refinement against this dataset improved the fit of the model. A batch scale factor for the ratio of the twin components refined to 0.1716(15).^[310]

5.6.6 Synthesis of [(TMDAE)Na(dpa)]₂, **23**

Dpa(H) (0.17 g, 1mmol) was introduced to a freshly prepared suspension of BuNa (0.08 g, 1mmol) in hexane (20ml) and the reaction mixture was stirred for 1 hour. TMDAE (0.38 ml, 2mmol) was subsequently added *via* syringe, which produced a

yellow solution. Cooling the resultant solution to -30 °C for 48 hours afforded a crop of colourless crystals [yield 0.13 g; 37% yield based upon the dpa(H) stoichiometry]. ^1H NMR (400.03 MHz, d_8 -THF, 300 K): δ = 7.99 [ddd, $^3\text{J}(\text{H},\text{H})$ = 5.0 Hz, $^4\text{J}(\text{H},\text{H})$ = 2.0 Hz, $^5\text{J}(\text{H},\text{H})$ = 1.0 Hz, 2H, H1-dpa], 7.30 [br. d, $^3\text{J}(\text{H},\text{H})$ = 8.4 Hz, 2H, H4-dpa] and 7.30 [ddd, $^3\text{J}(\text{H},\text{H})$ = 8.4, 6.8 Hz, $^4\text{J}(\text{H},\text{H})$ = 2.0 Hz, 2H, H3-dpa], 6.38 [ddd, $^3\text{J}(\text{H},\text{H})$ = 6.8, 5.0 Hz, $^4\text{J}(\text{H},\text{H})$ = 1.2 Hz, 2H, H2-dpa], 3.46 [t, $^3\text{J}(\text{H},\text{H})$ = 6.1 Hz, 4H, OCH_2 -TMDAE], 2.39 [t, $^3\text{J}(\text{H},\text{H})$ = 6.1 Hz, 4H, NCH_2 -TMDAE] and 2.17 ppm [s, 12H, $\text{N}(\text{CH}_3)_2$ -TMDAE]. $^{13}\text{C}\{\text{H}\}$ NMR (100.59 MHz, C_6D_6 , 300 K): δ = 163.2 (C5-dpa), 148.8 (C1-dpa), 136.9 (C3-dpa), 112.6 (C4-dpa), 112.3 (C2-dpa), 70.6 (OCH_2 -TMDAE), 59.9 (NCH_2 -TMDAE) and 46.3 ppm ($\text{N}(\text{CH}_3)_2$ -TMDAE).

Due to time restrictions, satisfactory C, H, N analyses were not obtained for **23**.

Crystal data for **23**: $\text{C}_{36}\text{H}_{56}\text{N}_{10}\text{Na}_2\text{O}_2$, M_r = 706.89, orthorhombic, space group P b c 21, a = 15.8743(8), b = 12.4146(7), c = 19.8597(11) Å, V = 3913.8(3) Å³, Z = 4, μ = 0.096 mm⁻¹, 36891 reflections, 9425 unique, R_{int} 0.0617, final refinement to full-matrix least squares on F^2 gave R = 0.0769 (F , 6569 obs. data only) and R_w = 0.2266 (F^2 , all data), GOF = 1.014.

5.6.7 Synthesis of [(H₆-TREN)Na(dpa)], **24**

To a freshly prepared suspension of BuNa (0.08 g, 1 mmol) in hexane (15ml), dpa(H) (0.17 g, 1 mmol) was added and the reaction mixture was allowed to stir for 1 hour. H₆-TREN (0.15 ml, 1 mmol) was added *via* syringe, followed by toluene (15ml) with gentle heating to produce a yellow-green solution. Gradual cooling to ambient temperature yielded colourless crystals [yield 0.31 g, 91% yield based upon the dpa(H) stoichiometry].

^1H NMR (400.03 MHz, d_8 -THF, 300 K): δ = 7.92 [ddd, $^3\text{J}(\text{H},\text{H})$ = 5.0 Hz, $^4\text{J}(\text{H},\text{H})$ = 1.8 Hz, $^5\text{J}(\text{H},\text{H})$ = 1.3 Hz, 2H, H1-dpa], 7.15 (br. m, 4H, H4-dpa and H3-dpa), 6.22 [ddd, $^3\text{J}(\text{H},\text{H})$ = 8.1, 5.0 Hz, $^4\text{J}(\text{H},\text{H})$ = 1.2 Hz, 2H, H2-dpa], 2.65 [t, $^3\text{J}(\text{H},\text{H})$ = 6.0 Hz, 6H, H_2NCH_2 -TREN], 2.40 [t, $^3\text{J}(\text{H},\text{H})$ = 6.0 Hz, 6H, NCH_2 -H₆-TREN] and 1.13 (br. s, 6H, NH_2 -H₆-TREN).

$^{13}\text{C}\{\text{H}\}$ NMR (100.59 MHz, C_6D_6 , 300 K): δ = 166.9 (C5-dpa), 148.9 (C1-dpa), 136.2 (C3-dpa), 112.8 (C4-dpa), 109.8 (C2-dpa), 59.1 ($\text{NCH}_2\text{-H}_6\text{-TREN}$) and 41.0 ppm ($\text{NCH}_2\text{-H}_6\text{-TREN}$).

Due to time restrictions, satisfactory C, H, N analyses were not obtained for **24**.

5.6.8 Benchmark Reactivity Studies: Nucleophilic Addition towards Benzophenone Method 5A - Work-Up Procedure

To the reaction mixture, deionised water (10 mL), 2 M HCl (20 mL) and diethyl ether (20 mL) were added. The organic layer was separated from the aqueous layer and the aqueous layer was washed with diethyl ether/hexane (3 x 20 mL). Magnesium sulfate was used to dry the combined organic layers. Solvent was removed in vacuo and the crude residue was spiked with 10 mol% hexamethylbenzene [0.0162 g, 0.1 mmol for 1 mmol scale (stoichiometric) reactions; 0.081 g, 0.5 mmol for 5 mmol scale (catalytic) reactions]. ^1H NMR spectroscopic analysis was performed in CDCl_3 solvent and the relative yields of 2- and 4-*tert*-butylbenzophenone, benzhydrol^[311] and diphenyl-*tert*-butylmethanol^[312] were determined by relative integration. Spectroscopic data show resonances that are in good agreement with the reference standard of commercially available samples of 2-*tert*-butylbenzophenone and 4-*tert*-butylbenzophenone.

5.6.9 Stoichiometric Reactions

A) Control Reaction

A standard solution of $^t\text{Bu}_2\text{Zn}$ (2 mL of a 0.5 M solution in hexane, 1 mmol) was transferred to a Schlenk flask under argon atmosphere. A further 6 mL of hexane was added, followed by benzophenone (0.18 g, 1 mmol). The reaction mixture was allowed to stir at ambient temperature for 18 hours prior to work-up as per Method 5A.

B) Donor Amines

A standard solution of $t\text{Bu}_2\text{Zn}$ (2 mL of a 0.5 M solution in hexane, 1 mmol) was introduced to a Schlenk flask under argon atmosphere, followed by 6 mL of hexane. Subsequently, a donor amine (either pyridine, 0.16 mL, 2 mmol or TMEDA, 0.15 mL, 1 mmol) was added. Upon addition of pyridine an orange solution was immediately produced. Benzophenone (0.18 g, 1 mmol) was then added and the reaction mixture was allowed to stir for 18 hours at ambient temperature, then was worked up according to Method 5A.

C) [(TMEDA)Na(μ -TMP)(μ - $t\text{Bu}$)Zn($t\text{Bu}$)], **1**

Crystalline sodium zincate **1** (0.46 g, 1 mmol) was dissolved in hexane (8 mL) to produce a pale yellow solution. Benzophenone (0.18 g, 1 mmol) was then added, producing a vivid colour change to emerald green. The reaction mixture was stirred at ambient temperature for 18 h, prior to work up as per Method 5A.

D) [(TMEDA) $_2$ Na $_2$ (μ -dpa) $_2$ Zn($t\text{Bu}$) $_2$], **19**

BuNa (0.16 g, 2 mmol) was suspended in hexane (6 mL) and dpa(H) (0.34 g, 2 mmol) was added. The resultant beige suspension was allowed to stir for 45 minutes at ambient temperature. To this, TMEDA was injected (0.30 mL, 2 mmol), followed by a hexane solution of $t\text{Bu}_2\text{Zn}$ (2 mL of a 0.5 M solution, 1 mmol). Benzophenone (0.18 g, 1 mmol) was subsequently added and the reaction was stirred at ambient temperature for 18 h, over which time a colour change from orange to green was observed. The reaction was worked up according to Method 5A.

E) [{Na(THF) $_6$ }] $^+$ {Zn($t\text{Bu}$) $_2$ (dpa)Zn($t\text{Bu}$) $_2$ } $^-$], **20**

Crystalline sodium zinczincate **20** (0.99 g, 1 mmol) was suspended in hexane (8 mL). To this, benzophenone (0.18 g, 1 mmol) was added and the reaction mixture was stirred for 18 hours at ambient temperature prior to work-up following the procedure outlined in Method 5A.

F) Variation of the Donor Ligand within [(donor)Na(dpa)]

BuNa (0.16 g, 2 mmol) was suspended in hexane (6 mL), dpa(H) (0.34 g, 2 mmol) was added and the reaction mixture was allowed to stir for 45 minutes at ambient temperature. To this, the donor ligand was injected [DMAP (0.24 g, 2 mmol); TEMPO (0.31 g, 2 mmol); TMEDA (0.30 mL, 2 mmol); PMDETA (0.42 mL, 2 mmol); TMDAE (0.38 mL, 2 mmol); H₆-TREN (0.30 mL, 2 mmol); or Me₆-TREN (0.52 mL, 2 mmol)]. A hexane solution of ^tBu₂Zn (2 mL of a 0.5 M solution, 1 mmol) was subsequently added, followed by benzophenone (0.18 g, 1 mmol) and the reaction was stirred for 18 h, either at ambient temperature or at 75 °C (see Table 5.5) prior to work up according to Method 5A.

G) Variation of the Alkali Metal (AM) within [(PMDETA)AM(dpa)]

Following the introduction of an organometallic reagent R'M [R'M = BuLi (1.25 mL, 1.6 M in hexanes solution, 2 mmol); BuNa (0.16 g, 2 mmol); or KR (0.25 g, 2 mmol) (where R is CH₂SiMe₃)] to hexane solvent (6 mL), dpa(H) (0.34 g, 2 mmol) was added *via* a solid addition tube. The resultant beige suspension was then stirred for 45 minutes at ambient temperature. To this, PMDETA was injected (0.42 mL, 2 mmol), followed by a hexane solution of ^tBu₂Zn (2 mL of a 0.5 M solution, 1 mmol). Benzophenone (0.18 g, 1 mmol) was subsequently added and the reaction was stirred for 18 hours at ambient temperature. The reaction was worked up following the procedure outlined in Method 5A.

H) Variation of the Solvent

BuNa (0.16 g, 2 mmol) was suspended in hexane (6 mL) and dpa(H) (0.34 g, 2 mmol) was added. The resultant beige suspension was allowed to stir for 45 minutes at ambient temperature, following which, all solvent was removed *in vacuo*. THF (6 mL), TMEDA (0.30 mL, 2 mmol), and ^tBu₂Zn (2 mL of a 0.5 M solution in THF, 1 mmol) were then added.^[a] Following the addition of benzophenone (0.18 g, 1 mmol), the reaction was allowed to stir at ambient temperature for 18 h, over which time a

colour change from orange to green was observed. The reaction was worked up as per Method 5A.

[a] When the reaction was performed in a mixed THF/hexane solvent system, hexane (4 mL), TMEDA (0.30 mL, 2 mmol), THF (2 mL) and ^tBu₂Zn (2 mL of a 0.5 M solution in THF, 1 mmol) were injected.

I) Variation of *tert*-butyl anion source: reaction with ^tBuLi or ^tBu₂Zn

Dpa(H) (0.34 g, 2 mmol) was added to a freshly prepared suspension of BuNa (0.16 g, 2 mmol) in hexane (6 mL). PMDETA (0.42 mL, 2 mmol) was subsequently introduced, followed by either ^tBu₂Zn (2 mL of a 0.5 M solution in hexane, 1 mmol), or ^tBuLi (1.18 mL of a 1.7 M solution in pentane, 2 mmol). Following the addition of benzophenone (0.18 g, 1 mmol), the reaction was stirred at ambient temperature for 18 hours prior to work up according to Method 5A.

J) Addition of TEMPO

BuNa (0.16 g, 2 mmol) was suspended in hexane (6 mL) and dpa(H) (0.34 g, 2 mmol) was added. PMDETA (0.42 mL, 2 mmol) was then injected, followed by ^tBu₂Zn (2 mL of a 0.5 M solution in hexane, 1 mmol). After the addition of benzophenone (0.18 g, 1 mmol) and TEMPO (0.31 g, 2 mmol), the reaction was allowed to stir at ambient temperature for 18 hours prior to work up following the procedure outlined in Method 5A. ¹H NMR spectroscopic resonances corresponding to TEMPO-^tBu were observed.^[304]

¹H NMR (400.03 MHz, CDCl₃, 300 K): δ = 1.48 (m, 4H, β-TEMPO), 1.30 (m, 2H, γ-TEMPO), 1.28 (s, 9H, ^tBu), 1.15 and 1.10 ppm (s, 6H, Me-TEMPO). ¹³C{¹H} NMR (100.60 MHz, CDCl₃, 300 K): δ = 77.3 (quat. ^tBu), 59.1 (α-TEMPO), 40.9 (β-TEMPO), 34.8 (Me-TEMPO), 29.7 (^tBu), 20.4 (Me-TEMPO) and 17.2 ppm (γ-TEMPO).

5.6.10 Sub-stoichiometric Reaction Conditions

Stoichiometric reactions A, C, D, E and F were repeated under sub-stoichiometric conditions. In hexane solvent (40 mL), ${}^t\text{Bu}_2\text{Zn}$ (0.90 g, 5 mmol) and the appropriate sodium reagent were combined [A, no sodium reagent; C, $\{(\text{TMEDA})\text{Na}(\text{TMP})\}$, 0.5 mmol; D, $\{(\text{TMEDA})\text{Na}(\text{dpa})_2\}$, 0.5 mmol; E, $\{\text{Na}(\text{THF})_6\}^+\{\text{Zn}({}^t\text{Bu})_2(\text{dpa})\text{Zn}({}^t\text{Bu})_2\}^-$, 0.5 mmol; F, $\{(\text{DMAP})\text{Na}(\text{dpa})\}$, 1.0 mmol, $\{(\text{PMDETA})\text{Na}(\text{dpa})\}$, 1.0 mmol, $\{(\text{TMDAE})\text{Na}(\text{dpa})\}$, 1.0 mmol]. Following the addition of benzophenone (0.90 g, 5 mmol), the reaction was allowed to stir at 75 °C for 18 hours prior to work up according to Method 5A.

5.6.11 Reaction of ${}^t\text{Bu}_2\text{Zn}$ and TEMPO

TEMPO (0.16 g, 1 mmol) was added to a hexane (5 mL) solution of ${}^t\text{Bu}_2\text{Zn}$ (0.18 g, 1 mmol), upon which the characteristic red-orange colour associated with TEMPO disappeared. After cooling the resultant colourless solution to -30 °C, a crystalline solid, $[(\text{TEMPO}^*)\text{Zn}({}^t\text{Bu})]$, was deposited after 24 hours (yield 0.08 g; 29%).

${}^1\text{H}$ NMR (500.13 MHz, C_6D_6 , 300 K): δ = 1.41 (s, 9H, ${}^t\text{Bu}$), 1.39 (m, 4H, β -TEMPO), 1.28 (m, 2H, γ -TEMPO) and 1.18 ppm (s, 12H, Me-TEMPO). ${}^{13}\text{C}\{\text{H}\}$ NMR (125.76 MHz, C_6D_6 , 300 K): δ = 40.4 (β -TEMPO), 34.0 (${}^t\text{Bu}$), 25.7 (Me-TEMPO) and 17.7 ppm (γ -TEMPO).

5.6.12 Reaction of 22, ${}^t\text{Bu}_2\text{Zn}$ and TEMPO

Dpa(H) (0.34 g, 2 mmol) was added to a freshly prepared suspension of BuNa (0.16 g, 2 mmol) in hexane (8 mL). Subsequently, PMDETA (0.42 mL, 2 mmol), ${}^t\text{Bu}_2\text{Zn}$ (2 mL of a 0.5 M solution in hexane, 1 mmol), and TEMPO (0.31 g, 2 mmol) were introduced to the reaction mixture. ${}^1\text{H}$ and ${}^{13}\text{C}\{\text{H}\}$ NMR spectroscopic data were consistent with those observed for $[(\text{TEMPO}^*)\text{Zn}({}^t\text{Bu})]$ (*vide supra*).

Chapter 6

Cooperative Bimetallics: Synthesis, Characterisation and Reactivity Studies of a New Sodium Zincate Derived from a Difunctional Amine

“Learn from yesterday, live for today, hope for tomorrow.
The important thing is to not stop questioning.”

Albert Einstein

German-born physicist

Nobel Prize for Physics, 1921

6.1 Summary

Attempting to create a cooperative bimetallic system with a key difference to existing systems, this part of the PhD project examines the incorporation of a difunctional organo-amide ligand into a sodium amidozincate reagent. Whilst sodium zincate chemistry primarily focuses on sterically demanding monofunctional amides such as TMP (2,2,6,6-tetramethylpiperidide), DA (diisopropylamine) and HMDS (1,1,1,3,3,3-hexamethyldisilazane), here we turned our attention to the donor appended amide BD [*N'*-benzyl-*N,N*-dimethylethylenediamide, $\text{PhCH}_2\text{NCH}_2\text{CH}_2\text{NMe}_2^-$], which facilitated the synthesis of a new sodium zincate. Through structural elucidation by X-ray crystallography, we reveal the influence of the tertiary amine donor arm of BD upon the molecular structure. In addition, the heteroleptic *tert*-butylzinc amide dimer derived from the precursor amine BD(H) is structurally characterised through an X-ray diffraction study, and its structure is shown to contain an unusual *trans*-5,4,5-fused ring system at its core. Preliminary reactivity studies appear promising, as the new difunctional-amido zincate base displays an intrinsic sodium-zinc cooperativity which enables metallation of the model aromatic substrates *N,N*-diisopropylbenzamide and anisole.

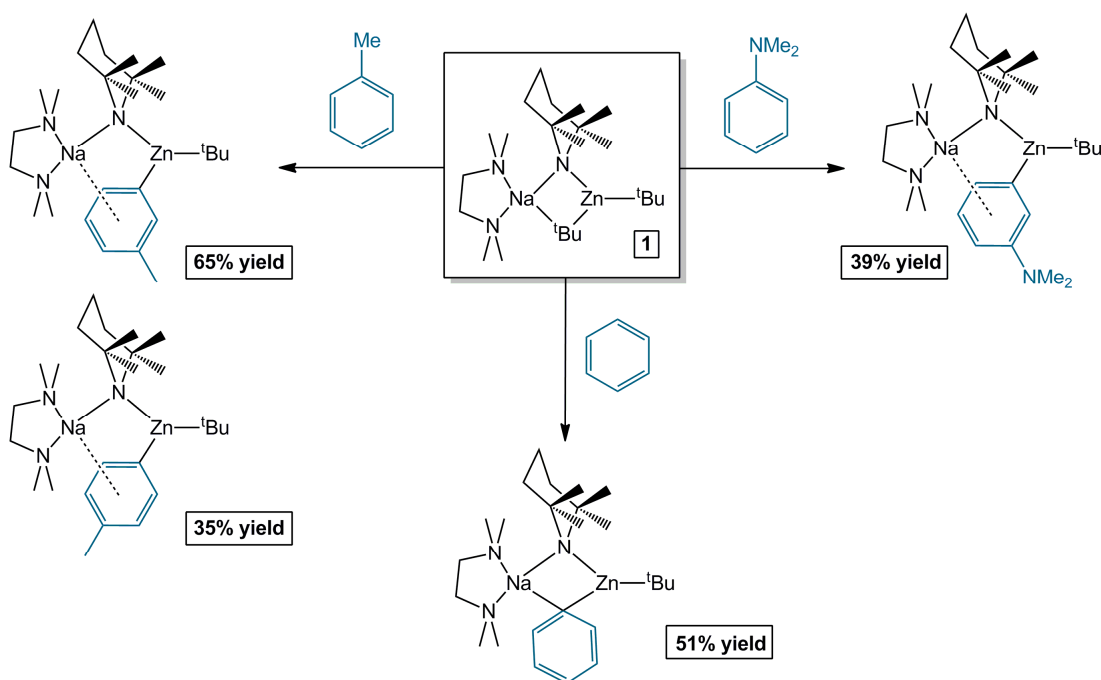
6.2 Introduction

6.2.1 It Takes Two: Advantages of Cooperative Bimetallic Bases

Bimetallic bases combining a hard, alkali metal with a softer metal Lewis acid (for example, most relevantly Zn, Mg, Al, Mn or Cd), within an organometallic framework, have been attracting increasing interest from synthetic chemists.^[72; 144; 149; 153; 201b; 202; 313] Germane to the results reported herein, the participation of a reactive alkali metal exports greater reactivity to zinc in executing deprotonation, whereupon *C-H* bonds inert to conventional neutral organozinc reagents

are converted to C-Zn bonds, opening a gateway to tandem functionalisation through cross-coupling methodologies (especially of the Negishi type). Concurrently, this transfer of reactivity appears to diminish the reactivity of the alkali metal. This usually circumvents the need for expensive sub-ambient temperature regimes, which are often required to avoid degradation reactions with sensitive functional groups when using conventional organoalkali metal reagents.^[314]

This cooperative reactivity between the alkali metal and the zinc or one of the other aforementioned softer metals has been termed “Alkali-Metal-Mediated Metallation” (AMMM), to reflect that the alkali metal is exporting its higher reactivity to the usually subordinate second metal *M*. This transfer of reactivity between metals is broad scoped as a range of bimetallic bases capable of executing low polarity direct metallation have been developed (including but not limited to Li/Zn, K/Mg, Li/Al, Li/Cd and Na/Mn pairings).^[72-73; 128; 149; 155; 202; 263b; 313a; 315] One of the most widely studied, most well defined examples in this ‘ate’ family is the sodium zincate [(TMEDA)Na(μ-TMP)(μ-^tBu)Zn(^tBu)], **1** (where the bulky secondary amide TMP is the kinetic engine behind its powerful Brønsted basicity).^[140a; 314] This synergically operative neutral heterometallic base offers decided advantages over both of its homometallic components (that is, NaTMP and ^tBu₂Zn). For example, it deprotonates benzene at ambient temperature, and can metallate toluene^[143a; 245] and *N,N*-dimethylaniline^[147; 316] in the challenging remote *meta*-position (Scheme 6.1). Significantly such reactivity and selectivity cannot be replicated by either NaTMP or ^tBu₂Zn acting in isolation with these aromatic substrates.



Scheme 6.1 A selection of zincation reactions executed by bimetallic zincate **1**.^[143a; 143c]

6.2.2 Introduction of a Donor Appended Amine to Sodium Zincate Chemistry

Our main objective within this study was to attempt to develop a sodium amidozincate base, but with an essential difference that made it novel in comparison to known reagents of this type. The reactivity enhancement that selected donor ligands (typified by TMEDA, *N,N,N',N'*-tetramethylethylenediamine) can often effect upon organolithium reagents has been long recognised.^[32a; 32d; 34-35; 317] Furthermore, it has recently been shown that amines with additional donor appendages can act as structural template changing ligands, leading to unconventional structures that can promote unexpected reactivities.^[293] Motivated by such precedents, we sought to incorporate *N-H* deprotonated difunctional *N'*-benzyl-*N,N*-dimethylethylenediamine [BD(H); PhCH₂N(H)CH₂CH₂NMe₂], a mixed secondary amine-tertiary amine hybrid (Figure 6.1), into a bimetallic sodium zincate

formulation. This donor-appended amine has the potential to simultaneously combine two roles of existing sodium bisalkyl-amidozincates, the most widely studied involving simple monofunctional amide ligands such as TMP (Figure 6.1). First, it provides an amido anion and second it provides a supporting tertiary amine donor. Compounds based upon the BD scaffold are found within skincare products^[318] and also have applications as antihistamine treatments for allergy relief.^[319] Although alkali metal^[320] and alkaline earth metal^[321] derivatives of this difunctional amine have been previously reported, prior to the work reported herein the zinc chemistry of this amine was very scant. To the best of our knowledge, hitherto no zinc derivative of BD(H) has ever been structurally characterised.^[178] However, of particular relevance to the work reported within this PhD study, BD has previously been incorporated into a bimetallic scaffold, within the homoleptic lithium magnesiate $[\text{Li}_2\text{Mg}(\text{BD})_4]$.^[322]

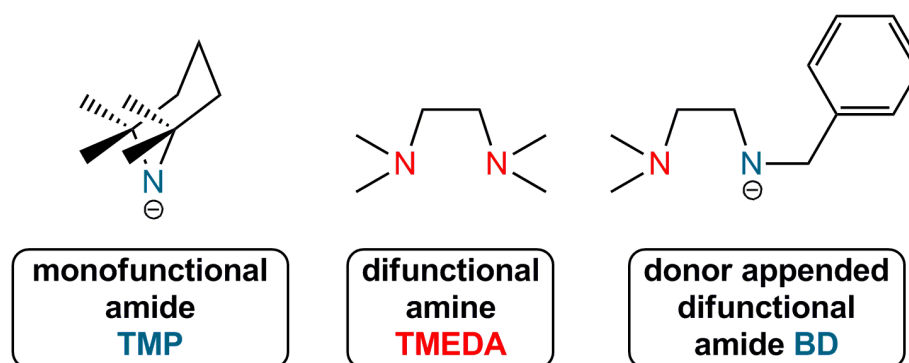


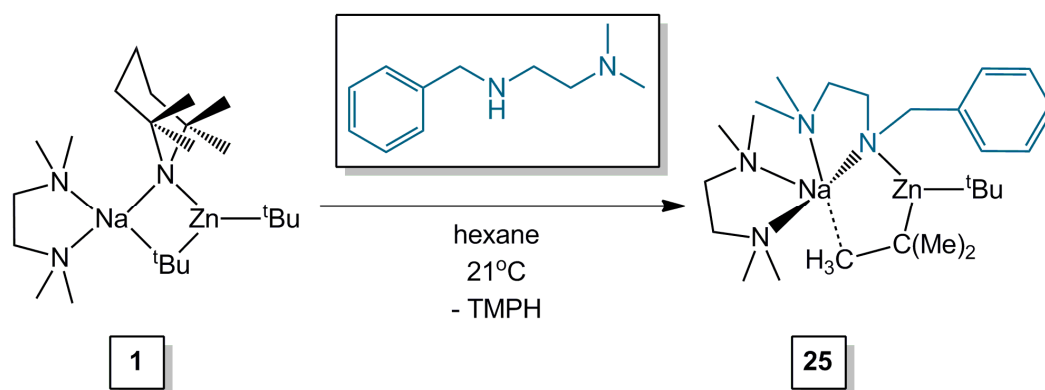
Figure 6.1 ChemDraw representations of the monofunctional amide TMP, donor ligand TMEDA and the difunctional amide BD.

Here in this part of the PhD project, we report the synthesis, isolation and characterisation of a new type of sodium amidozincate reagent, based on the difunctional amide BD. In addition, a homometallic alkylzinc amide dimer formed in the absence of TMEDA is described. Striving to explore the Brønsted base potential of the new difunctional-amidozincate, our initial investigations show promise towards the metallation of the test substrates *N,N*-diisopropylbenzamide and anisole.

6.3 Results and Discussion

6.3.1 Incorporation of a Donor Appended Amine into a Sodium Zincate Framework: Synthesis and Characterisation

Performed in hexane solution, the 1:1 stoichiometric reaction of sodium TMP-zincate **1** with the donor appended amine BD(H) instantaneously formed a bright pink solution (Scheme 6.2). Although the reaction was initially carried out at ambient temperature, cooling to 4 °C furnished a crop of crystalline [(TMEDA)Na(μ -BD)(μ -^tBu)Zn(^tBu)] (**25**) (yield 0.63g, 64%). Zincate **25** was characterised in solution using multinuclear (¹H and ¹³C{H}) NMR spectroscopy and its structure in the solid state was elucidated by X-ray crystallographic studies. From the formulation of **25** it is clear that overall a transamination reaction has occurred, with a difunctional BD unit replacing the monofunctional TMP bridge within a sodium zincate framework. This confirms that TMP is a stronger Brønsted base than its difunctional rival. NMR spectroscopic analysis of the filtrate following isolation of **25** revealed further resonances corresponding to **25**, in addition to noncoordinated TMP(H), so the absolute yield of **25** is higher than 64%.



Scheme 6.2 Formation of sodium amidozincate **25** through transamination.

Akin to the arrangement in **1**, the two metal centres of sodium zincate **25** (Figure 6.2) are connected through an amido bridge and an asymmetrical *tert*-butyl bridge, which involves a Zn-C_{quaternary} covalent bond [Zn1-C21, 2.0503(15) Å] and a significantly

weaker agostic $\text{Na}\cdots\text{C}_{\text{Me}}$ interaction [$\text{Na1}\cdots\text{C22}$, 3.0487(21) Å]. The bridging BD unit possesses a stereogenic centre (N1) as it bonds to four distinct atoms, namely Na1, Zn1, C10 and C17. This chirality is reflected by the spectroscopic inequivalence of the PhCH_2 and the BzNCH_2 resonances in the ^1H NMR spectrum (analysed in C_6D_6 solution, Spectrum 6.1). A two-dimensional ^1H - ^{13}C HSQC experiment confirmed the diastereotopicity of these hydrogen atoms, revealing that the two distinct PhCH_2 resonances (at 4.47 and 4.16 ppm) coordinate to one carbon centre, as do the two BzNCH_2 resonances (at 3.48 and 2.82 ppm).

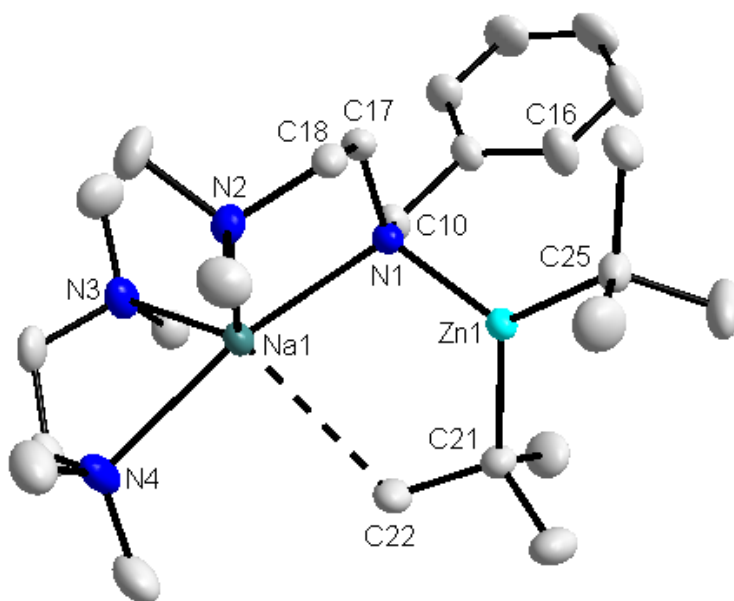


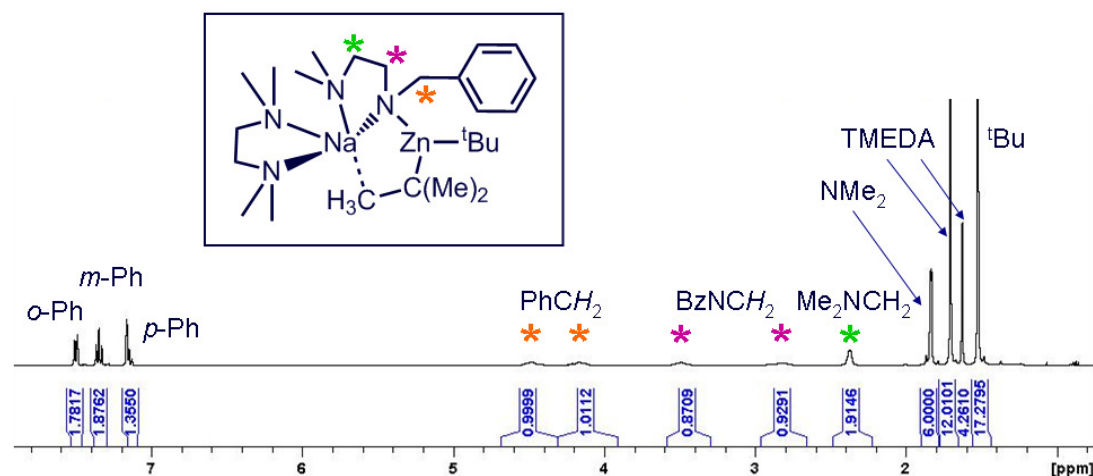
Figure 6.2 Molecular structure of **25** with thermal ellipsoids at 50% probability level and hydrogen atoms omitted for clarity. The dashed line represents a weak agostic interaction between Na1 and the methyl group of C22. Selected bond lengths (Å) and angles (°): Na1-N1, 2.4119(13); Na1-N2, 2.4771(14); Na1-N3, 2.5045(13); Na1-N4, 2.5398(15); Na1 \cdots C22, 3.0487(21); Zn1-N1, 2.0135(12); Zn1-C21, 2.0503(15); Zn1-C25, 2.0533(15); N1-Na1-N2, 76.96(4); N1-Na1-N3, 111.95(5); N1-Na1-N4, 169.55(5); N1-Na1-C22, 79.117(47); N2-Na1-N3, 115.11(5); N2-Na1-N4, 109.32(5); N2-Na1-C22, 126.130(51); N3-Na1-N4, 73.51(5); N3-Na1-C22, 118.516(50); N4-Na1-C22, 90.453(51); N1-Zn1-C21, 111.26(5); N1-Zn1-C25, 123.12(6); C21-Zn1-C25, 125.61(6); Na1-N1-Zn1, 103.91(5); Na1-N1-C10, 106.77(8); Na1-N1-C17, 100.54(9); Zn1-N1-C10, 115.10(9); Zn1-N1-C17, 118.58(9); C10-N1-C17, 109.94(11).

It may be expected that the tertiary amine arm of BD would stretch towards the stronger Lewis acid, to grasp the electropositive zinc centre through a dative interaction. Indeed, there is some precedent for lower-order, alkali metal zincate structures (defined by having a 1:1 alkali metal:zinc stoichiometry involving a monoanionic $[\text{ZnR}_3]^-$ moiety), where zinc adopts a distorted tetrahedral geometry.^[323] However, this is not the case within **25**, as the NMe_2 arm of BD instead reaches towards Na (closing a five-atom NaNCCN ring) whilst Zn maintains its distorted trigonal planar geometry. This preference to interact with Na probably has a steric origin as the zinc atom in **25** is surrounded by three bulky ligands.

The Na centre of **25** can be interpreted as being five-coordinate, in forming four Na-N bonds as well as an additional, agostic $\text{Na}\cdots\text{C}(\text{H}_3)$ interaction. In this regard, the five atoms surrounding Na1 (specifically N1, N2, N3, N4 and C22) form a distorted trigonal bipyramidal polyhedron. Whilst N1 and N4 occupy the axial positions [N1-Na1-N4 is $169.55(5)^\circ$], N2, N3 and C22 reside in the equatorial positions (where the sum of the angles is 359.8°).^[324]

Although the Na1-N1 and Zn1-N1 bond lengths within **25** are similar to those in **1**, [Na1-N1 is $2.4119(13)$ Å in **25** cf $2.412(6)$ Å in **1**; Zn1-N1 is $2.0135(12)$ Å in **25** cf $2.034(6)$ Å in **1**] the $\text{Na}\cdots\text{C}_{\text{Me}}$ separation length of **25** is significantly elongated [$3.0487(21)$ Å in **25** cf $2.75(1)$ Å in **1**], indicative of a very weak interaction. Despite observation of this weak interaction in the solid state, the two ^tBu groups are equivalent on the NMR timescale, as only one ^tBu singlet is present at 1.52 ppm in C_6D_6 solvent at 300 K. This suggests that in the solid state, **25** can be more accurately interpreted as having an open acyclic but curved NaNZnC motif rather than a 5-atom, 4-element (NaNZnCC) ring species, where the set trigonal planar geometry of Zn brings one ^tBu ligand into close proximity with Na, and thus the Na is best regarded as 4-coordinate, distorted tetrahedral (sum of bond angles 656.40° ; mean 109.4°). This weakening of the $\text{Na}\cdots\text{C}_{\text{Me}}$ interaction reflects both the electronic enhancement as well as the extra steric hindrance provided by the additional donor coordination at the Na centre. As a further consequence of the heightened steric strain, the TMEDA bite angle is narrowed from $76.4(2)^\circ$ in **1** to $73.51(5)^\circ$ in **25**.

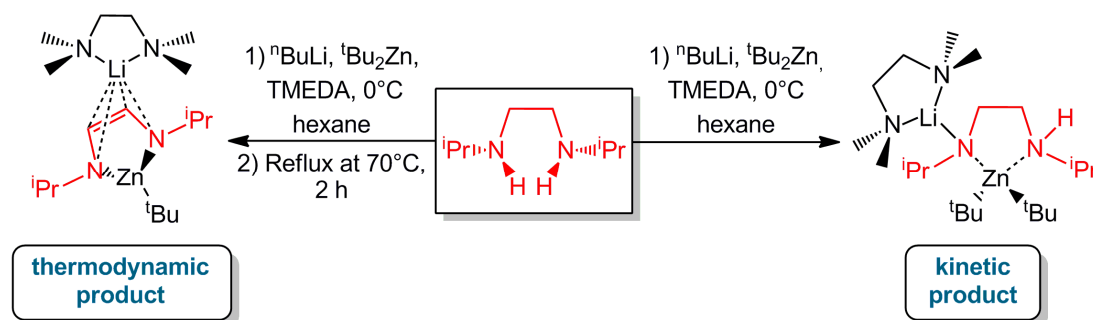
Comparison of the ^1H NMR resonances of **25** attributed to TMEDA with those of non-coordinated TMEDA revealed a significant upfield shift, where the respective NCH_3 and NCH_2 TMEDA resonances move from 2.12 and 2.36 ppm for free TMEDA, to 1.70 and 1.62 ppm in **25**. This suggests that despite the steric congestion at the Na centre, TMEDA remains coordinated in C_6D_6 solvent, mirroring the micro-coordinations observed in the solid state structure.



Spectrum 6.1 ^1H NMR (400.03 MHz, 300 K, C_6D_6) spectrum of **25**, highlighting the inequivalence of the PhCH_2 and the BzNCH_2 resonances. Inset shows the molecular structure of **25**.

Within this lower-order zincate **25**, Zn adopts a distorted trigonal planar coordination, where the sum of the bond angles is exactly 360.0° [N1-Zn1-C21 , $111.26(5)^\circ$; N1-Zn1-C25 , $123.12(6)^\circ$; C21-Zn1-C25 , $125.61(6)^\circ$]. Connected to Na mainly through an amido bridge, the tricoordinate geometry of Zn is complemented by a terminally bound ^tBu ligand [Zn1-C25 , $2.0533(15) \text{ \AA}$]. It seems likely that π -coordination of the face of the phenyl ring to either metal centre is blocked by the steric bulk and angular requirements of the ligand components, as the shortest metal $\cdots\text{C}_{\text{phenyl}}$ interaction ($\text{Zn1}\cdots\text{C16}$) is long at $3.3433(1) \text{ \AA}$. A search of the CCDB revealed that $\text{Zn}-\pi\text{C}$ interactions typically lie within the broad range between $1.8100(25)^{[325]}$, in $[\text{Zn}_3\{\text{OC}(\text{O})\text{Ph}\}_2(\text{hsalpn})_2]$ [where *hsalpn* is 1,3-bis(salicylideneamino)propan-2-ol] to $2.906(1) \text{ \AA}$, in the bis(2-methylallyl)zinc complex $[\text{Zn}\{\text{CH}_2\text{C}(\text{CH}_2)\text{CH}_3\}_2]_\infty$.^[326]

The most relevant literature comparison for **25** is possibly provided by the lithium zincate $[\text{}^t\text{Bu}_2\text{Zn}\cdot\{\text{}^i\text{PrN}(\text{Li}\cdot\text{TMEDA})\text{CH}_2\text{CH}_2\text{N}(\text{H})^i\text{Pr}\}]$ (Scheme 6.3).^[277; 327] Also a contacted ion pair, this lower order lithium zincate contains the symmetrical, difunctional *N,N'*-diisopropylethylenediamine, which, although closely related to BD(H), has a different set of terminal substituents that give rise to different steric and electronic properties. In spite of the similarity between the components of these two complexes, they differ structurally. A notable distinction is that within the lithium zincate, it is the more Lewis acidic Zn centre which is stabilised by dative bonding from the proton-carrying secondary amine. This could be attributed in part to the decrease in the van der Waal radius, from 2.27 Å for Na, to 1.82 Å for Li,^[18; 116] sterically blocking dative bonding to Li from occurring. Furthermore, the reduced steric constraints around zinc could make it more amenable towards four-coordination. Another structural disparity is that the central, 5-membered heteroatomic ring observed in **25** is absent.



Scheme 6.3 Kinetic (RHS) and thermodynamic (LHS) metallation of *N,N'*-diisopropylethylenediamine using a synergic lithium zincate base.

It is of interest to note that lithium zincate $[\text{}^t\text{Bu}_2\text{Zn}\cdot\{\text{}^i\text{PrN}(\text{Li}\cdot\text{TMEDA})\text{CH}_2\text{CH}_2\text{N}(\text{H})^i\text{Pr}\}]$ is the kinetic product of a reaction which, when provided with additional thermal energy, undergoes an intramolecular deprotonation, combined with loss of H_2 . Ultimately, a lithium/zinc stabilised diazaethene dianion is formed as the thermodynamic product (Scheme 6.3). The synthesis of **25** was repeated at 60°C , however ${}^1\text{H}$ NMR spectroscopic analysis showed no evidence of a similar oxidation of the ethylene backbone within the difunctional amine.

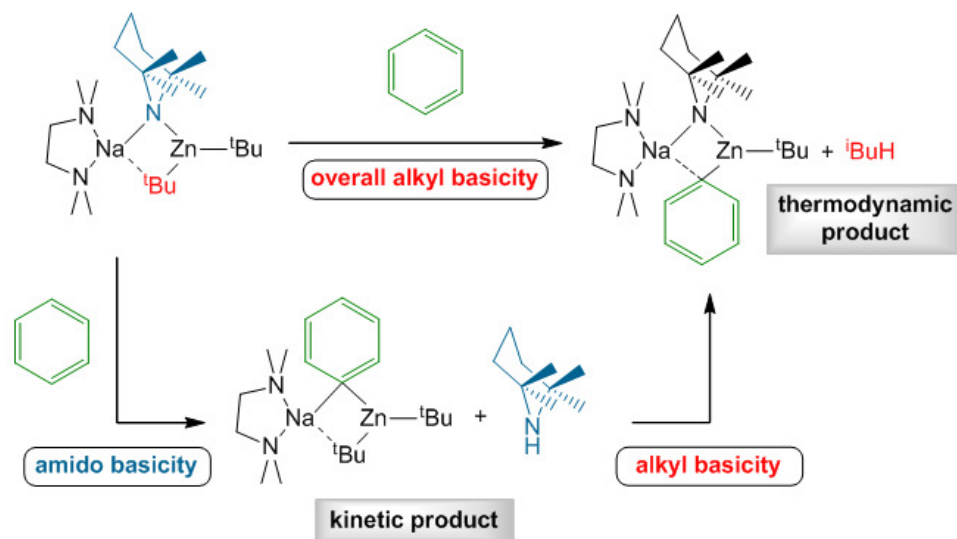
6.3.2 Mechanistic Insights: The Two-step Mechanism

With respect to the formation of **25**, heteroleptic bisalkyl-monoamidozincate **1** behaves as an amido base towards the diamine with concomitant protonation and elimination of TMP(H). This capacity to act as an amido base towards organic substrates is rarely witnessed,^[148] and deviates from the more commonly observed alkyl basicity.^[140a; 143a; 143c; 314] However, things are not always as straightforward as they seem.

To explain, a recent computational study investigating the modelled reaction of a simplified version of **1**, [(TMEDA)Na(μ -NMe₂)(μ -Me)Zn(Me)], with benzene, perceived that although **1** appears to act as an alkyl base, a step-wise mechanism is in fact in operation (Scheme 6.4).^[148] Firstly, the kinetically active amido ligand, TMP, instigates the initial deprotonation of an aromatic substrate. Secondly, TMP(H) re-enters the system as the irreversible thermodynamically driven protonation of the alkyl ligand occurs, to generate the thermodynamic sodium bisalkyl-monoamidozincate product and gaseous *iso*-butane.^[148] Furthermore, this computational study brought to light the reactivity enhancement role of the donor ligand TMEDA, which contributes towards the deprotonation capacity of the TMP ligand.

In view of these findings, experimental evidence supporting the two-step mechanism has since been published. Upon reaction of the related heteroleptic magnesiate base [(PMDETA)K(μ -TMP)(μ -CH₂SiMe₃)Mg(TMP)] with the well known aryl-alkyl ether anisole, the kinetic product arising from amide basicity, namely [(PMDETA)K(μ -TMP)(μ -C₆H₄-OMe)Mg(CH₂SiMe₃)], was yielded after 2 hours.^[328] In contrast, extension of the reaction time to 4 days yielded the thermodynamic product [(PMDETA)K(μ -TMP)(μ -C₆H₄-OMe)Mg(TMP)]. The identities of these crystalline, metallated derivatives of anisole were elucidated through X-ray diffraction studies and multinuclear NMR spectroscopy. Progress of this two-step reaction was then spectroscopically tracked through combining [(PMDETA)K(μ -TMP)(μ -CH₂SiMe₃)Mg(TMP)] with anisole in *d*₁₂-cyclohexane

solvent. After 1 hour, resonances diagnostic of the kinetic product [(PMDETA)K(μ -TMP)(μ -C₆H₄-OMe)Mg(CH₂SiMe₃)] and TMP(H) were observed. Once the reaction time reached 7 hours, resonances attributed to the thermodynamic product [(PMDETA)K(μ -TMP)(μ -C₆H₄-OMe)Mg(TMP)] began to arrive, in company with tetramethylsilane (Me₄Si).

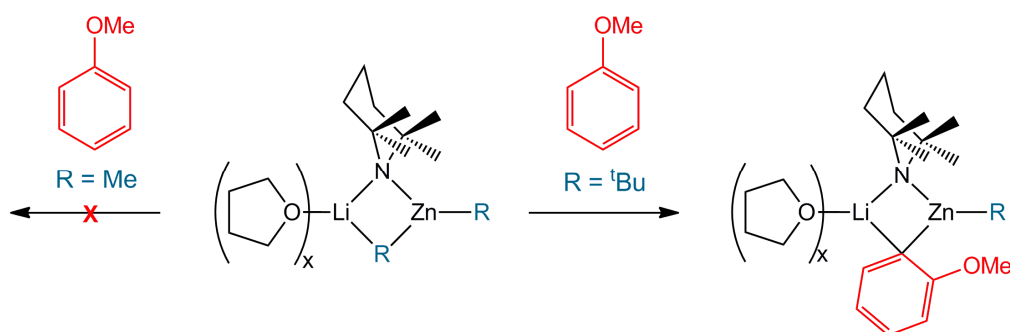


Scheme 6.4 Postulated two-step mechanism for the alkali-metal-mediated zincation of benzene.

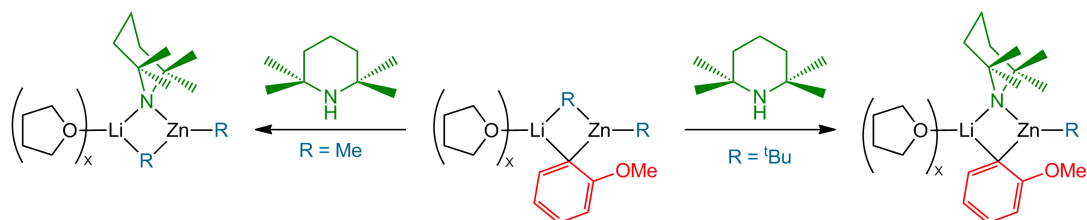
Bringing further clarity to the two-step mechanism, an insightful study probed the reaction of the lithium zincate [(THF)_xLi(μ -TMP)(μ -R)Zn(R)] with anisole (R = Me and R = *t*Bu).^[313a] When *tert*-butyl groups were employed as the alkyl ligands, [(THF)_xLi(μ -TMP)(μ -*t*Bu)Zn(*t*Bu)] appeared to act as an alkyl base and anisole was metallated in the *ortho*-position (Scheme 6.5). In contrast, when methyl ligands were present, no reaction was observed. However, it soon became apparent that the reaction system was far more complex than indicated by the initial results.

Hypothetical reaction intermediates were prepared based on the assumption that the reaction followed Uchiyama's two-step pathway and the kinetically active base TMP performed the initial deprotonation of anisole; namely [(THF)_xLi(μ -C₆H₄OMe)(μ -Me)Zn(Me)] and [(THF)_xLi(μ -C₆H₄OMe)(μ -*t*Bu)Zn(*t*Bu)]. Subsequently, the reaction

of the postulated intermediates with TMP(H) was monitored through ^1H and $^7\text{Li}\{\text{H}\}$ NMR studies. Surprisingly, $[(\text{THF})_x\text{Li}(\mu\text{-C}_6\text{H}_4\text{OMe})(\mu\text{-Me})\text{Zn}(\text{Me})]$ reacted to reform $[(\text{THF})_x\text{Li}(\mu\text{-TMP})(\mu\text{-Me})\text{Zn}(\text{Me})]$ and anisole. This informative result highlights that, whilst it may appear at first glance that no reaction has taken place, retro-reactions may in fact be occurring within the reaction system and the substrate metallated through a reversible process. In strict comparison, when introduced to $[(\text{THF})_x\text{Li}(\mu\text{-C}_6\text{H}_4\text{OMe})(\mu\text{-}^t\text{Bu})\text{Zn}(^t\text{Bu})]$, TMP(H) displaced an alkyl ligand in converting to the TMP anion, thus demonstrating the stronger basicity of *tert*-butyl groups in comparison with methyl groups.



Scheme 6.5 Overall reaction of lithium zincate $[(\text{THF})_x\text{Li}(\mu\text{-TMP})(\mu\text{-R})\text{Zn}(\text{R})]$ ($\text{R} = \text{Me}$, LHS; $\text{R} = ^t\text{Bu}$, RHS) with anisole.



Scheme 6.6 Reaction of postulated intermediates with TMP(H).

6.3.3 Transamination Reactions within Sodium Zincate Chemistry

Despite the scant few literature examples where **1** behaves as an amido base overall, the replacement of TMP by the amides of diisopropylamine (DA, N^iPr_2), chiral (*R*)-*N*-methylbenzylamine or hexamethyldisilazane (HMDS) have been described (Figure 6.3).^[275] Supplementary computational studies revealed that kinetic factors were

dominant in the production of three novel sodium bisalkyl-monoamidozincate complexes, namely the contact ion pair zincates [(TMEDA)NaZn(DA)(^tBu)₂], (*R,R*)-[(TMEDA)NaZn{N(CH₂Ph)(CH(CH₃)Ph)}(^tBu)₂] and the segregate (solvent separated ion pair ate complex)^[8] [{"(TMEDA)₂Na}⁺{Zn(HMDS)(^tBu)₂}⁻].^[275] Although theoretical studies predicted the thermodynamic preference for the deprotonation of the strongly acidic N-*H* of TMP by the *tert*-butyl unit to yield the corresponding sodium monoalkyl-bisamidozincate, this was not observed experimentally. In this regard, the two-step mechanism comes to a halt at the kinetic product.

It seems plausible that the bulk of the bridging amido ligands BD, DA, (*R*)-*N*-methylbenzylamine and HMDS prohibits sterically cumbersome TMP from re-entering the system and therefore blocks the second step of the two-step mechanism. Nonetheless, the major factor may be the higher acidity of these amines in comparison to TMP(H).^[275] Although the situation is more complicated for bimetallic systems, within simple monometallic systems, LiTMP is more basic than related lithium amides, as evidenced by the higher p*K*_a value of its conjugate acid (37.9) in comparison to those of LiDA (34.4) and LiHMDS (23.1).^[329] In the case of BD, the extra stability associated with the supporting tertiary amine arm and the chelate effect^[330] may also be a contributory factor in preventing the thermodynamically driven deprotonation of TMP(H).

6.3.4 Sodium Amidozincates and their Disproportionation Tendency

A search of the CCDB disclosed there are only eight examples of lower order sodium amidozincate complexes based upon ^tBu₂Zn or a fragment of ^tBu₂Zn (Figure 6.3).^[331] From this limited series, patterns have begun to emerge, revealing how the steric and electronic properties of the amido ligand influence the structure of the zincate. As structure and reactivity are intrinsically linked, improvement of our understanding of the structural influence of the amido ligand could aid the development of a cost efficient, reactivity tuned, sodium amidozincate base.

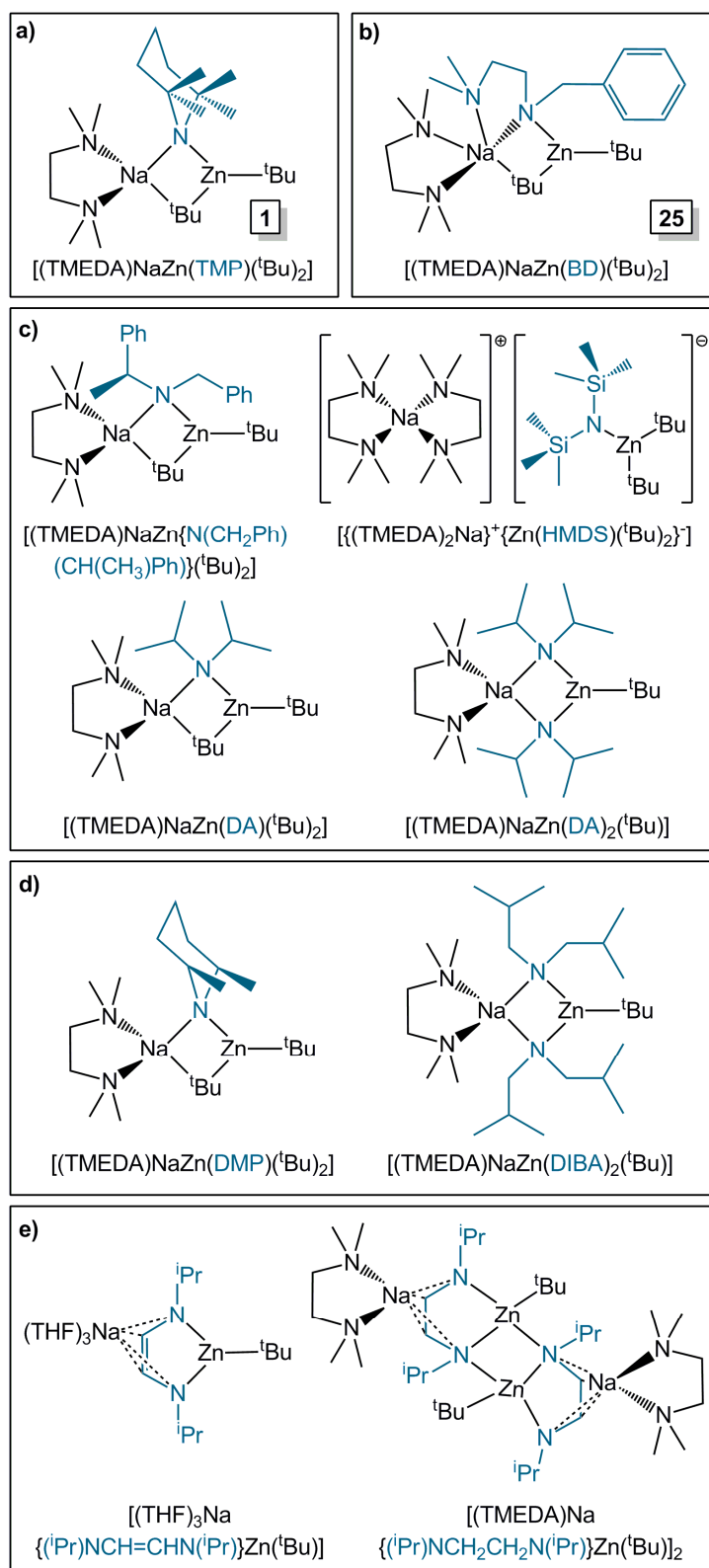


Figure 6.3 ChemDraw representation of the molecular structures of sodium amidozinc complexes a) ^[140a] b) this work c) ^[275] d) ^[332] and e) ^[327].

From the comparison of bond lengths presented in Table 6.1, it appears that the steric bulk of the amido component influences the molecular structure of the sodium zincate. For example, monoamidozincate **1** contains the sterically imposing amide TMP. Reflecting the steric bulk of TMP, the Na-N_{TMP} bond length is 2.412(6) Å, which lies towards the longest of such bond lengths in known sodium amidozincate structures (summarised in Table 6.1). Accordingly, no disproportionation of **1** is observed, where in this context, disproportionation refers to a redistribution of ligands around the zinc centre, but with no redox reaction taking place (Scheme 6.7).

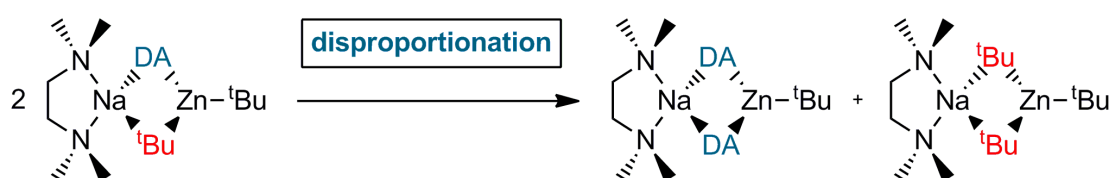
Table 6.1: Comparative bond length data for crystallographically characterised sodium amidozincate complexes.

Sodium Zincate	Na-N _{amide} bond length (Å)	Zn-N _{amide} bond length (Å)	Disproportionation observed?
[(TMEDA)NaZn(DIBA) ₂ (^t Bu)] ^[332]	2.4460(15)/ 2.4444(14)	2.0281(14)/ 1.9830(14)	No ^[a]
[(TMEDA)NaZn(TMP)(^t Bu) ₂], 1 ^[140a]	2.412(6)	2.034(6)	No
[(TMEDA)NaZn(BD)(^t Bu) ₂], 25	2.4119(13)	2.0135(12)	No
[(TMEDA)NaZn {N(CH ₂ Ph)(CH(CH ₃)Ph)}(^t Bu) ₂] ^[275]	2.374(4)	2.068(3)	No
[(TMEDA)NaZn(TMP)(CH ₂ SiMe ₃) ₂] ^[152]	2.359(3)	2.029(2)	No
[(TMEDA)NaZn(DA)(^t Bu) ₂] ^[275]	2.345(2)	2.050(2)	Yes ^[b]
[(TMEDA)NaZn(DMP)(^t Bu) ₂] ^[332]	2.342(5)	2.039(5)	Yes ^[c]
[{(TMEDA) ₂ Na} ⁺ {Zn(HMDS)(^t Bu) ₂ } ⁻] ^[275]	N/A ^[d]	2.0284(17)	No

a) This compound is itself a disproportionation product from [(TMEDA)NaZn(DIBA)(^tBu)₂]. [(TMEDA)NaZn(DIBA)(^tBu)₂] has not been structurally characterised, prohibiting a discussion of the relevant bond lengths; b) Disproportionation products [(TMEDA)NaZn(DA)₂(^tBu)] and [(TMEDA)NaZn(^tBu)₃] were observed; c) Disproportionation products [(TMEDA)NaZn(DMP)₂(^tBu)] and [(TMEDA)NaZn(^tBu)₃] were observed; d) [{(TMEDA)₂Na}⁺{Zn(HMDS)(^tBu)₂}⁻] exists as a segregated ion pair in the solid state.

In contrast, disproportionation was noted for the less sterically encumbered amides DMP (where DMP is *cis*-2,6-dimethylpiperidide) and DA, which bear the shorter Na-N_{amide} bond lengths of 2.342(5) and 2.345(2) Å respectively. Therefore, monoamidozincates [(TMEDA)NaZn(DMP)(^tBu)₂] and [(TMEDA)NaZn(DA)(^tBu)₂], disproportionated to give the bisamidozincate species [(TMEDA)NaZn(DMP)₂(^tBu)] and [(TMEDA)NaZn(DA)₂(^tBu)₂], in addition to the trisalkylzincate [(^tBu)₃Zn].

It can therefore be tentatively proposed that disproportionation is dependent on the steric bulk of the amido unit, and that as steric bulk decreases in the sequence TMP > DMP > DA > DIBA (where DIBA is diisobutylamide), the tendency to engage in disproportionation increases.^[275; 332] That BD has a significant steric profile is reflected by the relatively long Na-N_{amide} bond length within **25** [where Na-N_{amide} is 2.4119(13) Å], which lies close to the corresponding Na-N_{amide} bond length of **1** [2.412(6) Å]. Falling in line with this trend, disproportionation of **25** is not observed under the conditions studied. It is noteworthy that the Zn-N_{amide} bond lengths do not conform to this trend, suggesting that the Na-N_{amide} bond lengths are more significant markers in predicting which complexes will undergo disproportionation (Table 6.1).

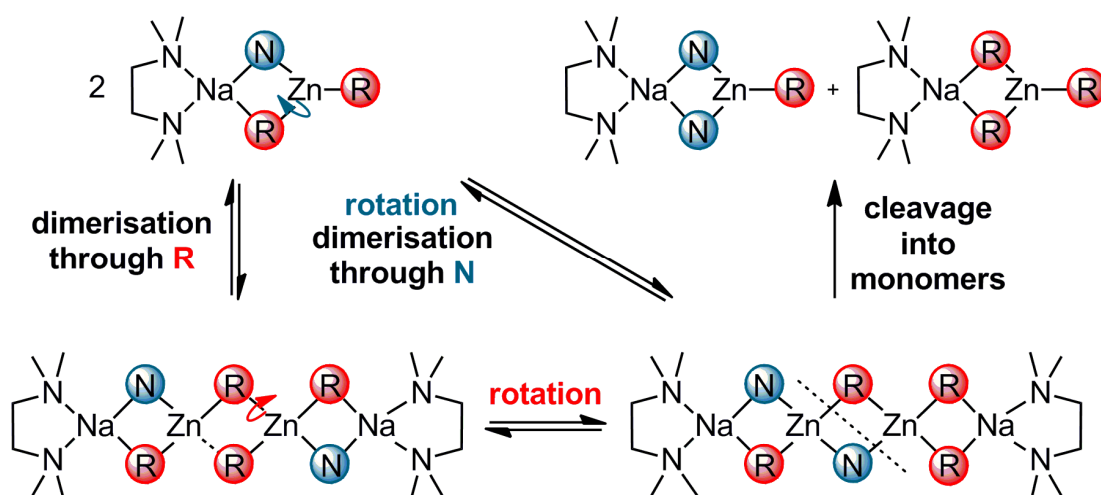


Scheme 6.7 Disproportionation of sodium diisopropylamidozincate [(TMEDA)NaZn(DA)(^tBu)₂] to bisamidozincate [(TMEDA)NaZn(DA)₂(^tBu)] and trisalkylzincate [(TMEDA)NaZn(^tBu)₃].

The basicity of the amide unit is also a potential factor in the likelihood of disproportionation for sodium amidozincates. As a result of its lesser acidity (*vide supra*), hence more powerful Brønsted basicity, TMP forms strong M-N_{TMP} bonds (where M is Na and/or Zn). In contrast the weaker, hence more labile M-N_{DA} bonds formed with the less basic DA unit could facilitate disproportionation.

Considering the strongly carbophilic nature of zinc, it seems unlikely that cleavage of a terminal Zn-^tBu bond is involved in the disproportionation mechanism, especially when the ^tBu unit is further stabilised through a long range agostic interaction with sodium. As reduced steric bulk appears to be a significant factor in promoting disproportionation, logic dictates that aggregation (dimerisation) may be operative in the mechanism. Through bringing two zinc centres into close proximity with each

other, dimerisation can facilitate the formation of a higher order dizincate species, as illustrated in Scheme 6.8. Although Scheme 6.8 depicts a contacted ion pair structure, it is also possible that the mechanism proceeds through a solvent separated segregated intermediate,^[8] with two [(TMEDA)Na]⁺ cations balancing the charge of a central [ZnN₂R₄]²⁻ dianionic core. “Opening” of this loosely coordinated dimer may then enable rotation about one of the Zn-R bonds, with the reformation of a dimeric species upon subsequent “closing”. Ensuing cleavage into two monomers could then generate a homoleptic sodium trisalkylzincate, alongside a sodium bisamido-monoalkylzincate species. It seems likely that the reverse reaction would be disfavoured, with the steric bulk and strong Zn-C bonds within the [(TMEDA)NaZn(^tBu)₃] product preventing dimerisation.



Scheme 6.8 Postulated mechanism for the disproportionation of sodium amidozincates.

6.3.5 In the Absence of TMEDA: Synthesis and Characterisation of a Neutral Alkylzinc Amide

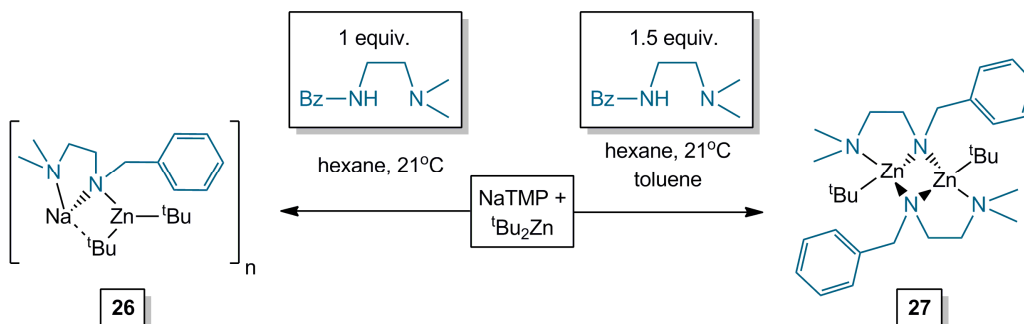
For comparative purposes, the corresponding reaction of “NaZn(TMP)(^tBu)₂” with BD(H) was performed in the absence of TMEDA. Upon the introduction of BD(H) into a 1:1 combination of NaTMP and ^tBu₂Zn in a hexane medium, a vibrant pink

suspension was formed immediately at ambient temperature. NMR spectroscopic analysis of the solid product suggested evidence of a transamination reaction, as resonances corresponding to TMP were absent from the ^1H and $^{13}\text{C}\{\text{H}\}$ NMR spectra. Furthermore, resonances attributed to BD and ^tBu were observed in a 1:2 ratio, suggesting that the product bears the general empirical formula “ $\text{NaZn}(\text{BD})(^t\text{Bu})_2$ ” (**26**, yield 0.45g, 66%). Altering the order of reagent addition, through firstly combining $^t\text{Bu}_2\text{Zn}$ with BD, followed by the introduction of NaTMP, did not change the reaction outcome as determined by ^1H NMR spectroscopy. As aforementioned it is worthy of note that a donor free, higher order lithium magnesiate species based upon difunctional BD has previously been reported in $[\text{Li}_2\text{Mg}(\text{BD})_4]$, where the central, dianionic $[\text{Mg}(\text{BD})_4]^{2-}$ core is balanced by two terminal Li cations.^[322] Each BD N(amido) unit bridges between Li and Mg, with dative bonding from the donor appended NMe_2 arm stabilising a tetracoordinate Li centre.

Running a second reaction combining this time NaTMP, $^t\text{Bu}_2\text{Zn}$ and BD(H), in an alternative 2:2:3 stoichiometry in hexane solution, with the addition of toluene for solubility purposes, deposited crystalline material upon cooling the bright pink solution to 4 °C (Scheme 6.9). X-ray crystallographic studies revealed this colourless product to be the dimeric alkylzinc amide, $[\{(\text{BD})\text{Zn}(^t\text{Bu})\}_2]$ (**27**, yield 0.17 g, 14% out of a maximum of 50% based upon the Zn stoichiometry). To balance the reaction stoichiometry, there must be another (sodium rich) product present in the reaction and accordingly, NMR spectroscopic analysis of the filtrate showed additional BD signals.

For completeness, the rational synthesis of **27** was attempted through the reaction of $^t\text{Bu}_2\text{Zn}$ with BD(H), in a 1:1 stoichiometry. NMR spectroscopic analysis of the resultant pale yellow solution revealed that the reaction afforded a coordination complex, with no deprotonation of the diamine N-H acidic bond. Diagnostic of BD(H) is a resonance at 1.76 ppm in the ^1H NMR spectrum, indicative of a NH group. This resonance disappears when the amine is metallated. However, after 1 month a crop of colourless crystals was deposited from the reaction solution, the

molecular structure of which was identified as **27** through X-ray crystallography and NMR spectroscopy. This suggests that whilst the deprotonation of BD(H) by ${}^t\text{Bu}_2\text{Zn}$ proceeds extremely slowly, there is a dramatic increase in the reaction rate driven by the cooperative combination of Na and Zn.



Scheme 6.9 Synthesis of proposed sodium zincate **26** (LHS) and the heteroleptic alkylzinc amide dimer **27** (RHS).

The crystal structure of the neutral alkylzinc amide **27** contains two independent molecules within its unit cell. However, as these are essentially identical, with only minor differences in bond parameters, for brevity only one molecule shall be discussed. This neutral zinc dimer (Figure 6.4), which has no crystallographically imposed symmetry, exhibits a *trans*-5,4,5-fused ring system at its core (Figure 6.4b). Therefore, **27** bears a strong resemblance to the closely related Mg dimer $[\{(\text{BD})\text{Mg}({}^t\text{Bu})\}_2]$,^[321] along with the solvated Mg dimers derived from the dianions of *N,N'*-diphenylethylenediamine and *N,N'*-dibenzylethylenediamine (Figure 6.5), namely $[\{\text{MgN}(\text{Ph})\text{CH}_2\text{CH}_2\text{N}(\text{Ph})\cdot 2\text{THF}(1.5\text{THF})\}_2]$ and $[\{\text{MgN}(\text{CH}_2\text{Ph})\text{CH}_2\text{CH}_2\text{N}(\text{CH}_2\text{Ph})\cdot \text{HMPA}\}_2]$.^[333] Each of these three Mg dimers also possess a *trans*-5,4,5-fused ring core. The central, four-membered $[\text{ZnN}]_2$ ring of **27** is almost a perfect square, with alternate Zn and N corners, displaying practically orthogonal N-Zn-N $[90.00(7)^\circ$ and $90.16(7)^\circ]$ and Zn-N-Zn endocyclic bond angles $[89.80(7)^\circ$ and $89.89(7)^\circ]$, which sum to 359.9° . All four Zn-N bond lengths are virtually equal, spanning the narrow range from 2.0877(16) to 2.0950(19) Å. Consequently, the transannular Zn1...Zn3 distance $[2.9548(3) \text{ \AA}]$ is almost identical to the corresponding N3...N5 distance $[2.9608(29) \text{ \AA}]$.

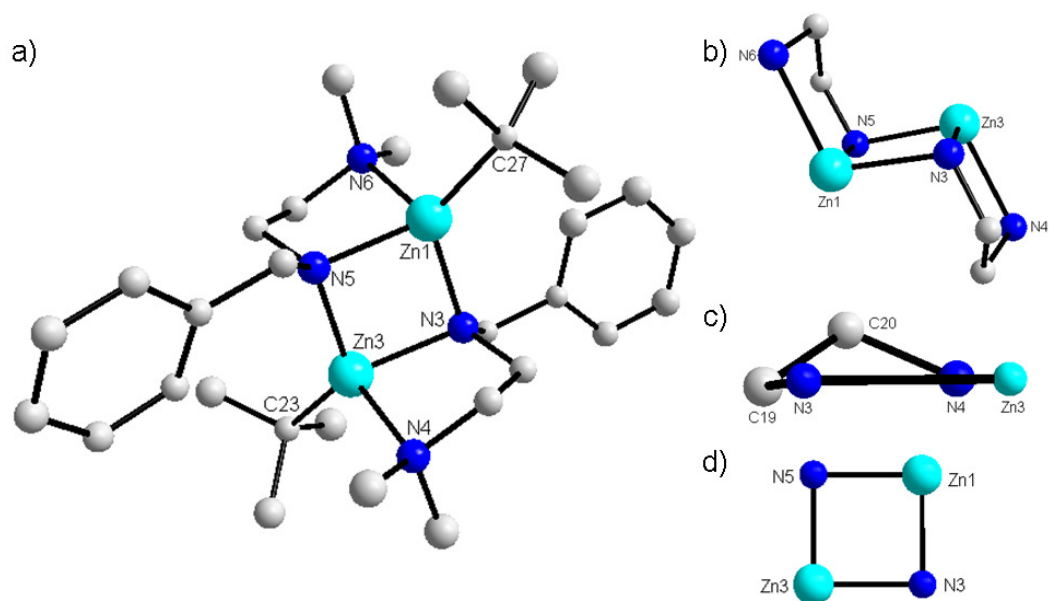


Figure 6.4 a) Molecular structure of **27** with thermal ellipsoids at 50% probability level, with hydrogen atoms and the second independent molecule omitted for clarity. Selected bond lengths (Å) and bond angles (°): Zn1-N3, 2.0922(16); Zn1-N5, 2.0950(19); Zn1-N6, 2.2339(18); Zn1-C27, 2.046(2); Zn3-N3, 2.094(2); Zn3-N4, 2.2284(18); Zn3-N5, 2.0877(16); Zn3-C23, 2.045(2); Zn1-N3-Zn3, 89.80(7); Zn1-N5-Zn3, 89.89(7); N3-Zn1-N5, 90.00(7); N3-Zn1-N6, 108.15(7); N3-Zn1-C27, 125.53(8); N5-Zn1-N6, 83.65(7); N5-Zn1-C27, 127.00(8); N6-Zn1-C27, 113.74(8); N3-Zn3-N4, 84.10(7); N3-Zn3-N5, 90.16(7); N3-Zn3-C23, 127.20(8); N4-Zn3-N5, 105.88(7); N4-Zn3-C23, 116.34(9); N5-Zn3-C23, 124.33(8); b) fragment of **27** highlighting the *trans*-5,4,5-fused ring system conformation; c) side-view of five-membered ring highlighting the apical C20 atom; d) central four-membered [ZnN]₂ ring, highlighting its near square geometry.

Extending from opposite sides of this central square are two five-membered ZnNCCN chelate rings. Owing to the constraints of this connected ring system, each Zn centre is held within a highly distorted tetrahedral geometry.^[334] Both five-membered rings have an envelope type appearance, with an apical C atom positioned *endo* to the [ZnN]₂ ring plane (Figure 6.4c), with dihedral angles (between the ZnNCCN plane and the NCC plane) of 49.7(1)° and 47.3(2)°. Adopting a pseudo-chair

conformation (Figure 6.4b), the dihedral angles between the central $[\text{ZnN}]_2$ ring plane and the ZnNCN ring plane (the apical C atoms were omitted) are $72.59(6)^\circ$ and $72.32(6)^\circ$.

Alkylzinc amides are well represented in the literature and typically possess a dimeric ring motif.^[335] However, examples that bear a structural resemblance to **27**, with a four-coordinate Zn centre and a tandem organozinc ring system (that is, a series of adjoining organometallic rings which contain a Zn centre) are less familiar. The best zinc based comparison for **27** is possibly the alkylzinc amidinate dimer $[\{^t\text{BuC}(\text{N}^i\text{Pr})_2\}\text{ZnMe}]_2$ (Figure 6.5).^[336] Both complexes have dimeric molecular structures that involve a connected organozinc ring system, however in the case of the amidinate, it is two four-membered rings which ensconce a central $[\text{ZnN}]_2$ core.

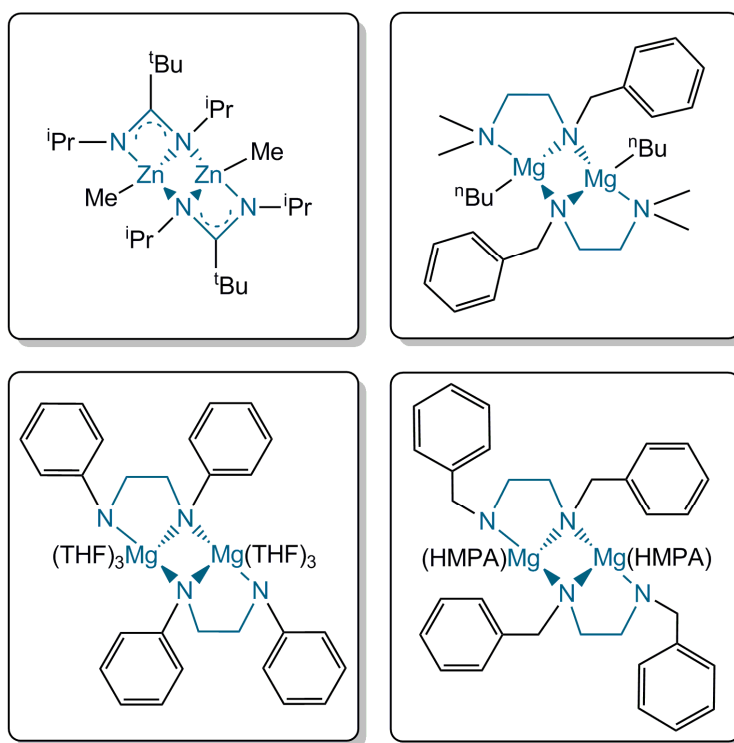


Figure 6.5 ChemDraw representation of the neutral zinc dimer $[\{^t\text{BuC}(\text{N}^i\text{Pr})_2\}\text{ZnMe}]_2$,^[336] and the related magnesium dimers $[\{(\text{BD})\text{Mg}(\text{nBu})\}]_2$,^[321] $[\{\text{MgN}(\text{Ph})\text{CH}_2\text{CH}_2\text{N}(\text{Ph})\cdot 2\text{THF}(1.5\text{THF})\}]_2$ ^[333] (the solvent THF molecules are omitted for clarity) and $[\{\text{MgN}(\text{CH}_2\text{Ph})\text{CH}_2\text{CH}_2\text{N}(\text{CH}_2\text{Ph})\cdot \text{HMPA}\}]_2$, highlighting the *trans*-fused ring systems.^[333]

6.3.6 Reactivity Studies: Metallation of *N,N*-diisopropylbenzamide

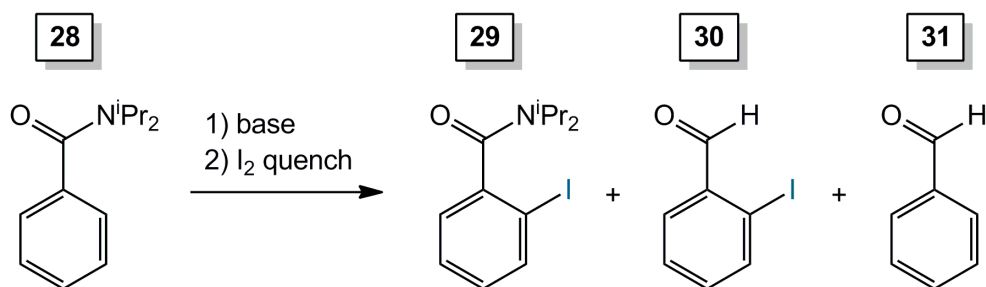
Intrigued as to how the reactivity would be affected upon the replacement of monofunctional TMP with difunctional BD, we decided to investigate sodium zincate **25** as a deprotonation agent. Initially, *N,N*-diisopropylbenzamide [$\text{C}_6\text{H}_5\text{C}(=\text{O})\text{N}^i\text{Pr}_2$] (**28**) was selected as the test organic substrate. Although tertiary amides are towards the strongest of the *ortho*-directing groups, their deprotonation is not necessarily straightforward. Organometallic reagents of considerable steric bulk, in conjunction with low reaction temperatures, can be required to prevent decomposition of the electrophilic amide group.^[337]

For control purposes the monometallic reagents NaBD and $\text{BD}(\text{H})\cdot^t\text{Bu}_2\text{Zn}$ were individually combined with benzamide **28** in a 1:1 molar ratio in hexane solvent. After 3 hours under reflux conditions, the reactions were quenched with iodine and worked up under aqueous conditions (Table 6.2, entries 3 and 4). Surprisingly, although no metallation was observed, a significant quantity of benzaldehyde was produced [NaBD, 20%; $\text{BD}(\text{H})\cdot^t\text{Bu}_2\text{Zn}$, 8%; where the yields were obtained by ^1H NMR spectroscopy using 10 mol% hexamethylbenzene as an internal standard]. For comparison, BD(H) and **28** were stirred together under reflux conditions in the absence of an organometallic reagent (entry 2). The formation of benzaldehyde persisted. However, in the absence of BD(H), only recovered **28** was observed (entry 1). From these preliminary findings, it seems likely that the difunctional amide is the culprit of the unexpected benzaldehyde formation.

Prior studies have proven the capability of sodium TMP zincate **1** to metallate **28** in the anticipated *ortho*-position.^[143b] With **1** exhibiting overall alkyl base behaviour, the molecular structure of the metallated intermediate $[(\text{TMEDA})\text{Na}(\mu\text{-TMP})\{\mu\text{-C}_6\text{H}_4\text{C}(=\text{O})\text{N}^i\text{Pr}_2\}\text{Zn}(^t\text{Bu})]$ was elucidated through X-ray crystallography and multinuclear NMR spectroscopy. Although a crystalline yield of 40% was achieved, uncertainty remained over the absolute metallation yield. Aiming to fill this gap in our knowledge, we began by combining crystalline **1** with **28** in a 1:1 ratio in a non-polar hydrocarbon medium, with a subsequent iodine quench after 3 hours at 75 °C.

These new findings show that under these reaction conditions, the absolute metallation yield is in fact much higher than 40%, as *ortho*-iodinated **28** was recovered in a good yield of 87% (entry 5).

Table 6.2: Reaction of polar metal amide bases with benzamide **28**.

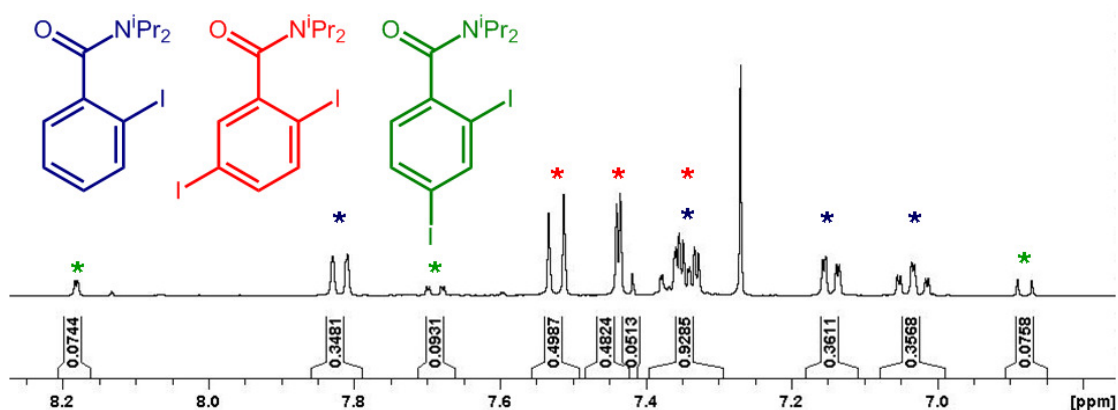


Entry	Base	Time (h)	Solvent	Base: Substrate Ratio	Product Yield ^{[a][b]} (%)		
					29	30	31
1	None	3	hexane	N/A	0	0	0
2	BD(H)	3	hexane	1:1	0	0	17
3	ⁿ BuNa + BD(H)	3	hexane	1:1	0	0	20
4	^t Bu ₂ Zn + BD(H)	3	hexane	1:1	0	0	8
5	1	3	hexane	1:1	87	0	0
6	1	3	hexane	2:1	36 ^[c]	0	0
7	1	18	hexane	2:1	33 ^[d]	0	0
8	25	3	hexane	1:1	43	0	14
9	25	3	THF	1:1	65	0	17
10	25 + BD(H)	3	hexane	1:1	4	0	15
11	25	3	hexane	2:1	40	40	20
12	25	18	hexane	2:1	18	25	19
13	3	3	hexane	2:1	20	28	21

a) Yields determined by ¹H NMR spectroscopy using hexamethylbenzene (10 mol%) as an internal standard; b) Conditions: **28** (1 mmol), base [donor amine {none; BD(H), 1 mmol}], monometallic reagent {ⁿBuNa, 1 mmol and BD(H), 1 mmol; ^tBu₂Zn, 1 mmol and BD(H), 1 mmol} or sodium zincate reagent (crystalline **1**; *in situ* preparation of **25** or **26**; 1 or 2 mmol as specified), solvent (10 mL) at 75 °C; c) In addition to *ortho*-iodinated **28**, diiodination products 2,5-diiodo-*N,N*-diisopropylbenzamide (49% yield) and 2,4-diiodo-*N,N*-diisopropylbenzamide (9% yield) were also observed; d) Diiodination products 2,5-diiodo-*N,N*-diisopropylbenzamide (45% yield) and 2,4-diiodo-*N,N*-diisopropylbenzamide (13% yield) were also obtained.

Surprisingly, upon increasing the base quantity to two equivalents, resonances corresponding to diiodinated **28** were observed in the ¹H NMR spectrum (Spectrum

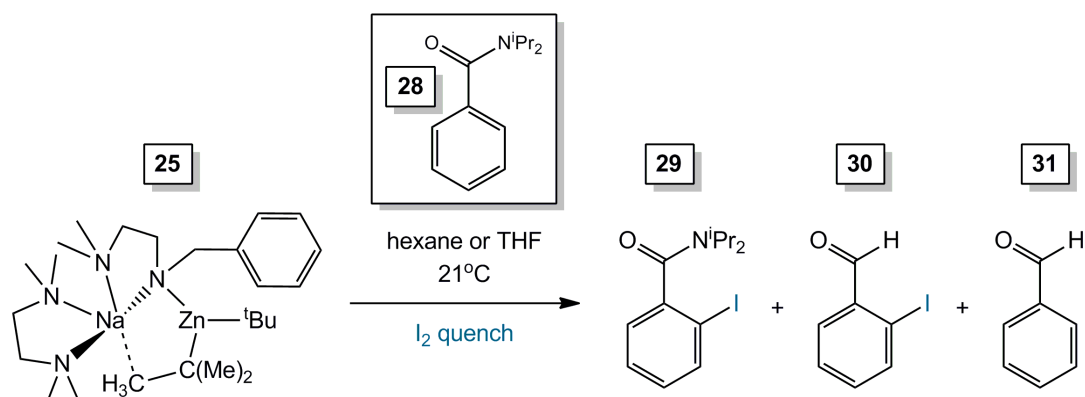
6.2). Specifically, 2,5-diiodo-*N,N*-diisopropylbenzamide (49% yield) having *ortho*, *meta*-substitution and 2,4-diiodo-*N,N*-diisopropylbenzamide^[338] (9% yield) having *ortho*, *para* substitution were obtained, in addition to the mono-*ortho*-iodinated **28** (36% yield). It was noted that increasing the reaction time from 3 hours to 18 hours did not improve the diiodination yields; the products yield and the product distribution remained constant within experimental error (entry 7).



Spectrum 6.2 ¹H NMR (400.03 MHz, 300 K, CDCl₃) spectrum of the crude reaction mixture upon the 2:1 stoichiometric reaction of sodium zincate base **1** with aromatic substrate **28** over 3 hours, highlighting the mono- and diiodination products observed upon iodine quenching.

The introduction of **28** into an *in situ* preparation of sodium zincate **25** in a hexane medium suggests that a synergic effect is operational within this bimetallic system. In spite of the failure of both homometallic components NaBD and BD(H)·^tBu₂Zn to individually metallate **28**, their simple combination within bimetallic **25** gave a 43% yield of *ortho*-iodinated **28** (Scheme 6.10; Table 6.2, entry 8). Different from the case with **1**, doubling the base quantity did not increase the yield of *ortho*-iodinated **28** (obtained in a 40% yield) and no diiodination products were observed. However, significantly higher yields of *ortho*-iodobenzaldehyde (40% *cf.*, 0% yield) and benzaldehyde (20% *cf.*, 14% yield) were achieved. Upon moving to a polar THF medium, an improved *ortho*-iodinated product yield of 65% was obtained (entry 9), alongside a reduced yield of benzaldehyde (17%) and no yield at all for *ortho*-iodobenzaldehyde. The milder reactivity of **25** in comparison to the ferocious base **1**

could in fact be advantageous, as its selectivity towards the deprotonation of **28** (and lack of reactivity towards polar solvents) may open the door to a wider range of available solvents for metallation chemistry.

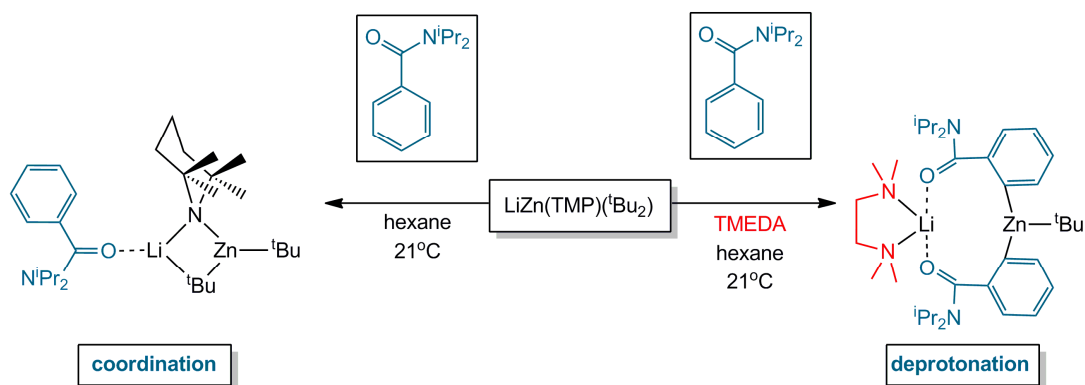


Scheme 6.10 The directed *ortho*-metallation of *N,N*-diisopropylbenzamide (**28**) using sodium amidozincate **25**, with subsequent iodine quenching.

Focussing on the Lewis donor TMEDA, our preliminary reactivity studies reveal that this chelating amine is an important component of **25**, as the *ortho*-metallation yield of **28** depends upon its presence. When the reaction of NaBD, ^tBu₂Zn and **28** was performed in the absence of TMEDA, the *ortho*-iodinated yield obtained halved to 20% (entry 13). Previous studies have highlighted the vital role TMEDA can play within metallation chemistry.^[142; 143b] For example, upon reaction with LiZn(TMP)(^tBu₂), **28** forms a terminal, dative interaction with the electropositive Li centre, to afford crystalline $[\{\text{PhC}(=\text{O})\text{N}^i\text{Pr}_2\}\text{Li}(\mu\text{-TMP})(\mu\text{-}^t\text{Bu})\text{Zn}(^t\text{Bu})]$.^[142] However, simply introducing TMEDA into this reaction system initiates the *ortho*-deprotonation of **28**, furnishing the bis(benzamido)zincate $[(\text{TMEDA})\text{Li}\{\mu\text{-C}_6\text{H}_4\text{C}(=\text{O})\text{N}^i\text{Pr}_2\}_2\text{Zn}(^t\text{Bu})]$ (Scheme 6.11), which is novel for surprisingly containing two *ortho*-deprotonated benzamide ligands.^[143b]

The introduction of an additional molar equivalent of BD into the reaction of **25** with **28** caused a substantial decrease in the yield of *ortho*-iodination, from 43% (entry 8) to an insignificant 4% (entry 10). As the addition of 1.5 equivalents of BD(H) to a mixture of NaBD and ^tBu₂Zn afforded the homometallic zinc species **27** (*vide*

supra), it seems plausible that the origin of this decreased yield lies with the destruction of the sodium-zinc cooperativity present in **25**.



Scheme 6.11 ChemDraw representation of the reaction of $\text{LiZn(TMP)(}^t\text{Bu}_2\text{)}$ with **28** in the absence (LHS)^[142] and presence (RHS)^[143b] of TMEDA.

To probe whether crystalline zincate **25** deprotonates **28** as an alkyl or an amido base (using a 1:1 stoichiometry), the reaction was monitored by ^1H NMR spectroscopy in C_6D_6 solvent. Although convoluted, the ^1H NMR spectrum provided evidence for the formation of ^tBuH , with the salient feature being the observation of a distinctive doublet at 0.87 ppm (Figure 6.6).^[313a] Observed after 6 hours at ambient temperature, this doublet continued to increase in intensity over a period of 1 week. In contrast, no ^1H NMR resonances corresponding to the noncoordinated amine BD(H) were observed, and so this study points towards **25** acting as an alkyl base overall. The resonances attributed to **28** at 0 hours experience an upfield shift to 6.97 and 7.06 ppm, in comparison to those of non-coordinated **28** (7.06 and 7.27 ppm). Indicative of dative coordination of **28** towards **25**, these values lie close to those found in previous studies where **28** coordinates to a metal centre.^[142; 337] Furthermore, the resonances corresponding to **28** disappear over time, and are replaced by a new set of aromatic resonances, indicating that **28** undergoes reaction with **25**. These observations suggest that ^tBuH is not simply a product of hydrolysis, as the resonances corresponding to the other expected hydrolysis products, namely BD(H) and **28**, are not witnessed. However, it cannot be unequivocally ruled out that

BD(H) and **28** are present in solution but experience a significant deviation in their chemical shift as a result of coordination to a metal centre.

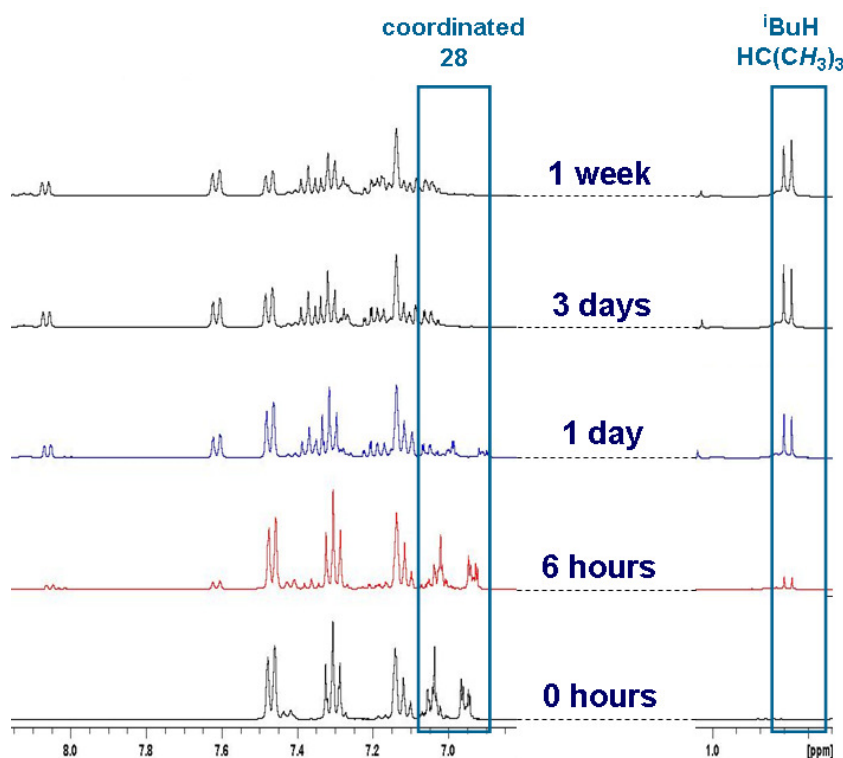
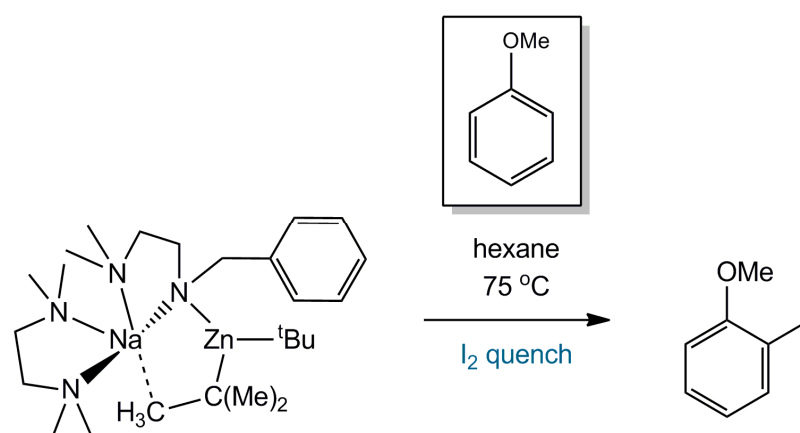


Figure 6.6 Variable time ^1H NMR (400.03 MHz, 300 K, C_6D_6) spectroscopic monitoring of the reaction of sodium zincate base **25** with aromatic substrate **28**, highlighting the formation of *iso*-butane and the disappearance of coordinated **28**.

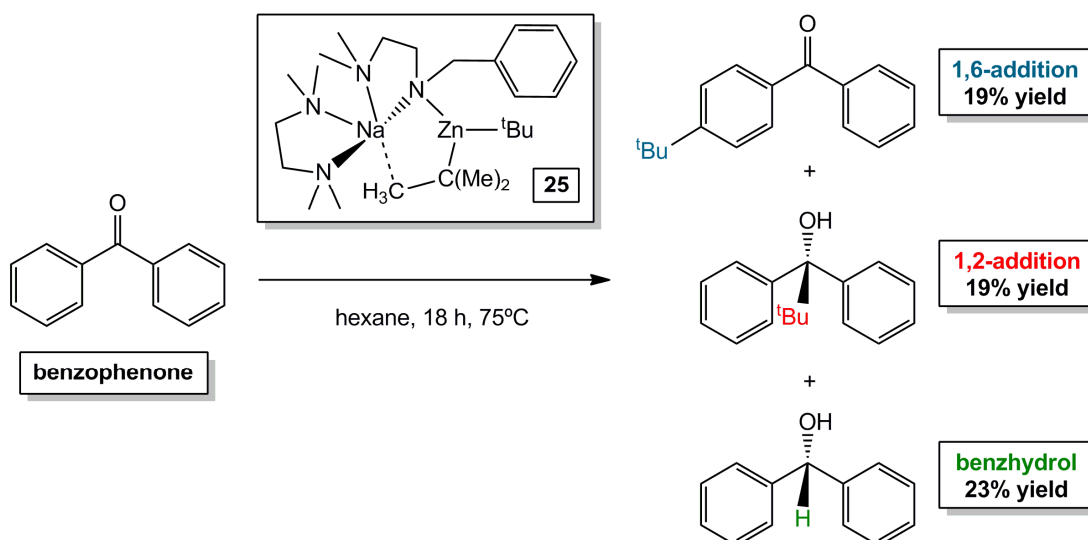
With a view to extending the scope of the metallation chemistry of **25**, preliminary investigations into the reaction of **25** with other test substrates were performed and appear promising. Anisole was selected as a more challenging substrate, owing to the weaker *ortho*-directing effect of a methoxy group in comparison to the amide group in *N,N*-diisopropylbenzamide. Under identical reaction conditions (stirred for 3 hours at 75 °C in hexane solvent), the *ortho*-metallation of anisole was achieved in a reasonable 49% yield (Scheme 6.12), demonstrating that the deprotonation capability of **25** extends to less activated substrates.

As the successful alkylation of benzophenone was previously achieved using a sodium zincate system with a difunctional amide component (Chapter 5), we

pondered whether **25** could also act as a *tert*-butyl transfer reagent. Benzophenone was selected as a benchmark substrate as its alkylation has been well studied and there are several competing reaction outcomes. Furthermore, prior studies have utilised sodium zincate reagents to achieve selective alkylation at the challenging 1,6-position.^[144; 293] While the alkylation of benzophenone was indeed achieved by **25** in a hexane medium (Scheme 6.13), the reaction was unfortunately not selective, ultimately producing a mixture of 1,2-addition across the carbonyl group (19% yield) and 1,6-addition at the *para*- position (19% yield), along with a significant quantity of the reduction product, benzhydrol (23% yield).



Scheme 6.12 The directed *ortho*-metallation of anisole using sodium amidozincate **25**, with subsequent iodine quenching.



Scheme 6.13 Attempted alkylation of benzophenone using sodium amidozincate **25**.

6.4 Conclusions

This study brings to light a new sodium amidozincate base (**25**), derived from the difunctional amine BD(H). Unexpectedly, within the molecular structure of **25**, as determined by X-ray crystallographic studies, the tertiary amine arm of BD reaches towards the weaker Lewis acid sodium, which creates extra steric hindrance around the metal centre in comparison to the monofunctional TMP-zincate precursor (**1**). Highlighting the importance of the donor amine and the difunctional amide stoichiometry, this study shows that a neutral zinc dimer is formed in the absence of TMEDA and the presence of an additional 0.5 molar equivalents of BD.

Significantly, preliminary reactivity studies have shown that replacing monofunctional TMP with difunctional BD diminishes the deprotonation capability of the bimetallic system. This is particularly noticeable when two molar equivalents of the base are employed. Whilst **1** gives not only *ortho*-iodination but also the diiodination products 2,5-diiodo-*N,N*-diisopropylbenzamide and 2,4-diiodo-*N,N*-diisopropylbenzamide, **25** returns only monoiodinated **28** in a moderate yield of 40%. However, this milder base still gives respectable quenched yields of *ortho*-iodinated **28** (65% in THF solvent) and *ortho*-iodoanisole (49% yield in hexane solvent). This less aggressive basicity could in fact pose an advantage, as **25** is stable towards benzene and THF, opening up a route to common solvents that are usually inaccessible with **1** because of its extreme reactivity. Importantly, these reactivity studies underscore the importance of the cooperation between the sodium and zinc metals, as the synergic reactivity seemingly achieved cannot be replicated by either homometallic constituent.

Certainly the findings presented within this chapter spark further questions. Although monitoring the reaction of sodium zincate **25** with benzamide **28** by ¹H NMR spectroscopy shows that **25** acts as an alkyl base overall, previous studies have shown that bimetallic bases can in fact operate through a two-step mechanism, where the amide component plays a key kinetic role.^[148; 313a; 328] However, the deprotonation of **28** by **25** may proceed through a different mechanism as a result of the

extra ligation within the bimetallic system, caused by the two metal binding points of the difunctional anion. Whether a one-step or a two-step mechanism is operational remains an open question.

6.5 Future Work

To capitalise on this work in the future, it would be important to attempt the rational preparation of **25** through the combination of BuNa, BD(H), $t\text{Bu}_2\text{Zn}$ and TMEDA, as this would provide a more time and cost efficient synthetic route. Future studies could then investigate the scope of this deprotonation chemistry by testing **25** with a range of organic substrates, such as aniline and trifluoromethylbenzene. Furthermore, the incorporation of alternative difunctional amides into this bisalkylmonoamidozincate system should be considered (Figure 6.7). Extending this study to include a range of difunctional amines, with varying degrees of steric bulk, would enable us to probe the structural outcome and assess the reactivity. Ideally, altering the amide, which acts as the key, kinetically active component of these synergic systems, will enable us to tune the reactivity of the bimetallic base. Moreover, the synthesis of a homoleptic difunctional amidozincate system should be explored, with the goal of designing an atom efficient base. The long-term aim would be to develop a range of synergic reagents, from which we can select the optimum base for a particular substrate.

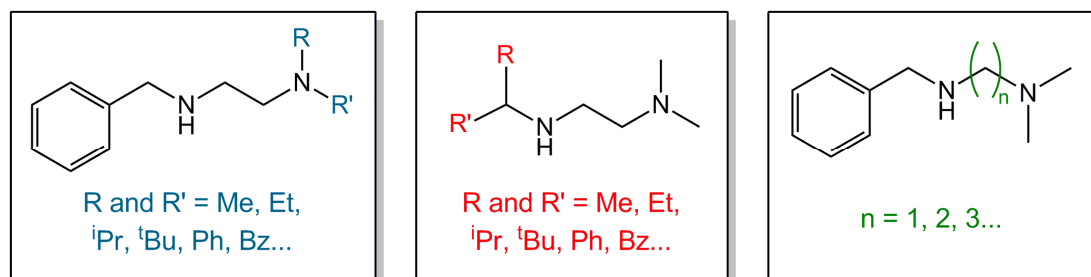


Figure 6.7 Structural representation of multifunctional amines that could be investigated within bimetallic systems.

To help achieve this end, there is the potential to extend the scope of this system beyond sodium and zinc, to alternative alkali metals, alkaline earth metals, and softer metal acids. Moreover, different stoichiometric combinations of the alkali metal and the softer metal components should be examined, to probe the synthesis of higher order bimetallic bases (defined by having a 2:1 alkali metal:zinc stoichiometry involving a dianionic $[\text{ZnR}_4]^{2-}$ moiety) that incorporate a donor appended amide.

Sodium zincate **25** has revealed itself to be a milder base than the parent compound **1**, and unlike **1**, it is stable towards arene solvents such as benzene.^[140a] That **25** displays the potential to execute metallation chemistry in arene solvents presents a potential advantage over **1**, through enabling access to a wider range of solvents. To this end, as the metallation of benzamide **28** by **25** in THF solvent gave decent yields of 65%, the alternative “green solvent” methyl-THF should also be investigated.^[339]

6.6 Experimental

6.6.1 Synthesis of $[(\text{TMEDA})\text{Na}(\mu\text{-BD})(\mu\text{-}^t\text{Bu})\text{Zn}(^t\text{Bu})]$, **25**

Ambient temperature: TMP(H) (0.34 mL, 2 mmol) was transferred *via* syringe to a suspension of freshly prepared $^n\text{BuNa}$ (0.16 g, 2 mmol) in hexane (10 mL) and the white suspension was allowed to stir for 1 hour at ambient temperature. A solution of $^t\text{Bu}_2\text{Zn}$ (0.36 g, 2 mmol) in hexane (10 mL) was consequently added to the suspension *via* cannula, followed by 0.30 mL (2 mmol) of TMEDA. Gentle heating produced a pale yellow solution, to which BD(H) (0.38 mL, 2 mmol) was injected, instantly forming a vivid pink solution. The reaction mixture was transferred to the refrigerator (4 °C) where a crop of pink crystals (yield 0.63 g, 64%) was deposited after 18 hours.

Elevated temperature: The reaction was repeated on a 1 mmol scale following the procedure outlined above. Following the addition of TMEDA, the reaction mixture was heated to 60 °C. After the addition of BD(H) (0.19 mL, 1 mmol), the reaction

was allowed to stir for 10 minutes at 60 °C. Multinuclear [^1H , $^{13}\text{C}\{\text{H}\}$] NMR spectroscopic analysis confirmed that **25** was the product of this reaction.

^1H NMR (400.03 MHz, C_6D_6 , 300 K): δ = 7.50 [d, $^3\text{J}(\text{H,H})$ = 7.0 Hz, 2H, $\text{H}_{ortho}\text{-Ph}$], 7.34 [t, $^3\text{J}(\text{H,H})$ = 7.7 Hz 2H, $\text{H}_{meta}\text{-Ph}$], 7.14 [t, $^3\text{J}(\text{H,H})$ = 7.5 Hz, 1H, $\text{H}_{para}\text{-Ph}$], 4.16 and 4.47 (br. s, 1H, PhCH_2), 3.48 and 2.82 (br. s, 1H, BzNCH_2), 2.37 (s, 2H, Me_2NCH_2), 1.83 (s, 6H, $\text{NCH}_3\text{-BD}$), 1.70 (s, 12H, $\text{NCH}_3\text{-TMEDA}$), 1.62 (s, 4H, $\text{NCH}_2\text{-TMEDA}$) and 1.52 ppm (s, 18H, ^tBu). $^{13}\text{C}\{\text{H}\}$ NMR (100.59 MHz, C_6D_6 , 300 K): δ = 146.3 ($\text{C}_{ipso}\text{-Ph}$), 128.6 ($\text{C}_{meta}\text{-Ph}$), 127.8 ($\text{C}_{ortho}\text{-Ph}$), 126.2 ($\text{C}_{para}\text{-Ph}$), 63.8 ($\text{Me}_2\text{NCH}_2\text{-BD}$), 62.4 (PhCH_2), 56.9 ($\text{NCH}_2\text{-TMEDA}$), 53.4 (BzNCH_2), 46.3 ($\text{NCH}_3\text{-TMEDA}$), 45.7 ($\text{NCH}_3\text{-BD}$), 35.7 (^tBu) and 23.2 ppm (quat. ^tBu).

Due to time restrictions, satisfactory C, H, N analyses were not obtained for **25**.

Crystal data for **25**: $\text{C}_{25}\text{H}_{51}\text{N}_4\text{NaZn}$, M_r = 496.06, triclinic, space group P-1, a = 9.0408(3), b = 11.2678(3), c = 15.1689(5) Å, α = 82.377(2), β = 82.929(2), γ = 74.824(3)°, V = 1471.87(8) Å³, Z = 2, μ = 0.866 mm⁻¹; 16520 reflections, 7728 unique, R_{int} 0.0289, final refinement to full-matrix least squares on F^2 gave R = 0.0330 (F , 6706 obs. data only) and R_w = 0.0793 (F^2 , all data), GOF = 1.035.

6.6.2 Synthesis of “NaZn(BD)(^tBu)₂”, **26**

A creamy suspension of $^n\text{BuNa}$ (0.16 g, 2 mmol) in hexane (10 mL) was prepared and $\text{TMP}(\text{H})$ (0.34 mL, 2 mmol) was subsequently added *via* syringe. After stirring for 1 hour at ambient temperature, a solution of $^t\text{Bu}_2\text{Zn}$ (0.36 g, 2 mmol) in hexane (10 mL) was added *via* cannula. $\text{BD}(\text{H})$ (0.38 mL, 2 mmol) was then added, which instantaneously produced a bright pink suspension (solid yield 0.45g, 66%).

^1H NMR (400.03 MHz, C_6D_6 , 300 K): δ = 7.22 [t, $^3\text{J}(\text{H,H})$ = 7.4 Hz, 2H, $\text{H}_{meta}\text{-Ph}$], 7.17 [d, $^3\text{J}(\text{H,H})$ = 7.9 Hz, 2H, $\text{H}_{ortho}\text{-Ph}$], 7.11 [t, $^3\text{J}(\text{H,H})$ = 7.2 Hz, 1H, $\text{H}_{para}\text{-Ph}$], 4.32 and 3.76 (br s, 1H, CH_2Ph), 3.36 and 2.76 (br s, 1H, CH_2NBz), 2.29 and 1.99 (br. s, 1H, CH_2NMe_2), 1.55 (s, 6H, NCH_3) and 1.39 ppm (s, 18H, ^tBu). $^{13}\text{C}\{\text{H}\}$ NMR (100.59 MHz, C_6D_6 , 300 K): δ = 147.3 ($\text{C}_{ipso}\text{-Ph}$), 129.1 ($\text{C}_{meta}\text{-Ph}$), 127.9 ($\text{C}_{ortho}\text{-Ph}$),

126.3 (C_{para} -Ph), 64.2 (CH_2NMe_2), 62.0 (CH_2Ph), 53.5 (BzNCH_2), 45.4 (NCH_3 -BD), 35.6 (^tBu) and 23.4 ppm (quat. ^tBu).

Due to time restrictions, satisfactory C, H, N analyses were not obtained for **26**.

6.6.3 Synthesis of $\{[(\text{BD})\text{Zn}(^t\text{Bu})]_2\}$, **27**

TMP(H) (0.34 mL, 2 mmol) was introduced to a white suspension of $^n\text{BuNa}$ (0.16 g, 2 mmol) in hexane (10 mL) *via* syringe. After 1 hour of stirring at ambient temperature, a solution of $^t\text{Bu}_2\text{Zn}$ (0.36 g, 2 mmol) in hexane (10 mL) was added, followed by BD(H) (0.57 mL, 3 mmol). The resultant, bright pink solution was immediately transferred to the refrigerator, where a crop of colourless crystals (yield 0.17 g, 14% out of a maximum of 50% based upon the Zn stoichiometry) was deposited after 18 hours.

^1H NMR (400.03 MHz, C_6D_6 , 300 K): δ = 7.44 [d, $^3\text{J}(\text{H,H})$ = 7.3 Hz, 2H, H_{ortho} -Ph], 7.33 [t, $^3\text{J}(\text{H,H})$ = 7.7 Hz 2H, H_{meta} -Ph], 7.15 [t, $^3\text{J}(\text{H,H})$ = 7.4 Hz, 1H, H_{para} -Ph], 4.32 (br s, 2H, CH_2Ph), 2.67 (br. s, 4H, CH_2NMe_2 and CH_2NBz), 1.86 (s, 6H, NCH_3) and 1.49 ppm (s, 9H, ^tBu). $^{13}\text{C}\{\text{H}\}$ NMR (100.59 MHz, C_6D_6 , 300 K): δ = 147.3 (C_{ipso} -Ph), 128.5 (C_{meta} -Ph), 128.0 (C_{ortho} -Ph), 126.6 (C_{para} -Ph), 63.4 (CH_2NMe_2), 62.0 (CH_2Ph), 52.1 (BzNCH_2), 47.1 (NCH_3 -BD), 36.1 (^tBu) and 22.4 ppm (quat. ^tBu).

Due to time restrictions, satisfactory C, H, N analyses were not obtained for **27**.

Crystal data for **27**: $\text{C}_{30}\text{H}_{52}\text{N}_4\text{Zn}_2$, M_r = 599.50, triclinic, space group P-1, a = 13.0422(5), b = 13.0894(5), c = 14.3441(5) Å, α = 75.391(3), β = 75.496(3), γ = 84.222(3)°, V = 2292.22(15) Å³, Z = 3, μ = 1.594 mm⁻¹; 15107 reflections, 9483 unique, R_{int} 0.0260, final refinement to full-matrix least squares on F^2 gave R = 0.0332 (F , 7995 obs. data only) and R_w = 0.0789 (F^2 , all data), GOF = 1.060.

6.6.4 Method 6A – Iodine Quenching and Work-Up Procedure

The *in situ* reaction mixture (1 mmol scale based on the substrate **28** or anisole) was treated with a freshly prepared solution of 1 M iodine in THF (4 mL, 4 mmol when 1

molar equivalent of the bimetallic base was used; 8 mL, 8 mmol when 2 molar equivalents of the bimetallic base were used) and allowed to stir for 1 hour. A 10 mL amount of NH_4Cl was added followed by saturated $\text{Na}_2\text{S}_2\text{O}_3$ until bleaching occurred (approximately 10 mL). The organic layer was then separated from the aqueous layer and the aqueous layer was washed with diethyl ether (3 x 15 mL). Magnesium sulfate was used to dry the combined organic layers. After filtration, the solvent was removed under vacuum and the crude residue was spiked with 10 mol% hexamethylbenzene [0.0162 g, 0.1 mmol for 1 mmol scale reactions (based upon the substrate)]. ^1H NMR spectroscopic analysis was performed in CDCl_3 solvent, and the relative yields of *ortho*-iodo-*N,N*-diisopropylbenzamide, *ortho*-iodobenzaldehyde and benzaldehyde were determined by relative integration. Spectroscopic data show resonances that are in good agreement with literature values for *ortho*-iodo-*N,N*-diisopropylbenzamide,^[337] *ortho*-iodobenzaldehyde^[340] and benzaldehyde.^[341]

6.6.5 Metallation of *N,N*-diisopropylbenzamide, **28**

The appropriate base [Table 6.2; none; BD(H), 0.19 mL, 1 mmol; $^n\text{BuNa}$, 0.08 g, 1 mmol and BD(H), 0.19 mL, 1 mmol; $^t\text{Bu}_2\text{Zn}$, 1 mL of a 1 M hexane solution, 1 mmol and BD(H), 0.19 mL, 1 mmol; crystalline **1**, 0.46 g, 1 mmol; **25** (prepared *in situ* from the reaction of **1**, 0.46g, 1 mmol, with BD(H), 0.19 mL, 1 mmol); **26** (prepared *in situ* by allowing $^n\text{BuNa}$, 0.16 g, 2 mmol, to stir with TMP(H), 0.34 mL, 2 mmol, for 1 hour, followed by addition of $^t\text{Bu}_2\text{Zn}$, 2 mL of a 1 M hexane solution, 2 mmol, and BD(H), 0.19 mL, 1 mmol] was dissolved in hexane (10 mL). Subsequently, *N,N*-diisopropylbenzamide (0.205 g, 1 mmol) was added. The reaction mixture was then stirred at 75 °C for either 3 hours, or 18 hours (Table 6.2), prior to iodine quenching using the procedure outlined in Method 6A.

6.6.6 ^1H NMR Monitoring of the metallation of **28** by zincate **25**

Isolated crystals of **25** (0.05 g, 0.1 mmol) and benzamide **28** (0.02 g, 0.1 mmol) were weighed into a Young's NMR tube in a drybox under argon atmosphere. After

dilution with C₆D₆ (approximately 0.5 mL), the Young's NMR tube was sealed and monitored by ¹H NMR spectroscopy over a period of 2 weeks.

6.6.7 Metallation of anisole

Sodium zincate **25** was prepared *in situ*, through the addition of BD(H) (0.19 mL, 1 mmol) to a freshly prepared solution of crystalline **1** (0.46 g, 1 mmol) in hexane (10 mL), which instantaneously produced a vivid pink solution. Anisole (0.11 mL, 1 mmol) was subsequently added and the reaction mixture was stirred for 3 hours at 75 °C. The resultant red suspension was then quenched and worked-up according to Method 6A. Spectroscopic data show resonances that are in good agreement with literature values for *ortho*-iodoanisole.^[199b]

6.6.8 Alkylation of benzophenone

Sodium zincate **25** was prepared *in situ* on a 1 mmol scale. Crystalline **1** was dissolved in hexane solvent (10 mL), and BD(H) (0.19 mL, 1 mmol) was injected, instantly forming a vivid pink solution. Upon the addition of benzophenone (0.18 g, 1 mmol) to this reaction mixture, a colour change from pink to brown occurred. The reaction was stirred for 18 hours at 75 °C, after which deionised water (10 mL), 2 M HCl (20 mL) and diethyl ether (20 mL) were added. The organic layer was separated from the aqueous layer and the aqueous layer was washed with diethyl ether/hexane (3 x 20 mL). Magnesium sulfate was subsequently used to dry the combined organic layers. Following filtration, solvent was removed *in vacuo* and the crude residue was spiked with 10 mol% hexamethylbenzene (0.0162 g, 0.1 mmol). ¹H NMR spectroscopic analysis was performed in CDCl₃ solvent and the relative yields of 2- and 4-*tert*-butylbenzophenone, benzhydrol^[311] and diphenyl-*tert*-butylmethanol^[312] were determined by relative integration. Spectroscopic data show resonances that are in good agreement with the reference standard of commercially available samples of 2-*tert*-butylbenzophenone and 4-*tert*-butylbenzophenone.

Chapter 7

The Outlook for Organometallic Chemistry

Past, Present and Future

“Truth in science can be defined as the working hypothesis
best suited to open the way to the next better one”

Konrad Lorenz

Austrian ethologist

Nobel Prize for Medicine, 1973

In comparison to other fields of chemistry such as organic, inorganic and physical, organometallic chemistry is still in its relative infancy. However, despite its effectual youth, organometallic research has dramatically changed the face of the chemical landscape.^[342] Highlighting the substantial importance of organometallic chemistry upon the scientific community, many Nobel Prizes in Chemistry have been awarded for landmark progressions within this field, especially in recent years. Catalysis represents one of the major real-world applications of organometallic chemistry and accordingly, Ziegler-Natta catalysts designed for the polymerisation of α -olefins earned their discoverers the Nobel Prize for Chemistry in 1963. Since the turn of the millennia, Grubbs, Schrock and Chauvin shared the Nobel Prize for Chemistry in 2005 for the development of organometallic catalysts for alkene metathesis. Five years later, Heck, Negishi and Suzuki shared the Nobel Prize for palladium catalysed cross-coupling reactions. These pioneering developments emphasise that organometallic chemistry is currently at the forefront of useful modern chemistry.

One of the most pertinent applications of organometallic chemistry, and certainly the most central to this PhD study, is that of C-H bond activation.^[8; 45] An issue of utmost importance for synthetic chemists, the conversion of a non-activated C-H bond to a more polar, hence more reactive C-metal bond is often a crucial step in constructing sophisticated molecular architectures from simple chemical building blocks. Although Grignard reagents have been used for C-H bond activation since their initial discovery more than a century ago,^[5] they have generally been superseded by more reactive organolithium analogues, especially with regard to the cleavage of challenging aromatic C-H bonds. Reflecting this fact, Collum, a leading world authority on the physical-organic chemistry of organolithium compounds, recently stated that:

“well over 95% of natural products syntheses rely upon lithium-based reagents in one form or another.”^[299a]

Prolific within modern synthetic methods, organolithium reagents are exploited in the synthesis of a vast library of everyday commodities that serve humankind;

including pharmaceuticals, agrochemicals, biochemicals, dyes and perfumes to name but a few. Contributing to this body of knowledge, the work described in Chapter 2 shows that the nature of the organometallic reagent (in this case ^tBuLi or ⁿBuNa) and the Lewis donor ligand (THF, TMEDA or PMDETA versus none) can have a substantial influence upon the yield and regioselectivity of the metallated derivatives of trifluoromethylbenzene. Whilst a mixture of regioisomers was observed using ^tBuLi/THF or ^tBuLi/TMEDA metallating systems, moving to ⁿBuNa/THF, ⁿBuNa/TMEDA or ⁿBuNa/PMDETA gave much more selective *ortho*-metallation. Providing insight into the regioselectivities observed, X-ray crystallographic, NMR spectroscopic and computational studies of the metallated intermediates suggest that the Na...F interactions observed for the sodium derivatives play a key role in the stabilisation of the *ortho*-product.

Given the remarkable chemistry that has been accomplished using organolithium reagents, this led us to ponder what potentially novel chemistry could be achieved using bimetallic systems. Although the field of bimetallic chemistry is relatively unexplored in comparison to that of classical homometallic reagents, phenomenal progress has already been made. Reflecting this, the well-known inorganic chemist Hahn recently said:

“If you look at the diverse chemistry of mononuclear complexes
imagine what the future would hold in polymetallic systems
for cooperative reactivity in catalysis or related fields.”^[4]

It has already been shown that pairing an alkali metal and a softer metal (in the hard soft acid base sense)^[343] within a single molecular environment can lead to enhanced reactivity and selectivity.^[143a; 143c] Expanding upon this principle, cooperative reactivity is observed with the novel sodium amidozincate developed in Chapter 6, which includes a difunctional amido unit within its bimetallic structure. This synergic base can deprotonate *N,N*-diisopropylbenzamide and anisole, in contrast to its monometallic constituents which are inactive under identical reaction conditions. One of the major advantages of cooperative bimetallic chemistry is that it can enable

reactions to be performed under ambient temperature conditions, circumventing the expensive, cryogenic cooling systems often required to prevent decomposition when utilising monometallic (typically organolithium) systems. This is demonstrated by the ambient temperature α -metallation of *N*-Boc pyrrolidine described in Chapter 4.

This synergic, metal-metal cooperativity could lead us to imagine a new, “hybrid” periodic table, where element pairs such as Li/Mg, Li/Al, Li/Cd, Na/Zn and K/Mn enable us to harness new reactivities that are completely separate to the “elemental” properties of either monometallic component. With the field of heterodinuclear chemistry still comparatively underdeveloped, the number of bimetallic “tools” that have been investigated is still somewhat limited, considering there is such a potentially vast elemental construction kit at our disposal:

“the toolbox is not even half full”.^[4]

Over the years, organometallic chemistry has made a substantial contribution to the discovery of new types of compounds. Hitherto unprecedented bonding modes have been uncovered, with groundbreaking examples including the electron deficient bonding in organolithium reagents,^[28a; 29; 31] the advent of a chromium-chromium quintuple bond^[344] and the discovery of metallocene complexes.^[345] Within this PhD project, novel sodium zinczincate and sodium-zinc donor-acceptor structures have been developed (Chapter 5), which break away from the typically observed “*Weiss motif*”.^[216b] Structure and reactivity are often intertwined and accordingly, these novel structures give unexpected reactivities, where sub-stoichiometric quantities of a sodium metalloligand donor component can activate the ^tBu₂Zn acceptor unit towards the *tert*-butylation of benzophenone. However, a full understanding of the mechanism of this special regioselective nucleophilic addition has yet to be deciphered.

With an increasing world population creating ever more demands upon the Earth’s resources, the relentless drive to move towards reaction efficiency, atom efficiency and environmentally benign reaction conditions present some of the next big

challenges faced by organometallic chemistry. Highlighting the importance assigned to this topic, the EPSRC selected “Dial-a-molecule – 100% efficient synthesis” as one of their four Grand Challenges. Recent developments within magnesiate chemistry have achieved the development of bases where all four ligand arms deprotonate an organic substrate.^[143e] Thus this suggests that the systems investigated within this PhD project could be further developed to achieve atom efficiency, where each anionic ligand arm can be used to deprotonate an aromatic substrate. Indeed, the successful synthesis of unprecedented homoleptic lower- and higher-order pyrrolyl zincate systems achieved in Chapter 3 hints that this could be a realistic future goal.

From here on in, the field of organometallic chemistry looks set to be one of the major players on the international stage for tackling important global issues. Although the use of organometallic compounds as catalysts is well established, this diverse class of reagents have many other potential applications, for example within CO₂ capture and usage.^[346] Furthermore, the high reactivity associated with organometallic complexes has also been successfully exploited in the activation of small molecules.^[1; 347] With the rapid decline of fossil fuel resources, in combination with increasing energy demands, water splitting^[348] and hydrogen storage^[349] are also likely to be key subjects of interest in the near future, and organometallic chemistry has already shown promise in these areas.

Chapter 8

General Experimental Techniques

“No amount of experimentation can ever prove me right;
a single experiment can prove me wrong”

Albert Einstein

German-born physicist

Nobel Prize for Physics, 1921

8.1 Schlenk Techniques

Many of the metal-based reagents and products encountered within this project are air- and moisture-sensitive. This necessitated the use of standard Schlenk techniques, including the routine employment of a high vacuum Schlenk line (Figure 8.1) and an argon filled glovebox. All manipulations, including analytical preparations, were therefore performed under a dry and inert argon atmosphere.

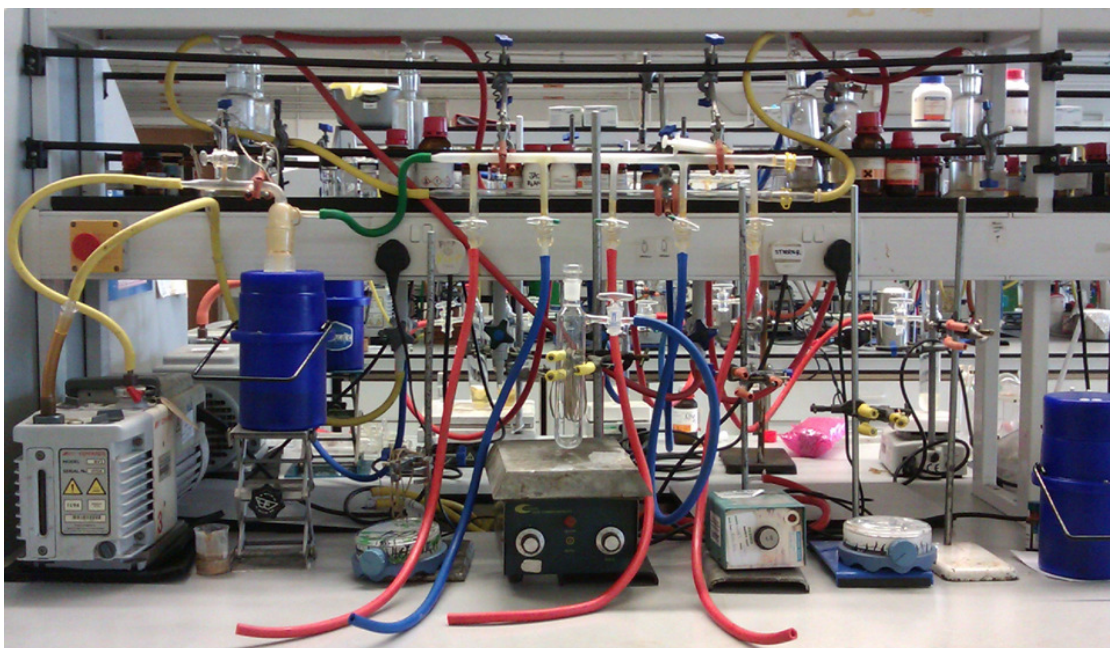


Figure 8.1 A typical Schlenk line in use.

A Schlenk line has two independent paths; one connected to a high vacuum pump and the other leading to a supply of dry, oxygen-free argon gas. The Schlenk line shown in Figure 8.1 has five connections which can be linked to Schlenk apparatus, most commonly Schlenk tubes. Each connection has a two-way tap (coated with high vacuum grease to ensure an efficient seal) and therefore a vacuum or argon source can be applied to the connected apparatus. A solvent trap, placed in a Dewar flask filled with liquid nitrogen, is included to condense any volatile substances prior to reaching and potentially damaging the pump. Also present is a pressure release Dreschel bottle, the function of which is to prevent pressure build-up within the apparatus. To ensure the absence of oxygen and moisture prior to each experiment, it

is routine practise to evacuate all the air from the Schlenk tube, then to refill with argon gas. This procedure is performed three times in total.

8.2 Glove Box

Storage and manipulation of all solid reactants and products (including NMR spectroscopic preparations, elemental microanalysis preparations, the determination of weights of solid reactants and products) had to be performed under an inert atmosphere to prevent their decomposition. An argon-filled, Saffron glove box was therefore employed to achieve these manipulations (Figure 8.2).

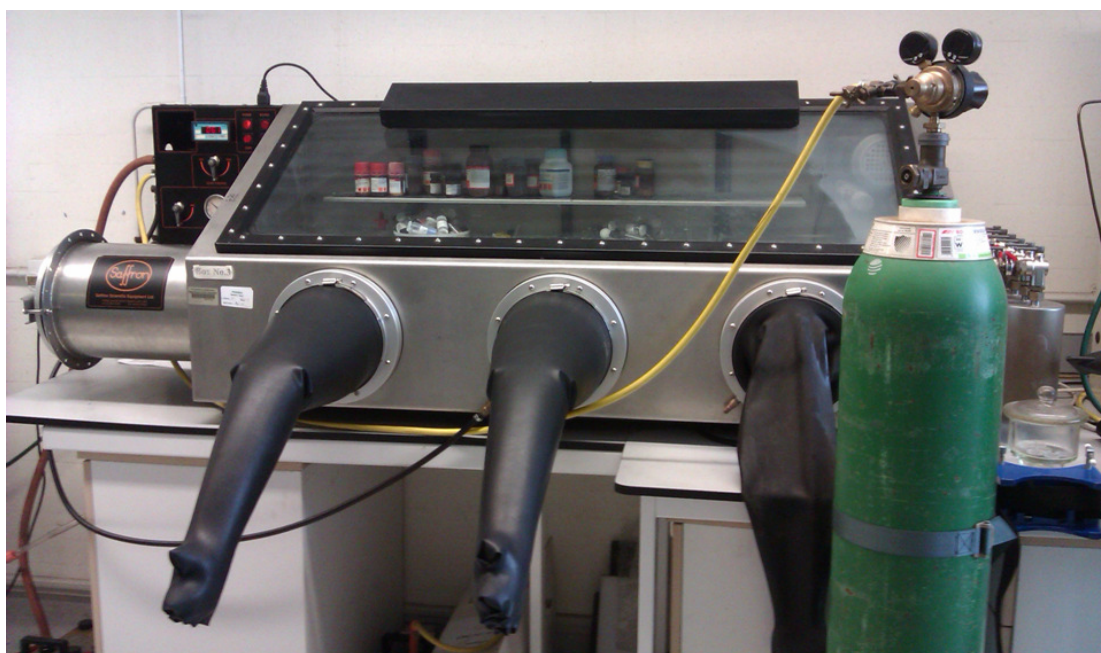


Figure 8.2 A typical research glove box with fitted argon gas recirculation and purification system.

The port on the left hand side of the glove box enables the transfer of chemicals and apparatus in and out of the glove box. Once the items have been placed in the port (*via* the outer port door), the door is sealed and, as with the Schlenk line, the port is evacuated for a minimum of ten minutes then refilled with argon gas. This process is

performed three times. The inner port door can then be opened safe in the knowledge that no, or negligible quantities of oxygen and water have entered the inert atmosphere of the main body of the glove box. To help ensure the absence of significant quantities of oxygen and water inside the glovebox, the oxygen and moisture levels are monitored by built in meters and are displayed on the LCD control panel. The box is regenerated as often as required to ensure these levels remain low (typically once every 2-3 months), by passing forming gas through the catalyst and removing water from the molecular sieves by heating under vacuum. Placing one's hands inside the neoprene gloves enables the user to manipulate materials stored inside the glove box. Solid products that have been isolated can be brought into the glovebox under vacuum. As long as the glassware joints are effectively sealed with high vacuum grease, the vacuum inside the apparatus will persist until it is opened inside the glovebox under argon atmosphere. Equally, solid reagents stored within the glovebox can be transferred to the bench for reactions, through placing clean, dry, greased glassware into the port, ensuring that the taps are open, and performing the aforementioned evacuation/argon flush procedure.

8.3 Solvent Purification

All the solvents used within this project (hexane, THF, toluene and diethyl ether) were purchased from Sigma-Aldrich. To ensure the absence of air and moisture, the presence of which could result in undesirable reactions occurring, all solvents were dried and degassed prior to use. Distillation of the solvents was carried out under a nitrogen blanket in the presence of sodium metal and benzophenone.^[350] The purpose of these chemicals is that they are used as an exceptional self-indicating method of ensuring the absence of oxygen and water from the solvent. Sodium reacts with benzophenone to yield an intensely blue ketyl radical. This species is extremely reactive towards oxygen and water and, if present, will yield colourless or yellow products. The colour difference provides an easily observable method of determining whether oxygen or water is present.

The dried solvent was then collected into a nitrogen-filled air tight flask that was sealed using a Subaseal[®]. This rubber seal provides an efficient means of removing a desired volume of solvent using a glass syringe and needle, without permitting air to enter the system. Prior to use, the syringe and needle were flushed three times with argon. To prevent a negative pressure arising within the system, a volume of argon gas was introduced to the system prior to the removal of solvent. If a negative pressure were to arise, solvent removal would become increasingly difficult to achieve, which could, in turn, lead to a gradual pull of atmospheric gases into the sealed flask as the pressure tries to re-equilibrate. This would cause contamination of the solvent.

8.4 NMR Solvent Purification

Each NMR solvent was transferred into an ampoule fitted with a J Young valve and dried over activated 4 Å molecular sieves. The solvent was subsequently degassed using the freeze-vacuum-thaw method,^[350] where the solvent was frozen under argon atmosphere using a Dewar flask of liquid nitrogen. Once frozen, a small vacuum was applied, to remove any volatile gases that had dissolved. As the solvent thawed, a small vacuum was introduced at regular intervals, to prevent any build up of pressure. Once the solvent had fully thawed, the system was returned to argon, and the ampoule sealed. The entire process was performed in triplicate.

8.5 Purification of Hydroscopic Liquids

Reagents such as TMP(H) and BD(H) were dried using activated 4 Å molecular sieves. The molecular sieves were activated by heating in the microwave, for fifteen minutes or until glowing red hot. At regular intervals, the flask was agitated to avoid the build up of hot spots.

Certain liquids used in this project were highly hygroscopic, such as amines. To ensure no contaminant moisture was present in these liquids, they were distilled for several hours in the presence of a desiccant (calcium hydride). The purified liquid was collected into a round bottomed flask, containing freshly activated 4 Å molecular sieves. The argon filled round bottomed flask was then sealed air tight with a Subaseal[®] for subsequent use in reactions.

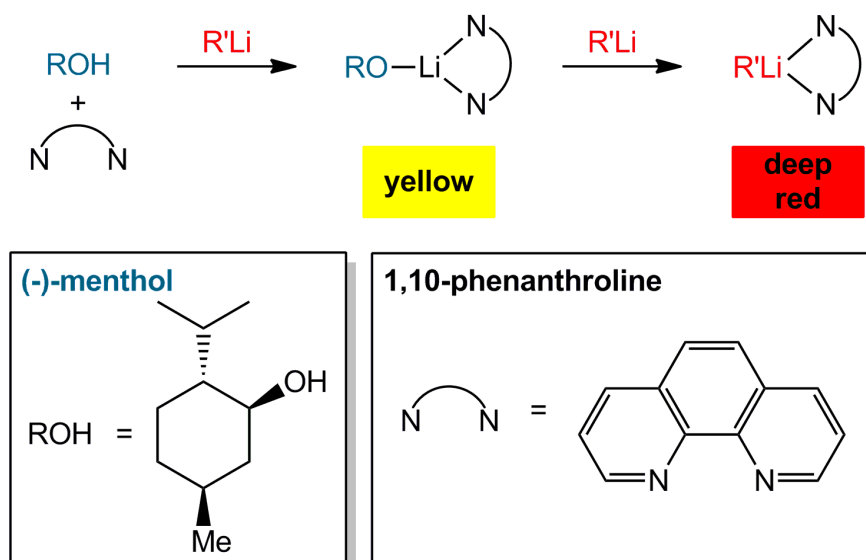
8.6 Commercial Reagents Used

The bulk of reagents employed were purchased from Sigma-Aldrich. Sodium alkoxide NaO^tBu, *N,N*-diisopropylbenzamide, TEMPO free radical, TMEDA and iodine were purchased from Alfa Aesar, while TMP(H) was purchased from Acros Organics.

8.7 Standardisation of Organolithium Reagents

Standardisation of commercial organolithium sources, such as ⁿBuLi in heptane, is required to ensure the solution has the correct molarity for the stoichiometry to be used in subsequent reactions. The molarity of the organolithium solution can change over time owing to evaporation of the solvent or reaction with air.

Standardisation of the organolithium reagents was performed by dissolving menthol (approximately 0.156 g, 1 mmol) and 1,10-phenanthroline (2-3 mg, present as an indicator) in 2 mL of dried THF solvent. This pale yellow solution was then titrated with the appropriate organolithium solution, RLi, until a persistent red colour was obtained (Scheme 8.1), at which point the volume of RLi added was recorded.^[351] The molarity of the RLi solution was then calculated using the formula in eqn. 8.1.



Scheme 8.1 Standardisation procedure for alkyllithium reagents.

Menthol:

Weight of menthol = **X** (g)

Number of moles of menthol = $\text{X}/156.27 = \text{Z}$ moles

(where the molecular weight of menthol = 156.27 g)

RLi:

Volume of RLi required to produce a colour change to red = **Y** (mL)

Molarity of RLi = $(\text{Z}/\text{Y}) \times 1000$

(eqn. 8.1)

8.8 Preparation of Common Starting Materials

Throughout this project, the homometallic reagents ${}^n\text{BuNa}$ and ${}^t\text{Bu}_2\text{Zn}$ were prepared on a regular basis according to the literature procedures outlined below.

8.8.1 Preparation and Isolation of ${}^n\text{BuNa}$ ^[352]

The highly pyrophoric sodium alkyl reagent ${}^n\text{BuNa}$ was prepared through a metathesis reaction. Firstly, the bulky alkoxide Na^tOBu (3.84 g, 40 mmol) was weighed into a Schlenk flask in the glovebox. The flask was subsequently transferred

to the bench. Hexane (50 mL) was then added and the resultant suspension was cooled to 0 °C in an ice bath. Upon the slow introduction of ⁿBuLi (25 mL of a 1.6 M solution, 40 mmol), a pyrophoric white solid precipitated. Following the complete addition of ⁿBuLi, the ice bath was removed and the reaction mixture was left to stir overnight at ambient temperature. The solid product deposited in the solution was collected by filtration and washed with dry hexane (3 x 20 mL aliquots). Finally, the white powder of ⁿBuNa was dried under high vacuum for one hour prior to isolation in the glovebox (typical yield, 2.4 g, 75%).

8.8.2 Preparation and Isolation of ^tBu₂Zn^[353]

Dried solid ZnCl₂ (40 mmol, 5.45g) was weighed into a Schlenk flask in the glovebox. After transferral of the Schlenk flask to the bench, the white powder was dissolved in diethyl ether (80 mL). The ZnCl₂ ethereal solution was subsequently cooled to 0 °C in an ice bath and ^tBuLi (80 mmol, 48 mL of a 1.7 M solution) was slowly added to form a white suspension. When the addition of ^tBuLi was complete, the ice bath was removed, the Schlenk flask was shielded from light (using a black plastic bag) to prevent decomposition and the reaction was stirred for 2-3 hours at ambient temperature.

The reaction mixture was subsequently filtered over Celite and glass wool to remove the solid lithium chloride by-product, and the filtrate was collected in a Schlenk flask under argon atmosphere. Under vacuum, solvent was removed until approximately 10 mL remained. Using a cannula, the colourless solution was then transferred to the sublimation apparatus (under argon atmosphere), where the remaining solvent was removed under vacuum. Once all the solvent was removed, the cold finger was filled with chilled *iso*-propanol (cooled through the addition of liquid nitrogen) and the temperature was held between -20 °C and -30 °C throughout the sublimation.

Once no crude solid remained, the *iso*-propanol was removed from the cold finger and the sublimation apparatus was transferred to the glovebox, where the purified

$^t\text{Bu}_2\text{Zn}$ was isolated, weighed and transferred into a clean, dry Schlenk flask (typical yield 5.0 g, 69%). Following removal from the glovebox, the bis-alkylzinc product was dissolved in the appropriate solvent (typically hexane or THF) and stored in the freezer at $-30\text{ }^\circ\text{C}$.

8.9 Instrumentation for Characterisational Procedures

8.9.1 Nuclear Magnetic Resonance (NMR) Spectroscopy

^1H NMR spectra were recorded on a Brüker AV3, AV400 or DRX 500 spectrometer, operating at 400.13, 400.03 or 500.13 MHz respectively. The same instruments, operating at 100.62, 100.60 or 125.77 MHz respectively were used to record $^{13}\text{C}\{\text{H}\}$ NMR spectra. All ^{13}C NMR spectra were proton decoupled. The chemical shifts are quoted relative to TMS at 0.00 ppm. Correlations between hydrogen atoms and carbon atoms were obtained through COSY (correlation spectroscopy) and HSQC (heteronuclear single quantum correlation) NMR spectroscopic methods.^[354] The NMR abbreviations are as follows: s (singlet); d (doublet); t (triplet); q (quartet); m (multiplet) and br (broad peak).

The Diffusion-Ordered Spectroscopy (DOSY) NMR experiments were performed on a Brüker AV400 NMR spectrometer operating at 400.13 MHz for proton resonance under TopSpin (version 2.0, Brüker Biospin, Karlsruhe) and equipped with a BBFO-z-atm probe with actively shielded z-gradient coil capable of delivering a maximum gradient strength of 54 G/cm. Diffusion ordered NMR data were acquired using the Brüker pulse program dstegp3s employing a double stimulated echo with three spoiling gradients. Sine-shaped gradient pulses were used with a duration of 3 ms together with a diffusion period of 100 ms. Gradient recovery delays of 200 μs followed the application of each gradient pulse. Data was accumulated by linearly varying the diffusion encoding gradients over a range from 2% to 95% of maximum for 64 gradient increment values. DOSY plot was generated by use of the DOSY

processing module of TopSpin. Parameters were optimized empirically to find the best quality of data for presentation purposes.

8.9.2 Elemental Microanalysis

Elemental (C, H, N) analysis was performed in order to obtain percentage values of the elemental composition of the compounds synthesised. This was carried out using a Perkin Elmer 2400 elemental analyser. Microanalysis samples were prepared in an argon filled glovebox, and were sealed in an air-tight box prior to removal from the glovebox. However, due to the extreme air- and moisture-sensitivity of the compounds synthesised, it was not always possible to obtain reliable microanalysis results despite several attempts.

8.10 X-Ray Diffraction Studies

Single crystals suitable for X-ray diffraction studies were grown in Schlenk flasks under an argon atmosphere, at various temperatures and concentrations. Single-crystal X-ray diffraction data were recorded on Oxford Diffraction Gemini S or Oxford Diffraction Xcalibur E diffractometers using graphite-monochromatic $\text{MoK}\alpha$ radiation ($\lambda = 0.71073 \text{ \AA}$) or $\text{CuK}\alpha$ radiation ($\lambda = 1.54180 \text{ \AA}$). The structures were solved by direct methods (SHELX-97) and refined on all unique F^2 values (SHELX).^[355]

Crystallographic data for the compounds synthesised within this PhD study are contained within the relevant Chapters. Additional crystallographic data can be found on the disk inserted at the back of the thesis.

Chapter 9

Bibliography

“Every honest researcher I know admits he's just a professional amateur.
He's doing whatever he's doing for the first time.
That makes him an amateur.
He has sense enough to know that he's going to have a lot of trouble,
so that makes him a professional.”

Charles Kettering
American engineer and inventor

- [1] J. A. Labinger, J. E. Bercaw, *Nature* **2002**, *417*, 507-514.
- [2] T. R. Verhoeven, D. Askin, *U.S. Pat.* **4,820,850**, **1989**.
- [3] O. Lohse, U. Beutler, P. Fünfschilling, P. Furet, J. France, D. Kaufmann, G. Penn, W. Zaugg, *Tetrahedron Lett.* **2001**, *42*, 385-389.
- [4] J. A. Gladysz, Z. T. Ball, G. Bertrand, S. A. Blum, V. M. Dong, R. Dorta, F. E. Hahn, M. G. Humphrey, W. D. Jones, J. Klosin, I. Manners, T. J. Marks, J. M. Mayer, B. Rieger, J. C. Ritter, A. P. Sattelberger, J. M. Schomaker, V. W.-W. Yam, *Organometallics* **2011**, *31*, 1-18.
- [5] V. Grignard, *Ann. Chim. Phys.* **1901**, *24*, 433-490.
- [6] T. T. Tidwell, *Angew. Chem. Int. Ed.* **2001**, *40*, 331-337.
- [7] W. Schlenk, J. Holtz, *Ber. Dtsch. Chem. Ges.* **1917**, *50*, 262-274.
- [8] R. E. Mulvey, *Dalton Trans.* **2013**, *42*, 6676-6693.
- [9] a) S. Ozaki, T. Akyama, A. Isaka, M. Machida, K. Kageyama, *JP 05032585*, **1993**, b) G. Wu, M. Huang, *Chem. Rev.* **2006**, *106*, 2596-2616.
- [10] a) K. Okuhara, K. Kodaira, *JP 62209083*, **1987**, b) R. Wingen, W. Schmidt, *JP 2001316323*, **2001**.
- [11] C. J. Hayes, N. S. Simpkins, *Org. Biomol. Chem.* **2013**, *11*, 8458-8462.
- [12] a) L. Viteva, T. Gospodova, Y. Stefanovski, M.-R. Mazières, J. G. Wolf, *Tetrahedron Lett.* **2001**, *42*, 7945-7948, b) C. Arbez-Gindre, B. R. Steele, G. A. Heropoulos, C. G. Screttas, J.-E. Communal, W. J. Blau, I. Ledoux-Rak, *J. Organomet. Chem.* **2005**, *690*, 1620-1626.
- [13] a) P. Kraft, *WO 2009129643*, **2009**, b) J. Smets, H. R. G. Denuette, A. Pintens, D. T. Stanton, K. v. Aken, I. H. H. Laureyn, B. Denolf, F. A. C. Vrielynck, *US 20100137178*, **2010**.
- [14] F. I. Chirskii, A. P. Boldyrev, N. N. Shapovalova, *RU2083599-C1*, Voronezhskintezkauchuk Stock Co. (Voro-Soviet Institute).
- [15] a) M. Winter, J. O. Besenhard, M. E. Spahr, P. Novak, *Adv. Mater.* **1998**, *10*, 725-763, b) M. S. Whittingham, *Chem. Rev.* **2004**, *104*, 4271-4301, c) P. G. Bruce, B. Scrosati, J. M. Tarascon, *Angew. Chem. Int. Ed.* **2008**, *47*, 2930-2946.
- [16] A survey of total syntheses compiled by Hans J. Reich and co-workers revealed lithium diisopropylamine to be the most commonly used reagent, reported in the database at <http://www.chem.wisc.edu/areas/reich/syntheses/syntheses.htm>.
- [17] Reported on the FMC company website <http://www.fmclithium.com/Portals/FMCLithiumEnergy/Content/Docs/Jefferies Conference Feb 2012 FINAL.pdf>.
- [18] A. Bondi, *J. Phys. Chem.* **1964**, *68*, 441-451.
- [19] F. M. Bickelhaupt, M. Solà, C. F. Guerra, *J. Mol. Model* **2006**, *12*, 563-568.
- [20] R. E. Mulvey, F. Mongin, M. Uchiyama, Y. Kondo, *Angew. Chem. Int. Ed.* **2007**, *46*, 3802-3824.
- [21] R. A. Olofson, C. M. Dougherty, *J. Am. Chem. Soc.* **1973**, *95*, 582-584.
- [22] R. E. Mulvey, S. D. Robertson, *Angew. Chem. Int. Ed.* **2013**, *52*, 11470-11487.
- [23] a) M. W. Rathke, R. Kow, *J. Am. Chem. Soc.* **1972**, *94*, 6854-6856, b) R. A. Olofson, C. M. Dougherty, *J. Am. Chem. Soc.* **1973**, *95*, 581-582.
- [24] a) J. Clayden, *Organolithiums: Selectivity for Synthesis*, *23*, 1st Edition, Elsevier Science Ltd., Oxford, UK, **2002**, b) T. Stey, D. Stalke, *The*

- Chemistry of Organolithium Compounds*, John Wiley and Sons, Ltd., Chichester, U.K., **2004**, c) H. W. Gschwend, H. R. Rodriguez, *Heteroatom-Facilitated Lithiations Organic Reactions*, John Wiley & Sons, Hoboken, New Jersey, **2005**, d) M. Schlosser, *Organometallics in Synthesis*, John Wiley and Sons, Inc., Hoboken, New Jersey, **2013**.
- [25] F. Faigl, M. Schlosser, *Tetrahedron Lett.* **1991**, 32, 3369-3370.
- [26] J. S. Nicholson, S. S. Adams, *GB 971700*, Boots Pure Drug Co. Ltd., **1964**.
- [27] M.-L. Hsueh, B.-T. Ko, T. Athar, C.-C. Lin, T.-M. Wu, S.-F. Hsu, *Organometallics* **2006**, 25, 4144-4149.
- [28] a) H. Dietrich, *Acta Cryst.* **1963**, 16, 681-689, b) H. Dietrich, *J. Organomet. Chem.* **1981**, 205, 291-299.
- [29] T. Kottke, D. Stalke, *Angew. Chem. Int. Ed.* **1993**, 32, 580-582.
- [30] T. Kottke, D. Stalke, *J. Appl. Cryst.* **1993**, 26, 615-619.
- [31] E. Weiss, E. A. C. Lucken, *J. Organomet. Chem.* **1964**, 2, 197-205.
- [32] a) A. J. Chalk, T. J. Hoozeboom, *J. Organomet. Chem.* **1968**, 11, 615-618, b) J. F. Remenar, B. L. Lucht, D. Kruglyak, F. E. Romesburg, J. H. Gilchirst, D. B. Collum, *J. Org. Chem.* **1997**, 62, 5748-5754, c) R. A. Rennels, A. J. Maliakal, D. B. Collum, *J. Am. Chem. Soc.* **1998**, 120, 421-422, d) J. L. Rutherford, D. Hoffmann, D. B. Collum, *J. Am. Chem. Soc.* **2002**, 124, 264-271, e) J. M. Gruver, L. R. Liou, A. J. McNeil, A. Ramirez, D. B. Collum, *J. Org. Chem.* **2008**, 73, 7743-7747.
- [33] D. B. Collum, *Acc. Chem. Res.* **1992**, 25, 448-454.
- [34] M. A. Nichols, P. G. Williard, *J. Am. Chem. Soc.* **1993**, 115, 1568-1572.
- [35] N. D. R. Barnett, R. E. Mulvey, W. Clegg, P. A. O'Neil, *J. Am. Chem. Soc.* **1993**, 115, 1573-1574.
- [36] T. Tatic, S. Hermann, M. John, A. Loquet, A. Lange, D. Stalke, *Angew. Chem. Int. Ed.* **2011**, 50, 6666-6669.
- [37] T. Tatic, H. Ott, D. Stalke, *Eur. J. Inorg. Chem.* **2008**, 3765-3768.
- [38] C. Strohmam, V. H. Gessner, *Angew. Chem. Int. Ed.* **2007**, 46, 4566-4569.
- [39] D. R. Armstrong, D. Barr, W. Clegg, S. M. Hodgson, R. E. Mulvey, D. Reed, R. Snaith, D. S. Wright, *J. Am. Chem. Soc.* **1989**, 111, 4719-4727.
- [40] B. Tecele, A. F. M. M. Rahman, J. P. Olivier, *J. Organomet. Chem.* **1986**, 317, 267-275.
- [41] P. Schorigin, *Ber. Dtsch. Chem. Ges.* **1908**, 41, 2723-2728.
- [42] M. C. Whisler, S. MacNeil, V. Snieckus, P. Beak, *Angew. Chem. Int. Ed.* **2004**, 43, 2206-2225.
- [43] M. Al-Aseer, P. Beak, D. Hay, D. J. Kempf, S. Mills, S. G. Smith, *J. Am. Chem. Soc.* **1983**, 105, 2080-2082.
- [44] D. R. Hay, Z. Song, S. G. Smith, P. Beak, *J. Am. Chem. Soc.* **1988**, 110, 8145-8153.
- [45] V. Snieckus, *Chem. Rev.* **1990**, 90, 879-933.
- [46] D. W. Slocum, T. K. Reinscheld, C. B. White, M. D. Timmons, P. A. Shelton, M. G. Slocum, R. D. Sandlin, E. G. Holland, D. Kusmic, J. A. Jennings, K. C. Tekin, Q. Nguyen, S. J. Bush, J. M. Keller, P. E. Whitley, *Organometallics* **2013**, 32, 1674-1686.
- [47] H. Nishiyama, K. Isaka, K. Itoh, K. Ohno, H. Nagase, K. Matsumoto, H. Yoshiwara, *J. Org. Chem.* **1992**, 57, 407-410.
- [48] D. E. Applequist, D. F. O'Brien, *J. Am. Chem. Soc.* **1963**, 85, 743-748.

- [49] M. Giannerini, V. Hornillos, C. Vila, M. Fañanás-Mastral, B. L. Feringa, *Angew. Chem. Int. Ed.* **2013**, *52*, 13329-13333.
- [50] H. J. Reich, D. P. Green, N. H. Phillips, *J. Am. Chem. Soc.* **1991**, *113*, 1414-1416.
- [51] H. J. Reich, N. H. Phillips, *J. Am. Chem. Soc.* **1986**, *108*, 2102-2103.
- [52] H. R. Rogers, J. Houk, *J. Am. Chem. Soc.* **1982**, *104*, 522-525.
- [53] H. J. Reich, N. H. Phillips, I. L. Reich, *J. Am. Chem. Soc.* **1985**, *107*, 4101-4103.
- [54] H. J. Reich, D. P. Green, N. H. Phillips, *J. Am. Chem. Soc.* **1989**, *111*, 3444-3445.
- [55] a) D. Barr, W. Clegg, R. E. Mulvey, R. Snaith, *J. Chem. Soc., Chem Commun.* **1984**, 226-227, b) D. Barr, W. Clegg, R. E. Mulvey, R. Snaith, *J. Chem. Soc., Chem Commun.* **1984**, 285-287, c) D. Barr, W. Clegg, R. E. Mulvey, D. Reed, R. Snaith, *Angew. Chem. Int. Ed.* **1985**, *24*, 328-329, d) K. Jens, J. Kopf, N. P. Lorenzen, E. Weiss, *Chem. Ber.* **1988**, *121*, 1201-1202, e) D. R. Armstrong, D. Barr, A. T. Brooker, W. Clegg, K. Gregory, S. M. Hodgson, R. Snaith, D. S. Wright, *Angew. Chem. Int. Ed.* **1990**, *29*, 410-411, f) D. R. Armstrong, D. Barr, P. R. Raithby, R. Snaith, D. S. Wright, P. v. R. Schleyer, *Inorg. Chem. Acta* **1991**, *185*, 163-167, g) Y. Tang, L. N. Zakharov, A. L. Rheingold, R. A. Kemp, *Polyhedron* **2005**, *24*, 1739-1748, h) P. C. Andrews, M. Minopoulos, E. G. Roberston, *Eur. J. Inorg. Chem.* **2006**, 2865-2870.
- [56] H. Reich, W. L. Whipple, *Can. J. Chem.* **2005**, *83*, 1577-1587.
- [57] W. B. Farnham, J. C. Calabrese, *J. Am. Chem. Soc.* **1986**, *108*, 2449-2451.
- [58] H. J. Reich, M. J. Bevan, B. Ö. Gudmundsson, C. L. Puckett, *Angew. Chem. Int. Ed.* **2002**, *41*, 3436-3439.
- [59] D. Bryce-Smith, *J. Chem. Soc.* **1956**, 1603-1610.
- [60] a) W. F. Bailey, J. J. Patricia, V. C. DelGobbo, R. M. Jarret, P. J. Okarma, *J. Am. Chem. Soc.* **1985**, *50*, 1999-2000, b) M. Newcomb, W. G. Williams, E. L. Crumpacker, *Tetrahedron Lett.* **1985**, *26*, 1183-1184.
- [61] a) H. R. Ward, R. G. Lawler, R. A. Cooper, *J. Am. Chem. Soc.* **1969**, *91*, 746-748, b) A. R. Lepley, R. L. Landau, *J. Am. Chem. Soc.* **1969**, *91*, 748-749, c) W. F. Bailey, J. J. Patricia, *J. Organomet. Chem.* **1988**, *352*, 1-46.
- [62] H. R. Ward, *J. Am. Chem. Soc.* **1967**, *89*, 5517-5518.
- [63] a) A. Thaler, D. Seebach, F. Cardinaux, *Helv. Chim. Acta.* **1991**, *74*, 617-627, b) A. Thaler, D. Seebach, F. Cardinaux, *Helv. Chim. Acta.* **1991**, *74*, 628-643.
- [64] L. Gupta, A. C. Hoepker, K. J. Singh, D. B. Collum, *J. Org. Chem.* **2009**, *74*, 2231-2233.
- [65] F. M. Piller, P. Appukkuttan, A. Gavryushin, M. Helm, P. Knochel, *Angew. Chem. Int. Ed.* **2008**, *47*, 6802-6806.
- [66] E. C. Ashby, S. R. Noding, *J. Org. Chem.* **1979**, *44*, 4371-4377.
- [67] E. Hevia, R. E. Mulvey, *Angew. Chem. Int. Ed.* **2011**, *50*, 6448-6450.
- [68] A. C. Hoepker, L. Gupta, Y. Ma, M. F. Faggini, D. B. Collum, *J. Am. Chem. Soc.* **2011**, *133*, 7135-7151.
- [69] a) E. C. Ashby, J. Laemmle, H. M. Neumann, *Acc. Chem. Res.* **1974**, *7*, 272-280, b) P. Knochel, W. Dohle, N. Gommermann, F. F. Kneisel, F. Kopp, T. Korn, I. Sapountzis, V. A. Vu, *Angew. Chem. Int. Ed.* **2003**, *42*, 4302-4320.

- [70] a) C. R. Hauser, H. G. Walker, *J. Am. Chem. Soc.* **1947**, *69*, 295-297, b) F. C. Frostick, C. R. Hauser, *J. Am. Chem. Soc.* **1949**, *71*, 1350-1352.
- [71] W. Schlenk, *Ber. Dtsch. Chem. Ges.* **1929**, *62*, 920-924.
- [72] A. Krasovskiy, P. Knochel, *Angew. Chem. Int. Ed.* **2004**, *43*, 3333-3336.
- [73] B. Haag, M. Mosrin, H. Ila, V. Malakhov, P. Knochel, *Angew. Chem. Int. Ed.* **2011**, *50*, 9794-9824.
- [74] P. García-Álvarez, D. V. Graham, E. Hevia, A. R. Kennedy, J. Klett, R. E. Mulvey, C. T. O'Hara, S. Weatherstone, *Angew. Chem. Int. Ed.* **2008**, *47*, 8079-8081.
- [75] D. R. Armstrong, P. García-Álvarez, A. R. Kennedy, R. E. Mulvey, J. A. Parkinson, *Angew. Chem. Int. Ed.* **2010**, *49*, 3185-3188.
- [76] S. H. Wunderlich, M. Kienle, P. Knochel, *Angew. Chem. Int. Ed.* **2009**, *48*, 7256-7260.
- [77] a) E. Frankland, *Liebigs Ann. Chem.* **1849**, *71*, 171-213, b) D. Seyferth, *Organometallics* **2001**, *20*, 2940-2955.
- [78] J. Bacsa, F. Hanke, S. Hindley, R. Odedra, G. R. Darling, A. C. Jones, A. Steiner, *Angew. Chem. Int. Ed.* **2011**, *50*, 11685-11687.
- [79] J. Lewiński, M. Dranka, W. Bury, W. Śliwiński, I. Justyniak, J. Lipkowski, *J. Am. Chem. Soc.* **2007**, *129*, 3096-3098.
- [80] a) S. Reformatsky, *Ber. Dtsch. Chem. Ges.* **1887**, *20*, 1210-1211, b) P. G. Cozzi, A. Mignogna, L. Zoli, *Pure Appl. Chem.* **2008**, *80*, 891-901.
- [81] J. A. Casares, P. Espinet, B. Fuentes, G. Salas, *J. Am. Chem. Soc.* **2007**, *129*, 3508-3509.
- [82] E. Negishi, T. Takahashi, A. O. King, *Org. Synth.* **1988**, *66*, 67-74.
- [83] A. O. King, N. Okukado, E. Negishi, *J. Chem. Soc., Chem Commun.* **1977**, 683-684.
- [84] E. Negishi, T. Takahashi, S. Baba, *Org. Synth.* **1988**, *66*, 60-66.
- [85] H. E. Simmons, R. D. Smith, *J. Am. Chem. Soc.* **1958**, *80*, 5323-5324.
- [86] S. Inoue, H. Koinuma, T. Tsuruta, *J. Polym. Sci., Part B* **1969**, *7*, 287-292.
- [87] G. W. Coates, D. R. Moore, *Angew. Chem. Int. Ed.* **2004**, *43*, 6618-6639 See references within.
- [88] D. J. Darensbourg, M. W. Holtcamp, *Macromolecules* **1995**, *28*, 7577-7579.
- [89] R. Eberhardt, M. Allmendinger, G. A. Luinstra, B. Rieger, *Organometallics* **2002**, *22*, 211-214.
- [90] a) M. Cheng, A. B. Attygalle, E. B. Lobkovsky, G. W. Coates, *J. Am. Chem. Soc.* **1999**, *121*, 11583-11584, b) L. R. Rieth, D. R. Moore, E. B. Lobkovsky, G. W. Coates, *J. Am. Chem. Soc.* **2002**, *124*, 15239-15248.
- [91] B. M. Chamberlain, M. Cheng, D. R. Moore, T. M. Ovitt, E. B. Lobkovsky, G. W. Coates, *J. Am. Chem. Soc.* **2001**, *123*, 3229-3238.
- [92] E. Frankland, *J. Chem. Soc.* **1962**, *15*, 363-381.
- [93] J. Lewiński, Z. Ochal, E. Bojarski, E. Tratkiewicz, I. Justyniak, J. Lipkowski, *Angew. Chem. Int. Ed.* **2003**, *42*, 4643-4646.
- [94] M. Kubisiak, K. Zelga, I. Justyniak, E. Tratkiewicz, T. Pietrzak, A. R. Keeri, Z. Ochal, L. Hartenstein, P. W. Roesky, J. Lewinski, *Organometallics* **2013**, *32*, 5263-5265.
- [95] J. Lewiński, M. Koscielski, K. Suwala, I. Justyniak, *Angew. Chem. Int. Ed.* **2009**, *48*, 7017-7020.

- [96] a) J. Lewiński, K. Suwala, M. Kubisiak, Z. Ochal, I. Justyniak, J. Lipkowski, *Angew. Chem. Int. Ed.* **2008**, *47*, 7888-7891, b) J. Lewiński, K. Suwala, T. Kaczorowski, M. Galezowski, D. T. Gryko, I. Justyniak, J. Lipkowski, *Chem. Commun.* **2009**, 215-217, c) N. Hollingsworth, A. L. Johnson, A. Kingsley, G. Kockiok-Kohn, K. C. Molloy, *Organometallics* **2011**, *30*, 4470-4470, d) P. Sobota, R. Petrus, K. Zelga, L. Makolski, D. Kubicki, J. Lewinski, *Chem. Commun.* **2013**, *49*, 10477-10479.
- [97] J. Lewiński, W. Marciniak, J. Lipkowski, I. Justyniak, *J. Am. Chem. Soc.* **2003**, *125*, 12698-12699.
- [98] J. Lewiński, W. Śliwiński, M. Dranka, I. Justyniak, J. Lipkowski, *Angew. Chem. Int. Ed.* **2006**, *45*, 4826-4829.
- [99] T. Cohen, H. Gibney, R. Ivanov, E. A. H. Yeh, I. Marek, D. P. Curran, *J. Am. Chem. Soc.* **2007**, *129*, 15405-15409.
- [100] a) T. E. Müller, M. Grosche, E. Herdtweck, A.-K. Pleier, E. Walter, Y.-K. Yan, *Organometallics* **1999**, *19*, 170-183, b) A. Zulys, M. Dochnahl, D. Hollmann, K. Löhnwitz, J.-S. Herrmann, P. W. Roesky, S. Blechert, *Angew. Chem. Int. Ed.* **2005**, *44*, 7794-7798, c) M. Dochnahl, J.-W. Pissarek, S. Blechert, K. Lohnwitz, P. W. Roesky, *Chem. Commun.* **2006**, 3405-3407, d) M. Dochnahl, K. Löhnwitz, J.-W. Pissarek, M. Biyikal, S. R. Schulz, S. Schön, N. Meyer, P. W. Roesky, S. Blechert, *Chem. Eur. J.* **2007**, *13*, 6654-6666, e) M. Biyikal, K. Löhnwitz, N. Meyer, M. Dochnahl, P. W. Roesky, S. Blechert, *Eur. J. Inorg. Chem.* **2010**, 1070-1081.
- [101] A. Ates, C. Quinet, *Eur. J. Org. Chem.* **2003**, 1623-1626.
- [102] M. R. Crimmin, I. J. Casely, M. S. Hill, *J. Am. Chem. Soc.* **2005**, *127*, 2042-2043.
- [103] F. Pohlki, S. Doye, *Chem. Soc. Rev.* **2003**, *32*, 104-114.
- [104] S. J. Hong, T. J. Marks, *Acc. Chem. Res.* **2004**, *37*, 673-686.
- [105] J. Hannedouche, E. Schulz, *Chem. Eur. J.* **2013**, *19*, 4972-4985.
- [106] R. Dorta, P. Egli, F. Zürcher, A. Togni, *J. Am. Chem. Soc.* **1997**, *119*, 10857-10858.
- [107] M. Utsunomiya, R. Kuwano, M. Kawatsura, J. F. Hartwig, *J. Am. Chem. Soc.* **2003**, *125*, 5608-5609.
- [108] a) M. Utsunomiya, J. F. Hartwig, *J. Am. Chem. Soc.* **2003**, *125*, 14286-14287, b) K. Li, K. K. Hii, *Chem. Commun.* **2003**, 1132-1133.
- [109] a) C. F. Bender, R. A. Widenhoefer, *J. Am. Chem. Soc.* **2005**, *127*, 1070-1071, b) J.-J. Brunet, N. C. Chu, O. Diallo, *Organometallics* **2005**, *24*, 3104-3110.
- [110] L. Fadini, A. Togni, *Chem. Commun.* **2003**, 30-31.
- [111] C. Brinkmann, A. G. M. Barrett, M. S. Hill, P. A. Procopiou, *J. Am. Chem. Soc.* **2012**, *134*, 2193-2207.
- [112] M. R. Crimmin, M. Arrowsmith, A. G. M. Barrett, I. J. Casely, M. S. Hill, P. A. Procopiou, *J. Am. Chem. Soc.* **2009**, *131*, 9670-9685.
- [113] M. Arrowsmith, M. S. Hill, G. Kociok-Köhn, *Organometallics* **2009**, *28*, 1730-1738.
- [114] A. G. M. Barrett, M. R. Crimmin, M. S. Hill, P. B. Hitchcock, G. Kociok-Köhn, P. A. Procopiou, *Inorg. Chem.* **2008**, *47*, 7366-7376.
- [115] I. Resa, E. Carmona, E. Gutierrez-Puebla, A. Monge, *Science* **2004**, *305*, 1136-1138.

- [116] L. Pauling, *The Nature of the Chemical Bond*, 3rd Edition, Cornell University Press, Ithaca, NY, **1960**.
- [117] D. H. Kerridge, S. A. Tariq, *J. Chem. Soc. A* **1967**, 1122-1125.
- [118] E. Carmona, A. Galindo, *Angew. Chem. Int. Ed.* **2008**, *47*, 6526-6536.
- [119] a) T. Li, S. Schulz, P. W. Roesky, *Chem. Soc. Rev.* **2012**, *41*, 3759-3771, b) J. Gao, S. Li, Y. Zhao, B. Wu, X.-J. Yang, *Organometallics* **2012**, *31*, 2978-2985.
- [120] S. P. Green, C. Jones, A. Stasch, *Science* **2007**, *318*, 1754-1757.
- [121] A. Grirrane, I. Resa, A. Rodríguez, E. Carmona, E. Alvarez, E. Gutiérrez-Puebla, A. Monge, A. Galindo, D. del Río, R. A. Andersen, *J. Am. Chem. Soc.* **2007**, *129*, 693-703.
- [122] Y. Wang, B. Quillian, P. Wei, H. Wang, X.-J. Yang, Y. Xie, R. B. King, P. v. R. Schleyer, H. F. Schaefer, G. H. Robinson, *J. Am. Chem. Soc.* **2005**, *127*, 11944-11945.
- [123] S. Schulz, D. Schuchmann, I. Krossing, D. Himmel, D. Bläser, R. Boese, *Angew. Chem. Int. Ed.* **2009**, *48*, 5748-5751.
- [124] S. Schulz, S. Gondzik, D. Schuchmann, U. Westphal, L. Dobrzycki, R. Boese, S. Harder, *Chem. Commun.* **2010**, *46*, 7757-7759.
- [125] T. Bollermann, K. Freitag, C. Gemel, R. W. Seidel, R. A. Fischer, *Organometallics* **2011**, *30*, 4123-4127.
- [126] A. Luhl, H. P. Nayek, S. Blechert, P. W. Roesky, *Chem. Commun.* **2011**, *47*, 8280-8282.
- [127] a) J. H. Clark, *Green Chem.* **1999**, *1*, 1-8, b) P. T. Anastas, M. M. Kirchhoff, *Acc. Chem. Res.* **2002**, *35*, 686-694, c) M. Poliakoff, J. M. Fitzpatrick, T. R. Farren, P. T. Anastas, *Science* **2002**, *297*, 807-810, d) D. J. C. Constable, P. J. Dunn, J. D. Hayler, G. R. Humphrey, J. L. Leazer, R. J. Linderman, K. Lorenz, J. Manley, B. A. Pearlman, A. Wells, A. Zaks, T. Y. Zhang, *Green Chem.* **2007**, *9*, 411-420.
- [128] Y. Kondo, M. Shilai, M. Uchiyama, T. Sakamoto, *J. Am. Chem. Soc.* **1999**, *121*, 3539-3540.
- [129] D. R. Armstrong, A. R. Kennedy, R. E. Mulvey, J. A. Parkinson, S. D. Robertson, *Chem. Sci.* **2012**, *3*, 2700-2707.
- [130] a) R. E. Mulvey, *Organometallics* **2006**, *25*, 1060-1075, b) R. E. Mulvey, *Acc. Chem. Res.* **2009**, *42*, 743-755, c) A. Harrison-Marchand, F. Mongin, *Chem. Rev.* **2013**, *113*, 7470-7562, d) A. Harrison-Marchand, F. Mongin, *Chem. Rev.* **2013**, *113*, 7563-7727.
- [131] H. J. Reich, *Chem. Rev.* **2013**, *113*, 7130-7178.
- [132] a) L. Lochmann, J. Pospíšil, D. Lím, *Tetrahedron Lett.* **1966**, *7*, 257-262, b) M. Schlosser, *J. Organomet. Chem.* **1967**, *8*, 9-16, c) M. Schlosser, *Pure Appl. Chem.* **1988**, *60*, 1627-1634, d) M. Schlosser, H. C. Jung, S. Takagishi, *Tetrahedron* **1990**, *46*, 5633-5648, e) C. Unkelbach, D. F. O'Shea, C. Strohmman, *Angew. Chem. Int. Ed.* **2013**, 10.1002/anie.201306884.
- [133] P. Caubère, *Chem. Rev.* **1993**, *93*, 2317-2334.
- [134] P. Fleming, D. F. O'Shea, *J. Am. Chem. Soc.* **2011**, *133*, 1698-1701.
- [135] P. Gros, Y. Fort, *Eur. J. Org. Chem.* **2002**, 3375-3383.
- [136] G. Wittig, F. J. Meyer, G. Lange, *Justus Liebigs Ann. Chem.* **1951**, *571*, 167-201.

- [137] L. Pauling, *General Chemistry An Introduction to Descriptive Chemistry and Modern Chemical Theory*, W.H. Freeman, San Francisco, California, **1947**.
- [138] J. A. Wanklyn, *Justus Liebigs Ann. Chem.* **1858**, *107*, 125-128.
- [139] J. S. Thayer, *J. Chem. Educ.* **1969**, *46*, 764.
- [140] a) P. C. Andrikopoulos, D. R. Armstrong, H. R. L. Barley, W. Clegg, S. H. Dale, E. Hevia, G. W. Honeyman, A. R. Kennedy, R. E. Mulvey, *J. Am. Chem. Soc.* **2005**, *127*, 6184-6185, b) A. Seggio, F. Chevallier, M. Vaultier, F. Mongin, *J. Org. Chem.* **2007**, *72*, 6602-6605.
- [141] E. Weiss, R. Wolfrum, *Chem. Ber.* **1968**, *101*, 35-40.
- [142] W. Clegg, S. H. Dale, E. Hevia, G. W. Honeyman, R. E. Mulvey, *Angew. Chem. Int. Ed.* **2006**, *45*, 2370-2374.
- [143] a) P. C. Andrikopoulos, D. R. Armstrong, D. V. Graham, E. Hevia, A. R. Kennedy, R. E. Mulvey, C. T. O'Hara, C. Talmard, *Angew. Chem. Int. Ed.* **2005**, *44*, 3459-3462, b) W. Clegg, S. H. Dale, R. W. Harrington, E. Hevia, G. W. Honeyman, R. E. Mulvey, *Angew. Chem. Int. Ed.* **2006**, *45*, 2374-2377, c) D. R. Armstrong, W. Clegg, S. H. Dale, E. Hevia, L. M. Hogg, G. W. Honeyman, R. E. Mulvey, *Angew. Chem. Int. Ed.* **2006**, *45*, 3775-3778, d) W. Clegg, S. H. Dale, E. Hevia, L. M. Hogg, G. W. Honeyman, R. E. Mulvey, C. T. O'Hara, *Angew. Chem. Int. Ed.* **2006**, *45*, 6548-6550, e) B. Conway, E. Hevia, A. R. Kennedy, R. E. Mulvey, *Chem. Commun.* **2007**, 2864-2866.
- [144] E. Hevia, G. W. Honeyman, A. R. Kennedy, R. E. Mulvey, *J. Am. Chem. Soc.* **2005**, *127*, 13106-13107.
- [145] D. R. Armstrong, W. Clegg, S. H. Dale, D. V. Graham, E. Hevia, L. M. Hogg, G. W. Honeyman, A. R. Kennedy, R. E. Mulvey, *Chem. Commun.* **2007**, 598-600.
- [146] A. R. Lepley, W. A. Khan, A. B. Giumanini, A. G. Giumanini, *J. Org. Chem.* **1966**, *31*, 2047-2051.
- [147] D. R. Armstrong, L. Balloch, E. Hevia, A. R. Kennedy, R. E. Mulvey, C. T. O'Hara, S. D. Robertson, *Beilstein J. Org. Chem.* **2011**, *7*, 1234-1248.
- [148] D. Nobuto, M. Uchiyama, *J. Org. Chem.* **2008**, *73*, 1117-1120.
- [149] Y. Kondo, J. V. Morey, J. C. Morgan, H. Naka, D. Nobuto, P. R. Raithby, M. Uchiyama, A. E. H. Wheatley, *J. Am. Chem. Soc.* **2007**, *129*, 12734-12738.
- [150] M. R. Crimmin, A. G. M. Barrett, M. S. Hill, D. J. MacDougall, M. F. Mahon, P. A. Procopiou, *Dalton Trans.* **2009**, 9715-9717.
- [151] A. Maercker, *Angew. Chem. Int. Ed.* **1987**, *26*, 972-989.
- [152] A. R. Kennedy, J. Klett, R. E. Mulvey, D. S. Wright, *Science* **2009**, *326*, 706-708.
- [153] E. Crosbie, P. García-Álvarez, A. R. Kennedy, J. Klett, R. E. Mulvey, S. D. Robertson, *Angew. Chem. Int. Ed.* **2010**, *49*, 9388-9391.
- [154] R. E. Mulvey, V. L. Blair, W. Clegg, A. R. Kennedy, J. Klett, L. Russo, *Nature Chem.* **2010**, *2*, 588-591.
- [155] B. Conway, A. R. Kennedy, R. E. Mulvey, S. D. Robertson, J. García-Álvarez, *Angew. Chem. Int. Ed.* **2010**, *49*, 3182-3184.
- [156] B. Conway, J. García-Álvarez, E. Hevia, A. R. Kennedy, R. E. Mulvey, S. D. Robertson, *Organometallics* **2009**, *28*, 6462-6468.
- [157] J. G. MacLellan, A. R. Kennedy, R. E. Mulvey, *Acta Cryst. C.* **2003**, *59*, 302-303.

- [158] G. Wittig, G. Fuhrmann, *Chem. Ber.* **1940**, *73*, 1197-1218.
- [159] H. Gilman, R. L. Bebb, *J. Am. Chem. Soc.* **1939**, *61*, 109-112.
- [160] W. Bauer, P. v. R. Schleyer, *J. Am. Chem. Soc.* **1989**, *111*, 7191-7198.
- [161] J. M. Saá, P. M. Deyá, G. A. Suñer, A. Frontera, *J. Am. Chem. Soc.* **1992**, *114*, 9093-9100.
- [162] M. Stratakis, *J. Org. Chem.* **1997**, *62*, 3024-3025.
- [163] S. Harder, J. Boersma, L. Brandsma, G. P. M. v. Mier, J. A. Kanters, *J. Organomet. Chem.* **1989**, *364*, 1-15.
- [164] a) G. Wittig, *Naturwissenschaften* **1942**, *30*, 696-703, b) R. Huisgen, H. Rist, *Naturwissenschaften* **1954**, *41*, 358-359, c) G. Wittig, *Angew. Chem. Int. Ed.* **1965**, *4*, 731-737.
- [165] a) H. J. Reich, B. Ö. Gudmundsson, *J. Am. Chem. Soc.* **1996**, *118*, 6074-6075, b) J. Belzner, D. Schär, U. Dehnert, M. Noltemeyer, *Organometallics* **1997**, *16*, 285-288, c) J. Clayden, R. P. Davies, M. A. Hendy, R. Snaith, A. E. H. Wheatley, *Angew. Chem. Int. Ed.* **2001**, *40*, 1238-1240, d) D. R. Armstrong, S. R. Boss, J. Clayden, R. Haigh, B. A. Kirmani, D. J. Linton, P. Schooler, A. E. H. Wheatley, *Angew. Chem. Int. Ed.* **2004**, *43*, 2135-2138, e) M. Linnert, C. Bruhn, T. Rüffer, H. Schmidt, D. Steinborn, *Organometallics* **2004**, *23*, 3668-3673, f) C. M. P. Kronenburg, E. Rijnberg, J. T. B. H. Jastrzebski, H. Kooijman, A. L. Spek, G. v. Koten, *Eur. J. Org. Chem.* **2004**, 153-159, g) K. L. Jantzi, I. A. Guzei, H. J. Reich, *Organometallics* **2006**, *25*, 5390-5395.
- [166] A. Ogawa, D. P. Curran, *J. Org. Chem.* **1997**, *62*, 450-451.
- [167] R. E. Banks, *Organofluorine Chemicals and their Industrial Applications*, Ellis Horwood LTD, Chichester, U.K. **1979**.
- [168] J. D. Roberts, D. Y. Curtin, *J. Am. Chem. Soc.* **1946**, *68*, 1658-1660.
- [169] a) M. Charton, *J. Org. Chem.* **1976**, *41*, 2217-2220, b) I. de Raggi, A. Virgili, M. de Moragas, C. Jaime, *J. Org. Chem.* **1995**, *60*, 27-31, c) C. Wolf, W. A. König, C. Roussel, *Liebigs Ann.* **1995**, 781-786.
- [170] a) A. A. Morton, G. H. Patterson, J. J. Donovan, E. L. Little, *J. Am. Chem. Soc.* **1946**, *68*, 93-96, b) A. A. Morton, M. E. T. Holden, *J. Am. Chem. Soc.* **1947**, *69*, 1675-1681, c) A. A. Morton, F. D. Marsh, R. D. Coombs, A. L. Lyons, S. E. Penner, H. E. Ramsden, V. B. Baker, E. L. Little, R. L. Letsinger, *J. Am. Chem. Soc.* **1950**, *72*, 3785-3792, d) H. L. Hsieh, C. F. Wofford, *J. Polym. Sci., Part A* **1969**, *7*, 449-460.
- [171] M. Schlosser, G. Katsoulos, S. Takagishi, *Synlett* **1990**, 747-748.
- [172] D. R. Armstrong, V. L. Blair, W. Clegg, S. H. Dale, J. García-Álvarez, G. W. Honeyman, E. Hevia, R. E. Mulvey, L. Russo, *J. Am. Chem. Soc.* **2010**, *132*, 9480-9487.
- [173] M. Uchiyama, H. Naka, Y. Matsumoto, T. Ohwada, *J. Am. Chem. Soc.* **2004**, *126*, 10526-10527.
- [174] M. Granitzka, A.-C. Pöpller, E. K. Schwarze, D. Stern, T. Schulz, M. John, R. Herbst-Irmer, S. K. Pandey, D. Stalke, *J. Am. Chem. Soc.* **2012**, *134*, 1344-1351.
- [175] W. N. Setzer, P. v. R. Schleyer, *Adv. Organomet. Chem.* **1985**, *24*, 353-451.
- [176] W. Bauer, G. Müller, R. Pi, P. v. R. Schleyer, *Angew. Chem. Int. Ed.* **1986**, *25*, 1103-1104.

- [177] a) K. Gregory, P. v. R. Schleyer, R. Snaith, *Adv. Inorg. Chem.* **1991**, *37*, 47-142, b) D. Barr, W. Clegg, L. Cowton, L. Horsburgh, F. M. Mackenzie, R. E. Mulvey, *J. Chem. Soc., Chem Commun.* **1995**, 891-892, c) A. R. Kennedy, J. Klett, C. T. O'Hara, R. E. Mulvey, G. M. Robertson, *Eur. J. Inorg. Chem.* **2009**, 5029-5035, d) J. A. Garden, A. R. Kennedy, R. E. Mulvey, S. D. Robertson, *Dalton Trans.* **2011**, *40*, 11945-11954.
- [178] Search performed 19/11/13, Version 1.15 F. H. Allen, *Acta Crystallogr. B.* **2002**, *58*, 380-388.
- [179] a) U. Schümann, U. Behrens, E. Weiss, *Angew. Chem. Int. Ed.* **1989**, *28*, 476-477, b) R. d. Besten, M. T. Lakin, N. Veldman, A. L. Spek, L. Brandsma, *J. Organomet. Chem.* **1996**, *514*, 191-196.
- [180] R. E. Dinnebier, U. Behrens, F. Olbrich, *J. Am. Chem. Soc.* **1998**, *120*, 1430-1433.
- [181] D. Thoennes, E. Weiss, *Chem. Ber.* **1978**, *111*, 3157-3161.
- [182] K. P. Huber, G. Herzberg, *Molecular Spectra and Molecular Structure, IV. Constants of Diatomic Molecules*, Van-Nostrand Reinhold Company, New York, New York, **1979**.
- [183] T. Kottke, K. S. Sung, R. J. Lagow, *Angew. Chem. Int. Ed.* **1995**, *34*, 1517-1519.
- [184] D. Stalke, K. H. Whitmire, *J. Chem. Soc., Chem Commun.* **1990**, 833-834.
- [185] D. Stalke, N. Keweloh, U. Klingebiel, M. Noltemeyer, G. M. Sheldrick, *Z. Naturforsch., B: Chem. Sci.* **1987**, *42*, 1237-1244.
- [186] H. Li, G.-H. Lee, S.-M. Peng, *J. Mol. Struct.* **2004**, *707*, 179-186.
- [187] B. M. Vedavathi, K. Vijayan, *Acta Cryst. B.* **1977**, *33*, 946-948.
- [188] G. B. Deacon, C. M. Forsyth, P. C. Junk, J. Wang, *Chem. Eur. J.* **2009**, *15*, 3082-3092.
- [189] a) D. R. Armstrong, A. R. Kennedy, R. E. Mulvey, R. B. Rowlings, *Angew. Chem. Int. Ed.* **1999**, *38*, 131-133, b) A. J. Martinez-Martinez, D. R. Armstrong, B. Conway, B. J. Fleming, J. Klett, A. R. Kennedy, R. E. Mulvey, S. D. Robertson, C. T. O'Hara, *Chem. Sci.* **2014**, *5*, 771-781.
- [190] W. Kohn, A. D. Becke, R. G. Parr, *J. Phys. Chem.* **1996**, *100*, 12974-12980.
- [191] A. D. McLean, G. S. Chandler, *J. Chem. Phys.* **1980**, *72*, 5639-5648.
- [192] a) Y. Zhao, C. Mao, Y. Li, P. Zhang, Z. Huang, F. Bi, R. Huang, Q. Wang, *J. Agric. Food Chem.* **2008**, *56*, 7326-7332, b) Y. Zhao, Y. Li, X. Ou, P. Zhang, Z. Huang, F. Bi, R. Huang, Q. Wang, *J. Agric. Food Chem.* **2008**, *56*, 10176-10182, c) X. Shao, Z. Li, X. Qian, X. Xu, *J. Agric. Food Chem.* **2009**, *57*, 951-957.
- [193] a) M. Powell, R. D. Bailey, C. T. Eagle, G. L. Schimek, T. W. Hanks, W. T. Pennington, *Acta. Crystallogr.* **1997**, *C53*, 1611-1613, b) M. Mathis, W. Harsha, T. W. Hanks, *Chem. Mater.* **1998**, *10*, 3568-3575.
- [194] H. Sato, E. Senbara, T. Ogawa, *Int. J. Nanosci.* **2002**, *1*, 489-494.
- [195] a) M. D. Liptak, T. C. Brunold, *J. Am. Chem. Soc.* **2006**, *128*, 9144-9156, b) X. Li, L. W. Chung, P. Paneth, K. Morokuma, *J. Am. Chem. Soc.* **2009**, *131*, 5115-5125, c) L. Mardini, J. Gasiorek, A. Derjuga, L. Carriere, M. Schranzhofer, B. H. Paw, P. Ponka, V. Blank, *Biochem. J.* **2010**, *432*, 145-151, d) A. Cruz-Castaneda, M. Lopez-Casamichana, J. J. Olivares-Trejo, *Biochem. J.* **2011**, *434*, 105-111, e) B. J. Reeder, D. A. Svistunenko, M. T. Wilson, *Biochem. J.* **2011**, *434*, 483-492.

- [196] M. Baumann, I. R. Baxendale, S. V. Ley, N. Nikbin, *Beilstein J. Org. Chem.* **2011**, *7*, 442-495.
- [197] a) I. Hasan, E. R. Marinelli, L. C. C. Lin, F. W. Fowler, A. B. Levy, *J. Org. Chem.* **1981**, *46*, 157-164, b) G. R. Martinez, P. A. Grieco, C. V. Srinivasan, *J. Org. Chem.* **1981**, *46*, 3760-3761, c) J. M. Muchowski, D. R. Solas, *J. Org. Chem.* **1984**, *49*, 203-205, d) F. Faigl, K. Fogassy, A. Thurner, L. Töke, *Tetrahedron* **1997**, *53*, 4883-4888, e) P. Anzenbacher, K. Jursikova, J. A. Shriver, H. Miyaji, V. M. Lynch, J. L. Sessler, P. A. Gale, *J. Org. Chem.* **2000**, *65*, 7641-7645.
- [198] S. H. Wunderlich, P. Knochel, *Angew. Chem. Int. Ed.* **2009**, *48*, 1501-1504.
- [199] a) M. Uchiyama, Y. Matsumoto, S. Usui, Y. Hashimoto, K. Morokuma, *Angew. Chem. Int. Ed.* **2007**, *46*, 926-929, b) J. M. L'Helgoual'ch, G. Bentabed-Ababsa, F. Chevallier, M. Yonehara, M. Uchiyama, A. Derdour, F. Mongin, *Chem. Commun.* **2008**, *44*, 5375-5377, c) K. Snegaroff, J. M. L'Helgoual'ch, G. Bentabed-Ababsa, T. T. Nguyen, F. Chevallier, M. Yonehara, M. Uchiyama, A. Derdour, F. Mongin, *Chem. Eur. J.* **2009**, *15*, 10280-10290.
- [200] G. Dayaker, A. Sreeshailam, F. Chevallier, T. Riosnel, P. R. Krishna, F. Mongin, *Chem. Commun.* **2010**, *46*, 2862-2864.
- [201] a) S. J. Birch, S. R. Boss, S. C. Cole, M. P. Coles, R. Haigh, P. B. Hitchcock, A. E. H. Wheatley, *Dalton Trans.* **2004**, 3568-3574, b) A. E. H. Wheatley, *New J. Chem.* **2004**, *28*, 435-443.
- [202] J. M. L'Helgoual'ch, A. Seggio, F. Chevallier, M. Yonehara, E. Jeanneau, M. Uchiyama, F. Mongin, *J. Org. Chem.* **2008**, *73*, 177-183.
- [203] H. N. Hunter, N. Hadei, V. Blagojevic, P. Patschinski, G. T. Achonduh, S. Avola, D. K. Bohme, M. G. Organ, *Chem. Eur. J.* **2011**, *17*, 7845-7851.
- [204] K. H. Thiele, M. Bendull, *Z. Anorg. Allg. Chem.* **1970**, *379*, 199-203.
- [205] a) A. A. Bothner-By, R. L. Stephens, J. Lee, C. D. Warren, R. W. Jeanloz, *J. Am. Chem. Soc.* **1984**, *106*, 811-813, b) A. Bax, D. G. Davis, *J. Mag. Res.* **1985**, *63*, 207-213.
- [206] G. Zhu, J. M. Tanski, G. Parkin, *J. Chem. Cryst.* **2002**, *32*, 469-475.
- [207] R. Goddard, O. Heinemann, C. Kruger, *Acta Crystallogr.* **1997**, *C53*, 1846-1850.
- [208] a) L. Wang, Z. Shi, L. Guanghua, Y. Fan, W. Fu, S. Feng, *Solid State Sci.* **2004**, *6*, 85-90, b) M. Bera, G. T. Musie, D. R. Powell, *Inorg. Chem. Commun.* **2008**, *11*, 293-299, c) P. A. M. Williams, L. G. Naso, G. A. Echeverria, E. G. Ferrer, *J. Mol. Struct.* **2010**, *978*, 124-130.
- [209] a) K. Barthelet, D. Riou, G. Férey, *Solid State Sci.* **2002**, *4*, 841-844, b) M. Kontturi, E. Laurila, R. Mattsson, S. Peraniemi, J. J. Vepsalainen, M. Ahlgren, *Inorg. Chem.* **2005**, *44*, 2400-2406, c) Z. Lai, R. Fu, S. Hu, X. Wu, *Eur. J. Inorg. Chem.* **2007**, 5439-5446.
- [210] a) Y. Diskin-Posner, G. K. Patra, I. Goldberg, *Eur. J. Inorg. Chem.* **2001**, 2515-2523, b) Y. Diskin-Posner, I. Goldberg, *New J. Chem.* **2001**, *25*, 899-904.
- [211] E. Alvarez, A. Grirrane, I. Resa, D. del Río, A. Rodríguez, E. Carmona, *Angew. Chem. Int. Ed.* **2007**, *46*, 1296-1299.
- [212] J.-Y. Zhang, A.-L. Cheng, Q. Sun, Q. Yue, E.-Q. Gao, *Cryst. Growth Des.* **2010**, *10*, 2908-2915.

- [213] According to the method published by Houser, the Na centre of **17** has a distorted tetrahedral geometry, with a τ_4 value of 0.68. The value of τ_4 indicates a sliding scale where 1.00 represents an ideal tetrahedral geometry and 0.00 indicates an ideal square planar geometry. L. Yang, D. R. Powell, R. P. Houser, *Dalton Trans.* **2007**, 36, 955-964.
- [214] E. S. J. Robles, A. M. Ellis, T. A. Miller, *J. Phys. Chem.* **1992**, 96, 3258-3265.
- [215] a) D. Barr, W. Clegg, R. E. Mulvey, R. Snaith, D. S. Wright, *J. Chem. Soc., Chem Commun.* **1987**, 716-718, b) B. Conway, D. V. Graham, E. Hevia, A. R. Kennedy, J. Klett, R. E. Mulvey, *Chem. Commun.* **2006**, 2638-2640.
- [216] a) C. Schade, P. v. R. Schleyer, *Adv. Organomet. Chem.* **1987**, 27, 169-278, b) E. Weiss, *Angew. Chem. Int. Ed.* **1993**, 32, 1501-1523, c) R. E. Mulvey, *Chem. Soc. Rev.* **1998**, 27, 339-346, d) S. Schade, G. Boche, *J. Organomet. Chem.* **1998**, 550, 359-379.
- [217] I. Heldt, U. Behrens, *Z. Anorg. Allg. Chem.* **2005**, 631, 749-758.
- [218] D. R. Armstrong, C. Dougan, D. V. Graham, E. Hevia, A. R. Kennedy, *Organometallics* **2008**, 27, 6063-6070.
- [219] T. Greiser, J. Kopf, D. Thoennes, E. Weiss, *Chem. Ber.* **1981**, 114, 209-213.
- [220] E. Hevia, K. W. Henderson, A. R. Kennedy, R. E. Mulvey, *Organometallics* **2006**, 25, 1778-1785.
- [221] T. J. Boyle, M. A. Rodriguez, D. Ingersoll, T. J. Headley, S. D. Bunge, D. M. Pedrotty, S. M. De'Angeli, S. C. Vick, H. Fan, *Chem. Mater.* **2003**, 15, 3903-3912.
- [222] a) J. Seixas de Melo, F. Elisei, R. S. Becker, *J. Chem. Phys.* **2002**, 117, 4428-4435, b) T. Nishinaga, M. Tateno, M. Fujii, W. Fujita, M. Takase, M. Iyoda, *Org. Lett.* **2010**, 12, 5374-5377, c) M. M. Oliva, T. M. Pappenfus, J. H. Melby, K. M. Schwaderer, J. C. Johnson, K. A. McGee, D. A. da Silva Filho, J.-L. Bredas, J. Casado, J. T. López Navarrete, *Chem. Eur. J.* **2010**, 16, 6866-6876, d) T. Nishinaga, T. Miyata, M. Tateno, M. Koizumi, M. Takase, M. Iyoda, N. Kobayashi, Y. Kunugi, *J. Mater. Chem.* **2011**, 21, 14959-14966, e) V. Tamilavan, M. Song, S.-H. Jin, M. H. Hyun, *Polymer* **2011**, 52, 2384-2390.
- [223] S. Tanaka, S. Tamba, D. Tanaka, A. Sugie, A. Mori, *J. Am. Chem. Soc.* **2011**, 133, 16734-16737.
- [224] M. Fujii, T. Nishinaga, M. Iyoda, *Tetrahedron Lett.* **2009**, 50, 555-558.
- [225] L. Balloch, J. A. Garden, A. R. Kennedy, R. E. Mulvey, T. Rantanen, S. D. Robertson, V. Snieckus, *Angew. Chem. Int. Ed.* **2012**, 51, 6934-6937.
- [226] Z. Guo, Q. Liu, X. Wei, Y. Zhang, H. Tong, J. Chao, J. Guo, D. Liu, *Organometallics* **2013**, 32, 4677-4683.
- [227] N. Blaquiere, S. Do, D. Dudley, A. J. Folkes, R. A. Goldsmith, R. Heald, T. Heffron, A. Kolesnikov, C. Ndubaku, A. G. Olivero, S. Price, S. Staben, B. Wei, *WO 20110076291 A1*, **2011**.
- [228] N. D. P. Cosford, L. Bleicher, A. Herbaut, J. S. McCallum, J.-M. Vernier, H. Dawson, J. P. Whitten, P. Adams, L. Chavez-Noriega, L. D. Correa, J. H. Crona, L. S. Mahaffy, F. Menzaghi, T. S. Rao, R. Reid, A. I. Sacaan, E. Santori, K. A. Stauderman, K. Whelan, G. K. Lloyd, I. A. McDonald, *J. Med. Chem.* **1996**, 39, 3235-3237.

- [229] D. S. Garvey, J. T. Wasicak, R. L. Elliott, S. Lebold, A.-M. Hettinger, G. M. Carrera, N.-H. Lin, Y. He, M. W. Holladay, *J. Med. Chem.* **1994**, *37*, 4455-4463.
- [230] R. R. Knowles, S. Lin, E. N. Jacobsen, *J. Am. Chem. Soc.* **2010**, *132*, 5030-5032.
- [231] X. Jia, Q. Huang, J. Li, S. Li, Q. Yang, *Synlett* **2007**, 806-808.
- [232] a) D. Hoppe, F. Hintze, P. Tebben, *Angew. Chem. Int. Ed.* **1990**, *29*, 1422-1424, b) D. Hoppe, A. Carstens, T. Krämer, *Angew. Chem. Int. Ed.* **1990**, *29*, 1424-1425.
- [233] P. Beak, W. K. Lee, *Tetrahedron Lett.* **1989**, *30*, 1197-1200.
- [234] G. Barker, P. O'Brien, K. R. Campos, *Org. Lett.* **2010**, *12*, 4176-4179.
- [235] K. M. B. Gross, P. Beak, *J. Am. Chem. Soc.* **2001**, *123*, 315-321.
- [236] C. J. Cordier, R. J. Lundgren, G. C. Fu, *J. Am. Chem. Soc.* **2013**, *135*, 10946-10949.
- [237] C. Agami, F. Couty, *Tetrahedron* **2002**, *58*, 2701-2724.
- [238] E. Hevia, A. R. Kennedy, M. D. McCall, *Dalton Trans.* **2012**, *41*, 98-103.
- [239] G. Wittig, *Angew. Chem.* **1958**, *70*, 65-71.
- [240] T. I. Yousaf, R. L. Williams, I. Coldham, R. E. Gawley, *Chem. Commun.* **2008**, 97-98.
- [241] R. E. Gawley, G. Barolli, S. Madan, M. Saverin, S. O'Connor, *Tetrahedron Lett.* **2004**, *45*, 1759-1761.
- [242] Search performed 06/01/14, Version 1.15 F. H. Allen, *Acta Crystallogr. B* **2002**, *58*, 380-388 CCDB.
- [243] P. Stanetty, H. Koller, M. Mihovilovic, *J. Org. Chem.* **1992**, *57*, 6833-6837.
- [244] A. Dobrev, C. Ivanov, A. Lattes, M. Bon, *B. Soc. Chim. Fr.* **1987**, *6*, 1084-1088.
- [245] D. R. Armstrong, J. García-Álvarez, D. V. Graham, G. W. Honeyman, E. Hevia, A. R. Kennedy, R. E. Mulvey, *Chem. Eur. J.* **2009**, *15*, 3800-3807.
- [246] J. Zabicky, *The Chemistry of Functional Groups* (Ed.: Z. Rappoport), John Wiley and Sons, Ltd., King's Lynn, U.K., **2009**.
- [247] D. Seebach, R. Amstutz, J. D. Dunitz, *Helv. Chim. Acta.* **1981**, *64*, 2622-2626.
- [248] K. W. Henderson, A. E. Dorigo, Q. Y. Liu, P. G. Williard, P. v. R. Schleyer, P. R. Bernstein, *J. Am. Chem. Soc.* **1996**, *118*, 1339-1347.
- [249] G. S. Manku, *Theoretical Principles of Inorganic Chemistry*, Tata McGraw-Hill, Delhi, India, **1980**.
- [250] T. Laube, J. D. Dunitz, D. Seebach, *Helv. Chim. Acta* **1985**, *68*, 1373-1393.
- [251] X. He, B. C. Noll, A. Beatty, R. E. Mulvey, K. W. Henderson, *J. Am. Chem. Soc.* **2004**, *126*, 7444-7445.
- [252] Y. Apeloig, I. Zharov, D. Bravo-Zhivotovskii, Y. Ovchinnikov, S. Y., *J. Organomet. Chem.* **1995**, *499*, 73-82.
- [253] P. G. Williard, G. B. Carpenter, *J. Am. Chem. Soc.* **1986**, *108*, 462-468.
- [254] A. I. Meyers, M. A. Seefield, B. A. Lefker, J. F. Blake, P. G. Williard, *J. Am. Chem. Soc.* **1998**, *120*, 7429-7438.
- [255] H. R. L. Barley, W. Clegg, S. H. Dale, E. Hevia, G. W. Honeyman, A. R. Kennedy, R. E. Mulvey, *Angew. Chem. Int. Ed.* **2005**, *44*, 6018-6021.
- [256] W. Clegg, B. Conway, P. García-Álvarez, A. R. Kennedy, J. Klett, R. E. Mulvey, L. Russo, *Dalton Trans.* **2010**, *39*, 62-65.

- [257] M. G. Davidson, D. García-Vivó, A. R. Kennedy, R. E. Mulvey, S. D. Robertson, *Chem. Eur. J.* **2011**, *17*, 3364-3369.
- [258] W. Clegg, K. W. Henderson, A. R. Kennedy, R. E. Mulvey, C. T. O'Hara, R. B. Rowlings, D. M. Tooke, *Angew. Chem. Int. Ed.* **2001**, *40*, 3902-3905.
- [259] W. Clegg, S. H. Dale, A. M. Drummond, E. Hevia, G. W. Honeyman, R. E. Mulvey, *J. Am. Chem. Soc.* **2006**, *128*, 7434-7435.
- [260] L. S. Bennie, W. J. Kerr, M. Middleditch, A. J. B. Watson, *Chem. Commun.* **2011**, *47*, 2264-2266.
- [261] R. E. Mulvey, S. D. Robertson, *Angew. Chem.* **2013**, *52*, 11470-11487.
- [262] F. Chevallerier, Y. S. Halauko, C. Pecceu, I. F. Nassar, T. U. Dam, T. Roisnel, V. E. Matulis, O. A. Ivashkevich, F. Mongin, *Org. Biomol. Chem.* **2011**, *9*, 4671-4684.
- [263] a) S. Duez, A. K. Steib, P. Knochel, *Org. Lett.* **2012**, *14*, 1951-1953, b) G. C. Clososki, C. J. Rohbogner, P. Knochel, *Angew. Chem. Int. Ed.* **2007**, *46*, 7681-7684.
- [264] a) H. Naka, J. V. Morey, J. Haywood, D. J. Eisler, M. McPartlin, F. García, H. Kudo, Y. Kondo, M. Uchiyama, A. E. H. Wheatley, *J. Am. Chem. Soc.* **2008**, *130*, 16193-16200, b) J. García-Alvarez, E. Hevia, A. R. Kennedy, J. Klett, R. E. Mulvey, *Chem. Commun.* **2007**, 2402-2404.
- [265] a) O. Bayh, H. Awad, F. Mongin, C. Hoarau, F. Trécourt, G. Quéguiner, F. Marsais, F. Blanco, B. Abarca, R. Ballesteros, *Tetrahedron* **2005**, *61*, 4779-4784, b) V. L. Blair, L. M. Carrella, W. Clegg, J. Klett, R. E. Mulvey, E. Rentschler, L. Russo, *Chem. Eur. J.* **2009**, *15*, 856-863, c) V. L. Blair, W. Clegg, B. Conway, E. Hevia, A. R. Kennedy, J. Klett, R. E. Mulvey, L. Russo, *Chem. Eur. J.* **2008**, *14*, 65-72.
- [266] a) S. Bernhardt, G. Manolikakes, T. Kunz, P. Knochel, *Angew. Chem. Int. Ed.* **2011**, *50*, 9205-9209, b) C. I. Stathakis, S. Bernhardt, V. Quint, P. Knochel, *Angew. Chem. Int. Ed.* **2012**, *51*, 9428-9432.
- [267] M. Lalia-Kantouri, M. Gdaniec, T. Choli-Papadopoulou, A. Badounas, C. D. Papadopoulos, A. Czapik, G. D. Geromichalos, D. Sahpazidou, F. Tsitouroudi, *J. Inorg. Biochem.* **2012**, *117*, 25-34.
- [268] Y. M. Lee, S. J. Hong, H. J. Kim, S. H. Lee, H. Kwak, C. Kim, S.-J. Kim, Y. Kim, *Inorg. Chem. Commun.* **2007**, *10*, 287-291.
- [269] K.-Y. Ho, W.-Y. Yu, K.-K. Cheung, C.-M. Che, *Dalton Trans.* **1999**, 1581-1586.
- [270] S. K. Seth, B. Dey, T. J. Kar, S. Mukhopadhyay, *J. Mol. Struct.* **2010**, *973*, 81-88.
- [271] H. Gornitzka, C. Hemmert, G. Bertrand, M. Pfeiffer, D. Stalke, *Organometallics* **2000**, *19*, 112-114.
- [272] Z. Zheng, M. K. Elmkaddem, C. Fischmeister, T. Roisnel, C. M. Thomas, J.-F. Carpentier, J.-L. Renaud, *New J. Chem.* **2008**, *32*, 2150-2158.
- [273] M. Pfeiffer, F. Baier, T. Stey, D. Leusser, D. Stalke, B. Engels, D. Moigno, W. Kiefer, *J. Mol. Model.* **2000**, *6*, 299-311.
- [274] a) J. E. Johnson, R. A. Jacobsen, *Acta Crystallogr.* **1973**, *B29*, 1669-1674, b) G. J. Pyrka, A. A. Pinkerton, *Acta Crystallogr.* **1992**, *C48*, 91-94, c) H. Schödel, C. Näther, H. Bock, F. Butenschön, *Acta Crystallogr.* **1996**, *B52*, 842-853.

- [275] D. R. Armstrong, W. Clegg, S. H. Dale, J. García-Álvarez, R. W. Harrington, E. Hevia, G. W. Honeyman, A. R. Kennedy, R. E. Mulvey, C. T. O'Hara, *Chem. Commun.* **2008**, *44*, 187-189.
- [276] a) F. A. Cotton, L. M. Daniels, G. T. Jordan IV, C. A. Murillo, *Polyhedron* **1998**, *17*, 589-597, b) H. Gornitzka, D. Stalke, *Eur. J. Inorg. Chem.* **1998**, 311-317, c) M. Pfeiffer, A. Murso, L. Mahalakshmi, D. Moigno, W. Kiefer, D. Stalke, *Eur. J. Inorg. Chem.* **2002**, 3222-3234.
- [277] R. Campbell, P. García-Álvarez, A. R. Kennedy, R. E. Mulvey, *Chem. Eur. J.* **2010**, *16*, 9964-9968.
- [278] S. E. Baillie, V. L. Blair, D. C. Blakemore, D. Hay, A. R. Kennedy, D. C. Pryde, E. Hevia, *Chem. Commun.* **2012**, *48*, 1985-1987.
- [279] H. Schumann, W. Genthe, E. Hahn, M. B. Hossain, D. van der Helm, *J. Organomet. Chem.* **1986**, *299*, 67-84.
- [280] W. Clegg, S. H. Dale, E. Hevia, L. M. Hogg, G. W. Honeyman, R. E. Mulvey, C. T. O'Hara, L. Russo, *Angew. Chem. Int. Ed.* **2008**, *47*, 731-734.
- [281] a) W. J. Evans, M. A. Ansari, J. W. Ziller, S. I. Khan, *Inorg. Chem.* **1996**, *35*, 5435-5444, b) W. J. Evans, D. S. Lee, D. B. Rego, J. M. Perotti, S. A. Kozimor, E. K. Moore, J. W. Ziller, *J. Am. Chem. Soc.* **2004**, *126*, 14574-14582, c) D. Kurzbach, S. Yao, D. Hinderberger, K. W. Klinkhammer, *Dalton Trans.* **2010**, *39*, 6449-6459.
- [282] D. J. Darensbourg, S. A. Niezgodna, J. D. Draper, J. H. Reibenspies, *Inorg. Chem.* **1999**, *38*, 1356-1359.
- [283] F. Antolini, P. B. Hitchcock, A. V. Khvostov, M. F. Lappert, *Eur. J. Inorg. Chem.* **2003**, 3391-3400.
- [284] a) F. F. Blicke, L. D. Powers, *J. Am. Chem. Soc.* **1929**, *51*, 3378-3383, b) M. S. Kharasch, S. Weinhouse, *J. Org. Chem.* **1936**, *1*, 209-230, c) E. C. Ashby, J. J. R. Bowers, *J. Am. Chem. Soc.* **1981**, *103*, 2242-2250, d) T. Holm, I. Crossland, *Acta Chem. Scand.* **1971**, *25*, 59-69, e) G. A. Olah, A. Wu, O. Farooq, *Synthesis* **1991**, 1179-1182, f) D. R. Armstrong, W. Clegg, P. García-Álvarez, M. D. McCall, L. Nuttall, A. R. Kennedy, L. Russo, E. Hevia, *Chem. Eur. J.* **2011**, *17*, 4470-4479.
- [285] a) M. Hatano, T. Matsumura, K. Ishihara, *Org. Lett.* **2005**, *7*, 573-576, b) M. Hatano, S. Suzuki, K. Ishihara, *J. Am. Chem. Soc.* **2006**, *128*, 9998-9999, c) M. Hatano, K. Ishihara, *Synthesis* **2008**, 1647-1675, d) M. Hatano, S. Suzuki, K. Ishihara, *Synlett* **2010**, 321-324.
- [286] a) I. Cragg-Hine, M. G. Davidson, A. J. Edwards, P. R. Raithby, R. Snaith, *J. Chem. Soc. Dalton Trans.* **1994**, 2901-2902, b) M. Karl, G. Seybert, W. Massa, K. Harms, S. Agarwal, R. Maleika, W. Stelter, A. Greiner, W. H. B. Neumüller, K. Dehnicke, *Z. Anorg. Allg. Chem.* **1999**, *625*, 1301-1309.
- [287] P. C. Andrews, W. Clegg, R. E. Mulvey, *Angew. Chem. Int. Ed. Engl.* **1990**, *29*, 1440-1441.
- [288] a) O. Vechorkin, A. Godinat, R. Scopelliti, X. Hu, *Angew. Chem. Int. Ed.* **2011**, *50*, 11777-11781, b) P. Ren, I. Salihu, R. Scopelliti, X. Hu, *Org. Lett.* **2012**, *14*, 1748-1751.
- [289] J. R. Allan, G. M. Baillie, L. A. Macindoe, A. J. Blake, H. J. Bowley, D. L. Gerrard, *Acta Crystallogr.* **1988**, *C44*, 1833-1834.
- [290] R. Campbell, E. Crosbie, A. R. Kennedy, R. E. Mulvey, R. A. Naismith, S. D. Robertson, *Aust. J. Chem.* **2013**, *66*, 1189-1201.

- [291] a) J. H. N. Buttery, N. C. Plackett, B. W. Skelton, C. R. Whitaker, A. H. White, *Z. Anorg. Allg. Chem.* **2006**, *632*, 1856-1869, b) D. R. Armstrong, M. G. Davidson, D. García-Vivó, A. R. Kennedy, R. E. Mulvey, S. D. Robertson, *Inorg. Chem.* **2013**, *52*, 12023-12032.
- [292] a) A. R. Kennedy, R. E. Mulvey, C. T. O'Hara, G. M. Robertson, S. D. Robertson, *Angew. Chem. Int. Ed.* **2011**, *123*, 8525-8528, b) D. M. Cousins, M. G. Davidson, C. J. Frankis, D. García-Vivó, M. F. Mahon, *Dalton Trans.* **2010**, *39*, 8278-8280.
- [293] D. R. Armstrong, J. A. Garden, A. R. Kennedy, R. E. Mulvey, S. D. Robertson, *Angew. Chem. Int. Ed.* **2013**, *52*, 7190-7193.
- [294] a) A. Macchioni, G. Ciancaleoni, C. Zuccaccia, D. Zuccaccia, *Chem. Soc. Rev.* **2008**, *37*, 479-489, b) D. Li, I. Keresztes, R. Hopson, P. G. Williard, *Acc. Chem. Res.* **2009**, *42*, 270-280.
- [295] a) S. Trefi, C. Routaboul, S. Hamieh, V. Gilard, M. Malet-Martino, R. Martino, *J. Pharmaceut. Biomed.* **2008**, *47*, 103-113, b) C. Su, R. Hopson, P. G. Williard, *Eur. J. Inorg. Chem.* **2013**, 4136-4141, c) C. C. Su, R. Hopson, P. G. Williard, *J. Am. Chem. Soc.* **2013**, *135*, 12400-12406.
- [296] O. L. Sydora, P. T. Wolczanski, E. B. Lobkovsky, C. Buda, T. R. Cundari, *Inorg. Chem.* **2005**, *44*, 2606-2618.
- [297] H. Schumann, M. Hummert, A. N. Lukoyanov, I. L. Fedushkin, *Chem. Eur. J.* **2007**, *13*, 4216-4222.
- [298] M. D. Rausch, D. J. Ciappenelli, *J. Organomet. Chem.* **1967**, *10*, 127-136.
- [299] a) D. B. Collum, *Acc. Chem. Res.* **1993**, *26*, 227-234, b) H. Oulyadi, C. Fressigné, Y. Yuan, J. Maddaluno, A. Harrison-Marchand, *Organometallics* **2012**, *31*, 4801-4809, c) A. Corruble, J.-Y. Valnot, J. Maddaluno, Y. Prigent, D. Davoust, P. Duhamel, *J. Am. Chem. Soc.* **1997**, *119*, 10042-10048.
- [300] H. Yamataka, Y. Kawafuji, K. Nagareda, N. Miyano, T. Hanafusa, *J. Org. Chem.* **1989**, *54*, 4706-4708.
- [301] a) G. C. Forbes, A. R. Kennedy, R. E. Mulvey, P. J. A. Rodger, *Chem. Commun.* **2001**, 1400-1401, b) L. Balloch, A. M. Drummond, P. García-Alvarez, D. V. Graham, A. R. Kennedy, J. Klett, R. E. Mulvey, C. T. O'Hara, P. J. A. Rodger, I. D. Rushworth, *Inorg. Chem.* **2009**, *48*, 6934-6944.
- [302] T. Vogler, A. Studer, *Synthesis-Stuttgart* **2008**, 1979-1993.
- [303] D. R. Armstrong, L. Balloch, J. J. Crawford, B. J. Fleming, L. M. Hogg, A. R. Kennedy, J. Klett, R. E. Mulvey, C. T. O'Hara, S. A. Orr, S. D. Robertson, *Chem. Commun.* **2012**, *48*, 1541-1543.
- [304] G. Sorin, R. M. Mallorquin, Y. Contie, A. Baralle, M. Malacria, J. P. Goddard, L. Fensterbank, *Angew. Chem. Int. Ed.* **2010**, *49*, 8721-8723.
- [305] C. C. L. Thum, G. N. Khairallah, R. A. J. O'Hair, *Angew. Chem. Int. Ed.* **2008**, *47*, 9118-9121.
- [306] C. Blomberg, R. M. Salinger, H. S. Mosher, *J. Org. Chem.* **1969**, *34*, 2385-2388.
- [307] a) M. H. Dickman, R. J. Doedens, *Inorg. Chem.* **1982**, *21*, 682-684, b) P. Jaitner, W. Huber, G. Hunter, O. Scheidsteger, *J. Organomet. Chem.* **1983**, *259*, C1-C5, c) J. Laugier, J. M. Latour, A. Caneschi, P. Rey, *Inorg. Chem.* **1991**, *30*, 4474-4477, d) M. K. Mahanthappa, K. W. Huang, A. P. Cole, R. M. Waymouth, *Chem. Commun.* **2002**, 502-503, e) D. J. Mindiola, R.

- Waterman, D. M. Jenkins, G. L. Hillhouse, *Inorg. Chim. Acta* **2003**, 345, 299-308.
- [308] a) T. Iwamoto, H. Masuda, S. Ishida, C. Kabuto, M. Kira, *J. Am. Chem. Soc.* **2003**, 125, 9300-9301, b) A. Naka, N. J. Hill, R. West, *Organometallics* **2004**, 23, 6330-6332, c) G. H. Spikes, Y. Peng, J. C. Fettinger, J. Steiner, P. P. Power, *Chem. Commun.* **2005**, 6041-6043, d) C. Jones, R. P. Rose, *New J. Chem.* **2007**, 31, 1484-1487.
- [309] W. J. Evans, J. M. Perotti, R. J. Doedens, J. W. Ziller, *Chem. Commun.* **2001**, 2326-2327.
- [310] R. I. Cooper, R. O. Gould, S. Parsons, D. J. Watkin, *J. Appl. Cryst.* **2005**, 35, 168-174.
- [311] N. J. Findlay, S. R. Park, F. Schoenebeck, E. Cahard, S. Zhou, L. E. A. Berlouis, M. D. Spicer, T. Tuttle, J. A. Murphy, *J. Am. Chem. Soc.* **2010**, 132, 15462-15464.
- [312] J. S. Lomas, S. Briand, D. Fain, *J. Org. Chem.* **1991**, 56, 166-175.
- [313] a) W. Clegg, B. Conway, E. Hevia, M. D. McCall, L. Russo, R. E. Mulvey, *J. Am. Chem. Soc.* **2009**, 131, 2375-2384, b) V. L. Blair, D. C. Blakemore, D. Hay, E. Hevia, D. C. Pryde, *Tetrahedron Lett.* **2011**, 52, 4590-4594, c) V. L. Blair, W. Clegg, A. R. Kennedy, Z. Livingstone, L. Russo, E. Hevia, *Angew. Chem. Int. Ed.* **2011**, 50, 9857-9860, d) J. J. Crawford, B. J. Fleming, A. R. Kennedy, J. Klett, C. T. O'Hara, S. A. Orr, *Chem. Commun.* **2011**, 47, 3772-3774, e) P. García-Álvarez, A. R. Kennedy, C. T. O'Hara, K. Reilly, G. M. Robertson, *Dalton Trans.* **2011**, 40, 5332-5341.
- [314] J. A. Garden, A. R. Kennedy, R. E. Mulvey, S. D. Robertson, *Chem. Commun.* **2012**, 48, 5265-5267.
- [315] R. E. Mulvey, D. R. Armstrong, B. Conway, E. Crosbie, A. R. Kennedy, S. D. Robertson, *Inorg. Chem.* **2011**, 50, 12241-12251.
- [316] D. R. Armstrong, W. Clegg, S. H. Dale, E. Hevia, L. Hogg, G. W. Honeyman, R. E. Mulvey, *Angew. Chem. Int. Ed.* **2006**, 45, 3775-3778.
- [317] J. F. Remenar, B. L. Lucht, D. Kruglyak, F. E. Romesberg, J. H. Gilchirst, D. B. Collum, *J. Org. Chem.* **1997**, 62, 5748-5754.
- [318] J. G. Rosa, B. Harichian, D. J. Drennan, J. S. Bajor, C. A. Bosko, *US 20120027700*, **2012**.
- [319] a) S. M. Feinberg, S. Friedlaender, *Am. J. Med. Sci.* **1947**, 213, 58-60, b) A. M. Fuchs, P. M. Schulman, M. B. Strauss, *J. Allergy* **1947**, 18, 385-390, c) H. Leibowitz, I. M. Kurtz, E. Schwartz, *New York State J. Med.* **1947**, 47, 989-991.
- [320] D. Barr, R. Snaith, D. S. Wright, R. E. Mulvey, K. Jeffrey, D. Reed, *J. Organomet. Chem.* **1987**, 325, C1-C6.
- [321] K. W. Henderson, R. E. Mulvey, W. Clegg, P. A. O'Neil, *J. Organomet. Chem.* **1992**, 439, 237-250.
- [322] W. Clegg, K. W. Henderson, R. E. Mulvey, P. A. O'Neil, *J. Chem. Soc., Chem. Commun.* **1993**, 969-970.
- [323] Within the alkyne derivative $[(\text{TMEDA})\text{Li}(\text{C}\equiv\text{CPh})_2\text{Zn}(\text{tBu})]_2(\text{TMEDA})$, two $(\text{TMEDA})\text{Li}(\text{C}\equiv\text{CPh})_2\text{Zn}(\text{tBu})$ fragments are connected via a bridging TMEDA ligand. Each Zn centre is coordinated to two C≡CPh anions and a *tert*-butyl anion, with the NMe₂ arm of TMEDA completing the coordination sphere. The related sodium zincate, $[(\text{TMEDA})\cdot\text{Na}(\text{C}\equiv\text{CPh})_2\text{Zn}(\text{tBu})]_2$, also

- exhibiting a tetrahedral lower order zinc centre, adopts a distorted cubane motif. W. Clegg, J. García-Álvarez, P. García-Álvarez, D. V. Graham, R. W. Harrington, E. Hevia, A. R. Kennedy, R. E. Mulvey, L. Russo, *Organometallics* **2008**, *27*, 2654-2663.
- [324] The sum of the equatorial angles [N2-Na1-N3, 115.11(5)°; N2-Na1-C22, 126.130(51)°; N3-Na1-C22, 118.516(50)°] is 359.8°, which corresponds to 99% equatorial trigonal bipyramidal character (TBP_e) according to the method proposed by Tamao and Ito. Defined by apical-to-equatorial bonds [N2-Na1-N4, 109.32(5)°; N3-Na1-N4, 73.51(5)°; C22-Na1-N4, 90.453(51)°], the axial trigonal bipyramidal character (TBP_a) is also high at 94%. K. Tamao, T. Hayashi, Y. Ito, M. Shiro, *Organometallics* **1992**, *11*, 2099-2114.
- [325] S. Uhlenbrock, R. Wegner, B. Krebs, *J. Chem. Soc., Dalton Trans.* **1996**, 3731-3736.
- [326] R. Benn, H. Grondey, H. Lehmkuhl, H. Nehl, K. Angermund, C. Krüger, *Angew. Chem. Int. Ed.* **1987**, *26*, 1279-1280.
- [327] R. Campbell, D. Cannon, P. García-Álvarez, A. R. Kennedy, R. E. Mulvey, S. D. Robertson, J. Saßmannshausen, T. Tuttle, *J. Am. Chem. Soc.* **2011**, *133*, 13706-13717.
- [328] W. Clegg, B. Conway, P. García-Álvarez, A. R. Kennedy, R. E. Mulvey, L. Russo, J. Saßmannshausen, T. Tuttle, *Chem. Eur. J.* **2009**, *15*, 10702-10706.
- [329] a) H. Ahlbrecht, G. Schneider, *Tetrahedron* **1986**, *42*, 4729-4741, b) A. Streitwieser, A. Facchetti, L. Xie, X. Zhang, E. C. Wu, *J. Org. Chem.* **2012**, *77*, 985-990.
- [330] R. D. Hancock, A. E. Martell, *Advances in Inorganic Chemistry*, *42* (Ed.: A. G. Sykes), Academic Press, Inc., San Diego, California, **1995**, pp. 89-146.
- [331] Search performed 08/11/13, Version 1.15 F. H. Allen, *Acta Cryst. B.* **2002**, *58*, 380-388.
- [332] R. Campbell, B. Conway, G. S. Fairweather, P. García-Álvarez, A. R. Kennedy, J. Klett, R. E. Mulvey, C. T. O'Hara, G. M. Robertson, *Dalton Trans.* **2010**, *39*, 511-519.
- [333] W. Clegg, L. Horsburgh, R. E. Mulvey, M. J. Ross, R. B. Rowlings, V. Wilson, *Polyhedron* **1998**, *17*, 1923-1930.
- [334] According to the method published by Houser, each Zn centre of **27** has a distorted tetrahedral geometry, with a τ_4 value of 0.76. The value of τ_4 indicates a sliding scale where 1.00 represents an ideal tetrahedral geometry and 0.00 indicates an ideal square planar geometry. L. Yang, D. R. Powell, R. P. Houser, *Dalton Trans.* **2007**, *36*, 955-965.
- [335] a) J. G. Noltes, J. Boersma, *J. Organomet. Chem.* **1969**, *16*, 345-355, b) M. Westerhausen, T. Bollwein, A. Pfitzner, T. Nilges, H.-J. Deiseroth, *Inorg. Chim. Acta* **2001**, *312*, 239-244, c) D. A. Walker, T. J. Woodman, M. Schormann, D. L. Hughes, M. Bochmann, *Organometallics* **2003**, *22*, 797-803, d) Y. Sarazin, J. A. Wright, D. A. J. Harding, E. Martin, T. J. Woodman, D. L. Hughes, M. Bochmann, *J. Organomet. Chem.* **2008**, *693*, 1494-1501, e) S. Javed, D. M. Hoffman, *Dalton Trans.* **2010**, *39*, 11439-11444.
- [336] Synthesised through the equimolar ligand redistribution reaction of [¹BuC(NⁱPr)₂]₂Zn] with ZnMe₂, [¹BuC(NⁱPr)₂]₂ZnMe] was isolated and characterised using single crystal X-ray diffraction analysis. S. Schmidt, S. Schulz, M. Bolte, *Z. Anorg. Allg. Chem.* **2009**, *635*, 2210-2213.

- [337] D. R. Armstrong, J. A. Garden, A. R. Kennedy, S. M. Leenhouts, R. E. Mulvey, P. O'Keefe, C. T. O'Hara, A. Steven, *Chem. Eur. J.* **2013**, *19*, 13492-13503.
- [338] S. Usui, Y. Hashimoto, J. V. Morey, A. E. H. Wheatley, M. Uchiyama, *J. Am. Chem. Soc.* **2007**, *129*, 15102-15103.
- [339] F. M. Kerton, *Alternative Solvents for Green Chemistry*, Royal Society of Chemistry, Cambridge, U.K., **2009**.
- [340] J. M. Hoover, S. S. Stahl, *J. Am. Chem. Soc.* **2011**, *133*, 16901-16910.
- [341] R. J. Abraham, M. Mobli, R. J. Smith, *Magn. Reson. Chem.* **2003**, *41*, 26-36.
- [342] J. Halpern, *Pure Appl. Chem.* **2001**, *73*, 209-220.
- [343] a) T. L. Ho, *Chem. Rev.* **1975**, *75*, 1-20, b) R. G. Pearson, *Coord. Chem. Rev.* **1990**, *100*, 403-425.
- [344] M. Brynda, L. Gagliardi, P.-O. Widmark, P. P. Power, B. O. Roos, *Angew. Chem. Int. Ed.* **2006**, *45*, 3804-3807.
- [345] T. J. Kealy, P. L. Pauson, *Nature* **1951**, *168*, 1039-1040.
- [346] a) H. Lu, A. Khan, P. G. Smirniotis, *Ind. Eng. Chem. Res.* **2008**, *47*, 6216-6220, b) K. Sumida, D. L. Rogow, J. A. Mason, T. M. McDonald, E. D. Bloch, Z. R. Herm, T.-H. Bae, J. R. Long, *Chem. Rev.* **2011**, *112*, 724-781, c) J. Liu, P. K. Thallapally, B. P. McGrail, D. R. Brown, J. Liu, *Chem. Soc. Rev.* **2012**, *41*, 2308-2322.
- [347] a) R. H. Crabtree, *J. Chem. Soc., Dalton Trans.* **2001**, 2437-2450, b) A. M. Chapman, M. F. Haddow, D. F. Wass, *J. Am. Chem. Soc.* **2011**, *133*, 18463-18478.
- [348] a) J. L. Dempsey, B. S. Brunshwig, J. R. Winkler, H. B. Gray, *Acc. Chem. Res.* **2009**, *42*, 1995-2004, b) G. J. Kubas, *J. Organomet. Chem.* **2009**, *694*, 2648-2653.
- [349] a) S. Harder, J. Spielmann, J. Intemann, H. Bandmann, *Angew. Chem. Int. Ed.* **2011**, *50*, 4156-4160, b) E. Hevia, R. E. Mulvey, *Angew. Chem. Int. Ed.* **2011**, *50*, 9242-9243, c) S. Harder, *Chem. Commun.* **2012**, *48*, 11165-11177.
- [350] D. F. Shriver, M. A. Derezdon, *The Manipulation of Air-Sensitive Compounds*, 2nd ed., Wiley and Sons, New York, New York, **1986**.
- [351] a) S. C. Watson, J. F. Eastham, *J. Organomet. Chem.* **1967**, *9*, 165-168, b) H.-S. Lin, L. A. Paquette, *Synth. Commun.* **2007**, *24*, 2503-2506.
- [352] C. Schade, W. Bauer, P. v. R. Schleyer, *J. Organomet. Chem.* **1985**, *295*, 25-28.
- [353] P. C. Andrikopoulos, D. R. Armstrong, H. R. L. Barley, W. Clegg, S. H. Dale, E. Hevia, G. W. Honeyman, A. R. Kennedy, R. E. Mulvey, *J. Am. Chem. Soc.* **2005**, *127*, 6184-6185.
- [354] D. H. Williams, I. Fleming, *Spectroscopic Methods in Organic Chemistry*, 5th ed., McGraw-Hill, Maidenhead, **1995**.
- [355] G. M. Sheldrick, *Acta Crystallogr.* **2008**, *A64*, 112-122.